Wisconsin Highway Research Program

Structural Analysis of Sign Bridge Structures and Luminaire Supports

Christopher M. Foley, Ph.D., P.E.
Scott J. Ginal
John L. Peronto
Raymond A. Fournelle, Ph.D., P.E.
Marquette University
Department of Civil and Environmental Engineering

March, 2004

WHRP 04-03

Technical Report Documentation Page

1. Report No. 04-03	2. Government Accession No.	3. Recipient's Catalog No.
4. Title and Subtitle Structural Analysis Of Sign Bridge Structures And Luminaire Supports		5. Report Date March 31, 2004
		6. Performing Organization Code SPR-0092-00-0016
7. Authors Christopher M. Foley, Ph.D., P.E. Raymond A. Fournelle, Ph.D., P.E. Scott J. Ginal John L. Peronto		8. Performing Organization Report No. 0092-00-0016
9. Performing Organization Name and Address Department of Civil & Environmental Engineering Marquette University 1515 W. Wisconsin Avenue Milwaukee, WI 53233		10. Work Unit No. (TRAIS)
		11. Contract or Grant No. WHRP Project No. 0092-00-16
12. Sponsoring Agency Name and Address Wisconsin Department of Transportation 4802 Sheboygan Avenue Madison, WI 73707-7965		13. Type of Report and Period Covered Final Report
		14. Sponsoring Agency Code

15. Supplementary Notes
This research was funded by the Wisconsin DOT and FHWA through the Wisconsin Highway Research Program. Wisconsin DOT Contact: Stanley Woods (608) 266-8348.

16. Abstract
The Wisconsin Department of Transportation has experienced failures of a high-mast luminaire (HML) support structure and a full-span overhead sign support structure. Furthermore, cracking has been found in many sign support structures composed of welded round hollow structural shapes (HSS). The purpose of the research conducted was to provide fatigue life estimates for these structures, which could then shed light onto the causes of the cracking found and the failures experienced. The analytical and experimental effort conducted was also used to establish rational inspection intervals for these structures and recommend changes (as required) to the procedures for design of high-mast luminaire and full-span sign support structures targeted to improve in-service performance.

17. Key Words Sign Support Structures, High-Mast Luminaire Support Structures, Fatigue Life Prediction, Finite Element Analysis	18. Distribution Statement No restriction. This document is available to the public through the National Technical Information Service, 5285 Port Royal Road, Springfield, VA 22161		
19. Security Classification (of this report) Unclassified	20. Security Classification (of this page) Unclassified	21. No. of Pages	22. Price

Form DOT F 1700.7 (8-72) Reproduction of completed page authorized.

NOTICE:

This research was funded through the Wisconsin Highway Research Program by the Wisconsin Department of Transportation and the Federal Highway Administration under Project # (0092-00-0016). The contents of this report reflect the views of the authors who are responsible for the facts and the accuracy of the data presented herein. The contents do not necessarily reflect the official views of the Wisconsin Department of Transportation or the Federal Highway Administration at the time of publication.

Table of Contents

This page intentionally left blank.

Acknowledgements

As is the case in any large project, there are many, many individuals that contribute to its success and completion. The authors would like to acknowledge the indispensable help of many individuals in completion of this effort.

The authors would like to thank the following individuals at the Wisconsin Department of Transportation for their time and expertise. Without these individuals this project would never have been completed:

District 1:	District 2:
Kent Bahler	Thomas Heydel
Joel Alsum	Charles N. Landey
Craig Wehrle	Arlo Tessmer

Special thanks are extended to Stanley Woods for his understanding and patience.

The authors would also like to acknowledge the help of, and thank, Jackie Jiran at the Wisconsin Highway Research Program.

Obtaining specimens from decommissioned sign support structures would not have been possible without the help of Charlie Johanek of The Kuehne Company and Owen Wade of Arbor Green.

Helpful comments, suggestions on improving the work, general information, and aid in visiting sites, have been provided by many individuals. The authors would like to acknowledge the help of the following:

Terence Browne of Collins Engineers, Inc.
Jeff Gerbensky of Wilbur, Smith and Associates, Inc.
Mark Huntoon (formerly of Wilbur, Smith and Associates, Inc.)
Bruce Peterson of Edwards and Kelcey
Justin Ocel of the University of Minnesota
Prof. Al Ghorbanpoor of the University of Wisconsin – Milwaukee
Prof. Robert Dexter of the University of Minnesota

A very big “thank you” is extended to Mike Henke and his firm, Construction Supply & Erection of Germantown, Wisconsin. It is safe to say that the highly-important experimental portion of this work would not have been possible without Mike and C.S. & E.

This Page Intentionally Left Blank

Executive Summary

Project Summary

The Wisconsin Department of Transportation has experienced failures of a high-mast luminaire (HML) support structure and a full-span overhead sign support structure. Furthermore, cracking has been found in many sign support structures composed of welded round hollow structural shapes (HSS). The purpose of the research conducted was to provide fatigue life estimates for these structures, which could then shed light onto the causes of the cracking found and the failures experienced. The analytical and experimental effort conducted was also used to establish rational inspection intervals for these structures and recommend changes (as required) to the procedures for design of high-mast luminaire and full-span sign support structures targeted to improve in-service performance.

Background

The motivation for the present study stems from the collapse of several luminaire assembly support masts (both high- and low-) in the Milwaukee area, instances of cracking in welded truss structures throughout the state, and the near collapse of a full-span sign support truss in Eau Claire, Wisconsin.

In 1998, there was a collapse of a (approximately) 40-foot tall luminaire assembly support mast (Core-Ten steel material) into IH 894 in West Allis, Wisconsin. This collapse initiated data collection and inspection of 474 of these luminaire support masts in the metro-Milwaukee area. The research conducted revealed that the majority had their bases founded within the "salt-spray area" of the roadway leading to a 20% loss of wall thickness near the base. A similar experience with Core-Ten luminaire mast material was seen in Eau Claire, Wisconsin. WisDOT also experienced a collapse of a high-mast luminaire support structure at the Zoo Interchange in Milwaukee, Wisconsin. This failure was attributed to loose anchor rod nuts exhibited by wear marks on the base plate in the anchor rod holes.

Perhaps the most disconcerting in-service performance failure that WisDOT has seen to date was the excessive vibration of a full-span sign support bridge in Eau Claire, Wisconsin. This structure was put into service in August 1996 and was removed from service in February 1997. An extensive inspection of the decommissioned structure revealed extensive cracking in the vertical diagonals and cracks that had migrated into the bottom chord of the welded truss. A failure analysis was performed and electron microscopy indicated that the crack surfaces in each piece studied were covered with a zinc-rich coating. This indicated that the cracks were present at the time the truss section was galvanized and the cracking that was found was said to be initiated or caused by liquid metal embrittlement during the galvanizing process. The forensic investigation of this failed structure was very important to the present

research investigation. First of all, the performance of this structure appears to be consistent and indicative of a large portion of the poor in-service performance of sign support structures seen across the United States. Secondly, the results of the failure investigation of this structure point to a "fabrication" problem rather than a "design" problem. Much of the research efforts in the last 5-7 years sponsored by the National Cooperative Highway Research Program (NCHRP) have focused on the "loading side" of the design equation. These efforts have sought to develop conservative loading scenarios and fatigue detail category data that will result in sign, luminaire, and traffic signal support structures that have infinite design lives. These efforts have resulted in very complicated design provisions that may or may not solve the in-service performance problems.

The present research draws upon several efforts conducted by the National Cooperative Highway Research Program. It provides performance-related information related to the full-span overhead sign support structures and high-mast luminaire structures not considered in these past efforts. The present study also provides the most detailed analytical effort to date for ancillary highway support structures in the United States.

The research was conducted at Marquette University in Milwaukee, Wisconsin. The research team was composed of Dr. Christopher M. Foley, P.E.; Dr. Raymond A. Fournelle, P.E.; Scott J. Ginal, M.S.; and John L. Peronto, M.S. Scott Ginal and John Peronto were graduate research assistants and their contributions to the Project were in the form of masters theses in partial fulfillment of their Master of Science Degrees. Dr. Foley is a member of the civil and environmental engineering department at Marquette and is a structural engineer. Dr. Fournelle is a metallurgical engineer in the department of mechanical engineering at Marquette. The MS theses for Mr. Ginal and Mr. Peronto are available through the Marquette University libraries.

Process

The present research effort focused on detailed structural analysis, evaluation of the susceptibility to aerodynamic instability, and fatigue life prediction of high-mast luminaire and full-span steel sign support structures within the State of Wisconsin. The research effort provides a review and synthesis of the literature related to the state-of-the-art design and analysis methodologies for sign and luminaire support structures. Data collection and analysis were undertaken to provide data necessary to predict wind speed and direction probabilities for the metro-Milwaukee area. This analysis set the stage for generating fatigue-life predictions for full-span sign and luminaire support structures. An experimental effort was undertaken to generate statistical variability measures for the *ET* detail category found in the welded HSS sign support trusses. A procedure was described whereby natural wind can be simulated and used as

loading in a finite element analysis for the structures considered with subsequent rainflow counting and fatigue life predictions. An analytical model for a truck-induced gust pressure pulse was developed for subsequent use in finite element analysis to generate fatigue damage estimates for full-span overhead sign support structures resulting from passing trucks.

Three full-span sign support structures were selected from those managed by WisDOT District 2. These structures were S-40-156, S-40-404, and S-67-402. Vibration characteristics of the structures were studied including the effect of base fixity on the modal vibration shapes. The susceptibility of these structures to the aerodynamic instability phenomena of galloping and vortex-shedding was evaluated. An experimental program was undertaken to determine fatigue life statistical variability of the fully-welded joints found in round HSS trusses. Using the experimental fatigue life information obtained and the finite element analysis, fatigue lives for these structures were computed and critical components that governed the fatigue lives were pointed out. The susceptibility of full-span sign support structures to damage resulting from truck-induced pressure pulses was also evaluated.

Two high-mast luminaire support structures were selected from the database of structures managed by WisDOT District 2. These structures were HML-40-061 and HML-67-006. A detailed stress analysis of the base conditions and a study of the stress distribution in the mast wall at the base were provided including recommendations for stress-concentration factors for both base conditions. Modal analysis for the HML structures was conducted and the impact of base plate thickness and anchor rod stand off height on the natural frequencies of vibration for the HML structures was evaluated. The susceptibility of the HML structures to vortex-shedding induced vibrations was also evaluated. Finally, fatigue life predictions were made and critical components that limit the fatigue life of the HML structures considered were identified.

The research effort began in October 2000 and was completed in March 2004. The research effort was intended to provide information suitable for development of modifications to national design specifications for high-mast luminaire and full-span sign support structures, and to provide WisDOT with valuable information for establishing design requirements for these structures and inspection protocols to ensure suitable in-service performance.

Findings and Conclusions

There are several conclusions that can be drawn from the completed study with regard to full-span sign support structures. The design of sign support structures of the configurations examined need not consider galloping vibrations and vortex shedding induced vibrations. Truck-induced pressure pulses

were found to cause stress ranges of magnitude less then 1/2 the constant amplitude fatigue limit for the tri-chord sign support structure examined (S-40-156). Therefore, truck-induced gust pressures need not be considered in the design of structures using this configuration. Truck-induced pressures may be required as a design consideration for longer spans (*e.g.* greater than 100 feet) in the four-chord configuration.

Tri-chord sign support structures (*e.g.* S-40-156) are likely to have service lives that are less than a 50-year target service life (95% confidence). Diagonal web members in the front face of the truss are likely to be the controlling members when determining the fatigue life of the structure. Four-chord box trusses with VMS and grouted base plates are likely to attain a 50-year target service life. However, the fatigue life of 4-chord box trusses with stand-off heights in the anchor rods is likely to be less than the 50-year target. The analytical study conducted showed that the anchor rods for this configuration (S-67-402) are the fatigue-critical component and therefore, control the fatigue life of this structure. It is surmised that if the anchor rods did not have such a severe stand-off (*e.g.* less than one anchor rod diameter), the ability to omit bending stresses in the anchor rods when considering fatigue would likely have improved the fatigue life to the extent that it would extend into the target range of 50-years or more. Aside from the anchor rods, the diagonal web members are the fatigue-critical components in the four-chord box truss configuration and fatigue lives (with the exception of the tri-chord configuration) will exceed 50 years.

There are several conclusions that one can draw regarding the analysis of the high-mast luminaire support structures considered in this study. Anchor bolt stand off heights have very little impact on the natural frequencies of the first five modes of vibration for the structures evaluated. Variation in base plate thickness has a greater impact than anchor rod stand-off height in causing the modal frequencies (first five modes) to deviate significantly from that of the fixed base condition. If base plate thicknesses are 1-1/2 inches or greater, there is no concern. If base plate thicknesses become thinner than this threshold, higher-mode frequencies may differ considerably from the fixed base condition.

Four bolt anchor rod arrangements cause a 40% increase in the stress in the wall of the mast when bending is considered. This stress concentration should be considered when establishing fatigue-life stress ranges for the mast base. Eight anchor rod arrangements do not have the same stress raiser condition and can be treated as a fixed base for stress computations. Four anchor rod arrangements result in significant bending stresses in the anchor rods. The magnitude of bending stress is significantly reduced in the eight anchor arrangement. Overall, it is suggested that 4 anchor rod arrangements be avoided in HML structures. The 8 anchor rod arrangement has a much smoother stress distribution at the base of the mast and the bending stresses in the anchor rods are lessened.

The analytical study of the HML structures considered suggests that vortex-shedding need not be considered in the design. The senior author personally watched HML-67-006 for nearly one hour in 25-35 mph measured winds (reported). There was no across-wind vibration of the mast indicative of vortex-shedding vibrations. The equivalent projected area of the luminaire assembly and the ever decreasing shaft diameter makes along-wind first-mode vibration shapes dominant in the response.

Both HML structures studied have no difficulty in attaining their 50-year target service life with 95% confidence. The analysis of both structures ignored degradation of cross-section through corrosion. However, the 264 year fatigue life, in the case of HML-40-061, with "perfect" anchor rods leaves ample room for consideration of cross-section reduction without concern. Furthermore, if mean stress effects are omitted, changing the cross-sections (through corrosion) will not change the magnitude of the stress ranges. Therefore, fatigue lives are not expected to differ.

By eliminating consideration of: truck-induced pressures for design of full-span sign support structures; vortex shedding evaluation from full-span sign and high-mast luminaire support structures; and galloping evaluation from the design of full-span sign support structures; the design of full-span overhead sign and high-mast luminaire support structures will become far less tedious than the efforts currently undertaken. As a result, there will be greater economy of design achieved.

If a structure is inspected with great detail during fabrication (*e.g.* immediately after galvanizing) and immediately after erection with no flaws being found, the structure can be put into service with inspection intervals much longer than the current 2-year cycles (*e.g.* 10 years). In the case of high-mast luminaire support structures, this initial inspection may lead to an "inspection free" service life. This will result in significant economic savings to WisDOT. In the case of full-span overhead sign support structures, the 2-year inspection interval can be lengthened. Considering that there are nearly 1,000 sign and luminaire support structures in Wisconsin, lengthening the inspection cycle will result in much more efficient use of monetary resources.

The tri-chord welded truss configuration has been shown to have a reduced fatigue life when compared to the four-chord configuration and therefore, it should be utilized with less sign area that that of S-40-156 considered in this study. In general, it is recommended that tri-chord trusses not be used due to the significant twisting deformations that are present in the structures when subjected to natural wind.

The results of the present effort can be expected to contribute to a better understanding of the fatigue lives for sign and luminaire support structures and a streamlined design methodology more consistent with reality. The results are expected to contribute to the knowledge base currently under

development in the National Cooperative Highway Research Program regarding ancillary highway structures.

Recommendations for Further Action

The bending of anchor rods with stand-off heights in HML and sign support structures needs further study. It would be very useful to have experimental work done on anchor rods with significant bending in them (*e.g.* beyond the 1:40 out-of-plumb currently assumed in the sign and luminaire design specifications). Furthermore, having statistical information regarding the fatigue life of these anchors would improve design methodologies and fatigue life evaluation significantly.

In general, a better understanding of the statistical variability in the fatigue life of typical details found in sign and luminaire support structures would lead to a better understanding of why some of these structures have had questionable in-service performance, and more importantly, why others have had stellar in-service performance records.

Last, but certainly not least, a better understanding of the galvanizing process and its effect on high-strength steels, welded HSS connections, and the impact of partial dip galvanizing on welded truss structures is urgently needed. This will help in understanding exactly why poor in-service performance has been obtained for some structures and its apparent link to the galvanizing process and fabrication.

It is expected that many of the results of the current effort can be implemented immediately by WisDOT and other DOTs. The results can be used to formulate WisDOT design methodologies for these structures. Furthermore, the results can be used to establish rational inspection protocols for these structures. Completion of the recommended work recommended previously would solidify thinking, but it is expected that WisDOT can implement these recommendations today.

Chapter 1

Introduction

1.1 Problem Statement

The Wisconsin Department of Transportation (WisDOT) has experienced several instances of inadequate in-service performance of ancillary highway structures (*e.g.* sign supports and luminaire supports). WisDOT personnel have documented cases of: high-mast luminaire (HML) support failure; full-span overhead sign support structure (near) failure; Core-Ten luminaire support mast through-thickness corrosion; and many, many instances of cracking found in the members comprising sign support structures. Inadequate in-service performance of these structures is not limited to WisDOT. In fact, as recently as November 2003, there was a collapse of a high-mast luminaire support structure in Iowa. Dexter and Ricker (2002) have documented instances of cracking and excessive vibration in these and traffic signal support structures throughout the United States.

The majority of performance issues related to these structures have been reported as loose anchor rods (HML and sign support structures); cracking in truss structures composed of round structural steel HSS members with welded connections; cracking in truss structures composed of round aluminum pipe members with welded connections; cracking at the base of HML masts; and even instances of collapse of cantilevered sign, HML, and low-rise luminaire support structures. Cracking has been specifically reported as fatigue cracking even though a probabilistic evaluation of wind loading and fatigue detail strengths for these structures has yet to occur. The determination that cracking was a result of fatigue has been nearly anecdotal.

The causes of the perceived fatigue cracking in these structures have been attributed to: (a) truck-induced wind pressures; (b) vortex-shedding induced vibration; (c) galloping-induced vibration; and (d) natural wind turbulence. NCHRP research efforts have focused on cantilevered highway sign support structures, traffic signal support structures, and low luminaire support structures. There has been very little (if any) research efforts devoted to the structural analysis and fatigue-related performance of high-mast luminaire support structures and full-span structures supporting Type 1 (aluminum) and variable message signs (VMS). Furthermore, there has been very little analytical work geared toward quantifying the reasons for the cracking seen in these ancillary structures to justify the assertions that the cracking is indeed related to fatigue, truck-induced pressures, aeroelastic wind phenomena, or natural wind turbulence.

1.2 Project Background and Research Objectives

The Wisconsin Department of Transportation has always taken a pro-active role in seeking solutions to the problems related to inadequate in-service performance of highway structures. The motivation for the present study stemmed from the collapse of several luminaire assembly support masts (both high- and low-) in the Milwaukee area, many instances of cracking in welded truss structures throughout the state, and the near collapse of a full-span sign support truss in Eau Claire, Wisconsin. Although an issue of national scope, the present study focused on cracking and poor in-service performance of ancillary highway structures within the state of Wisconsin.

WisDOT has seen its share of cracking and corrosion in ancillary structures. In 1998, there was an instance of a collapse of a (approximately) 40-foot tall luminaire assembly support mast (Core-Ten steel material) into IH 894 in West Allis, Wisconsin. This collapse initiated data collection and inspection of 474 of these luminaire support masts in the metro-Milwaukee area. The research conducted with these structures found that the majority had their bases founded within the "salt-spray area" of the roadway. The "salt-spray area" was defined to be the median strip between traffic lanes (opposing directions). The Core-Ten poles located in this region exhibited very high levels of corrosion resulting from a brine-laden snow pack being deposited during snow removal efforts and the continual spray of brine from the passing cars and trucks. The wall thickness of these support masts near the base were found to have lost 20% or more of their cross-section thickness. A similar experience with Core-Ten luminaire mast material was seen in Eau Claire, Wisconsin.

WisDOT also experienced a collapse of a high-mast luminaire support structure at the Zoo Interchange in Milwaukee, Wisconsin. This failure was attributed to loose anchor rod nuts exhibited by wear marks on the base plate in the anchor rod holes. Other than the failure of the anchor rod, the base of the mast (mast to base plate connection) appeared intact. WisDOT undertook inspection of several other high-mast luminaire support structures with specific goals being to determine the condition of the anchor rods and mast-to-base plate connection.

Perhaps the most disconcerting in-service performance failure that WisDOT has seen to date was the excessive vibration of a full-span sign support bridge in Eau Claire, Wisconsin. This structure was put into service in August 1996 and was removed from service in February 1997. An extensive inspection of the decommissioned structure revealed "numerous additional cracks in the vertical diagonals". Furthermore, "two additional transverse cracks in the bottom chord" were found (Fish 1997). This structure is quite interesting because its investigation included examination of the material microstructure and provided other very detailed discussions of the visual inspection undertaken.

A failure analysis was performed by an independent consultant. Visual inspection and scanning electron microscopy of the crack surfaces in each piece submitted indicated "…the majority of the prior crack surfaces in each piece are covered with a zinc-rich coating. This indicates that the cracks were present at the time the truss section was hot dip galvanized after welding." (Fish 1997). The cracking that was found was said to be initiated or caused by liquid metal embrittlement during the galvanizing process. This is known to be a very important phenomenon to the galvanizing industry (AGA 2000a,b; 2001). The investigation also suggested that the cracks, initially formed during the galvanizing process, resulted in a pre-cracked condition of the diagonals that promoted "fatigue crack propagation found in both samples" tested.

The findings of this investigation and the report for structure S-18-44 are very important to the present research investigation. First of all, the performance of this structure appears to be consistent and indicative of a large portion of the poor in-service performance of sign support structures seen across the United States. Secondly, the results of the failure investigation of this structure point to a "fabrication" problem rather than a "design" problem. Much of the research efforts in the last 5-7 years sponsored by the National Cooperative Highway Research Program (NCHRP) have focused on the "loading side" of the design equation. These research efforts have sought to develop conservative loading scenarios and fatigue detail category data that will result in sign, luminaire, and traffic signal support structures that have infinite design lives. These efforts have resulted in very complicated design provisions that may or may not solve the in-service performance problems. For example, the result of the failure investigation of S-18-44 seems to indicate a dichotomy. The in-service cracking has resulted from the fabrication and galvanizing process with subsequent propagation through transient loading, OR the in-service cracking is independent of the galvanizing process and is caused by the transient loading seen during the service life.

The first step in resolving the dichotomy is to understand and characterize the fatigue life expected for sign and luminaire support structures designed using current specifications and realistic loading expected during the service life. If the fatigue life estimates match well with service lives seen prior to crack formation, then one can state (with engineering "certainty") that the cracking seen in these structures is a result of transient in-service loading. However, if the fatigue life estimates are grossly different from those seen prior to cracking, then one can say (with engineering "certainty") that the cracking was present prior to service loading and fabrication is the issue that needs to be addressed with these structures.

The present effort is devoted to full-span overhead sign support structures (Type 1 and VMS) and high-mast luminaire support structures. Addressing the dichotomy that appears to exist between fabrication and service of these structures was the over-riding concern of the present research effort. Furthermore, the development of rationally-based inspection intervals for sign and luminaire support structures for economic dispersion of public monies earmarked for structure inspection, and minimization of disruption to the

motoring public were of the utmost importance to the effort. The objectives for the research can be outlined as follows.

1.) Develop realistic loading models for truck-induced gust pressures and natural turbulent wind that can be used as part of transient finite element analysis of sign and luminaire support structures.

2.) Thoroughly evaluate (analytically) the susceptibility of full-span sign and high-mast luminaire support structures to excessive vibration resulting from aeroelastic instability (*e.g.* vortex-shedding and galloping).

3.) Generate detailed finite element models capable of capturing all important phenomenological aspects to structure response for HML and sign support structures including; bending and axial stresses in the anchor rods; eccentric mass of VMS and catwalk supports on sign structures; uplift and suction pressures on catwalk and sign elements for full-span overhead structures from passing trucks; concentration of stress at the mast-to-base plate welded connections in HML structures; and bending of base plates for HML and sign support structures that include significant anchor rod stand off heights.

4.) Assemble statistical information needed to generate probabilistically-based loading scenarios suitable for generating fatigue life estimates for these structures.

5.) Gather and develop (as required) the necessary statistical information related to the fatigue performance of pertinent details needed to generate fatigue lives with levels of confidence.

6.) Develop a methodology for predicting fatigue life estimates for various levels of confidence and generate fatigue life estimates for sign and luminaire support structures for these confidence levels. These estimates can then be used to address the fabrication/design dichotomy as well as establish rational inspection protocols for these structures.

Through achievement of the objectives set out for this effort, the design of ancillary highway structures can be done in a rational manner resulting in greater economy in design and construction of these structures, greater economy in inspection of these structures, and minimized disruption to the motoring public through inspection intervals established using state-of-the-art analytical methods.

1.3 Organization of the Report

The report presents the results of analytical studies undertaken to achieve the objectives previously laid out. As mentioned previously, the analytical work is limited to full-span sign support structures and high-mast luminaire support structures. The NCHRP research efforts have undertaken significant study regarding

cantilevered sign support structures and traffic signal support structures. Therefore, these were not considered.

Chapter 2 contains a detailed synthesis of the currently available literature related to sign and luminaire support structures. A brief summary of current inspection procedures for these structures is provided and how they relate to development of inspection protocols. Several concerns with the galvanizing process are highlighted as well. Detailed discussion of damping used in the finite element models is provided. The chapter also includes derivation of an analytical loading model for truck-induced gust pressure that is consistent with experimental results. Analytical models for turbulent-wind pressure are also presented and discussed. A detailed study of wind speed probability, wind direction probability, and combined probabilities of wind speed and direction is also included in the chapter. The chapter includes a detailed discussion of the NCHRP and AASHTO procedures that can be used to generate fatigue-life estimates with defined levels of confidence as well as the results of an experimental effort conducted as part of the present research to generate statistical information describing the fatigue life variability of *ET* fatigue details (specifically, welded connections for round HSS members).

Chapter 3 presents and discusses the research findings related directly to the objectives outlined previously. The study related to full-span sign support structures is outlined first. The test group structures are described and a detailed discussion of the finite element modeling for these structures is then undertaken. Vibration characteristics for each of the three test group structures are discussed in detail. A detailed discussion of the aerodynamic damping assumed in the FEA is also provided as this can be a significant source of damping for the sign support structures. The response of the three test structures to truck-induced wind pressures is discussed as well as the impact of truck-induced gust pressure on the fatigue life of full-span sign support structures. An in-depth evaluation of the three test structures to aeroelastic instability is also provided. Fatigue life predictions for three confidence levels and a discussion of cumulative damage for various wind speeds for each sign support structure considered are provided. Detailed discussion of aeroelastic instability, stress computations, cumulative damage due to naturally turbulent wind, and fatigue life predictions for two luminaire support structures are also given in the chapter.

Chapter 4 provides conclusions related to the research study conducted and also provides recommendations for future research efforts.

This page intentionally left blank.

Chapter 2

Literature Synthesis and Background Research

2.1 Introduction

The large number of cantilevered and overhead sign support structures found along major highways across the country suggests that they are well-engineered structures void of any problems. However, these structures have suffered from performance problems, which have lead to great concerns for departments of transportation throughout the United States and Canada. Poor performance of these structures can be attributed to a complex loading scheme, the use of fatigue sensitive details, the quality of fabrication, and combinations thereof. While these structures are subjected to both static and dynamic loads, it is the dynamic component that more directly affects their fatigue performance. Transient loading components can arise from several sources (Kaczinski *et al.* 1998):

1.) The natural turbulence of wind as it flows over the earth's boundary layer.
2.) Gust pressures induced on the sign or support as trucks pass beneath the structure.
3.) Vortex shedding-induced vibrations, which are dependent upon the free-stream wind velocity and the geometry of the structure and supported sign.
4.) Galloping-induced vibrations, which result from the interaction of the structure's deformations with the free stream wind velocity component (*i.e.* change in the angle of attack with respect to the free stream velocity direction).

Quantifying the magnitudes of these transient wind loading components has been the focus of many research efforts undertaken in the last two decades.

Furthermore, there is a significant portion of typical sign support structures assembled using welded connections. Most of the connections commonly used can be characterized as category E, E', or ET details, which have constant amplitude fatigue limits (CAFL) as described in the standard specifications (AASHTO 2001). The susceptibility of details in these categories to fatigue-induced failure is evaluated by using corresponding stress-life (*S-N*) curves. These curves provide the current basis for fatigue performance predictions of structures that utilize these details. Accurate computation of stress ranges in these structures is required in order to make appropriate estimates of fatigue performance.

The purpose of this chapter is to provide a synthesis of former research efforts. This synthesis is important as it provides the background information needed to understand the direction taken in the present research effort. A portion of this chapter is also devoted to providing research results generated in

the present study used to establish a foundation for the sign support and high-mast luminaire support research to follow.

2.2 Synthesis of Past Research

Appendix B contains a full review of the research literature pertaining to sign-support structures and high-mast luminaire assembly support structures. This section is limited to a synthesis of the literature that resulted from this review.

It appears that the majority of research into sign and signal support structures has occurred in the past decade. Much of the research effort has been instigated from in-service failures of these structures. The following general conclusions can be drawn after reviewing the body of literature related to sign and luminaire support structures.

1. There is a well-documented body of knowledge regarding truck-induced gust pressures. Experimental results have provided relatively consistent estimates for the shape of truck-induced truck pulses as well as the magnitudes of the peak pressures. These values can be used to generate analytical simulations of truck-induced gust pressures to be used in subsequent finite element analysis.
2. No research efforts have been undertaken to assess the aerodynamic instability of full-span overhead sign support structures of truss-type configuration with VMS and traditional signs attached. The work of Irwin and Peeters (1980) attacked the problem for monotube sign supports, but the truss configuration has received little attention.
3. The body of research completed to date suggests that base plate flexibility should be included in analytical models for luminaire supports. One might argue that base plate flexibility should be included in all analytical models. Furthermore, anti-symmetric anchor bolt configurations may cause elevated stress levels in the mast wall. Addressing this in the fatigue life evaluation is important.
4. There is a general consensus in all research results and recommendations that natural wind turbulence, aerodynamic instability effects, and truck-induced gust pressures are important to assessing fatigue lives of ancillary highway structures.
5. Research has demonstrated that finite element analysis of these structures is capable of producing accurate analytical simulations of a structure's vibrational characteristics as well as structure response to loading.

6. Static methods of analysis are likely to overestimate the fatigue-life of sign support structures by a significant margin. This suggests that transient analysis is a better candidate for generating fatigue-life estimates.
7. There is significant concern that the aeroelastic phenomena of vortex-shedding and galloping are contributing to reduced fatigue lives of sign support structures and luminaire support masts.
8. There appears to be very little information and understanding of the behavior of high-mast luminaire support structures. These structures constitute a very large portion of the ancillary highway structures maintained by departments of transportation.
9. The latest thinking regarding sign and luminaire support structures contained in Dexter and Ricker (2002) should be included in any work conducted in the present study.
10. There is support in the Literature for developing analytical simulations of turbulent wind and predicting fatigue lives of complicated support structures.

One item should be discussed prior to closing this literature synthesis. It is unfortunate that the "galloping" and "vortex-shedding" discussion appears to remain an issue of confusion in the research literature. In simple terms, the aeroelastic phenomena of galloping requires that the angle of attack between the wind flow direction and the face of the bluff body presented to the wind stream suddenly change and "diving" or "lifting" instability results in self-perpetuating vibrations. If the angle of attack remains stationary relative to the bluff-body, galloping cannot occur. However, vortex-shedding induced vibrations can occur in situations where the bluff-body's orientation remains fixed relative to the wind stream. These situations occur in *both* circular HML masts and box-shaped variable message signs.

The first author has personally observed wind-induced vibrations in a cantilever VMS support structure (insert structure number here) during sustained 25-35 mph winds. The vibration of this structure *did not* include angle of attack change of either the monotube mast arm or the VMS box. There was simply a sustained vertical vibration of the VMS box and arm with 6-12 inch amplitude. The lack of angle of attack change suggests that vortex shedding is the aeroelastic phenomenon present in the response observed. The sustained vibration seen in the long-term monitoring of Johns and Dexter (1998b) also suggests that vortex shedding is present in the response. Ginal (2003) includes a detailed study of aeroelastic phenomena as related to full-span sign support structures. This report will highlight the findings of this work and can hopefully lead to reduced confusion regarding galloping as a loading source for VMS support structures.

There has also been some significant variability in the recommendations of vortex shedding as a loading consideration in the design of high-mast luminaire (HML) support structures. Dexter and Ricker

(2002) outline these concerns and it is recommended that vortex-shedding be included in the design of HML supports. This issue needs to be resolved as the design procedures for HML structures including vortex shedding are quite complicated and will result in reduced design economy for these structures.

2.3 Current Inspection Procedures

Dexter and Ricker (2002) outline commonly used inspection procedures and recommendations for inspection intervals for sign support and luminaire support structures. The inspection intervals recommended in this document are especially germane to the present effort. Luminaires and cantilevered sign support structures (mounted to the ground) should be inspected every 4 years (Dexter and Ricker 2002). Less frequent inspection intervals are recommended for luminaire supports "if they cannot fall in traffic lanes" (Dexter and Ricker 2002). It is also recommended that a "walk-through" of the sign bridge structure be performed rather than ground-based inspection. The Wisconsin DOT currently performs sign bridge inspections in this manner. It is also reported that inspection of anchor rods in Michigan is undertaken every two years.

A very useful description of inspection methods as well as inspection checklists is provided in Dexter and Ricker (2002). The Wisconsin Department of Transportation already follows many of the procedures recommended. The WisDOT procedures for luminaire and sign support structures have been heavily influenced by the work of Fish (1994, 1995) and have been proven to be effective in locating structures with in-service deficiencies. Dexter and Ricker (2002) also outline retrofit measures that can be taken when "problem structures" are found.

It is apparent that the inspection cycles outlined in the Literature are based on ad-hoc recommendations developed through experience and adaptation of the "fracture critical" inspection intervals recommended by AASHTO. It certainly appears that "rationally" established inspection intervals for sign and luminaire support structures are missing. A rational inspection interval can be developed if one understands the fatigue damage accumulated by a structure during its service life. For example, if one could be 95% confident that a structure installed without cracks would last 25 years, then a detailed inspection could take place at 25 years. One could certainly "hedge" a bit and establish an initial in-service inspection at 12 years and 25 years. Therefore, a rationally established inspection interval would result in 2 inspections rather than 12. Considering there are hundreds of these structures in the State, the economic impact from rational inspection intervals is non-trivial.

2.4 Concerns with Galvanizing Process

The fact that sign support and luminaire support structures are exposed to weather makes corrosion resistance of paramount importance. There has been progress made in corrosion prevention methods over the last 30 years in Wisconsin. Initially steel support structures exposed to environmental degradation were painted with coatings that have been affectionately referred to as "red-lead" paint. This coating was eventually replaced by galvanizing and "weathering steels".

Examination of the database of sign support structures in Wisconsin reveals that the majority of those with crack monitoring or repairs is Aluminum or has been erected since 1985. In fact, there appears to be a rash of in-service cracks found in structures erected in Milwaukee County in 1995. This evidence tends to suggest that there may be forces at work causing cracks in sign support and luminaire support structures other than natural wind turbulence, vortex-shedding, and truck-induced gusts.

Galvanizing structural steel components has long been known to be an effective mechanism for preventing corrosion. However, the process is also known to develop significant residual stresses in, and distortion of, the components being galvanized (AGA 2000a,b, 2001; Bigot and Iost 1999; Cresdee *et al.* 1993). Considering the galvanizing bath is typically maintained at 894 degrees Fahrenheit, the process of "double-dipping" sign support truss structures is certainly capable of inducing significant thermal gradient through the structure. Although the impact of double dipping of a truss-type component of a full-span sign support structure remains to be quantified, subjecting a fully-welded structure to significant thermal gradient along portions of its length is potentially detrimental to the structure.

Liquid metal embrittlement is another very sinister possibility with galvanizing. This is thought to be the source of poor in-service performance and eventual decommissioning of a sign support structure in Wisconsin (Fish 1997b). Embrittlement of galvanized steel is said to be very rare (AGA 2001). However, there is a caveat to this statement that mentions embrittlement is "usually the result of using high-strength steel" (AGA 2001). It is interesting to note that sign support structures are usually composed of ASTM A53 or A500 round HSS shapes. If A500 steel is provided, these have yield strengths on the order of 40-50 ksi and could be classified as high-strength steel. Experimental testing done as part of the present study showed round HSS shapes composed of materials with yield stress magnitudes on the order of 55 ksi. One could argue that this is high-strength steel. Personal communications (Engtsrom 2003; Fisher 2003) have also suggested that the galvanizing process itself may be causing cracking in fabricated structures prior to erection.

If steel embrittlement resulting from the galvanizing process is a cause of cracks that are not detected prior to erection of the structure, it is likely that the cracks found in many sign support structures

are caused by the fabrication process rather than fatigue-induced failures from vortex shedding, galloping, truck-induced gust pressure, and natural wind turbulence. It is of paramount importance to generate rational predictions of fatigue lives of these structures to determine if the galvanizing process is a culprit causing severe revisions to the design methodologies for these structures.

2.5 Damping Model for Sign Support Structures

Damping is a dynamic characteristic that is usually measured experimentally. However, this study has relied upon experimental field measurements of damping ratios from previous research efforts in order to approximate the damping ratio of full-span sign support structures. Table 2.1 is a brief summary highlighting some past research efforts and measurements of damping ratio.

The range of damping ratios for each cantilevered sign support structure given in Table 2.1 was determined by measuring damping in 1 or 2 vibration modes. Generally, the two modes considered were a vertical "hatchet" mode and an out-of-plane "twisting" mode. In all cases the "twisting" mode produced a higher damping ratio. This is expected because the damping measured in each study was "total" damping, which includes both inherent structural and aerodynamic damping components. The "twisting" mode involves "pushing" the supported sign/signal through the air, which can generate a significant aerodynamic damping component. Damping ratios from this mode make up the high-end of the range of damping ratios listed in the Table.

Table 2.1: Summary of Past Research Efforts Measuring Damping Ratios for Cantilevered Sign and Signal Support Structures.

Research Effort	Structure Description	Sign Type	Damping Ratio (% of Critical)
Creamer, *et al* (1979)	Four chord cantilevered pipe truss supported by monotube upright	Type I	0.40 – 1.11
Gilani, *et al* (1997)	Monotube cantilevered mast arm and vertical support	VMS	0.50 – 0.70
Johns and Dexter (1998)	Two-chord cantilevered pipe truss supported by monotube upright	VMS	0.25 – 0.57
South (1994)	Tapered cantilevered monotube mast-arm and upright traffic signal support	NA	0.60
Edwards and Bingham (1984)	Two- and four-chord cantilevered pipe truss supported by monotube upright	Type I	0.58 – 1.85
Kaczinski, *et al* (1998)	Cantilevered sign and signal support structures of varying configurations	Type I	0.12 – 0.62

Many of the sign support structures listed in Table 2.1 were constructed using welded HSS connections. This is advantageous because the structures evaluated in the present study utilize the same connection configurations and therefore, similar levels of damping could be expected. The "target" damping ratio used in the present study was determined by taking an average of the low-end damping ratios of the six experimentally measured values listed in Table 2.1. This low-end average value (0.40 % of critical) was selected to represent the *inherent structural damping* present in the structures.

Ginal (2003) presented a detailed derivation of aerodynamic damping for the single degree of freedom oscillator. The aerodynamic damping ratio (as a percentage of the critical damping ratio) is computed using,

$$\zeta_a = \frac{\rho C_d A \bar{U}}{2\sqrt{mk}} \tag{2.1}$$

where: ρ is the density of the air; C_d is the drag coefficient for the sign; A is the projected area of the sign; $\bar{U}$ is the mean wind speed; m and k is the mass and stiffness of the SDOF oscillator. Equation (2.1) indicates that each and every mean wind speed considered in an analysis will have a corresponding aerodynamic damping ratio. Furthermore, this ratio will have to be based upon an equivalent SDOF oscillator model for the sign support structure.

The total damping is therefore composed of two components: (a) inherent structural damping; and (b) aerodynamic damping. Mathematically, the total damping *ratio*, ζ_{total}, can be written as,

$$\zeta_{total} = \zeta_s + \zeta_a \tag{2.2}$$

Equation (2.1) demands that any structure to be modeled can be represented as an SDOF oscillator with appropriate mass and stiffness. This aspect to the analytical model is discussed in Chapter 3 of the report when individual structures are discussed.

2.6 Analytical Truck-Induced Pressure Pulse

Over the past ten years, a truck-induced pressure pulse has become a necessary loading scenario for the design of overhead sign support structures. The heightened sense of awareness regarding this type of loading is partially attributed to the increasing use of Variable Message Signs (VMS) by numerous state Departments of Transportation (DOTs).

The VMS has a relatively large surface area both perpendicular and parallel to the flow of traffic when compared to the traditional light gauge Type I aluminum printed signs. The surface area of the VMS parallel to the flow of traffic (*i.e.* "soffit") is subjected to a pressure pulse and/or suction from each passing truck. This "push-pull" excitation of the supporting structure, caused by high-volume truck

traffic, could potentially coincide with a natural frequency and mode shape of the sign support structure and possibly create a resonant condition. Truck-induced oscillations have been blamed for the sudden failure of at least one cantilevered sign structure that supported a VMS (DeSantis and Haig 1996). While researchers agree that overhead sign support structures are subjected to truck-induced pressure pulses, the magnitude, duration, and shape of this pulse are varied.

This section consists of the present study's attempt to synthesize a typical truck-induced pressure pulse based on field measurements from previous research efforts. The present study utilized pressure versus time plots for 23 random truck "events," which were recorded as part of the experimental work and field measurements conducted by Cook *et al.* (1996). A brief overview of field measurements made by this and other research endeavors is provided. The formulation of the typical truck pulse is then discussed, which includes using a Fourier analysis to evaluate the frequency content and pressure magnitudes of the pulses from the 23 random truck "events."

A number of past research efforts have published field measurements of truck-induced pressure pulses. While it is generally accepted that a truck-induced pressure pulse is a triangular impulse loading, not all studies agree on the time duration and peak magnitude of this pulse, how the pressure varies with elevation, and the existence of a suction component. This section gives a brief overview of field measurements from past research endeavors and the methods by which these measurements were recorded. From this discussion, field measurements are extracted and used to develop a typical truck pulse that is representative of this type of loading.

Since the breakthrough work of Creamer *et al.* (1979) regarding the formulation of a loading function for truck-induced pressures, many other research efforts have also performed field measurements of truck pulses in order to quantify this loading scenario. Table 2.2 is a brief summary of the field measurements recorded by some of these endeavors. From Table 2.2 it appears that past research efforts have resulted in similar values for the peak dynamic pressure of a truck pulse.

The former research also suggests that the pressure pulse from trucks passing beneath a sign should include both a pressure and suction component. Based upon the relatively consistent pressure magnitudes contained in Table 2.2 and the detailed results of multiple truck test data the research team decided to use the work of Cook *et al.* (1996) as the basis for developing an analytical truck-induced wind pressure.

A Fourier analysis was performed on each of the 23 random truck "events" recorded by Cook *et al.* (1996). This analysis was used to evaluate the frequency components of each measured truck "event." In order to perform a Fourier analysis on the measured truck-induced pressure pulses, the recorded time

versus pressure plots needed to be represented as continuous repeating functions. This was achieved by first fitting each plot with a linear piecewise function. Figure 2.1 illustrates the linear model concept.

Table 2.2: Summary of Field-Measurements for Truck-Induced Pressure Pulses

Researcher	Technique	Peak Pressure
Creamer *et al.* (1979)	Recorded member strains for various truck "events" and back-calculated an equivalent *dynamic* loading function	1.23 psf
Johns and Dexter (1998b)	Recorded member strains for various truck "events" and back-calculated an equivalent *static* pressure	1.2 – 2.4 psf (1)
Edwards and Bingham (1984)	Recorded wind speed from truck "events" and used Bernoulli's Equation to calculate *dynamic* pressure	1.41 psf
Cook *et al.* (1996)	Recorded pressure versus time for various truck "events" and synthesized *dynamic* design pressures	0.92 to 1.43 psf

Notes:
(1) The literature review included a modification of the back-calculated pressure of 11 psf provided in Johns and Dexter (1998b). The response measured for the three test trucks (Figure B.8) suggests the magnitudes listed in the Table.

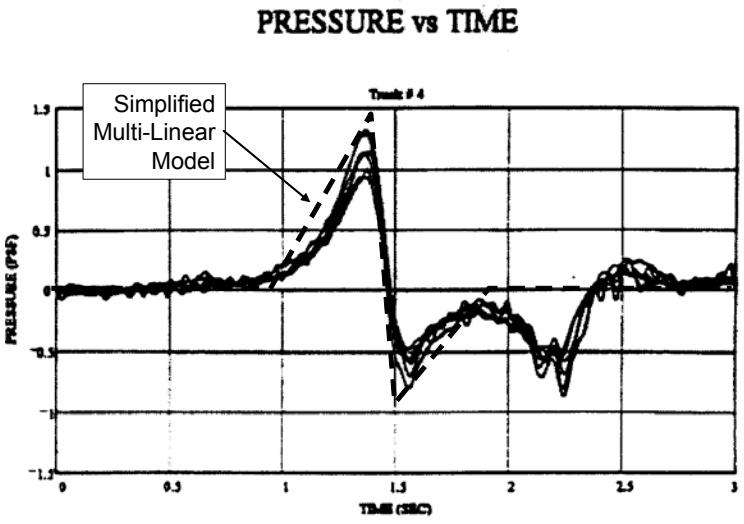

Figure 2.1: Typical Plot of Pressure versus Time for Simplified Impulse Function Superimposed on Pressure Pulse Measured by (Cook *et al.* 1996).

The peaks for each pulse were set so that they would envelope the maximum positive and negative pressure readings from the seven pressure transducers. The fitted pulse duration (*i.e.* period, T) was determined by using both the general trend of the recorded pressure as well as utilizing the truck's picture

and recorded speed to determine how long the truck would take to pass beneath the testing apparatus. The simplified impulse functions used in the ensuing Fourier analysis are believed to be well representative of the actual in-service conditions.

Ginal (2003) linearized each truck event measured by Cook *et al.* (1996) and developed Fourier series representations with ten Fourier coefficients to study the frequency content of the truck pulses. Fourier spectra were then created for all 23 truck pressure-pulse events and utilized to generate a single spectrum, which could be used to develop a single characteristic truck pulse that captured the frequency content of all measured events. This combined spectrum (shown in Figure 2.2) reinforces the notion that the higher harmonic frequencies (*i.e.* n > 3 and $f > 2$ Hz) contribute very little to the truck impulse function, $p(t)$. This is expected since the plot of the *typical* truck pulse is quite similar to that of a sine function, and therefore, the function can be expressed accurately using a relatively small number of sine and cosine terms. From the above combined spectrum there is evidence of some variability among the individual truck pulses with respect to the contribution of the corresponding lower harmonic frequencies. The range of pulse durations and positive and negative peak pulse magnitudes of the individual truck pulses generated this variability.

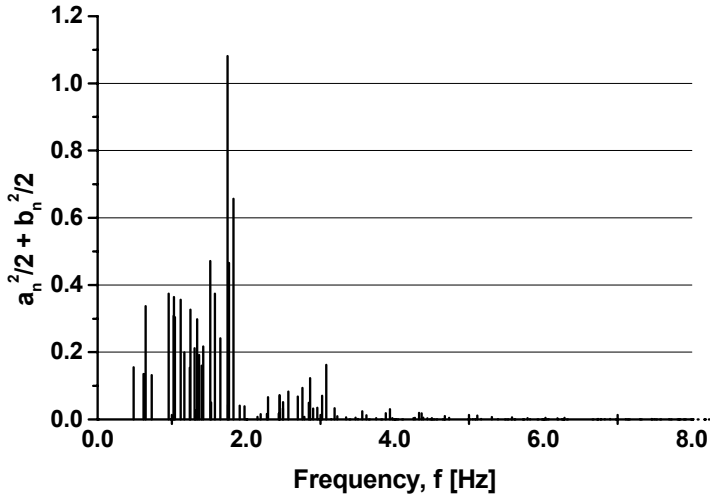

Figure 2.2: Combined Frequency Spectrum of Truck Impulse Functions (Ginal 2003).

The harmonic frequencies and the corresponding spectral values or frequency contributions of each linearized pulse represented in the combined spectrum were averaged in order to create the *typical* truck pulse spectrum. Three frequency components were used in the Fourier representations and therefore, the Fourier representation was nonlinear (Figure 2.3). The nonlinear Fourier representation was enveloped with a linear representation (Figure 2.3) with the following characteristics:

$p(t = 0) = 0$ *psf*

$p(t = 0.35) = 1.0 \;\; psf$

$p(t = 0.57) = -1.0 \;\; psf$

$p(t = 0.82) = 0 \;\; psf$

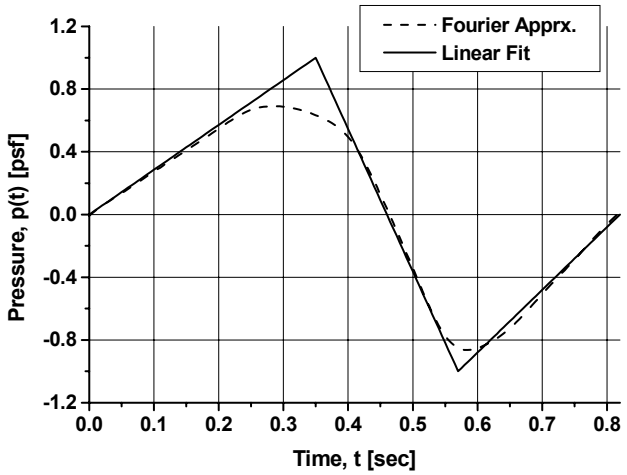

Figure 2.3: *Typical* Truck Pulse Fourier Approximation and Linear Fit (Ginal 2003).

The most important characteristics of the *typical* truck pulse loading function are the location and duration of its peak pressure magnitudes and its period. These characteristics should be representative of the field measured truck pulses. This was checked visually through superimposing the *typical* truck pulse loading function onto a plot of a selective group of the measured truck pulses. This plot is illustrated in Figure 2.4.

The *typical* truck pulse, generated using the average frequency spectrum, does a good job of representing the measured truck pulses. The peak pressure magnitudes are a good average of the measured values and the period and overall shape of the *typical* truck pulse capture the general trend of the measured data. From these observations it was confirmed that the *typical* truck pulse loading function developed is a good representation of the pressure magnitudes and frequency content of an actual truck-induced pressure pulse.

The correct application of this load to the analytical models can be somewhat confusing without a visual picture of the actual directions recorded by the pressure transducers. It is obvious from the recorded pressure pulses that an upward pressure is applied to horizontal surfaces of the structure (*e.g.* catwalk/light assemblages and VMS "soffit") as the truck starts to pass beneath. As the end of the truck passes beneath the structure, this pressure acts downward and becomes a suction type load. The direction of the pressure applied to the vertical surfaces during the pulse is less obvious. When the truck first starts to pass beneath the structure it exerts a pressure in the direction of traffic on the front vertical surfaces

(*e.g.* the sign face). Then as the end of the truck passes beneath the structure, the airflow around the truck creates a pressure loading on the back vertical surfaces in the direction opposite the flow of traffic. These directionalities are illustrated qualitatively in Figure 2.5.

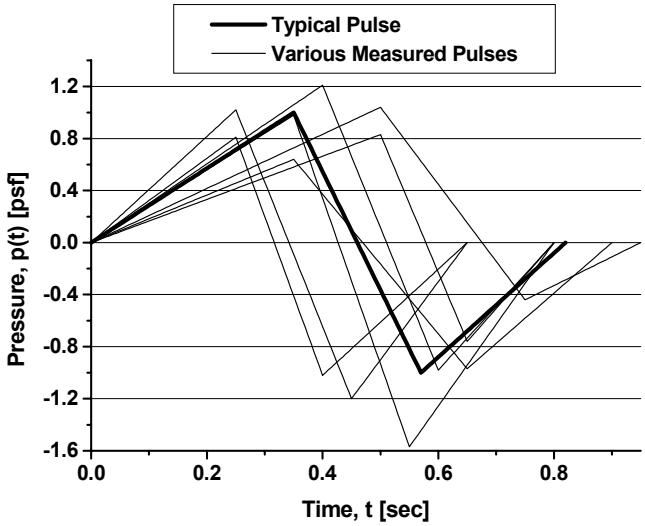

Figure 2.4: Comparison *Typical* Truck Pulse to Field Measured Truck Pulses (Ginal 2003).

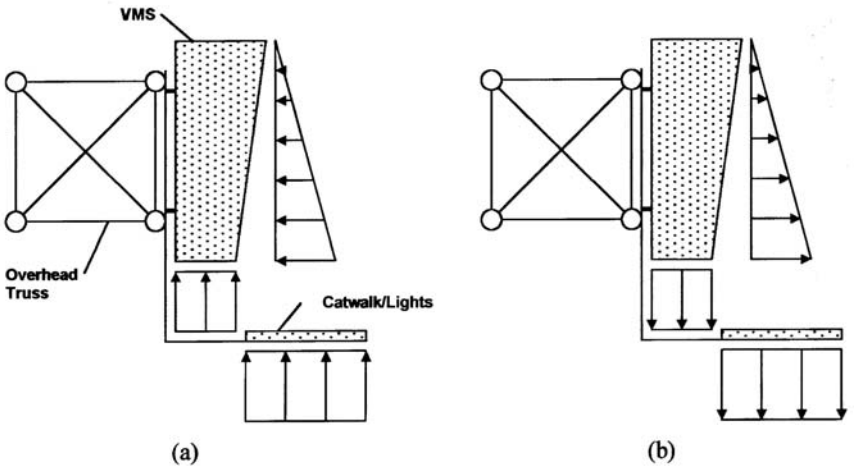

Figure 2.5: Direction of Truck-Induced Pressure Applied to VMS and Catwalk: (a) Positive Pressure; and (b) Negative Pressure (Ginal 2003).

Experimental work by Cook *et al.* (1996) found that truck-induced pressures vary linearly with elevation above the roadway surface. A parametric study performed by Cook *et al.* (1996) established, on average, a 10 % reduction in pressure magnitude for every one-foot increase in elevation of the supported sign and catwalk components above a reference height. The pressure magnitudes of the *typical* truck pulse developed in the previous section were established for a height of 17 feet above the roadway surface. Therefore, the pressure magnitudes used for each analytical model were modified accordingly in

order to account for the elevations of the structure's sign and catwalk elements above this reference height. Appendix A includes the elevations of the sign and catwalk components for each structure. Utilizing the pressure versus elevation relationship, all horizontal surfaces (*i.e.* VMS "soffit" and/or catwalk) were loaded with a uniform pressure/suction while all vertical surfaces (*i.e.* sign face) were loaded with a linearly varying pressure (refer to Figure 2.5). It should also be noted that the uniform pressures applied to the catwalk components were reduced to account for the void ratio of the grating.

2.7 Analytical Simulation of Turbulent-Wind

Natural wind velocity has been characterized as having two components: (a) mean speed; and (b) fluctuating component that represents turbulence. Mathematically, these can be expressed as (Buchholdt 1997),

$$U(z,t) = U(z) + u(z,t) \tag{2.3}$$

where: $U(z)$ is the mean wind velocity component, which varies with height z above the surface; and $u(z,t)$ is the fluctuating turbulent component that varies with both height z and time t.

In general, a constant height can be established for both velocity components in equation (2.3), and therefore, the spatial variability implied in this expression can be removed. This results in the following:

$$U_z(t) = \bar{U}_z + u_z(t) \tag{2.4}$$

where: $\bar{U}_z$ is the mean wind speed (constant value) at a height z above the ground; and $u_z(t)$ is the turbulent component (transient) at a height z above the ground (to be discussed).

The mean wind speed component defined in equation (2.4) has well-developed models (*e.g.* the power law) for generating mean wind speeds that vary with height. Furthermore, wind recording stations (*i.e.* NCDC ASOS sites) provide contiguous records of mean wind speeds that can be used to create statistical models for the mean wind speed component. The turbulent component of wind is *not* measured at ASOS sites. In fact, by design, the wind records have *averaged and removed* the turbulent component using the *averaging time* concept. Therefore, the turbulent component of the transient wind speed must be *simulated*. This section of the Report describes how transient wind-speed records are generated using equation (2.4).

2.7.1 Mean Wind Speed Component

Two empirical relationships are commonly used to describe the variation of mean wind speed with elevation above the Earth's surface within the *atmospheric boundary layer*: (a) the *Logarithmic Law*; and (b) the *Power Law*. The *Logarithmic Law* is considered slightly more accurate for larger heights (Simiu

and Scanlon 1996), but is also more difficult to use. However, both the *Logarithmic Law* and the *Power Law* produce similar profiles at the heights of the sign and luminaire support structures presently considered. Therefore, the *Power Law* was used in the present study to model mean wind speed with height.

Using the *Power Law*, the speed at any height above the ground can be determined using the following expression (Liu 1991; Simiu and Scanlon 1996),

$$\bar{U}_z = \bar{U}_{ref}\left(\frac{z}{z_{ref}}\right)^{\alpha} \tag{2.5}$$

where: $\bar{U}_z$ is the desired mean wind speed at a height z above the ground; and $\bar{U}_{ref}$ is a reference wind velocity measured at a reference height, z_{ref}, above the ground.

The power-law exponent, α, attempts to consider boundary layer roughness in the variation of wind speed with height. In general, smooth terrain (*e.g.* open water) has a smaller value of α than rough terrain (*e.g.* urban terrain). The reference height, z_{ref}, used to define the mean wind speed was taken to be 33 feet. The height above the ground will depend upon whether a sign support structure or high-mast luminaire support tower is being considered. Open terrain was assumed for all structures considered, and therefore, $\alpha = 0.15$.

2.7.2 Turbulent Wind Speed Component

The turbulent component of wind can be considered a random variable that is a function of a number of parameters, one of which is time. The transient variation of turbulent wind is necessary for quantifying the dynamic response of structures subjected to natural wind gusts. However, in order to simulate turbulent wind using a straightforward analysis, wind must be considered a stationary ergodic random variable. Without this assumption simulating wind for general engineering purposes becomes intractable.

Figure 2.6 illustrates a typical wind speed record. It should be noted that the mean wind speed U in the figure corresponds to the mean wind speed component in equations (2.4) and (2.5), and the turbulent wind speed component, u, corresponds to the turbulent component in equation (2.4). The time over which turbulent wind is averaged for recording purposes called the averaging time, T. As one can see, a wind speed record given by equation (2.4) will be turbulent over T and the turbulent component of the wind speed, $u_z(t)$, contains many frequencies, and, as implied in the symbol for this component, it will vary with height. There have been many frequency spectrum models proposed for turbulent wind.

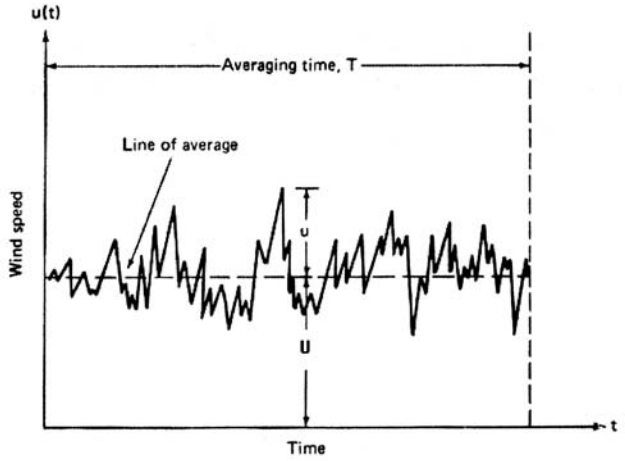

Figure 2.6: Variation in Wind Speed with Time (Liu 1991).

The "classical" model of the wind turbulence spectrum is attributed to Davenport (1961a, b). Several modifications have been made to the Davenport model. The present study utilizes the modified wind turbulence spectrum proposed by Kaimal (1972). Using this model, the spectral density of the turbulent wind component is approximated by,

$$S_K(f) = \frac{200 \cdot U_*^2 \cdot z}{\bar{U}_z \left(1 + 50 f z / \bar{U}_z\right)^{5/3}} \tag{2.6}$$

where: $\bar{U}_z$ is the desired mean wind speed at a height, z, above the ground surface; f is the frequency (Hz); and U_* is the friction or shear velocity, which accounts for wind speed turbulence. The desired mean wind speed is determined using equation (2.5). The Kaimal spectrum includes the effect of height on the turbulent wind component, and it has been found to be quite accurate in the higher frequency range for which most engineered structures respond (Simiu and Scanlon 1996). For these reasons the power spectral density function given by equation (2.6) was used to simulate turbulent wind speed records for the time history analyses of the test group structures.

Random time histories of turbulent wind can be simulated using a variety of techniques. The techniques frequently used involve generation of the zero mean random turbulent component of wind using a predetermined *target* spectrum. The *target* spectrum ensures that the simulated wind records have frequency content comparable to measured wind. One approach commonly used to generate histories that fit a *target* spectrum is to generate the turbulent component of wind using summations of sine functions (Irvine 1999) or cosine functions (Shinozuka and Jan 1972). Presently, wind simulation can be accomplished for records of moderate length through summation of cosine functions of varying frequencies and a randomly generated phase angle. The following discussion is a brief overview of this

technique and the process used to validate the resulting simulations of the turbulent component of natural wind.

As mentioned previously, the power spectral density function of naturally occurring wind given by equation (2.6) was used in the present study as the target spectrum for the simulated wind histories. These histories were developed using superimposed cosine waves of various frequencies and randomly generated phase angles. The random turbulent wind speed component of these histories was simulated using (Iannuzzi and Spinelli 1987; Levy 1996; Shinozuka and Jan 1972),

$$u_z(t) = \sum_{k=1}^{N} \sqrt{2 \cdot S_K(f_K)\Delta f} \cdot \cos\left(2\pi f + \phi_K\right) \tag{2.7}$$

where,

$$f_K = k \cdot \Delta f$$

and N is the number of frequencies for which the given spectrum, $S_K(f_K)$, has been evaluated for specific frequencies, f_K; Δf is the frequency increment assumed; and t is the time value in the simulation. The randomly generated phase angle, ϕ_K, is a Gaussian random number distributed uniformly between 0 and 2π which is chosen for each central frequency, f_K. Equation (2.7) has been evaluated by Iannuzzi and Spinelli (1987), and it has been found to generate accurate wind histories when compared to measured wind records.

Simulating wind histories requires the spectrum be defined at frequencies beyond excitable frequencies found in the structures. Therefore, an upper-limit frequency of 100 *Hz* and a lower-limit frequency of 0.1 *Hz* were used. These limits were set in order to ensure the simulation followed the *target* spectrum over the excitable frequency ranges of the sign support structures being studied, and to ensure a good representation of the frequency content of natural wind. The length of the simulated wind record is dependent upon computation power and available statistical data of measured wind velocities. With the improvement in analytical tools in recent years, computation power is rarely an issue. However, statistics of measured wind velocities are crucial to accurate fatigue life predictions.

A "sample" turbulent wind simulation was developed with a 5-second *averaging time* in order to validate the simulation algorithm. The parameters for this simulation were set to values similar to those used to develop the simulations for the analytical study. Equation (2.7) was utilized to develop the random turbulent wind speed component of this simulation. As mentioned previously, a frequency range from 0.1 *Hz* to 100 *Hz* was used. The frequency increment was set at 0.01 *Hz*. The spectrum given by equation (2.6) was established as the *target* spectrum for the simulation. A reference height of $z_{ref} = 33$

feet and a simulation height of $z = 27$ feet were also used. The friction velocity was defined as (Buchholdt 1997),

$$U_* = \sqrt{\frac{\sigma_u^2}{6}} \tag{2.8}$$

where the variance of the turbulent wind component, σ_u^2, was taken as (Levy 1996),

$$\sigma_u^2 = 6 \cdot K \cdot \bar{U}_{ref} \tag{2.9}$$

The surface drag coefficient, *K*, was set at 0.005, which corresponds to open terrain. The mean wind speed, $\bar{U}_{ref}$, was set at 30 mph and the mean wind speed at the simulation height was then determined using equation (2.5) with $\alpha = 1/7$ for open terrain. The resulting simulated wind record, including the adjusted mean wind speed, is given in Figure 2.7.

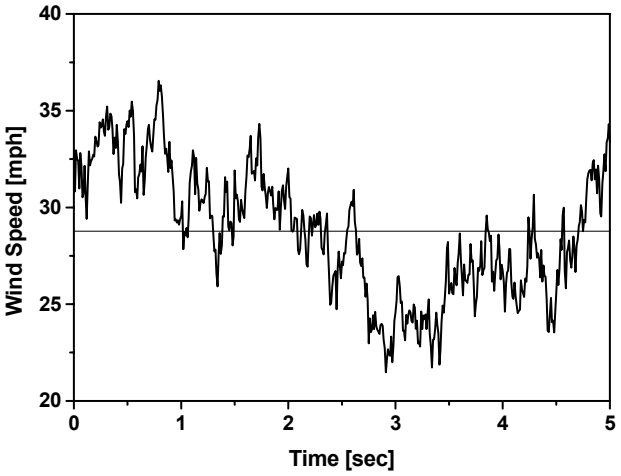

Figure 2.7: Simulated Wind History including Mean Wind Speed (Ginal 2003).

The simulated wind speed record shown in Figure 2.7 was evaluated with respect to its frequency content by computing the power spectral density (PSD) for the signal and comparing it with the target spectrum. Figure 2.8 illustrates the comparison of the PSD for the simulated record shown in Figure 2.7 and the target spectrum given by equation (2.6).

In order for a simulated spectrum to more closely follow the *target* spectrum, multiple wind histories need to be considered. To illustrate this, ten simulated wind records were generated using the same parameters discussed previously. The power spectral density function was then computed for each simulation. At each frequency the values of each spectra were averaged. This averaged spectrum was then compared with the original spectrum. The comparison of these two spectra is given in Figure 2.9.

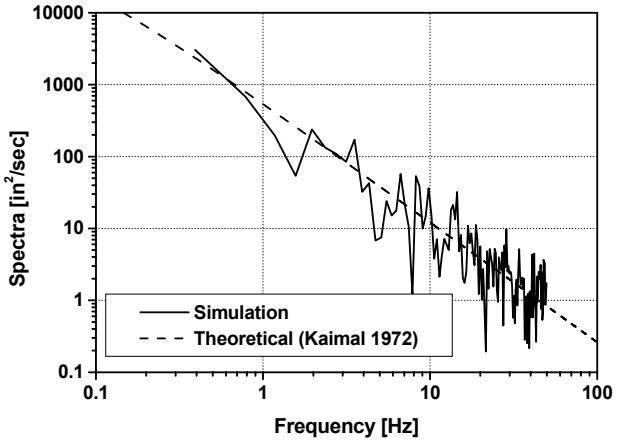

Figure 2.8: Comparison of Target Kaimal Spectrum and Spectrum Obtained Using Simulated Wind History (Ginal 2003).

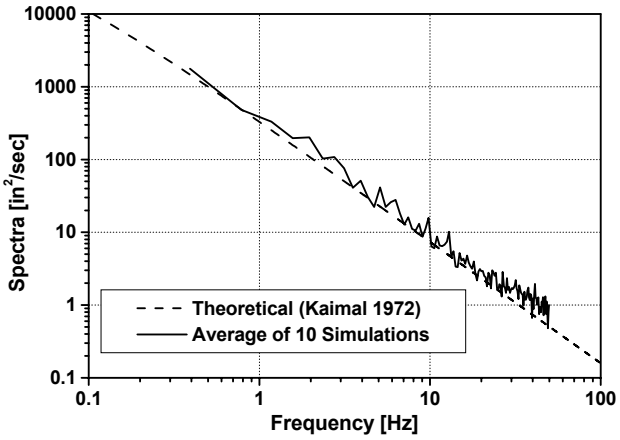

Figure 2.9: Comparison of Target Kaimal Spectrum and Averaged Spectrum Obtained Using 10 Simulated Wind Histories (Ginal 2003).

The plot in Figure 2.9 illustrates that the averaging of 10 simulations resulted in a closer representation of the original spectrum. However, it may take upwards of 100 simulations in order for the averaged spectrum to fall exactly on the *target* spectrum. Nonetheless, the plots illustrated in Figures 2.8 and 2.9 demonstrate that the simulation algorithm is accurately capturing the frequency content of natural wind in the resulting simulations.

The "random process" contained in the simulation algorithm (*i.e.* turbulent wind speed component) also required validation to ensure that the magnitude of the turbulent component of the simulated wind record followed a Gaussian frequency distribution about the mean wind speed. The original "sample" simulation was checked using a frequency count histogram of the turbulent wind speed magnitude. This

histogram is shown in Figure 2.10 and it illustrates that the simulated wind speed certainly varies about the mean speed of 30 mph in the form of a Gaussian (normal) distribution.

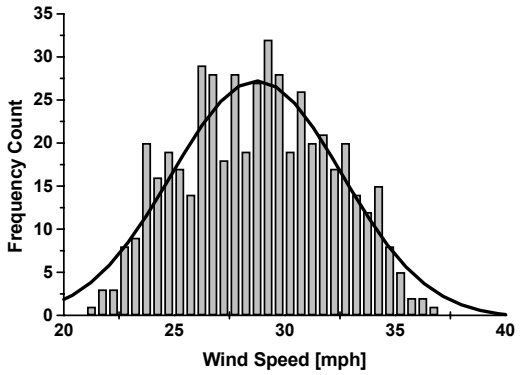

Figure 2.10: Comparison of Turbulent Wind Speed Histogram for Simulated Wind Record with "Best-Fit" Gaussian Distribution (Ginal 2003).

2.8 Natural Wind-Speed Statistics

Wind speed and direction data is recorded continuously at numerous Automated Surface Observing System (ASOS) stations throughout Wisconsin. The National Weather Service (NWS) and the Federal Aviation Administration (FAA) maintain these ASOS stations. This wind speed and direction data is accessible through the National Climatic Data Center (NCDC) website. Discussions of this data and how it was utilized to develop combined probabilities for use in the following fatigue analysis are the focus of this subsection.

Wind data used in the present study was taken from the ASOS station located at Milwaukee County's Mitchell International Airport. The data utilized in the present study consists of daily peak mean wind speed and corresponding direction readings as well as mean wind speed and corresponding direction readings recorded hourly. Wind recording stations do not report instantaneous wind speeds, but report mean wind speeds averaged over differing time intervals (*i.e.* averaging times). Typical time intervals for averaging wind speeds are 5 seconds and 2 minutes. Wind speeds averaged over these two time intervals are conveniently referred to as 5-second and 2-minute wind speeds. Generally, as the averaging time is increased, the mean wind speed over that time period is reduced.

Sometimes it is necessary to compare mean wind speeds that have been averaged over different time intervals. In order to do this, the mean wind speeds must be modified to reflect a consistent *averaging time*. It is often convenient to use an hourly mean wind speed (*averaging time* is 1 hour) to convert mean wind speeds. Wind loading standards (ASCE 1998) utilize the curve proposed by Durst (1960) for smooth terrain depicted in Figure 2.11 to convert wind speeds to different averaging times.

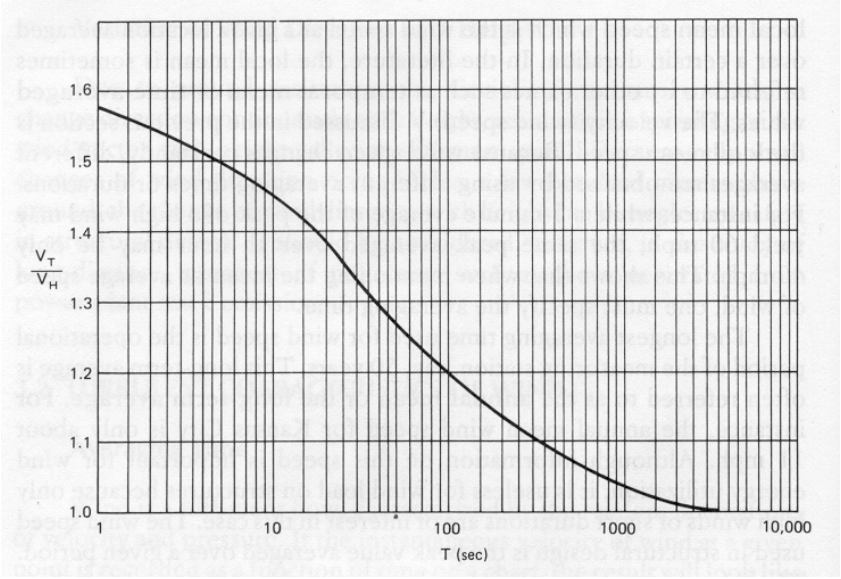

Figure 2.11: Wind Speed Variation with Averaging Time (Liu 1991).

The wind data gathered from the ASOS station located at Mitchell International Airport consisted of daily *peak* mean wind speed and corresponding direction readings and also mean wind speed and corresponding direction readings that were recorded hourly. The data used in the present study was collected from July 1996 to November 2001. The daily *peak* mean wind speed readings were recorded with both a 5-second and a 2-minute averaging times, and the hourly readings were all recorded based on a 2-minute averaging time. All mean wind speed data values were converted to a 5-second averaging time using the Durst curve (Figure 2.11). Mean wind speeds with a 5-second averaging time will be higher than mean wind speeds averaged over longer time intervals.

Histograms were developed for both the mean wind speed data and the direction data. The histogram plot for the mean wind speed data is illustrated in Figure 2.12, and the histogram plot for the corresponding direction data is illustrated in Figure 2.13. The mean wind speed histogram (Fig. 2.12) was developed using a bin size of 1.5 mph. Frequency data for the wind directionality histogram was established with a bin size of 10 degrees. It should be noted that in the wind directionality histogram, 0 degrees corresponds to winds out of the North. Over 56,000 wind speed and direction readings were used to develop these histograms. This relatively large sample of data is more than adequate to establish yearly wind speed and direction trends for Milwaukee.

The histograms, illustrated in Figure 2.12 and Figure 2.13, represent the probability of occurrence for both mean wind speed and wind direction, respectively. The wind data used to construct these histogram plots was also used to develop mean wind speed and wind direction combined probabilities. A discussion of how these combined probabilities were developed follows.

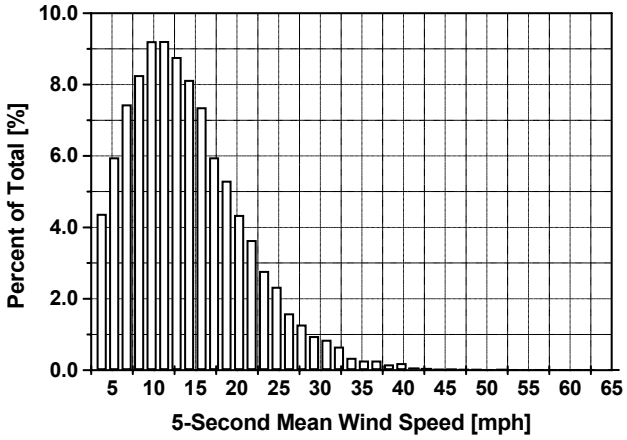

Figure 2.12: Histogram of 5-Second Mean Wind Speed Data Recorded at Mitchell International Airport from July 1996 to November 2001 (Ginal 2003).

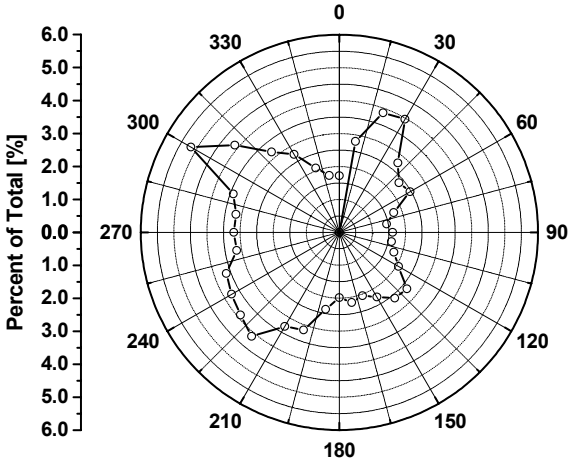

Figure 2.13: Wind Directionality Histogram for Wind Data Recorded at Mitchell International Airport from July 1996 to November 2001 (Ginal 2003).

Both mean wind speed and wind direction are *continuous* random variables with *sample spaces* of $\{0 \le \bar{U} < \infty \; mph\}$ and $\{0 \le \theta < 360 \deg\}$, respectively. Both mean wind speed and wind direction were assumed to be *discrete* random variables. Mean wind speed was divided into 5 mph increments in order to correlate with the time history analyses, and wind direction was divided into 10 deg increments since the available wind direction data was recorded in this increment. An additional frequency count was performed on the mean wind speed data in order to reflect the 5 mph bin size. The resulting histogram is illustrated in Figure 2.14. A frequency count of the wind direction data was already performed using 10 deg increments and, therefore, the histogram illustrated in Figure 2.13 was not modified.

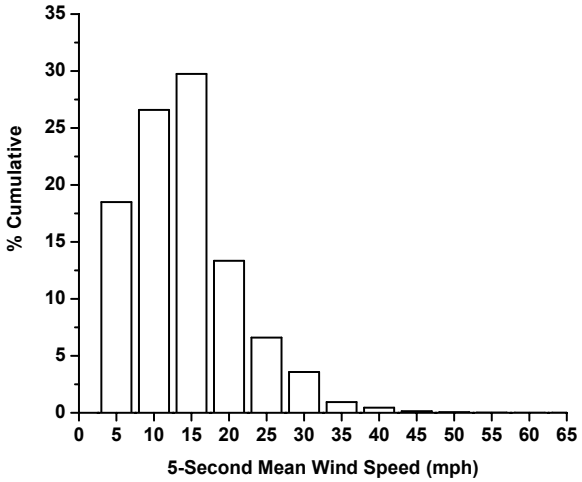

Figure 2.14: Probability Histogram for Mean Wind Speed (Ginal 2003).

Converting mean wind speed into *discrete* random variables requires a few underlying assumptions. As stated above, mean wind speed data was analyzed using 5 mph increments from 0 to 50 mph. Therefore, mean wind speed readings that did not fall on one of the 5 mph increments had to be lumped appropriately. For example, all mean wind speed readings that are in the range of 12.5 to 17.5 mph, inclusive, are lumped under the 15 mph increment. This assumes that the response data from a wind load time history analysis with a 15 mph mean wind speed represents an average response for mean wind speeds ranging from 12.5 to 17.5 mph.

It should be noted that the highest mean wind speed used in the analytical work was 50 mph. This limit was established based on the mean wind speed statistical data, which suggests a very small probability of occurrence for mean wind speeds greater than 50 mph (approximately 0.039 %). Peak wind speeds (gusts) in excess of 50 mph will occur, but mean wind speeds with a 5-second averaging time will rarely exceed 50 mph in Southeast Wisconsin. Additionally, any peak wind gusts above 50 mph were captured in the 30 to 50 mph turbulent wind simulations. Second, it was assumed that response data from a wind load analysis using a mean wind speed of 0 mph will be the average for mean wind speeds from 0 to 2.5 mph. In other words, it was assumed that mean wind speeds from 0 to 2.5 mph do not inflict damaging response in full-span overhead sign support and high-mast luminaire support structures.

Converting wind direction into a *discrete* random variable also requires assumptions. As stated previously, wind direction data was analyzed using 10 deg increments from 0 to 360 deg. This was convenient since wind direction data was recorded in 10 deg increments. Wind direction data was lumped, however, into primary and secondary cardinal direction sectors. Sectors were established both for the primary cardinal directions (*e.g.* North) and for the secondary cardinal directions (*e.g.* Southwest).

For example, wind direction readings in the range of 340 to 20 deg, inclusive, are lumped under North. This assumes that any response data generated by applying the wind load out of the North is an average response for wind loads applied out of directions 20 deg West (340 deg) to 20 deg East (20 deg) of North. Similarly, wind direction readings in the range of 110 to 160 deg, exclusive, are lumped under Southeast and therefore, any response data generated by applying the wind load out of the Southeast is an average response for wind loads applied out of directions 20 deg North (110 deg) to 20 deg South (160 deg) of Southeast.

The *combined* probabilities of mean wind speed and wind direction were then calculated based on the assumption that these two events are *statistically dependent*. This assumption has undergone extensive validation by Ginal (2003). The statistical data used to generate the conditional probabilities can be found in the histograms of Figures 2.15 and 2.16. Conditional probabilities were then extracted from these histograms. These conditional probabilities represent the probability of occurrence for wind direction given that mean wind speeds of 5 mph to 50 mph, in 5 mph increments, have already occurred. Table 2.3 lists these conditional probabilities. Mean wind speed and wind direction combined probabilities were then calculated using the conditional probabilities listed in Table 2.3 and the individual probabilities for mean wind speed listed in Table 2.4.

The necessary statistical information to determine combined probabilities of wind speed and direction (*i.e.* the intersection of statistically dependent events) is contained in Tables 2.3 and 2.4. The intersection of a particular wind speed event, E_1, with a particular direction event, E_2, can be written as,

$$P(E_1 \cap E_2) = P(E_1) \cdot P(E_2 \mid E_1) \tag{2.10}$$

where: $P(E_1)$ is the probability that event 1 will occur; and $P(E_2 \mid E_1)$ is the probability that event 2 will occur given that event 1 has occurred. This can be written more explicitly in terms of the wind speed and directionality probabilities currently discussed as,

$$P(40\ mph \cap Southwest) = P(40\ mph) \cdot P(Southwest \mid 40\ mph) \tag{2.11}$$

In words, equation (2.11) states, the probability that the wind speed will be 40 mph out of the Southwest is equal to the probability that the wind speed will be 40 mph (Table 2.4) multiplied by the probability that the wind will be from the Southwest given that it has a speed of 40 mph (Table 2.3).

A quick example computation for the wind speed and direction contained in equation (2.11) can be carried out as follows:

$$P(40\ mph \cap Southwest) = (0.00463) \cdot (0.23462) = 0.00109$$

The calculation above and those for the remaining wind speeds from 0 to 50 mph and the 8 directions considered can be found in Table 2.5.

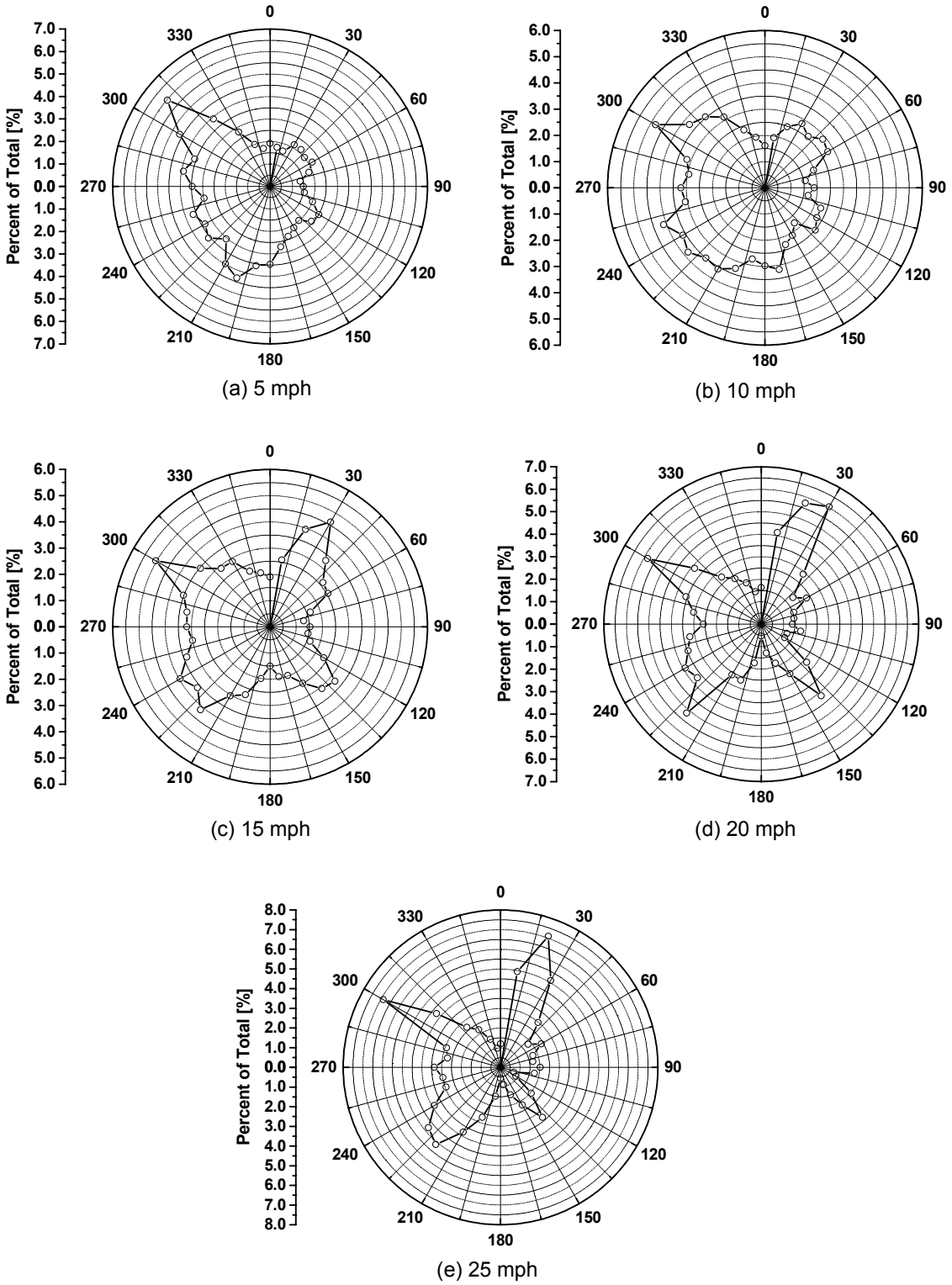

Figure 2.15: Directionality Histograms for the Calculation of Wind Direction *Conditional* Probabilities for Given Mean Wind Speeds: (a) – (e) 5 mph to 25 mph (Ginal 2003).

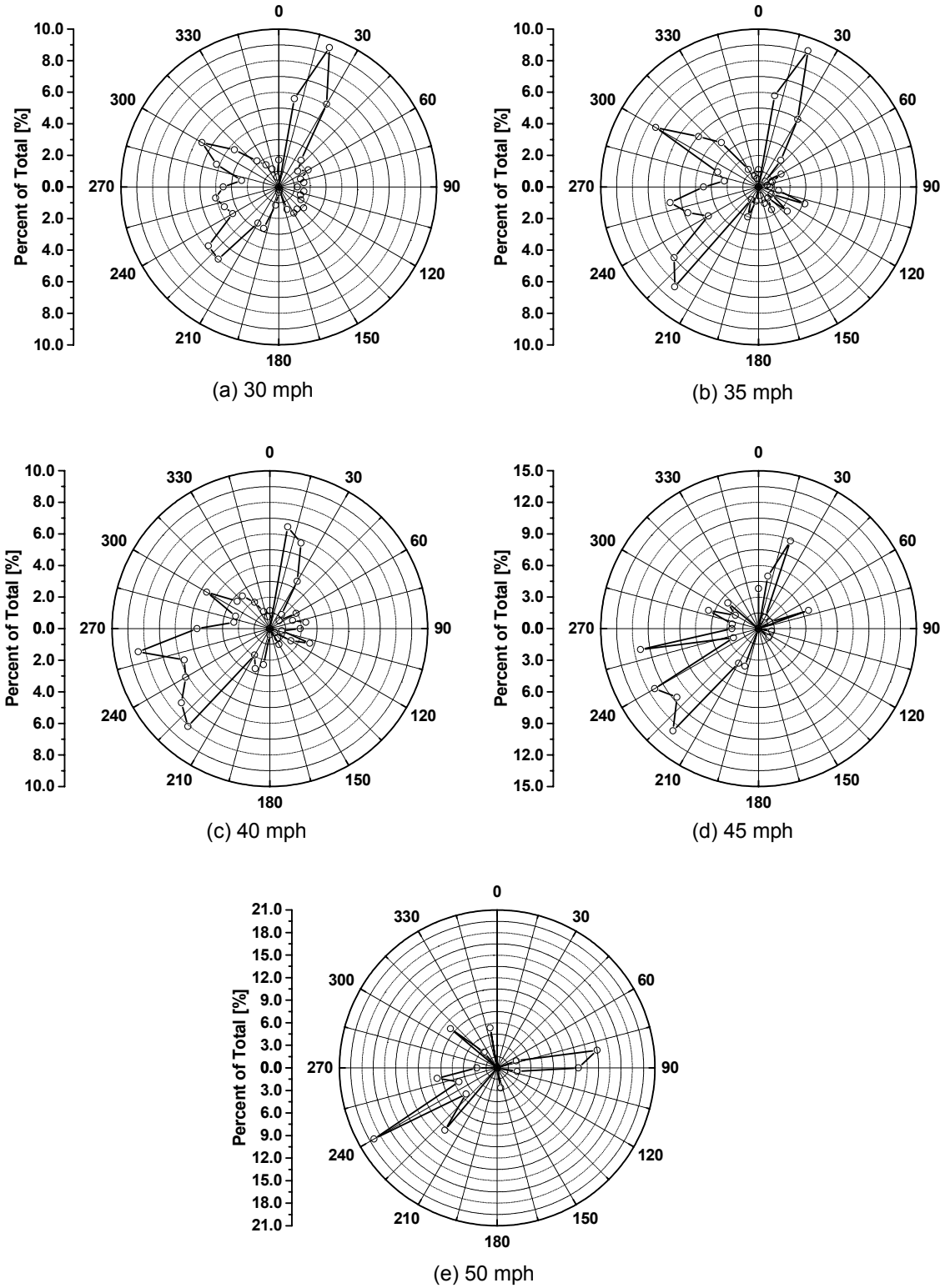

Figure 2.16: Directionality Histograms for the Calculation of Wind Direction *Conditional* Probabilities for Given Mean Wind Speeds: (a) – (e) 30 mph to 50 mph (Ginal 2003).

Table 2.3: Wind Direction Conditional Probabilities for Given Mean Wind Speeds (Ginal 2003).

		Wind Direction								
		North	Northeast	East	Southeast	South	Southwest	West	Northwest	**SUM**
Mean Wind Speed	5 mph	0.09053	0.08443	0.08242	0.09013	0.16455	0.13924	0.17555	0.17315	1.00000
	10 mph	0.10328	0.11027	0.09355	0.08635	0.14459	0.14499	0.16485	0.15212	1.00000
	15 mph	0.12784	0.13086	0.07541	0.11149	0.10159	0.14727	0.16279	0.14276	1.00000
	20 mph	0.14906	0.13085	0.07400	0.10540	0.08086	0.15367	0.15855	0.14761	1.00000
	25 mph	0.15711	0.12288	0.07909	0.08466	0.07139	0.17569	0.14942	0.15977	1.00000
	30 mph	0.18622	0.11975	0.07331	0.07380	0.06012	0.17791	0.17840	0.13050	1.00000
	35 mph	0.17431	0.09358	0.06606	0.05872	0.04587	0.19817	0.18899	0.17431	1.00000
	40 mph	0.15385	0.07308	0.09231	0.03846	0.05385	0.23462	0.23462	0.11923	1.00000
	45 mph	0.17722	0.02532	0.06329	0.01266	0.03797	0.37975	0.24051	0.06329	1.00000
	50 mph	0.05405	0.00000	0.29730	0.00000	0.02703	0.35135	0.16216	0.10811	1.00000

Table 2.4: Mean Wind Speed *Individual* Probability of Occurrence (Ginal 2003).

Mean Wind Speed	Probability of Occurrence
5 mph	0.17788
10 mph	0.26704
15 mph	0.30036
20 mph	0.13489
25 mph	0.06704
30 mph	0.03640
35 mph	0.00970
40 mph	0.00463
45 mph	0.00141
50 mph	0.00066
SUM	1.0000

Table 2.5: Mean Wind Speed and Wind Direction *Combined* Probabilities Based on Wind Direction *Conditional* Probabilities (Ginal 2003).

		Wind Direction								
		North	Northeast	East	Southeast	South	Southwest	West	Northwest	**SUM**
Mean Wind Speed	5 mph	0.01610	0.01502	0.01466	0.01603	0.02927	0.02477	0.03123	0.03080	0.17788
	10 mph	0.02758	0.02945	0.02498	0.02306	0.03861	0.03872	0.04402	0.04062	0.26704
	15 mph	0.03840	0.03930	0.02265	0.03349	0.03051	0.04423	0.04890	0.04288	0.30036
	20 mph	0.02011	0.01765	0.00998	0.01422	0.01091	0.02073	0.02139	0.01991	0.13489
	25 mph	0.01053	0.00824	0.00530	0.00568	0.00479	0.01178	0.01002	0.01071	0.06704
	30 mph	0.00678	0.00436	0.00267	0.00269	0.00219	0.00648	0.00649	0.00475	0.03640
	35 mph	0.00169	0.00091	0.00064	0.00057	0.00044	0.00192	0.00183	0.00169	0.00970
	40 mph	0.00071	0.00034	0.00043	0.00018	0.00025	0.00109	0.00109	0.00055	0.00463
	45 mph	0.00025	0.00004	0.00009	0.00002	0.00005	0.00053	0.00034	0.00009	0.00141
	50 mph	0.00004	0.00000	0.00020	0.00000	0.00002	0.00023	0.00011	0.00007	0.00066
	SUM	0.12218	0.11530	0.08160	0.09592	0.11704	0.15048	0.16540	0.15208	1.00000

Table 2.5 contains all wind speed and direction statistical data needed to assign probabilities for the subsequent fatigue life analysis of the sign and luminaire support structures considered in the present study.

2.9 NCHRP and AASHTO Procedures for Fatigue Life Estimation

The *Standard Specifications for Structural Supports for Highway Signs, Luminaires and Traffic Signals* (AASHTO 2001) is the latest design standard for ancillary highway structures. The fatigue analysis portion of these specifications is geared toward design (not fatigue-life estimation) and 95% confidence in attaining infinite fatigue life. However, procedures have been developed for determining varying confidence levels in attaining fatigue life performance (Moses *et al.* 1987) and making rational predictions for fatigue lives within the context of the AASHTO (2001) procedure. This section of the report describes the methodology used to generate fatigue life predictions using analytical models for wind loading applied to full-span sign support structures and luminaire support structures. Full details of the procedure related to sign support structures can be found in Ginal (2003).

2.9.1 AASHTO Stress-Life Procedure

The method currently recommended by the AASHTO design standards for the evaluation of fatigue in overhead sign support structures is the "stress-life" method (AASHTO 2001). The "stress-life" method contains a relatively quick and easy analysis procedure that provides conservative fatigue life predictions (*i.e*. shorter than expected) for 95% confidence levels. It produces good fatigue results for "infinite life" design and is applicable to those structures that will experience a large number of cycles (> 10e6 cycles) at relatively low stress magnitudes (*i.e. elastic* strains). This is appropriate for overhead sign support structures, which are designed to undergo elastic stress cycles and will experience millions of loading intervals during a typical service-life. The "stress-life" method relies heavily upon experimental testing of parts/materials as well as modifications of experimental results for use in practical design scenarios. The fatigue design procedure outlined in the AASHTO Specification is based upon an extensive inventory of material and component experimental data as well as a "good" understanding of required modification factors. The "stress-life" method also has the advantage of being well documented and accepted.

The fundamental element of the "Stress-Life" method that is relied upon to generate accurate fatigue life predictions is the *S-N* diagram. The general form of the *S-N* curve (expressed in log-log space) used in the specifications (AASHTO 2001) is shown in Figure 2.17. The present study considers fatigue life predictions for auxiliary highway structures. Therefore, focus will be on the linear portion of the *S-N* diagram and not the constant amplitude fatigue life (CAFL) limit. The linear portion of the curve can be written as,

$$\log N = \log A - m \log S \tag{2.12}$$

or

$$N \cdot S^m = A \tag{2.13}$$

The simple schematic shown in Figure 2.17 does not adequately illustrate the level of uncertainty in the linear expression used to determine the number of cycles to failure for a given stress range.

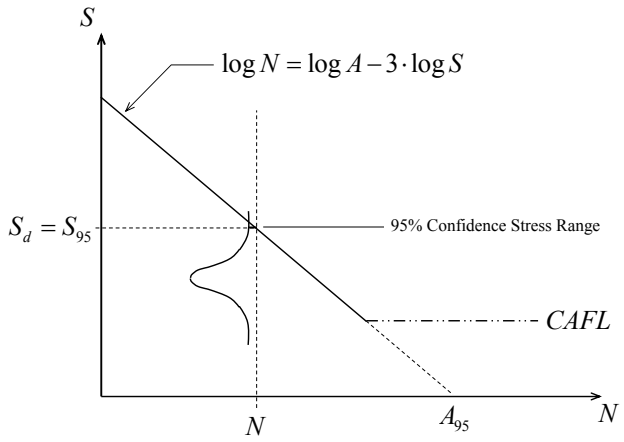

Figure 2.17: Schematic Stress-Life (*S*-*N*) Curve Used for Design.

If one considers design, establishing confidence levels for stress ranges (given a number of cycles to failure), or the number of cycles to failure (given a stress range) would certainly be the most important tasks if rational design procedures are to be developed. The AASHTO (2001) methodology establishes a stress range, S_{95}, in the following manner. Consider a set number of cycles to failure, N, for which only 5% of all stress ranges achieving N were above the stress range, S_{95}. Therefore, S_{95} denotes the highest stress range (with 95% confidence) that achieved N cycles before failure. AASHTO (2001) defines this stress range as the design stress range, S_D. Equation (2.12) can then be used to define an A value that corresponds to the 95% confidence level stress range. The AASHTO (2001) design *S*-*N* diagram is defined as,

$$\log N = \log A_{95} - m \log S_{95} \tag{2.14}$$

The "slope" of the *S*-*N* curve, m, is taken to be 3 and the x-axis intercept is A_{95}. Equation (2.14) is the basis for the fatigue design provisions for a large variety of detail categories. Each detail category has its own S_{95}, A_{95}, and $CAFL_{95}$ values. The slope remains constant ($m = 3$).

The AASHTO and AWS detail categories that most commonly apply to connections found in overhead highway sign support and luminaire support structures are D, E, E', and ET (AASHTO 2001;

AWS 1999). These fatigue detail categories are sufficient for most sign support structures regardless of the structural geometry (*e.g.* tri-chord, four-chord, etc.) and member cross-sections (*e.g.* angular members, tubular members, etc.). However, since the present study evaluates full-span overhead sign support structures composed of round HSS members and luminaire support structures, the connection details and appropriate fatigue detail categories associated with these types of structural members will be highlighted. Table 2.6 lists the typical detail categories found in the auxiliary highway structures considered in the present study.

Table 2.6: Typical Detail Categories for Auxiliary Highway Structures (AASHTO 2001).

Detail		**Detail Category**	$A_{95} \times 10^8$	$CAFL_{95}$ **(psi)**
Sign Support Structures	Truss Chord Splice	E'	3.90	2,600
	Truss Chord	E	10.6	4,500
	Truss Web Member	ET	0.80	1,200
	Anchor Rods	E' (1)	3.90	7,000
High-Mast Luminaire Support Structures	Slip-Joint Splice	B (2)	n.a.	n.a.
	Anchor Rods	E' (1)	3.90	7,000
	Mast-to-Base Plate Connection (full-penetration groove weld)	E'	3.90	2,600
	Reinforced Hand-Hole (Length > 4 inches; t =1/2 inch)	E	10.6	4,500

Notes:
(1) Dexter and Ricker (2002) recommend that double-nut, non-pretensioned anchor rods be evaluated as an E' detail with constant amplitude fatigue limit (CAFL) taken to be that of a category *D* detail. This recommendation is taken in this study.
(2) The slip-joint splice was not considered in the present study. These have not been reported to suffer from questionable in-service performance other than reports of splitting due to "packing corrosion".

The detail category data shown in Table 2.6 and equation (2.14) can be used to define stress ranges, or cycle counts for 95% confidence levels. However, these singular values do not give the engineer any "real indication" as to the ranges of fatigue life that can be experienced for these structures. To understand the fatigue-life range, one must examine alternate confidence levels.

Figure 2.18 illustrates typical details found in the full-span overhead sign support structures considered in the present study and Figure 2.19 illustrates typical details found in high-mast luminaire support structures.

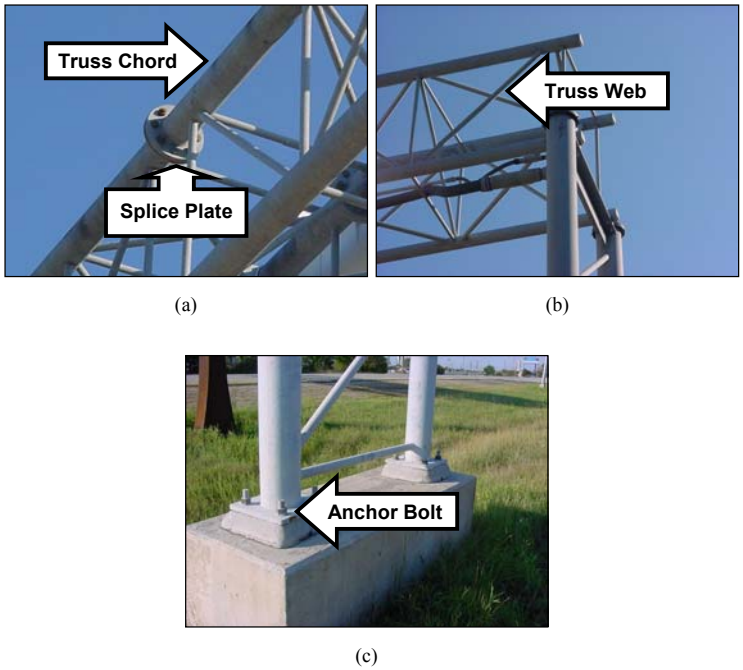

Figure 2.18: Typical Connection Details Found in Highway Sign Support Structures Composed of Round HSS Members (Ginal 2003).

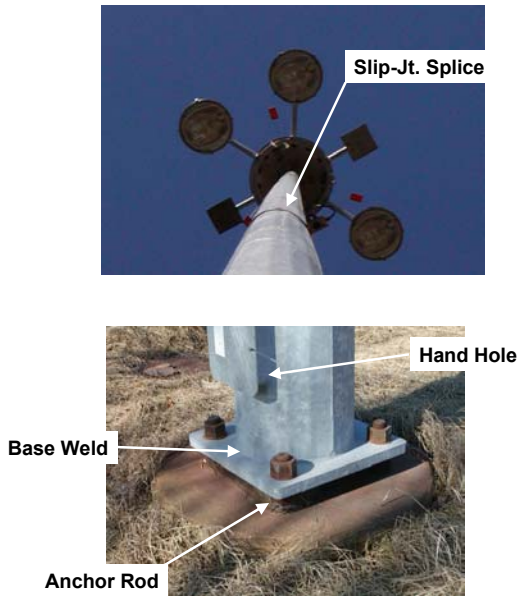

Figure 2.19: Typical Details Found in High-Mast Luminaire Support Structures.

2.9.2 NCHRP-Based Methodology for Fatigue Life Prediction

The NCHRP, as part of an overall fatigue evaluation of steel bridges, conducted a reliability study pertaining to predictions of remaining service life of highway bridge structures (Moses *et al.* 1987). Statistical properties of the experimental fatigue test results were used to associate a confidence level with the *S-N* curves that correspond to the AASHTO detail categories. The following points highlight the assumptions used in this study (Moses *et al.* 1987):

1.) The stress range, S, for each fatigue detail category is assumed to have a known statistical distribution at any number of cycles to failure, N.

2.) Mean values of S obtained from the experimental fatigue test results were used to evaluate the confidence level associated with values of S from the AASHTO *S-N* design curves.

3.) AASHTO *S-N* curves at varying confidence levels for a given detail category are all assumed to be parallel and have a slope of 3.0.

Assuming that a given detail category's statistical distribution follows the lognormal model, the following expression can be used to formulate a cumulative distribution function (Nowak and Collins 2000):

$$P\left[S_r \le S_{rD}\right] = \Phi\left(\frac{\ln\left(S_{rD}\right) - \mu_{\ln(S_r)}}{\sigma_{\ln(S_r)}}\right) \tag{2.15}$$

where: $P\left[S_r \le S_{rD}\right]$ represents the probability that a particular stress range, S_r, will be less than or equal to the design curve stress range, S_{rD}, for a given number of cycles to failure, N; and $\mu_{\ln(S_r)}$ and $\sigma_{\ln(S_r)}$ are the mean and standard deviation, respectively, of the lognormal of the experimental data. Φ denotes the cumulative distribution function (CDF) for standard normal variables.

For a lognormal random variable S_r, the mean and standard deviation of the lognormal of S_r can be calculated using the following equations (Nowak and Collins 2000):

$$\mu_{\ln(S_r)} = \ln\left(S_{rm}\right) - \frac{1}{2}\sigma^2_{\ln(S_r)} \tag{2.16}$$

$$\sigma_{\ln(S_r)} = \sqrt{\ln\left(\mathrm{cov}\left(S_r\right) + 1\right)} \tag{2.17}$$

where: $\mathrm{cov}\left(S_r\right)$ is the covariance of the random variable S_r. Moses *et al.* (1987) contains the statistical data needed to utilize equations (2.16) and (2.17) to generate *S-N* expressions for alternate confidence levels. Table 2.7 contains the statistical data for many of the fatigue detail categories contained in Figures 2.18 and 2.19.

It should be noted that statistical information for the *ET* detail category was not contained in this former research effort. Furthermore, evaluation of the remaining fatigue life of sign support structures

demands an understanding of the *S-N* behavior of existing (in-service) structures. As a result, the present effort set out to generate statistical information for the *ET* detail category found in the fatigue-critical details of sign support structures (Ginal 2003). Generation of the statistical information for the *ET* detail category will be undertaken later in this chapter of the report.

Table 2.7: Statistical Data used to Develop AASHTO *S-N* Design Curves with Varying Confidence Levels (Moses *et al.* 1987).

Detail Category	S_{rm} (ksi)	$\mathrm{cov}(S_r)$
D	13.00	0.142
E	9.50	0.097
E′	7.20	0.132

The mean and covariance data found in Table 2.7 can be used in conjunction with equations (2.15) through (2.17) to generate x-axis intercept values (*i.e. A*-values) for the design confidence level (95%) and other confidence levels that can be used to quantify fatigue lives of structures containing *D*, *E*, and E' detail categories. Table 2.8 contains the stress range for a set confidence level and the corresponding *A* value.

Table 2.8: *S-N* Design Curve Parameters for AASHTO *Fatigue Detail Categories* (Ginal 2003).

Detail Category	**Confidence Level**	S_{rD} **(ksi)**	$A_D \ \left(x10^8\right)$	$CAFL_D$
D	20%	14.50	61.0	7,000
E	20%	10.25	21.5	4,500
E′	20%	7.98	10.2	2,600
D	50%	13.00	43.9	7,000
E	50%	9.50	17.1	4,500
E′	50%	7.20	7.46	2,600
D	70%	11.95	34.1	7,000
E	70%	9.00	14.6	4,500
E′	70%	6.67	5.93	2,600
D	95%	10.30	21.9	7,000
E	95%	8.10	10.6	4,500
E′	95%	5.80	3.90	2,600

Overhead sign support structures undergo a relatively complex loading scheme, which can be characterized as *variable amplitude loading*. Structures subjected to this type of loading exhibit complex stress histories that make fatigue evaluation cumbersome. First, a procedure to "extract" and count stress ranges of varying amplitudes from the complex stress histories is needed. Once these stress ranges have been counted, a damage summation or accumulation method is required to assess the level of fatigue in the structure. Numerous counting methods have been developed to transform a complex stress history into an array of pseudo-constant-amplitude stress ranges. The two methods commonly used in structural engineering applications are the reservoir and rainflow methods (Fisher *et al.* 1998). Both methods produce similar results, but the rainflow method was used in the present study since it is more easily adapted to a computer algorithm.

The fatigue accumulation method utilized in the present study is based upon linear damage theory first proposed by Palmgren (1924) and furthered developed by Miner (1945). This theory is commonly known as the Palmgren-Miner rule, or Miner's rule. The basic premise of this theory is that the level of damage in a detail resulting from any one stress range of an array of stress ranges is a linear function of the number of cycles at that stress range. The total damage is then the sum of all fractional damages caused by each stress range level. Failure according to this theory is assumed to take place when the summation of damage fractions equals 1. This theory can be expressed in the following equation:

$$\sum D_i = \sum \frac{n_i}{N_i} = 1 \tag{2.18}$$

Equation (2.18) states that the sum of the individual fractional damages, D_i, at stress range levels S_i is equal to the sum of the cycle ratios, n_i/N_i. In the cycle ratio n_i/N_i, n_i is the number of cycles at stress range S_i, and N_i is the fatigue life, in cycles, at stress level S_i.

The Palmgren-Miner rule provides a quick and relatively easy method for fatigue life predictions. However, this theory possesses a few shortcomings when compared to observed material behavior. First, the Palmgren-Miner rule does not consider sequence effects (Bannantine *et al.* 1990). This theory assumes that the damage caused by an individual stress range is independent of its position in the stress history. The second major shortcoming of the Palmgren-Miner rule is that it assumes the rate of damage accumulation is independent of mean stress level (Bannantine *et al.* 1990). However, in structural applications where residual stresses are high and the number of stress range cycles is on the order of 10^4 or higher, these factors have only a small influence (Fisher *et al.* 1998). These observations are typical for most bridge structures as well as ancillary highway structures. In addition, theoretical data based on the Palmgren-Miner rule correlates well with experimental fatigue test data for these types of structures.

All of these factors have contributed to the AASHTO Specification's recommendation of the Palmgren-Miner rule for the linear accumulation of fatigue damage (AASHTO 2001).

Application of the Palmgren-Miner rule for the fatigue evaluation of overhead sign support structures is rather straightforward. The following example will be used to illustrate this procedure as applied in the present study.

Given:
AASHTO Fatigue Detail Category E ; 95% confidence level; $A_{95} = 10.6x10^8$; $m = 3.0 ksi/cycle$.
$S_1 = 5 ksi$ & $n_1 = 5x10^5 cycles$; and $S_2 = 2 ksi$ & $n_2 = 2x10^7 cycles$.

Determine:
Compute the percentage of accumulated damage due the two stress range magnitudes.

Solution:

$$N_i S_i^m = A \tag{2.13}$$

$$N_i = AS_i^{-m}$$

$$N_1 = \left(10.6x10^8\right)\cdot\left(5\right)^{-3.0} = 8.48x10^6 cycles$$

$$N_2 = \left(10.6x10^8\right)\cdot\left(2\right)^{-3.0} = 1.325x10^8 cycles$$

$$\sum D_i = \sum \frac{n_i}{N_i} \tag{2.18}$$

$$\therefore \sum D_i = \frac{n_1}{N_1} + \frac{n_2}{N_2} = \frac{5x10^5}{8.48x10^6} + \frac{2x10^7}{1.325x10^8} = 0.059 + 0.151 = 0.21 = 21\%$$

The accumulated damage for the AASHTO *Fatigue Detail Category* E in the above example is equal to 21% based on a confidence level of 95%. In other words, given the above stress ranges and corresponding cycles, a category E detail will have a 95% chance of accumulating a level of damage less than or equal to 21%.

The wind speed and direction probability study discussed previously makes determining the number stress-range cycles a little bit cumbersome, but nonetheless, it is possible to create a rational procedure for computing fatigue damage accumulation. The basic procedure for predicting the number of stress range cycles for a fatigue-sensitive component is described in the following:

1. Conduct a transient analysis (5-second duration) of the structure considered using a turbulent wind pressure record for a user-defined mean wind speed (*e.g.* 40 mph). Record the stress history of the desired component within the structure (*e.g.* an anchor rod). Repeat the analysis for all desired mean wind speeds (*e.g.* 5, 10, 15, 20, 25, 30, 35, 40, 45, 50 mph).
2. Use a rainflow counting procedure (Bannantine *et al.* 1990; Fuchs and Stephens 1980) to count the stress cycles in the stress history, $N_{\Delta\sigma,5-\text{sec}}$.

3. Determine the combined probabilities for mean wind speed and direction (*e.g.* probability of 45-mph wind out of the NE direction) using the procedure developed by Ginal (2003).
4. Determine the number of tensile stress cycles for a given mean wind speed for a one year exposure period. The example calculation below is for 40-mph mean wind (5-second averaging time) out of the SW direction;

$$\begin{aligned} N_{\Delta\sigma} &= N_{\Delta\sigma,5-\text{sec}} \cdot N_{5-\text{sec/yr}} \cdot P\left(\bar{V}_{5-\text{sec}} = 40\right) \cdot P\left(D = SW \middle| \bar{V}_{5-\text{sec}} = 40\right) \\ &= N_{\Delta\sigma,5-\text{sec}} \cdot N_{5-\text{sec/yr}} \cdot P\left(40 \cap SW\right) \end{aligned} \tag{2.19}$$

where: $N_{5\text{-sec/yr}}$ is the number of 5-second intervals in one year; $P\left(\bar{V}_{5\text{-sec}} = 40\right)$ is the probability that the mean 5-second wind speed is 40 mph; and $P\left(D = SW \middle| \bar{V}_{5\text{-sec}} = 40\right)$ is the probability that the wind direction will be southwest given that the 5-second mean wind speed is 40 mph. Equation (2.19) allows each stress range from the rainflow counting procedure to be extrapolated to the number of stress ranges in a full-year of exposure to mean-wind considered. Data used in the evaluation of equation (2.19) can be found in Table 2.5.
5. Use the AASHTO stress-life equations to assign yearly damage and the linear damage accumulation assumption (Miner 1945) to predict fatigue life.

The basic procedure described in steps 1 through 5 above has some subtle modifications that will be discussed when each structure type (*e.g.* sign support, or high-mast luminaire support) is considered. These modifications will be discussed in greater detail in Chapter 3.

Before continuing, a few concluding comments regarding the AASHTO fatigue analysis procedure are warranted. When designing a highway structure, the AASHTO Specification allows the designer to omit a fatigue assessment when the maximum stress range falls below the constant amplitude fatigue limit (CAFL).

Each AASHTO fatigue detail category has its own CAFL. When conducting a fatigue analysis, any structural detail that experiences a maximum stress range below the CAFL is assumed to have an infinite life. However, AASHTO recommends that all stress ranges greater than one half the CAFL are considered damaging and must be evaluated in the fatigue analysis. Since fatigue life predictions do not make a distinction between life being defined by crack formation or fracture, these lower stress ranges can be ignored because their impact on the fatigue life of the detail is not significant until near fracture.

Researchers, taking a theoretical point of view, have debated the notion of a CAFL for many years. The two sides of the debate disagree on whether or not this *limit* actually exists. The one side feels that every structural detail and/or material has a threshold stress range below which no stress ranges cause any

fatigue damage. The other side feels that all stress ranges, regardless of their magnitude, cause damage. The present study does not take a side in this debate, but rather follows AASHTO's recommendation, which is to assume that all stress ranges below one half the CAFL do not cause damage. However, even this approach, outside the central issue, is open to debate when various confidence levels are considered.

If the *S-N* curve for a fatigue detail category is adjusted to reflect a certain confidence level, one might also wonder if the CAFL should be adjusted as well. Again, this secondary discussion hinges on whether or not the CAFL actually exists. For example, consider the *S-N* curve at a 20% confidence level and the *S-N* curve at a 95% confidence level for AASHTO *Fatigue Detail Category E* . The CAFL for the curve representing a 20% confidence level can be determined in one of two ways. It either can be the same value as the CAFL for the curve with a 95% confidence level or it can be adjusted to a value above the 95% confidence level value. If the CAFL remains at the value for the curve with a 95% confidence level, this suggests that the detail achieves an infinite fatigue life at a larger number of cycles. This discrepancy in determination of cyclic value for infinite fatigue life is alleviated if the CAFL is eliminated from the curves and if all stress ranges are assumed to be damaging. In the present study the CAFL for all confidence levels of each detail category was set at the appropriate value for a 95% confidence level. This approach was taken for both simplicity and to produce conservative results in the fatigue life predictions.

2.10 Fatigue-Life Parameters for ET Detail Category

The generation of fatigue-life estimates for welded round HSS connections requires that statistical information, similar to that found in Moses *et al.* (1987) found in Table 2.7, be available for the *ET* detail category. Unfortunately, this statistical information is not available and generating reliable fatigue-life estimates for these detail categories was not possible.

The research team conducted an experimental program to generate the needed statistical information for *ET* fatigue detail categories (specifically welded round HSS connections). The experimental program examined existing and fabricated Y-joint specimens composed of round HSS shapes. Details of the experimental study can be found in Peronto (2003). The present section will highlight important results from this study and will provide a statistical model for the fatigue life variability of these detail categories suitable for later use in generating fatigue lives of welded sign support structures.

2.10.1 Specimen Fabrication and Experimental Fixturing

Three groups of specimens were fabricated and then tested. The first group of specimens, denoted MTS, consisted of 12 Y-Joint specimens fabricated from ASTM A513 DOM (Drawn Over Mandrel) material.

Three of the specimens included “back-grinding” to insure a better fit of the branch member against the chord requiring less filler weld metal around the joint. The difference in branch “fit” is shown in Figure 2.20. The welding parameters for the MTS specimens are given in Table 2.9. The dimensions of the specimen branch and chord members are given in Table 2.10.

(a) (b)

Figure 2.20: Saddle Connectivity: (a) Back-ground or Fish-Mouth Specimen; (b) Non-Back-Ground or Straight-Cut Specimen (Peronto 2003).

Table 2.9: Welding Parameters Used in Specimen Preparation (Peronto 2003).

Electrode (1)	Wire Diameter (2)	Voltage (3)	Amperage (4)	Wire Feed (5)	Shielding Gas (6)
E7056	0.035 in.	24 V	190 A	636 in./min.	75% - Argon 25% - CO_2

The second specimen group is denoted as ES. This group was composed of 8 K-Joint specimens that were cut from a decommissioned WisDOT sign support structure. The WisDOT designation number was S-40-10 indicating the structure resided in Milwaukee County (-40-) and it was structure number 10 (eastbound IH 94 immediately north of Miller Park). The structure went into service in 1962 and was decommissioned in 2002. Each joint cut from the existing structure was a K-Joint. Only one branch was subjected to tensile loading during the fatigue testing. Shop drawings for this structure were not available, but subsequent chemical composition analysis and tensile testing provided information regarding the material used. Dimensions for the branch and chord members are contained in Table 2.10.

The final specimen group, MTSx, was a replacement for the MTS group. The A513 DOM material used in the MTS specimens is not allowed per the design specifications (AASHTO 2001). Therefore, the

MTSx specimen group was composed of ASTM A500 or A53 Gr. B material. Therefore, these 6 Y-Joints were fabricated as "replacements" to the MTS specimens.

Table 2.10: Fatigue-Test Specimen Dimensions (Peronto 2003). (B.G. indicates that the specimen has been fabricated using back-grinding.)

Specimen Group	Specimen I.D.	Chord Member		Branch Member	
		O.D. (in.)	t_w (in.)	O.D. (in.)	t_w (in.)
MTS	1	4.50	0.194	1.66	0.131
	2	4.50	0.190	1.66	0.130
	3	4.50	0.193	1.65	0.129
	4	4.50	0.194	1.66	0.128
	5	4.50	0.195	1.68	0.128
	6	4.50	0.194	1.66	0.138
	7 (B.G.)	4.50	0.192	1.65	0.130
	8 (B.G.)	4.50	0.194	1.65	0.130
	9	4.50	0.196	1.65	0.135
	10	4.50	0.198	1.65	0.130
	11	4.50	0.194	1.65	0.129
	12 (B.G.)	4.50	0.195	1.65	0.130
ES	1	5.625	0.284	1.91	0.149
	2	5.625	0.289	1.90	0.152
	3	5.625	0.281	1.93	0.153
	4	5.625	0.275	1.90	0.156
	5	5.625	0.290	1.92	0.157
	6	5.625	0.275	1.89	0.160
	7	5.625	0.290	1.89	0.158
	8	5.625	0.285	1.91	0.160
MTSx	1	4.50	0.237	1.66	0.140
	2	4.50	0.237	1.66	0.140
	3	4.50	0.237	1.66	0.140
	4	4.50	0.237	1.66	0.140
	5	4.50	0.237	1.66	0.140
	6	4.50	0.237	1.66	0.140

The Marquette University testing facilities include a 20-kip capacity hydraulic closed-loop MTS 810 testing machine. Using this target testing machine, an experimental fixture had to be designed and constructed. Figure 2.21 illustrates the test fixture used for the fatigue testing. Figure 2.21(a) contains an ES specimen in the test fixture. The MTS and MTSx fixtures had slightly different fixturing with respect to the "actuator side" of the experimental setup and is shown in Figure 2.21 (b,c). However, the fixture setups resulted in negligible difference in the fatigue data generated. Further details regarding the experimental setup can be found in Peronto (2003).

(a)

(b)

(c)

Figure 2.21: Typical Specimen Support Fixture in MTS Machine: (a) ES Specimen Fixturing; (b) MTS and MTSx Fixturing with Strain Gauge Mounting; (c) MTSx Fixturing.

2.10.2 Material Characterization

The materials from which the fatigue specimens were fabricated were characterized using chemical composition analysis, microscopic examination, and tensile testing. Samples were taken from the chord and branch members and these samples were machined into ASTM 8-96a compliant tension test specimens. The specimens were machined such that the axis of the specimen was parallel to the direction of the rolling and parallel to the axis of the cyclic loading applied to the branch. Four tensile test

specimens were generated for the MTS joints, three specimens were fabricated for the MTSx joints, and three specimens were fabricated for the ES joints. All specimens were fabricated from chord material.

The tensile testing setup is shown in Figure 2.22. An extensometer was mounted to the specimens and modulus of elasticity data was obtained. The modulus of elasticity data indicates that the materials have the expected range of Young's modulus values for structural steels (*i.e.* 28,000 ksi). Further details can be found in Peronto (2003).

(a) (b)

Figure 2.22: Tensile Testing Machine and Fixturing Used for Material Characterization Study.

Unfortunately, an extensometer capable of providing full stress-strain response data was not available in the laboratory. Therefore, the tension testing provided data for plotting applied stress (engineering stress) versus displacement of the testing machine cross-head. While this cannot allow stress-strain data to be generated, it certainly allows yield stress, ultimate tensile stress, and percentage elongation at rupture to be determined. These were felt to be sufficient to characterize the materials. Figures 2.23 through 2.25 illustrate the tensile testing data generated for all specimens.

The stress-extension behavior of the ES material had a well-defined yield plateau typical of hot-rolled, mild-carbon structural steel. The yield plateau was utilized to define the yield stress by selecting the "lower yield point". The MTS and MTSx materials had stress-extension characteristics typical of cold-drawn steels and as a result, there was no well-defined yield stress. The 0.2% offset technique was utilized to define the yield stress for these materials.

The percentage elongation of the various materials is one indication of the material's ductility. Table 2.11 indicates the average percentage elongations for the tensile tests conducted for each specimen group. There is a significant difference in percentage elongation in the MTS material when compared to the MTSx and ES materials. The MTS material had an average percent elongation of 10.6. The ductility

of this material was significantly less than the MTSx and ES materials, which had average percentage elongations on the order of 26. The ramifications of this lack of ductility in the material will be related to the fatigue life of joints composed of this material as well as the material's microstructure.

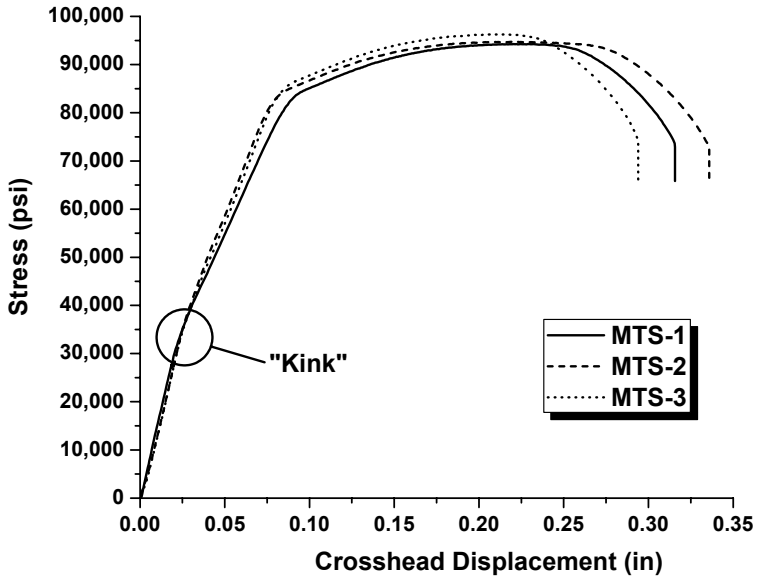

Figure 2.23: Stress-Extension Behavior of Material Comprising MTS Specimen Group.

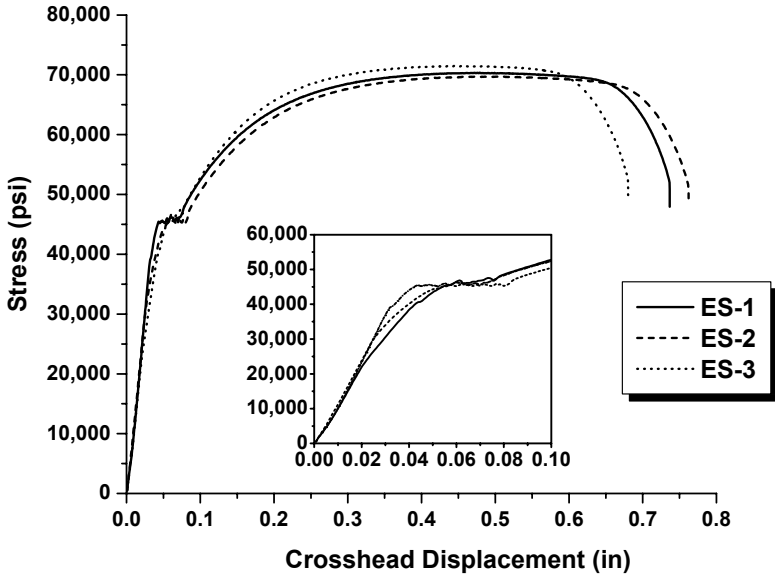

Figure 2.24: Stress-Extension Behavior for Material Comprising ES Specimen Group.

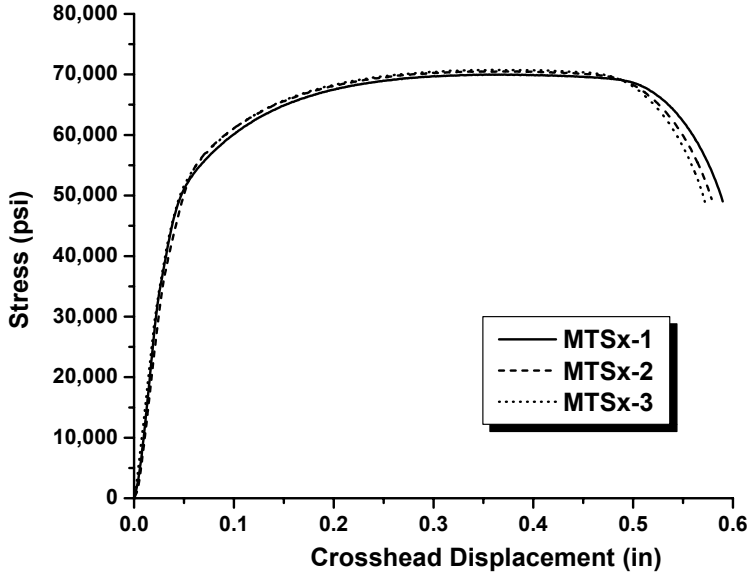

Figure 2.25: Stress-Extension Behavior for Material Comprising MTSx Specimen Group.

Table 2.11: ASTM Minimum Tensile Test Data Requirements and Properties Determined via Tensile Testing (Peronto 2003).

ASTM Designation or Specimen Designation		F_y (ksi)	F_u (ksi)	Percentage Elongation
A53	A53 Gr. B	35	60	
A500	A500 Gr. B	42	58	23
	A500 Gr. C	46	62	21
A513 (AISI 1026)	Sink Drawn	55	70	7
	Mandrel Drawn	70	80	5
	Mandrel Drawn Stress-Relieved	65	75	10
Present	MTS (avg.)	47.5	95.2	10.6
	MTSx (avg.)	46.3	70.4	26.0
	ES (avg.)	45.4	70.5	26.8

The “kink” in the stress-elongation response seen in Figure 2.23 is very interesting from a metallurgical point of view. Several tests with extensometer were conducted to verify that this “kink” indeed existed in the response. It was initially thought that this might be “slip” in the grips of the testing machine. The presence of this kink will be re-visited after the material’s microstructure is analyzed and discussed.

Table 2.11 contains minimum yield strength and minimum ultimate tensile strength requirements for ASTM A500 (Gr. B and C), A53 (Gr. B and C), and the various flavors of A513 material. The average yield stress and average ultimate tensile stress for the specimens tested are also contained in the

Table. The MTSx and ES specimen groups both demonstrate yield stress, ultimate stress, and ductility similar to that required for ASTM A500 Gr. B and C materials. The MTS specimens exhibited much lower ductility. The yield stress, ultimate tensile stress, and ductility values determined for this material via testing indicate that it meets requirements for A513 Mandrel-Drawn (DOM) material. The ductility magnitudes seen in the test results for the MTS material indicate that it is likely "stress-relieved".

Rockwell B hardness tests were also conducted for the chord material, the branch material, and the weld material (Peronto 2003). Measured Rockwell B data were typical for mild-carbon steels and the weld electrode material. The weld material, branch material, and chord material showed consistent Rockwell B values in the range 76 to 91 (Peronto 2003).

Several of the joints (MTS and ES) were examined for weld penetration into the base material at the fillet welds. The study indicated that the joints examined had very good welding penetration into the base metal (Peronto 2003).

The material characterization continued with examination of the material's microstructure under the electron microscope. Three regions were examined for each of the specimens (MTS, MTSx, and ES). The chord material, branch material, and material in the heat affected zone (HAZ) were examined. The material microstructure for all materials is shown in Figures 2.26 through 2.28. It is important to note that the darker regions in the figures are pearlite and the lighter regions are the proeutectoid ferrite in the material. A greater percentage of pearlite in the field of view relative to the ferrite indicates greater carbon content in the steel. From Figures 2.26 through 2.28, it appears that the MTS and MTSx material has higher carbon content than the ES material. This is illustrated in the yield plateau of the ES material and the lack of yield plateau in the MTS and MTSx material.

The ES and MTSx material microstructure exhibit nice "mixture" of pearlite and ferrite and therefore, the material ductility is at the levels demanded for structural engineering purposes. However, the material in the MTS specimens is heavily banded. The proeutectoid ferrite and the pearlite form well-defined layers parallel to the rolling direction and the longitudinal direction of the chord. This banding results from the micro-segregation of alloy elements, especially carbon, during solidification of the steel at its initial stage in production. This extreme banding can result in anisotropic behavior in the steel. Banding in the microstructure can have an adverse affect on the materials fatigue life. Furthermore, the banding could lead to micro-cracking in the base material during weld-cooling.

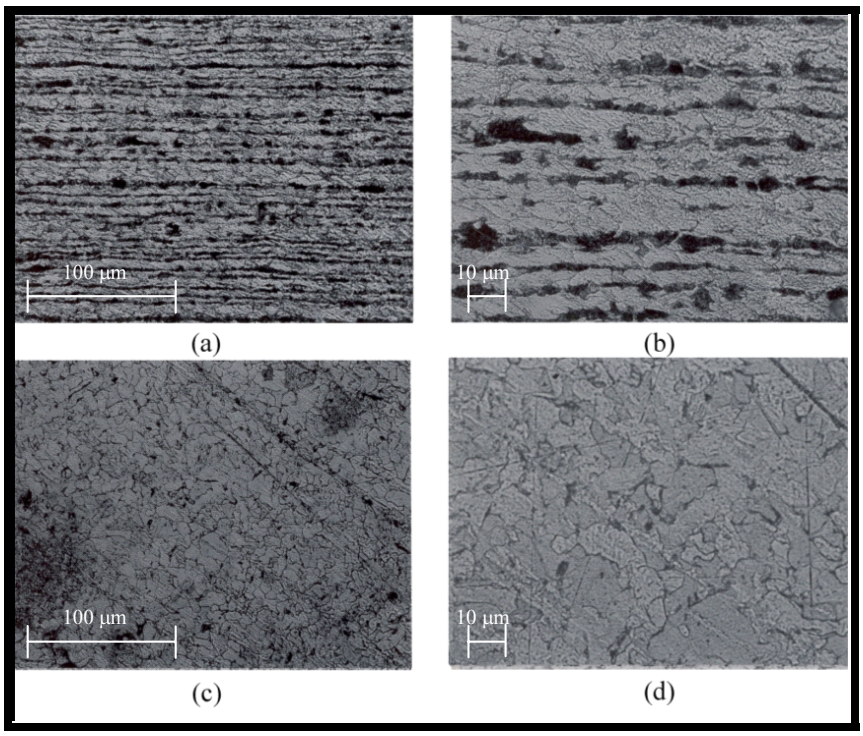

Figure 2.26: MTS Microstructure; (a) 200x Chord, (b) 500x Chord, (c) 200x Branch, (d) 500x Branch (Peronto 2003).

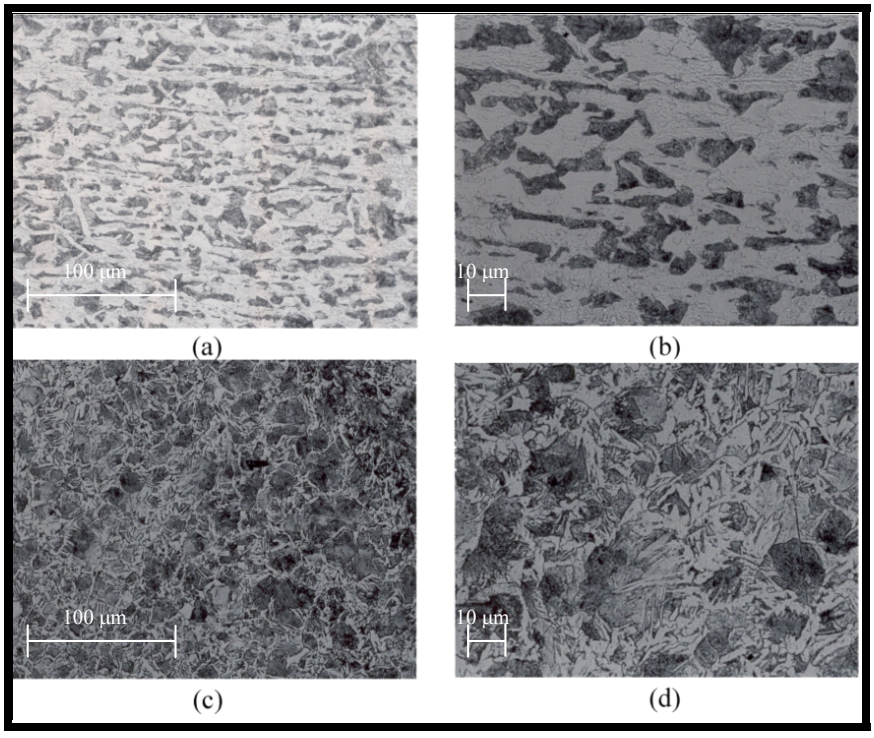

Figure 2.27: ES Microstructure; (a) 200x Chord, (b) 500x Chord, (c) 200x Branch, (d) 500x Branch (Peronto 2003).

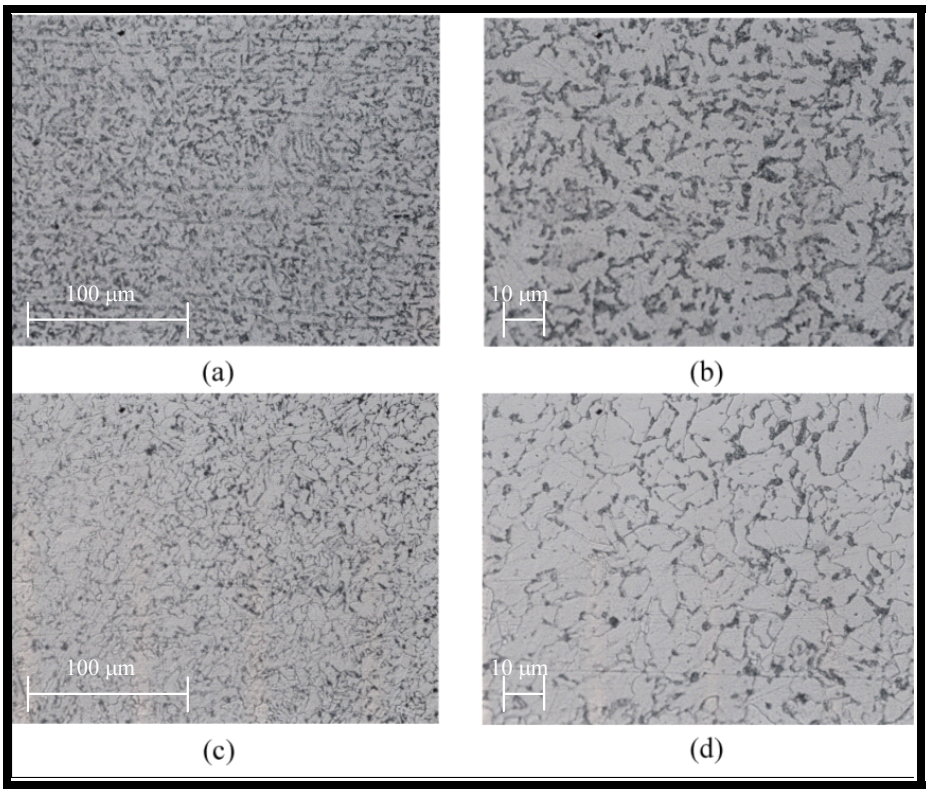

Figure 2.28: MTSx Microstructure; (a) 200x Chord, (b) 500x Chord, (c) 200x Branch, (d) 500x Branch (Peronto 2003).

Material banding is also a possible explanation for the "kink" in the stress-elongation response for the MTS material shown in Figure 2.23. One thing to note at this point is that the A513 DOM material comprising the MTS specimens would likely appear "okay" to specify if only ultimate stress and yield stress were the specification criteria. However, as will be illustrated, the banding has a definite effect on the fatigue life and should not be allowed in fatigue-resistant design. The formation of this "kink" and its impact is under further study, but is outside the scope of the present research effort.

All of the specimen material chemical compositions were determined via an external testing laboratory (Anderson Laboratories in Greendale, Wisconsin). Tables 2.12 and 2.13 provide the material chemistries determined for the MTS, MTSx and ES specimen materials. Both the chord and branch material was examined.

The MTSx and ES material chemistries satisfy ASTM A500 Grade B and C and ASTM Gr. B chemical composition requirements. The MTS specimen material appears to satisfy ASTM A513 material chemical composition requirements. The branch material appears to be out of the acceptable ranges of Manganese and Carbon content.

Table 2.12: Material Chemistries for MTSx and ES Specimen Material (Peronto 2003).

	ASTM	MTSx		ES		ASTM	
Element (1)	A53 Gr. B Type S & E (2)	Chord (1022) (3)	Branch (1010) (4)	Chord (1026) (5)	Branch (1022) (6)	A500 Gr. B (7)	A500 Gr. C (8)
Si	n/a	0.02	0.03	0.02	0.13	n/a	n/a
S	0.045	0.006	0.004	0.027	0.019	0.045	0.045
P	0.05	0.014	0.017	0.007	0.011	0.045	0.045
Mn	1.20	0.70	0.56	0.76	0.71	1.40	1.40
C	0.30	0.22	0.07	0.26	0.23	0.30	0.27
Cr	0.40	0.01	0.07	0.07	0.04	n/a	n/a
Ni	0.40	0.01	0.06	0.05	0.02	n/a	n/a
Mo	0.15	< 0.01	0.01	0.02	< 0.01	n/a	n/a
Cu	0.40	0.02	0.10	0.08	0.04	0.18	0.18
V	0.08	< 0.005	< 0.005	< 0.005	< 0.005	n/a	n/a
Pb	n/a	< 0.01	< 0.01	< 0.01	< 0.01	n/a	n/a
Al	n/a	0.047	< 0.033	0.028	0.021	n/a	n/a
Ti	n/a	< 0.005	< 0.005	n/a	n/a	n/a	n/a

Table 2.13: Material Chemistries for MTS Specimen Material (Peronto 2003).

	ASTM	MTS		ASTM		
Element (1)	A513 (1026) (2)	Chord (1026) (3)	Branch (1008) (4)	A53 Gr. B Type S & E (5)	A500 Gr. B (6)	A500 Gr. C (7)
Si	n/a	0.03	0.01	n/a	n/a	n/a
S	< 0.035	0.007	0.007	0.045	0.045	0.045
P	< 0.035	0.012	0.016	0.05	0.045	0.045
Mn	0.60 – 0.90	0.71	0.43	1.20	1.40	1.40
C	0.22 – 0.28	0.24	0.08	0.30	0.30	0.27
Cr	n/a	0.03	0.03	0.40	n/a	n/a
Ni	n/a	0.02	0.01	0.40	n/a	n/a
Mo	n/a	< 0.01	< 0.01	0.15	n/a	n/a
Cu	n/a	0.02	0.02	0.40	0.18	0.18
V	n/a	< 0.005	< 0.005	0.08	n/a	n/a
Pb	n/a	< 0.01	< 0.01	n/a	n/a	n/a
Al	n/a	0.042	0.06	n/a	n/a	n/a
Ti	n/a	n/a	n/a	n/a	n/a	n/a

One very interesting aspect to the chemical composition analysis is that the MTS material appears to satisfy the chemical composition requirements for both ASTM A53 and A500 materials. Based upon the fatigue results to follow, one must be diligent in specifying *both* material stress-strain data (ultimate tensile stress, yield stress, and percentage elongation at rupture) and chemical composition data. This will be further elaborated upon when the fatigue testing results are discussed.

2.10.3 Fatigue Testing and Variability Analysis

As mentioned earlier in this section, determination of an adequate statistical model for the *ET* detail category was of paramount importance to predict the fatigue lives of welded HSS sign support structures. The goal of this section of the report is to outline the experimental work done to generate a statistical model for the MTSx, and ES specimens. The MTS material was heavily banded (as described earlier). This affected the fatigue lives and since A513 material is not allowed for sign structures (AASHTO 2001), statistical information for the fatigue performance of the MTS specimens was not developed. However, the testing of these specimens does indeed shed light on the fatigue performance of welded round HSS joints composed of heavily banded material.

All specimens that underwent fatigue testing were loaded axially through the branch member using the fixturing described in Figures 2.21. The loading applied had constant amplitude and the frequency varied from 1 to 2 Hz. A force-controlled procedure that followed established protocols (ASTM 1998; 1999; 2002) was utilized. Failure of a specimen during the testing was defined as one of two scenarios (Peronto 2003): separation of the branch member from the chord by 0.5 inches; or the instant when the specimen could not support the maximum loading in the loading range (5% tolerance on this magnitude).

Many of the specimens were outfitted with strain gauges (4 total) mounted around the perimeter of the branch member in 90 degree intervals. Figure 2.21(b) illustrates the typical location of the strain gauges. These gauges were utilized to quantify the stress-range gradient across the branch member diameter inherent in the specimen fixturing. The strain gauges were mounted at a distance of at least one branch diameter from the fillet weld. The strains measured indicated that there was bending in the branch member as a result of the experimental fixture. The specimen results indicated that the mean stress range gradient across the branch diameter (*i.e.* the cyclic bending) was 5.3 and 7.6 ksi for the MTS and ES specimens, respectively (Peronto 2003). The mean stress ranges were 17.9 and 22.8 ksi (averages) for the ES and MTS specimens, respectively (Peronto 2003). As a result, there was bending in the branch member during the fatigue testing. However, the failure modes seen in the experiments were very similar to those seen in the field and therefore, the experimental fixturing was felt to be a good representation of the behavior in the field.

The failure modes of the MTS, MTSx and ES specimens varied slightly from one another. All specimens in the MTS group had failure defined by the loading tolerance. As expected, a crack initiated at the weld toe at the toe-side of the branch member. This crack propagated around the circumference of the branch member until the failure criteria was met. Figure 2.29 illustrates the typical failure modes for the specimens tested.

(a)

(b) (c)

Figure 2.29: Typical Specimen Failures: (a) MTS Material Specimens; (b) ES Material Specimens; and (c) MTSx Material Specimens.

The failures of the MTSx and ES specimens were triggered by the 0.5 inch branch member deflection tolerance after a very small number of loading cycles (less than 10). These specimen failures are also shown in Figure 2.29. The failure of the MTSx and ES specimens indicate that the material was significantly tougher than that in the MTS specimens. This is exhibited by the "tearing" of the branch member away from the chord member in the MTSx and ES group as shown in Figures 2.29(b) and

2.29(c). This suggests that the joint could still carry the applied load range, but was undergoing significant deformations at the chord wall prior to failure.

An example of the fracture surface of a selected ES specimen was examined under the electron microscope (Peronto 2003). Fatigue crack striations were observed on the fracture surface indicating that this material did indeed support fatigue crack growth. The material testing performed for the MTSx and ES specimens indicated that the material did have significant toughness and that stable growth of fatigue cracks would be possible. The limited ductility of the MTS specimen material would not support this and this is evident in the lack of "tearing" in the MTS specimens at failure.

The in-service failures seen in these structures are similar to those seen in the experiments. Several of the in-field failures are shown in Figure 2.30.

Figure 2.30: Typical Cracking Observed During Sign Support Structure Service Life.

The cracking exhibited in Figure 2.30 is very similar to that seen in the experimental work (see Figure 2.29). The experimental results are an adequate simulation of in-service loading conditions and the fatigue life predictions are suitable for the engineering analysis conducted.

The culmination of the experimental effort undertaken in this study was the generation of statistical information regarding the fatigue life variability of the welded round HSS connection suitable for generating fatigue life estimates for various confidence levels. The stress-life procedure used by design specifications (AASHTO 2001) was shown in Figure 2.17. The present study utilizes an experimental stress range, S, and examines the statistical variation in the number of cycles to failure at that stress range. This process is schematically shown in Figure 2.31. Two target stress ranges, S_r^1 and S_r^2, are defined. There will be a statistical variation in the number of cycles to failure at these stress ranges (shown in the Figure as "bell curves"). One can then assume that each of these distributions at the two stress ranges will have N_1^{95} and N_2^{95} defining the number of cycles to failure that are exceeded by 95% of

all experimental results. This technique is, of course, simplistic because it ignores the possibility for the statistical variation in the target stress range. However, if the lines defining the 95% confidence level stress ranges are "close" or "on top" of one another, this variation in stress range can then be ignored (for practical design).

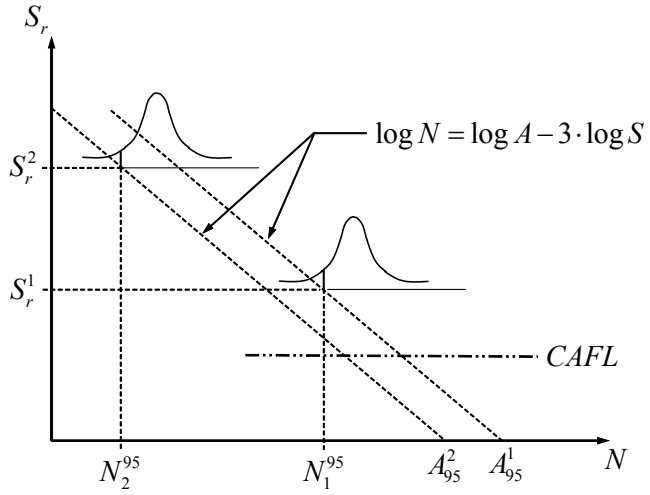

Figure 2.31: Schematic of the Approach Used to Establish Stress-Life Curves for Fatigue-Life Estimation in Regions Outside the CAFL.

The linear *S-N* diagram in log-space then allows x-intercept values, A_1^{95} and A_2^{95}, to be defined for each linear model. These then can be used to set 95% confidence-levels for alternative stress ranges not covered via experiment.

The statistical variation in the number of cycles to failure for the MTS, MTSx, and ES specimens are given in Table 2.14. Peronto (2003) determined that the variability in the number of cycles to failure was adequately modeled using a lognormal cumulative distribution function. Given the lognormal model, the probability that a number of stress cycles to failure, N, will exceed a defined (design) value, N_D, can be computed using (Nowak and Collins 2000);

$$P\left[N \geq N_D\right] = 1.0 - \Phi\left[\frac{\ln N_D - \mu_{\ln N}}{\sigma_{\ln N}}\right] \tag{2.20}$$

where: $\mu_{\ln N}$ and $\sigma_{\ln N}$ are the mean and standard deviation in the number of cycles to failure.

Equation (2.20) can be used to establish cycle counts that correspond to user-established confidence levels. Using the data in Table 2.14 for the MTSx specimens and equation (2.20), the following can be stated,

$$P[N \geq 22{,}710] = 0.95$$

This allows one to state that there is 95% confidence that the number of cycles to failure for the MTSx specimens (at the defined stress range) will be at least 22,710 cycles. It should be noted that this corresponds to a single stress range (*i.e.* no statistical variability in stress range).

Table 2.14: Fatigue Testing Statistics for Specimens Tested (Peronto 2003).

Parameter (1)		MTS (2)	MTSx (3)	ES (4)
S_r (ksi)		19.1	17.9	14.0
μ (cycles)		18,224	55,785	128,979
σ (cycles)		2,410	14,260	35,374
COV		0.132	0.256	0.274
median (cycles)		18,862	56,572	144,569
$\mu_{\ln N}$		0.352	0.477	0.492
$\sigma_{\ln N}$		9.748	10.815	11.646
N	95%	9,595	22,710	50,850
	70%	13,502	36,070	81,970
	50%	17,120	49,760	114,240
A	95%	0.67e8	1.30e8	1.40e8
	70%	0.94e8	2.07e8	2.25e8
	50%	1.19e8	2.85e8	3.13e8

The region in stress-life space that is of interest in the present study corresponds to stress ranges that are above the constant amplitude fatigue limit (CAFL). This deviates from the infinite life approach used in most design specifications for fatigue. Using the 95% confidence level number of cycles to failure, equation (2.14) can be modified as,

$$\log N^{95} = \log A_{95} - 3\log S_r \tag{2.21}$$

where A_{95} is the x-axis intercept corresponding to the 95% confidence number of cycles to failure at the defined constant amplitude stress range. If several experiments are performed, equation (2.21) can be used to solve for multiple x-axis intercepts.

Figure 2.31 illustrates the concept that there may be multiple A values possible for describing the fatigue behavior. The most desirable scenario would result in a single A value being suitable for each confidence level desired for fatigue life estimations. The validity of this scenario was investigated. Table 2.14 indicates that the 95% confidence A value for the ES and MTSx specimens were $1.30e8$

and $1.40e8$, respectively. It is important to note that there is a little less than 8% difference between these values. A conservative approach would be to set $A = 1.30e8$. Using the "conservative value", $A = 1.3e8$, one can establish a 95% confidence-level *S-N* diagram for the ES and MTSx specimens. The linear model using this x-intercept value is shown in Figure 2.32. The MTS, MTSx, and ES specimen experimental results are included on the graph.

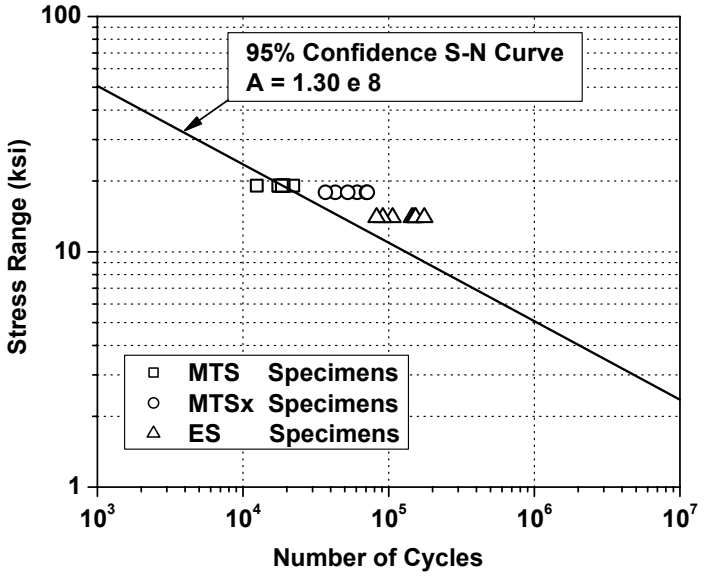

Figure 2.32: S-N Data and Recommended 95% Confidence S-N Curve (Peronto 2003).

The lognormal statistical model allows *S-N* diagrams for other confidence levels to be established. Peronto (2003) computed linear model parameters for 95%, 70%, and 50% confidence levels. These *A* values are shown in Table 2.15. The experimental work undertaken did not allow the constant amplitude fatigue limit (CAFL) to be addressed. One might surmise that there is statistical variability in this value, but it would be much more difficult to quantify. As a result, it was assumed that the 95% confidence-level CAFL would be used to define infinite life for all detail categories. These magnitudes are included in Table 2.15 as well. The data in Table 2.15 serves as the basis for estimating fatigue lives of detail categories in the present effort.

It is very interesting at this point to examine the fatigue performance of the MTS specimens composed of the heavily banded material. The results in Table 2.14 indicate that the number of cycles to failure for the MTS specimens were very low when compared to the lower stress range of the MTSx specimens. Therefore, the material microstructure of these specimens has a very large impact on the fatigue performance. A513 DOM material should not be allowed for sign support structures because the fatigue performance of this material is severely impacted by the banded microstructure that is likely to result in round HSS shapes.

Table 2.15: *S-N* Design Curve Parameters for AASHTO *Fatigue Detail Categories* (Ginal 2003; Peronto 2003).

Confidence Level	**Detail Category**	$A_D \ \left(x10^8\right)$	$CAFL_{95}$ **(psi)**
50%	*D*	43.9	7,000
	E	17.1	4,500
	E′	7.46	2,600
	ET	2.85	1,200
75%	*D*	34.1	7,000
	E	14.6	4,500
	E′	5.93	2,600
	ET	2.22	1,200
95%	*D*	21.9	7,000
	E	10.6	4,500
	E′	3.90	2,600
	ET	1.30	1,200

This Page Intentionally Left Blank

Chapter 3

Research Findings

3.1 Introduction

The immediately preceding chapter provided a literature synthesis of efforts related to the study of sign and luminaire support structures. It also included additional information derived as part of the present study necessary to conduct the analytical effort devoted to full-span Type 1 sign and VMS support structures and high-mast luminaire support structures. The chapter is broken down into two parts. Part one is devoted to the study of the full-span sign support structures. Three structure configurations commonly found in Wisconsin are used as test cases. The susceptibility of these structures to vortex-shedding-induced vibrations and galloping vibrations is discussed in detail. The damage expected due to truck-induced gust pressures for these structures is also discussed. Fatigue life estimates of the sign support structures considered are generated using procedures previously outlined. Part two includes the analytical study of two high-mast luminaire support structures chosen from the database of those managed by WisDOT District 2. The concentration of stress in unique four anchor rod base plate configurations is discussed as well as the susceptibility of these structures to vortex-shedding-induced vibrations. Fatigue life estimates for the HML structures are also discussed.

3.2 Full-Span Sign Support Structures

The review of past research related to sign support structures clearly indicates that research efforts have examined cantilevered sign support structures quite extensively. Therefore, the present study will focus its efforts on the analysis and fatigue evaluation of full-span overhead sign support structures. An emphasis on these types of structures will provide the greatest contribution to the body of knowledge and it is consistent with the recommendations of Kaczinski *et al.* (1998).

WisDOT District 2 currently has jurisdiction over approximately 560 sign support structures. The age of these structures ranges from less than one year to over 30 years. Within this population is a wide variety of full-span overhead sign support structures whose configurations are typical of full-span overhead sign support structures found in numerous states. It was felt that a thorough evaluation of the sign support structures under WisDOT District 2 jurisdiction would produce a diversified database of structures for selection of a representative test group.

The standard configuration for full-span sign support structures is 4-5 foot square box trusses supported on full-height uprights composed of two-chord pipe trusses as shown in Figure 3.1.

Figure 3.1: Four-Chord Pipe Truss Configuration used by WisDOT.

WisDOT has been systematically replacing aluminum structures with those constructed using structural steel. WisDOT also utilizes a tri-chord pipe truss configuration (Figure 3.2).

Figure 3.2: Tri-Chord Pipe Truss Configuration currently used by WisDOT.

Full-span box trusses now include a WT section, or "seat", which is welded between the truss chords of the two uprights. This is illustrated in Figure 3.3. The modification of the connection shown in Figure 3.1 to that shown in Figure 3.3 was motivated by ease in erection. Welded round HSS (hollow pipe) shapes continue to be used as the main supporting members for these structures.

Figure 3.3: WT Support Strut used in WisDOT Sign Support Structures

An investigation of retrofitted sign support structures under WisDOT District 2 jurisdiction revealed a variety of problems. Table 3.1 is a brief listing of these problem structures, which includes a description of retrofits/repairs made. From Table 3.1 it is apparent that both aluminum and steel structures of varying ages have required retrofit measures such as weld repair and/or replacement of truss members. It is also evident from this listing that most of the sign support structures containing the WT section have required repair of the T-stub detail. The structures included in this database are not only representative of the types of full-span overhead sign support structures in-service over Wisconsin roadways, but they also exhibit many of the performance problems that have plagued these types of structures.

Many State Departments of Transportation (DOT) have become aware of the performance problems associated with these pipe truss structures. Over the last five years, measures have been taken to improve the design of these structures. Many of the welded pipe-to-pipe connections in the sign support structures listed in Table 3.1 are an AASHTO *Category ET Fatigue Detail*, which has a relatively low Constant Amplitude Fatigue Limit (AASHTO 2001). Current design trends of sign support structures have tried to eliminate the use of *ET* details in order to improve the fatigue performance of these structures and at the same time decrease member sizes. One such design currently being used by WisDOT is similar to the original four-chord box truss with full uprights. One major difference is the truss web members for both the overhead portion and the uprights are angles bolted to gusset plates that are welded to the truss chords. This is illustrated in Figure 3.4.

The Minnesota Department of Transportation has also adopted a similar technique for the design of its full-span overhead sign support structures. The "Minnesota Design" consists of a four-chord box truss made up of welded angles for the chords and web members. The horizontal truss is supported on top of two monotube uprights. This configuration is shown in Figure 3.5. WisDOT has used this configuration for a handful of full-span overhead sign support structures that support VMS.

Figure 3.4: Four-Chord Bolted Angles and Welded Gusset Plates Truss Configuration currently used by WisDOT.

Table 3.1: Database of Retrofitted/Repaired Full-Span Overhead Sign Support Structures under WisDOT District 2 Jurisdiction

Structure Designation	Year	Location	Structure Placement	Sign Placement	Structure Type	Material	Span	Clearance	Retrofits / Repairs	Sign
S-30-12	1993	IH 94 @ Ramp to Tourist Info Center (STA 391+25)	NB Traffic (E-W)	S. face	Tri-Chord Truss connected w/ U-bolts to monotube uprights	Steel Pipe	46 ft	19 ft (min.)	Weld repair	Type I
S-40-40	1964	IH 43 S. of Green Bay Ave. (STA 1417+00)	SB Traffic (E-W)	N. face	Four-Chord Box Truss w/ full height uprights	Aluminum Pipe	97 ft	16 ft (min.)	Removed in 1999	Type I
S-40-144	1969	IH 43 W. of Layton Ave. (STA 93+40)	EB Traffic (N-S)	W. face	Four-Chord Box Truss w/ full height uprights	Aluminum Pipe	75 ft	17 ft (min.)	Replaced column strut & weld repair	Type I
S-40-148	1971	STH 145 @ Water St. (STA 355+03)	EB Traffic (N-S)	W. face	Four-Chord Box Truss w/ full height uprights	Aluminum Pipe	66 ft	17 ft (min.)	Replaced truss member(s)	Type I
S-40-152	1972	IH 94 @ Hawley Rd. (STA 293+50)	EB & WB Traffic (N-S)	W. & E. faces	Four-Chord Box Truss w/ full height uprights	Steel Pipe	77 ft	17 ft (min.)	Replaced truss member(s)	Type I
S-40-166	1969	IH 794 Hoan Bridge (STA 105+00)	SB Traffic (E-W)	N. face	Four-Chord Box Truss w/ full height uprights	Steel Pipe	110 ft	17 ft (min.)	Weld repair	Type I
S-40-404	1995	STH 119 E. of 6th St. (Mitchell Airport Spur)	WB Traffic (N-S)	E. face	Four-Chord Box Truss *U-bolted* to WT "seat" welded to uprights	Steel Pipe	106 ft	18 ft (min.)	Replaced truss member(s) & T-stub retrofit	VMS
S-40-56	1992	IH 43 @ Ramp to Silver Spring Dr. (STA 117+70)	NB Traffic (E-W)	S. face	Tri-Chord Truss connected w/ U-bolts to monotube uprights	Steel Pipe	56 ft	18 ft (min.)	T-stub retrofit	Type I
S-40-156	1995	IH 894 S. of Greenfield Ave. (STA 152+60)	NB Traffic (E-W)	S. face	Tri-Chord Truss *U-bolted* to WT "seat" and upright	Steel Pipe	67 ft	18 ft (min.)	T-stub retrofit	Type I
S-40-400	1995	USH 45 N. of Burleigh St.	SB Traffic (E-W)	N. face	Four-Chord Box Truss *U-bolted* to WT "seat" welded to uprights	Steel Pipe	86 ft	18 ft (min.)	T-stub retrofit	VMS
S-40-402	1995	IH 43 N. of Locust St.	SB Traffic (E-W)	N. face	Four-Chord Box Truss *U-bolted* to WT "seat" welded to uprights	Steel Pipe	81 ft	18 ft (min.)	T-stub retrofit	VMS
S-40-403	1995	IH 94/43 N. of Kinickinnic River	NB Traffic (E-W)	S. face	Four-Chord Box Truss *U-bolted* to WT "seat" welded to uprights	Steel Pipe	66 ft	18 ft (min.)	T-stub retrofit	VMS
S-40-405	1995	IH 94 S. of Ramsey Ave.	NB Traffic (E-W)	S. face	Four-Chord Box Truss *U-bolted* to WT "seat" welded to uprights	Steel Pipe	76 ft	18 ft (min.)	T-stub retrofit	VMS

Table 3.1: *(continued)*

Structure Designation	Year	Location	Structure Placement	Sign Placement	Structure Type	Material	Span	Clearance	Retrofits / Repairs	Sign
S-40-406	1995	IH 894 S. of Cleveland Ave.	NB Traffic (E-W)	S. face	Four-Chord Box Truss *U-bolted* to WT "seat" welded to uprights	Steel Pipe	86 ft	18 ft (min.)	T-stub retrofit	VMS
S-45-01	1969	IH 43 0.2 miles N. of JCT STH 33	SB Traffic (E-W)	N. face	Four-Chord Box Truss w/ full height uprights	Aluminum Pipe	115 ft	17 ft (min.)	Replaced truss member(s)	Type I
S-45-03	1969	IH 43 0.6 miles N. of JCT STH 33	SB Traffic (E-W)	N. face	Four-Chord Box Truss w/ full height uprights	Aluminum Pipe	125 ft	17 ft (min.)	Replaced truss member(s)	Type I
S-64-01	1975	IH 43 0.1 miles E. of CTH NN	EB Traffic (N-S)	W. face	Four-Chord Box Truss w/ full height uprights	Aluminum Pipe	91 ft	n.a.	Replaced truss member(s)	Type I
S-64-06	1975	USH 12 0.3 miles E. of IH 43	WB Traffic (N-S)	E. face	Four-Chord Box Truss w/ full height uprights	Aluminum Pipe	55 ft	n.a.	Replaced truss member(s)	Type I
S-66-01	1985	USH 41/45 0.5 miles S. of split of USH 41 & USH 45	NB Traffic (E-W)	S. face	Four-Chord Box Truss w/ full height uprights	Aluminum Pipe	100 ft	17 ft (min.)	Replaced truss member(s)	Type I
S-67-32	1995	IH 94 @ Hwy J Off Ramp (STA 180+50)	EB Traffic (N-S)	W. face	Four-Chord Box Truss w/ full height uprights	Aluminum Pipe	101 ft	18 ft (min.)	Weld repair	Type I
S-67-13	1975	USH 41/45 @ Pilgrim Rd.	NB Traffic (E-W)	S. face	Four-Chord Box Truss w/ full height uprights (formerly S-51-03)	Aluminum Pipe	69 ft	n.a.	Replaced truss member(s)	Type I
S-67-400	1995	USH 41/45 S. of Main St. (STH 74 & 100)	SB Traffic (E-W)	N. face	Four-Chord Box Truss *U-bolted* to WT "seat" welded to uprights	Steel Pipe	86 ft	18 ft (min.)	T-stub retrofit	VMS
S-67-402	1995	IH 94 W. of Elm Grove Rd.	EB Traffic (N-S)	W. face	Four-Chord Box Truss *U-bolted* to WT "seat" welded to uprights	Steel Pipe	71 ft	18 ft (min.)	Weld repair	VMS
S-67-401	1995	IH 94 W. of Brookfield Rd.	EB Traffic (N-S)	W. face	Four-Chord Box Truss *U-bolted* to WT "seat" welded to uprights	Steel Pipe	76 ft	18 ft (min.)	T-stub retrofit	VMS
S-67-403	1995	IH 43 W. of Beloit Rd.	NB Traffic (E-W)	S. face	Four-Chord Box Truss *U-bolted* to WT "seat" welded to uprights	Steel Pipe	56 ft	18 ft (min.)	T-stub retrofit & replaced column strut(s)	VMS
S-20-06	1999	USH 151 @ VVV, near USH 41 (STA 26+240)	NB Traffic (E-W)	S. face	Four-Chord Box Truss w/ full height uprights	Steel Pipe	112 ft	18 ft (min.)	"No Retrofit Drawings"	Type I

Figure 3.5: "Minnesota Design" currently used by WisDOT to Support VMS.

3.2.1 Test Group Structures

To select the most representative test group from this listing, the structures contained in Table 3.1 were grouped first using the following criteria:

1.) Overhead truss configuration (tri-chord/four-chord);
2.) Structural material (aluminum/steel);
3.) Sign type (Type I/VMS).

The resulting smaller groups allowed for a comparison of similar structures using a tailored list of criteria to eliminate nonessential structures. WisDOT's transition from aluminum to steel sign support structures has made the evaluation of aluminum structures somewhat dated. Therefore, these structures were eliminated immediately from consideration in the test group. This lowered the total number of structures considered to 16. The remaining support structures were then evaluated using the supported sign type.

Figure 3.6 illustrates the two types of signs these structures support: (a) the Variable (or changeable) Message Sign (VMS); and (b) the Type I aluminum sign. These two sign types have markedly different geometries, which is an important aspect to consider when evaluating a support structure's dynamic response to wind loading phenomenon such as vortex shedding and galloping instability, as well as its dynamic response to truck-induced pressures. The VMS boxes have a much larger soffit dimension than the Type I signs, which may cause the support structure to be more susceptible to the shedding of vortices. The relatively large surface area of the soffit will also allow for a greater resultant pressure and/or suction on the structure from truck-induced pressures. The mass in Figure 3.6(a) is also severely eccentric to the center of stiffness of the box truss. This also will affect the dynamic characteristics of the structure.

It is evident from Table 3.1 that structures supporting VMS, which were installed in 1995, have already required retrofitting of the T-stub detail. This is evidence of a fatigue concern that may be attributed to characteristics of these structures, which includes the supported VMS. Therefore, the

research team decided to focus the present research effort on full-span structures that support VMS. The limited amount of research devoted to full-span structures that supports VMS, as evidenced by the literature review and the growing popularity of these types of signs further supports this direction taken by the study.

(a) (b)

Figure 3.6: Sign Types used in Wisconsin: (a) Variable Message Sign (VMS); (b) Type I Aluminum Printed Sign.

The condensed set of structures was reduced to a group of three test group structures based on a refined set of criteria. As mentioned earlier, the large soffit of the VMS box increases the surface area available to truck-induced pressure pulses, which may adversely affect the fatigue performance of these structures. Therefore, it was deemed necessary to consider sign support structures in service over thoroughfares that have substantial truck traffic. A representative group of structures was then selected based on span length, structure orientation, and sign orientation. The test group, which consists of three full-span overhead sign support structures, is discussed below. Specific reasons for the selection of each structure are also provided.

Structure **S-67-402** is shown in Figure 3.7. It is a steel four-chord pipe truss structure that was installed in 1995. Within the first five years of its service, this structure required both weld repairs and retrofitting of its T-stub details. This structure is in service over eastbound lanes of Interstate Highway 94 about 10 miles west of Milwaukee, which sees significant high-speed truck traffic volume. This structure is typical of many VMS support structures used throughout southeast Wisconsin. The span of this structure is roughly 71 ft, which is average for structures contained in the WisDOT database. The analysis of this structure and subsequent results can be extrapolated to other sign support structures of similar configuration and vintage (*e.g.* S-67-400, S-67-401, S-67-403, S-40-400, S-40-402, S-40-403, S-40-405).

Figure 3.7: Sign Bridge S-67-402 Located in Waukesha County over Eastbound IH 94.

Structure **S-40-404** is a steel four-chord pipe truss structure that was installed in 1995. The structure is shown in Figure 3.8.

Figure 3.8: Sign Bridge S-40-404 Located on the "Airport Spur" in Milwaukee.

This structure also required both weld repairs and retrofitting of its T-stub details within the first five years of its service. This structure supports a VMS and is located over westbound lanes of the "airport spur" near Milwaukee County's Mitchell International Airport. Although similar in configuration to the S-67-4yy and S-40-4yy series structures discussed previously, the span of this structure is (on average) approximately 30 feet longer. Furthermore, this structure's close proximity to Mitchell International Airport is beneficial since that is where weather data is recorded. The location of this structure is such that it experiences a low to moderate amount of truck traffic. On the basis of these observations, this structure was thought to be a valuable addition to the test group.

Structure **S-40-156** (shown in Fig. 3.9) is a steel tri-chord pipe truss structure, which was also installed in 1995. This structure is in-service over northbound lanes of Interstate Highway 894 about one mile west of Milwaukee city limits. This structure supports large Type I aluminum signs and has significant high-speed truck traffic beneath it, and the sign area covers a majority of the truss' span. Both the tri-chord configuration and Type I sign make this structure unique when compared to the two

structures discussed above. Furthermore, this structure has also required retrofitting of its T-stub details. It was thought that this structure would make a valuable addition to the test group because of its unique attributes and also because its configuration is used by many State DOTs. The analytical results from this structure can also be extrapolated to other tri-chord support structures (*e.g.* S-40-56, S-30-12).

Figure 3.9: Sign Bridge S-40-156 Over IH 894 in Milwaukee, County.

3.2.2 Analytical Model Development and Modal Analysis

This section describes the FE software used for the analytical study, including its advantages and disadvantages. The development of each model is then discussed in detail, including selected element types, material properties, and analytical concerns, damping ratio assumptions, etc.

The FE software selected to perform the three-dimensional dynamic time history analyses of the test group sign support structures is ANSYS (SAS 2000b). This software package was chosen for a number of reasons. First, members of the research team involved with this study were already familiar with this software package, which allowed for preliminary modeling and analysis obstacles to be avoided. ANSYS was also selected because it is a very powerful package with a large database of element types, a comprehensive analysis component, and excellent graphics capability. ANSYS also has an internal programming language, called the ANSYS Parametric Design Language (APDL), which allows time intensive analyses to be automated by writing macros. The disadvantages of ANSYS can be attributed to the longevity of its original coding. The software has never been completely rewritten since its first distribution in 1971. Therefore, some implementation procedures can seem cryptic. The most difficult obstacle encountered with ANSYS was extracting analysis results data for further manipulation outside the ANSYS environment. This obstacle was overcome using APDL macros.

Development of these models began with retrieving design (or fabrication) drawings for each structure from WisDOT offices in Waukesha and Madison, Wisconsin. The available drawings from these offices were design drawings and copies of shop drawings stored on microfiche. These drawings

proved to be sufficient for the creation of the analytical models, and a field investigation of each structure verified approximate structure dimensions, support conditions, and sign and catwalk placement. A summary of each analytical model used for the test group sign support structures is located in *Appendix A*. These summaries include a list of material properties, member sizes, and element types used for the various components of each model.

Three element types were used to model the different components of each test group structure. Since all three sign support structures consist of welded pipe trusses, a three-dimensional pipe element (PIPE16) was selected to model the web and chord members. PIPE16 is a three-dimensional uniaxial elastic beam element with tension-compression, torsion, and bending capabilities, and it includes simplifications due to its symmetry and standard pipe geometry (SAS 2000a). This element has six degrees of freedom at two nodes, which allows for translation in three coordinate directions and rotation about three axes. It was noted that each of the sign support structures utilizes the WT section, or "seat" to connect the overhead portion of the structure to its vertical uprights. Element BEAM4 (SAS 2000a) was used to model this WT section. BEAM4 is actually the element on which PIPE16 is based. Therefore, these two elements are quite similar except that BEAM4 allows for the input of a more general cross-section. Element BEAM4 was also used to model elements of the sign and catwalk for each structure, which will be discussed later in this subsection. A three-dimensional elastic shell element (SHELL63) was used to model the sign and catwalk of each structure. A discussion of this aspect of the development of the analytical models follows.

During development of the analytical models, it was decided to include both the supported sign and catwalk in each model. This was done for several reasons. First, it was deemed necessary to incorporate these components into the analytical models in order to capture the in-service dynamic behavior of each structure. Second, the inclusion of these elements allowed for a more direct and accurate tracking of applied loads to the structure. In the time history analyses of each structure, both turbulent wind pressures and truck-induced pressures were applied directly to the sign and/or catwalk elements. Modeling the supported sign and catwalk allowed the inherent stiffness of each structure to dictate how the loading was distributed among its supporting members.

Both the sign and catwalk components were modeled using element SHELL63. SHELL63 is a three-dimensional elastic shell element that has both bending and membrane capabilities (SAS 2000a). This element has one node at each corner, each with six degrees of freedom, which allow for translation in three coordinate directions and rotation about three axes. In all three analytical models, the catwalk was modeled with a course mesh of SHELL63 elements whose material and section properties, specifically density and thickness, were adjusted in order to model the mass and stiffness of the actual catwalk. The

supports used to mount both the catwalk and sign to each sign bridge were modeled with BEAM4 elements whose material and section properties were set as those of the actual supports. A view of a typical FE model illustrating these elements is shown in Figures 3.10.

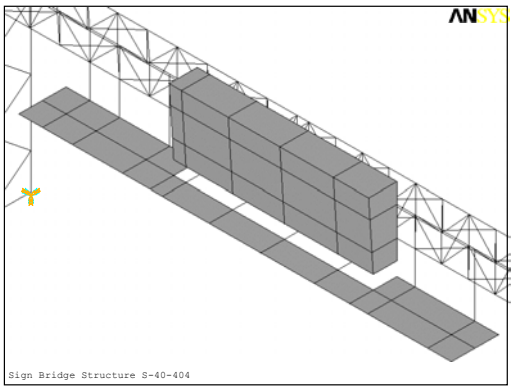

Figure 3.10: Portion of FE Model for Sign Bridge S-40-404 including Typical Catwalk and VMS Box Models (Ginal 2003).

Sign support S-40-156, which supports Type 1 signs, used a coarse mesh of SHELL63 elements, whose material and section properties were modified accordingly, to model the planar Type 1 sign. The sign components of each model were attached to the overhead truss portion of the model via coincident nodes of the shell, pipe, and beam elements, which are located at specific support points along each structure's span as dictated by the reference design and shop drawings. The FE model illustrating the tri-chord model and its Type I sign is shown in Figure 3.11.

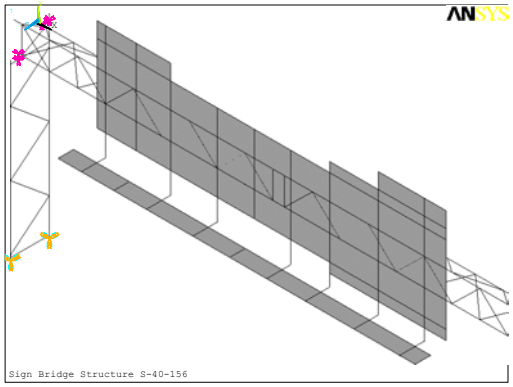

Figure 3.11: Portion of FE Model for Sign Bridge S-40-156 including Catwalk and Type I Sign Models (Ginal 2003).

The VMS boxes supported by sign bridges S-40-404 and S-67-402 were modeled with SHELL63 elements. Using dimensions of an actual VMS, a hollow box model was constructed using a coarse mesh of SHELL63 elements for the sides, top, and bottom (refer to Fig. 3.10). Again, material and section

properties were modified accordingly. As mentioned previously, *Appendix A* has a complete description of the three analytical models described above.

Before the sign and catwalk were added to each analytical model, a modal analysis was performed in order to provide a benchmark for the natural frequencies and mode shapes of each model. During these preliminary analyses, the support conditions for each structure were assumed fixed and the first 10 modes of vibration were extracted. These models also excluded the additional mass that would be present on the structure if the VMS or Type 1 sign were present. Table 3.2 lists the natural frequencies and periods of the first 10 mode shapes for each of the three analytical models. Next, each structure's supported sign and catwalk were added to the models. Again, a modal analysis, assuming fixed supports, was performed on each model, and the first 10 modes of vibration were extracted. Table 3.3 lists the results of this analysis.

Table 3.2: Natural Frequencies and Periods of Vibration from Modal Analysis of Support Structures *Without* Sign and Catwalk (Ginal 2003).

Vibration Mode	S-40-156		S-40-404		S-67-402	
	Frequency (Hz)	Period (sec.)	Frequency (Hz)	Period (sec.)	Frequency (Hz)	Period (sec.)
1	2.504	0.399	1.104	0.906	1.566	0.639
2	6.184	0.162	3.033	0.330	5.820	0.172
3	6.934	0.144	3.465	0.289	6.717	0.149
4	14.603	0.0685	8.545	0.117	13.389	0.075
5	14.811	0.0675	10.682	0.094	16.762	0.060
6	20.906	0.0478	12.151	0.082	20.193	0.050
7	21.202	0.0472	13.145	0.076	20.709	0.048
8	22.521	0.0444	18.533	0.0540	21.781	0.046
9	24.581	0.0407	18.560	0.0539	22.223	0.045
10	26.613	0.0376	19.663	0.051	25.158	0.040

These modal analyses illustrated irregularities in the resulting mode shapes and natural frequencies. With the addition of the sign and catwalk to the analytical models for sign bridges S-40-404 and S-67-402, the natural frequencies decreased (refer to Table 3.2 & Table 3.3).This result is expected since a significant amount of mass was added to the models by virtue of the VMS and catwalk, while the stiffness of the two models remained relatively unchanged. However, the fifth through tenth modes of vibration for S-40-404 and the fourth through the tenth for S-67-402 displayed vibration modes of the catwalk and not the supporting structure. Figure 3.12 illustrates this phenomenon in mode shape 5 of sign structure S-40-404.

Table 3.3: Natural Frequencies and Periods of Vibration from Modal Analysis of Support Structures *With* "Unstiffened" Sign and Catwalk (Ginal 2003).

Vibration Mode	S-40-156		S-40-404		S-67-402	
	Frequency (Hz)	Period (sec.)	Frequency (Hz)	Period (sec.)	Frequency (Hz)	Period (sec.)
1	1.692	0.591	0.801	1.248	0.949	1.054
2	1.913	0.523	2.124	0.471	3.154	0.317
3	2.261	0.442	2.338	0.428	3.647	0.274
4	2.821	0.354	4.188	0.239	6.035	0.166
5	3.425	0.292	5.829	0.172	6.094	0.164
6	4.022	0.249	7.222	0.138	8.338	0.120
7	4.182	0.239	7.871	0.127	8.420	0.119
8	4.503	0.222	9.308	0.107	9.574	0.104
9	4.944	0.202	9.609	0.104	10.111	0.099
10	5.549	0.180	10.225	0.098	11.955	0.084

The frequencies of S-40-156, which supports a Type I sign, decreased significantly as well (refer to Tables 3.2 and 3.3). This is partially justified by the increase in mass due to the addition of the Type I sign and catwalk, but it does not completely explain the poor separation of frequencies in the higher modes of vibration. The mode shapes of S-40-156 shown in Figure 3.13 depict vibration modes of the sign. From these results, it was evident that the models containing the sign and catwalk needed to be adjusted in order to limit the excitation of these undesirable mode shapes.

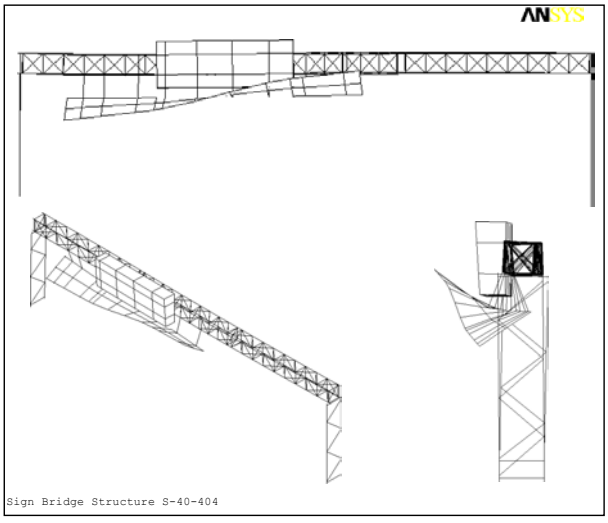

Figure 3.12: Mode Shape 5 of Sign Bridge S-40-404 Illustrating "Unstiffened" Catwalk Vibration Mode (Ginal 2003).

In order to ensure a relevant set of mode shapes and corresponding natural frequencies, modifications were made to all three analytical models. Massless stiffening elements were added to the catwalk and

sign components in the analytical models. The stiffening members were modeled using the BEAM4 element (SAS 2000a). The material properties used for this element were that of steel, except for the density, which was set at zero so that it would not add mass to the structure.

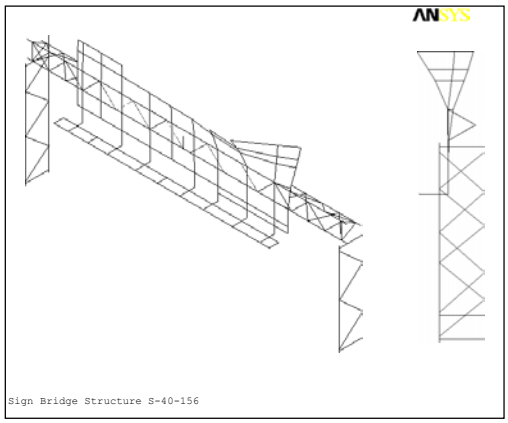

Figure 3.13: Mode Shape 4 of Sign Bridge S-40-156 Illustrating "Unstiffened" Sign Vibration Mode (Ginal 2003).

These stiffening elements were also given a low axial stiffness but a relatively large bending and torsional stiffness (see *Appendix A*) so as not to constrict the expansion and contraction of the sign and catwalk stiffening elements. The relatively large bending and torsional stiffness used for these elements limited contribution of these deformations to the structures' mode shapes. The stiffening elements were added in a grid pattern to the catwalks of S-40-404 and S-67-402 and to both the catwalk and sign of S-40-156. Another modal analysis, similar to before, was then performed on each of the three modified models. Again, the first 10 mode shapes and corresponding natural frequencies are listed in Table 3.4.

Table 3.4: Natural Frequencies and Periods of Vibration from Modal Analysis of Support Structures *With* "Stiffened" Sign and Catwalk (Ginal 2003).

Vibration Mode	S-40-156		S-40-404		S-67-402	
	Frequency (Hz)	Period (sec.)	Frequency (Hz)	Period (sec.)	Frequency (Hz)	Period (sec.)
1	1.916	0.522	0.802	1.247	0.950	1.053
2	4.545	0.220	2.132	0.469	3.201	0.312
3	5.780	0.173	2.355	0.425	3.691	0.271
4	8.385	0.119	4.212	0.237	6.289	0.159
5	11.304	0.088	6.287	0.159	7.080	0.141
6	12.841	0.078	7.596	0.132	9.722	0.103
7	20.151	0.050	9.350	0.107	10.125	0.099
8	20.654	0.048	10.289	0.097	10.580	0.094
9	22.675	0.044	11.209	0.089	15.112	0.066
10	23.698	0.042	11.488	0.087	16.506	0.061

A comparison of the natural frequencies listed in Table 3.2 and Table 3.4, as well as a visual comparison of the corresponding mode shapes indicates that the natural frequencies extracted from the modal analyses for the models that contained the "stiffened" sign and catwalk were consistently lower than the benchmark frequencies. Again, this is valid because of the increased mass in these models. It is also evident that the first 10 modes of vibration for each structure are well separated. The mode shapes of these models also improved visually from those of the "unstiffened" models. Figure 3.14 illustrates mode shapes from the following analytical models and corresponding modal analyses for S-40-156.

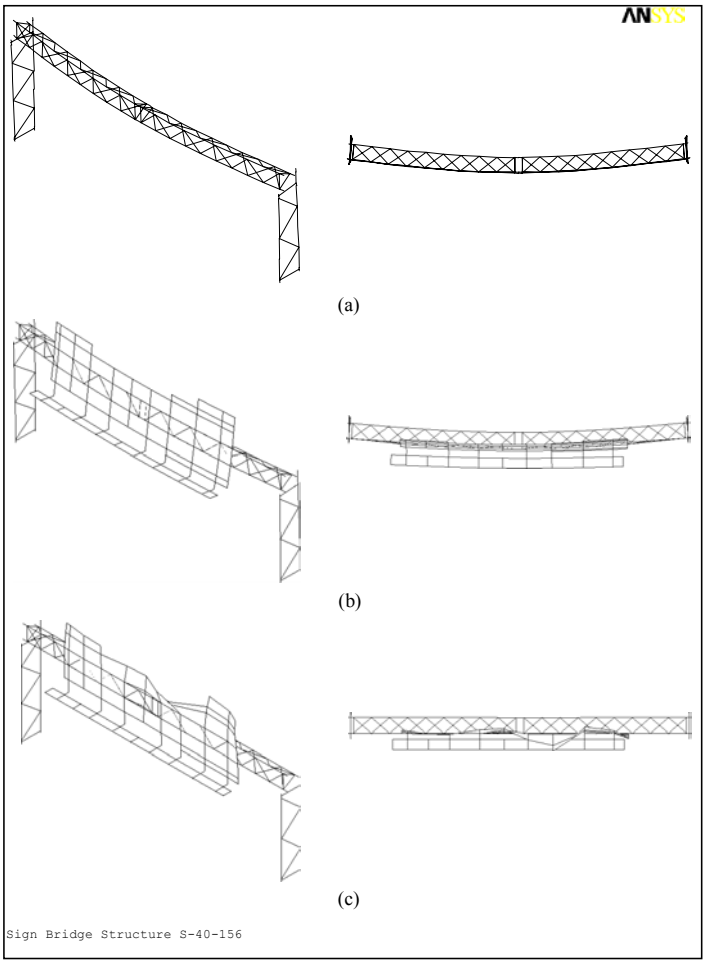

Figure 3.14: Modes of Vibration for Various Analytical Models: (a) 2nd Mode Shape *without* Sign and Catwalk (f = 6.1839 Hz); (b) 2nd Mode Shape *with* "Stiffeners" (f = 4.5433 Hz); (c) 8th Mode Shape *without* "Stiffeners" (f = 4.5033 Hz) (Ginal 2003).

The mode shapes depicted in Figure 3.14 were chosen based on similar vibration frequencies among the three modal analyses. A reduced frequency was selected for the models that included the sign and catwalk because of the expected lower frequency of these models due to their increased mass. As evident in Figure 3.14, the mode shapes from the "benchmark" modal analysis and the "stiffened" sign and

catwalk modal analysis agree quite well. However, the mode shape from the "unstiffened" sign and catwalk model, which is actually the eighth mode of vibration, compared to the second mode from the other two analyses depicts excitation of one of the supported sign's mode shapes. The comparison depicted in Figure 3.14 was typical of the modal analyses performed on S-40-156 as well as those of S-40-404 and S-67-402. Therefore, it was determined that the analytical models containing the "stiffened" sign and/or catwalk components were adequate for capturing the dynamic behavior of these structures.

3.2.3 Support Conditions

A structure's dynamic characteristics, specifically natural frequencies and mode shapes, are influenced by the structure's support stiffness. A modal analysis was again used to evaluate the dynamic behavior given varying support conditions. A comparison study of the resulting natural frequencies and mode shapes was conducted in order to determine appropriate support conditions for each model. This comparison study, along with a field inspection of each structure, was then used to justify the support conditions that were used.

Two modal analyses were performed on each model in order to evaluate dynamic properties for varying support type. The two support conditions used in these analyses were "fixed" bases and "pinned" bases. The "fixed" base condition simulates anchor rods with a sufficient embedment length and a fully grouted base plate whose thickness is adequate to prevent rotation of the sign support structure's vertical uprights. A "pinned" base condition allows for rotation of the vertical uprights while moment is not transferred from the uprights to the supporting foundation. Table 3.5 lists the vibrational frequencies from each structure's modal analysis for both the "fixed" and "pinned" base condition.

Table 3.5: Natural Frequencies (Hz) of Vibration from Modal Analysis of Sign Support Structures Assuming "Pinned" and "Fixed" Base Conditions (Ginal 2003).

Vibration Mode	S-40-156		S-40-404		S-67-402	
	Pinned	Fixed	Pinned	Fixed	Pinned	Fixed
1	0.684	1.916	0.069	0.802	0.701	0.950
2	4.456	4.545	2.107	2.132	3.192	3.201
3	5.760	5.780	2.352	2.355	3.670	3.691
4	8.334	8.385	4.210	4.212	6.286	6.289
5	11.087	11.304	6.228	6.287	7.065	7.080
6	12.660	12.841	7.492	7.596	9.659	9.722
7	14.880	20.151	9.348	9.350	10.120	10.125
8	17.423	20.654	10.171	10.289	10.495	10.580
9	18.229	22.675	11.049	11.209	13.431	15.112
10	19.385	23.698	11.362	11.488	15.100	16.506

It is important to note that structure S-67-402 contains a special base condition. Subsequently, the pinned and fixed support conditions were limited to only one vertical upright rather than both uprights. The effects on the dynamic analysis from modeling the supports in this manner are discussed in detail later.

From Table 3.5 it is evident that the support conditions for structures S-40-404 and S-67-402, excluding the first mode, contribute little to the dynamic behavior of each structure. Sign structure S-40-156, however, experienced a variation in natural frequencies in the first mode of vibration and modes above the fifth. Even though it is apparent that the support conditions affect the dynamic behavior of S-40-156 in its higher modes, these modes will not be excited in the analyses conducted as part of this study. This statement is valid because the simulated wind histories used in these subsequent analyses are modeled using the Kaimal spectrum (Kaimal 1972), which utilizes turbulent wind frequencies of less than 10 Hz.

As mentioned above, the first mode of vibration for each structure is affected differently by the two support conditions. The reason for this is that the first mode shape of each structure involves a lateral sway vibration of the uprights as illustrated in Figure 3.15.

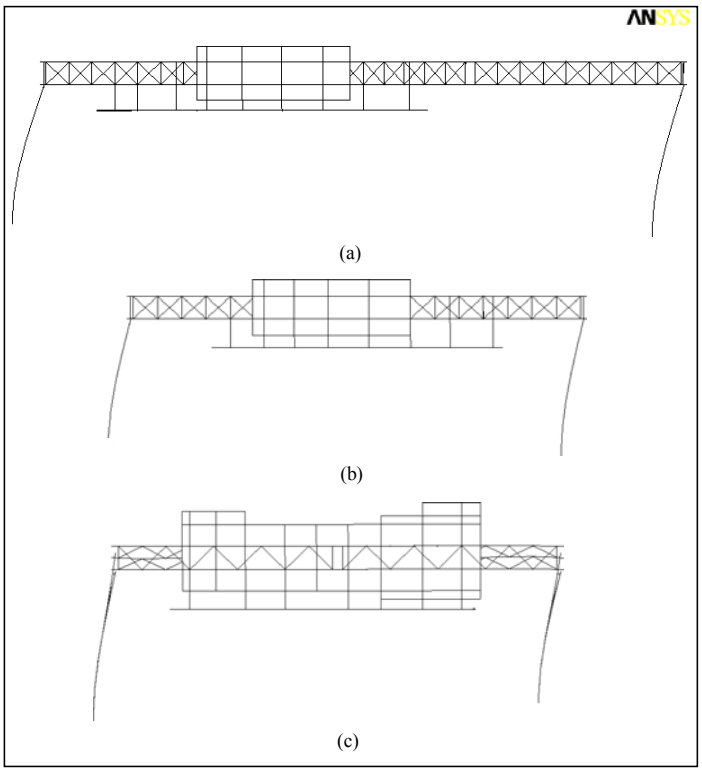

Figure 3.15: First Vibrational Mode Shape from Modal Analysis for Structures Studied with "Fixed" Bases: (a) S-40-404; (b) S-67-402; (c) S-40-156 (Ginal 2003).

The very small natural frequency for the "pinned condition" of S-40-404 should be noted at this point. The magnitude of this frequency appeared questionably low when compared to a similar structure (S-67-402). Details regarding dimensions of both structures are given in *Appendix A*.

As mentioned previously, the fundamental natural frequencies of S-67-402 given in Table 3.5 were obtained from an FE model that included "special" base plate modeling at one of the vertical uprights. The FE model was "adjusted" in order to remove these "special" modeling considerations for the qualitative comparison. A model was constructed for this structure that would allow true "fixed" and "pinned" base plate conditions. The modified structure yielded the following fundamental frequencies for the varying support conditions: fixed – 0.986 Hz; and pinned – 0.103 Hz. Table 3.5 shows that S-40-404 has fundamental frequencies of 0.802 Hz and 0.069 Hz for the fixed and pinned support condition, respectively.

Ginal (2003) validated the results of the modal analysis conducted using simplified single degree of freedom (SDOF) analogies. This small analytical study also suggested that the support conditions used for the analytical models have little influence on dynamic behavior as it pertains to the present study. Therefore, "fixed" supports were used in all three analytical models (an exception was the special base plate modeling in S-67-402), which are believed to give a similar dynamic response to "pinned" bases and any level of support stiffness in-between. A field inspection of each support structure revealed fully grouted base plates for most structures (an exception is the uprights near the roadway median for S-67-402), which further validated the use of "fixed" supports.

As mentioned above, each structure's in-service support conditions were observed during a field inspection. From this inspection it was noted that most of the sign support uprights were attached to fully grouted base plates. However, the inspection of sign bridge S-67-402 revealed one of its uprights as having fully grouted base plates while the base plates of the other included anchor bolts stand-off heights of approximately three inches (refer to Fig. 3.16). The unique base plate condition of this structure motivated the inclusion of the base plates and anchor bolts in the analytical model to evaluate stresses in the anchor rods. The base plate was modeled with a relatively fine mesh of SHELL63 (SAS 2000a) elements and the anchor rods were modeled with BEAM4 (SAS 2000a) elements. Figure 3.17 illustrates the special modeling conditions. The spatial beam and 3D shell elements were "married" in the analytical model using constraint equations that define *rigid regions*. Ginal (2003) carried out an analytical study to verify the validity of the constraint equation modeling. This effort illustrated that the constraint equations could adequately capture anchor rod axial loading distributions.

Figure 3.16: In-Service Base Plate Condition of Sign Bridge S-67-402 (Ginal 2003).

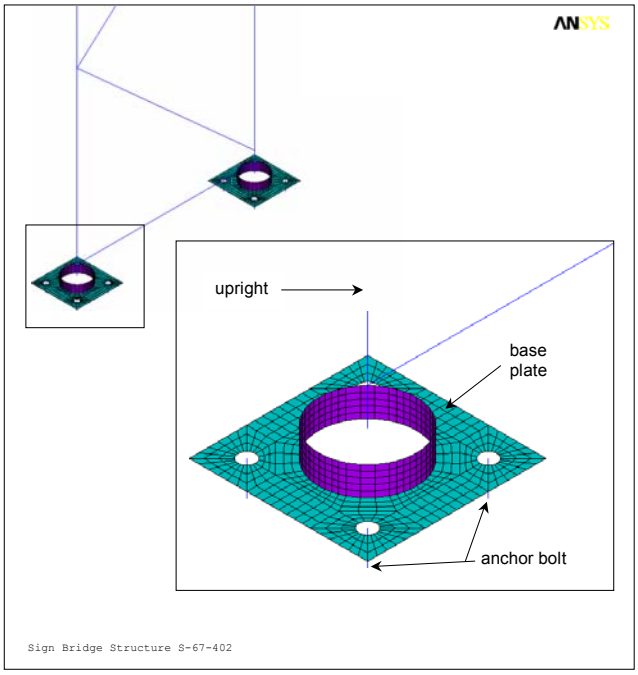

Figure 3.17: Analytical Base Plate Condition for Sign Bridge S-67-402 (Ginal 2003).

3.2.4 Damping Assumed in the FEA

One final aspect of the analytical model development requires discussion is damping. Studies have shown that most auxiliary highway structures, including cantilevered sign support structures (refer to Chapter 2), have relatively low levels of damping (*e.g.* ≤ 5 % of critical). Therefore, damping will not significantly affect the natural frequencies of the test group structures. However, determining an accurate level of damping, regardless of its magnitude, is an important aspect to consider when evaluating the fatigue life of a structure. It is important to include an accurate level of damping in these analytical models in order to generate accurate stress histories for subsequent fatigue life estimations.

ANSYS (SAS 2000a) utilizes classical (Rayleigh) damping with user-defined quantities. Rayleigh damping is an experimentally supported technique for constructing a classical damping matrix for transient analysis of multiple degree of freedom (MDOF) systems. Classical damping for a MDOF system can be assumed to consist of two parts: (1) a portion proportional to mass; and (2) a second portion proportional to stiffness. Rayleigh (classical) damping attempts to combine these two damping components into a single damping matrix while ensuring reasonable (averaged) values for damping in all modes contributing significantly to the response of the system. The single damping matrix is written as,

$$\mathbf{C} = \alpha\mathbf{M} + \beta\mathbf{K} \tag{3.1}$$

where, $\mathbf{M}$ and $\mathbf{K}$ are the system's mass and stiffness matrices, respectively, and α and β are the mass and stiffness matrix multipliers generated in a manner such that a target damping ratio is present (approximately) over a user-defined range of vibration modes.

The coefficients α and β are determined using specified damping ratios ζ_i and ζ_j for the *i*th and *j*th vibrational modes from the following equation:

$$\frac{1}{2}\begin{bmatrix} 1/\omega_i & \omega_i \\ 1/\omega_j & \omega_j \end{bmatrix}\begin{Bmatrix} \alpha \\ \beta \end{Bmatrix} = \begin{Bmatrix} \zeta_i \\ \zeta_j \end{Bmatrix} \tag{3.2}$$

These two algebraic equations are solved to determine the coefficients α and β. If both modes in the above equation are assumed to have the same target damping ratio, ζ, the above system of equations can be rewritten in the following two equations:

$$\alpha = \zeta\frac{2\omega_i\omega_j}{\omega_i + \omega_j} \tag{3.3}$$

$$\beta = \zeta\frac{2}{\omega_i + \omega_j} \tag{3.4}$$

Equations (3.3) and (3.4) were used to calculate the appropriate mass and stiffness matrix multipliers for use in the subsequent dynamic time history analyses.

The time history analysis used as the basis for fatigue life estimations requires that Rayleigh (classical) damping coefficients computed using equations (3.3) and (3.4) include aerodynamic damping contributed by the supported sign moving through the air. Aerodynamic damping ratios were calculated at each mean wind speed considered in the analytical study. Static analyses were performed to determine the appropriate mass and stiffness to be used in the aerodynamic damping ratio calculations. The mass of the entire structure was used in the calculations in order to give a somewhat conservative response (*i.e.* smaller value of ζ_a). The stiffness of each model was determined by placing a 1000-lb. load at a node near the center of the supported sign area, recording the average deflection at that location, and then

dividing by the load magnitude. Table 3.6 contains the parameters used to calculate the aerodynamic damping ratios for each model using the procedures discussed previously in Chapter 2.

Table 3.6: Parameters Used to Compute Aerodynamic Damping Ratios for Sign Support Structures (Ginal 2003).

Parameter	S-40-156	S-40-404	S-67-402
Sign Area, A (ft^2)	495	221	221
Mass, m (lb-s^2/ft)	266.04	552.59	394.14
Stiffness, k (lb/ft)	100,487	71,728	136,907

Using the structural parameters contained in Table 3.6 for each of the structures, aerodynamic damping ratios for each mean wind speed considered in the fatigue-life estimation were computed. Table 3.7 contains the contribution of aerodynamic damping at each mean wind speed.

Table 3.7: Aerodynamic Damping Coefficients Associated with Mean Wind Speeds Used in the Transient FE Analysis (Ginal 2003).

Mean Wind Speed $\bar{U}$ (mph)	Aerodynamic Damping, $[\zeta_a]_{\bar{U}}$		
	S-40-156	S-40-404	S-67-402
5	0.00100	0.00052	0.00045
10	0.00200	0.00104	0.00089
15	0.00301	0.00156	0.00134
20	0.00401	0.00208	0.00178
25	0.00501	0.00260	0.00223
30	0.00601	0.00312	0.00268
35	0.00701	0.00364	0.00312
40	0.00801	0.00416	0.00357
45	0.00902	0.00468	0.00401
50	0.01002	0.00520	0.00446

It is apparent that the aerodynamic damping resulting from the supported signs results in relatively large increase in total damping of the system. The literature review indicated that the amount of inherent structural damping assumed in these structures is 0.4 % of critical damping (*i.e.* $\zeta_s = 0.004$). Aerodynamic damping will significantly increase the damping in each structure when along-wind response is considered. For every 5 mph increase in mean wind speed, the total damping ratio for sign bridge S-40-156 increases by 25%, and the total damping ratio for sign bridges S-40-404 and S-67-402 increases by approximately 15%. This added damping has a significant influence on the response of these structures during sustained turbulent wind.

The target damping ratios for each structure are required at each mean wind speed considered in the transient analysis. The total damping is made up of two components: (a) inherent structural damping; and (b) aerodynamic damping corresponding to the mean wind speed considered. The total damping ratio can be computed using,

$$\zeta_T = \zeta_s + [\zeta_a]_{\bar{U}} \tag{3.5}$$

The damping ratio given by equation (3.5) is then used to compute the Rayleigh damping coefficients using equations (3.3) and (3.4). The present study established Rayleigh damping coefficients averaged over vibration modes 1 through 5.

3.2.5 Truck-Induced Wind Pressure

Time history analyses were conducted in which the analytical models were loaded with surface pressures and loading protocols intended to simulate truck-induced gust pressures. The transient loading used in the FE analysis was based upon the truck-pulse model described in Chapter 2 of this report. A comparison study was performed in which each analytical model's response to a single truck "event" is compared to its response to consecutive truck "events." The results of these analyses were then used to evaluate the likely fatigue damage to full-span overhead sign support structures resulting from truck-induced pressure pulses.

3.2.5.1 Single Truck Event Time History Analysis

ANSYS finite element (FE) software (SAS 2000b) was used for the time history analyses of the test group analytical models subjected to the synthesized truck pulse loading. Each model was loaded with pressures from a single truck "event" and then allowed to oscillate in free-vibration for a specified length of time after the impulse load duration. The response of each structure, including stress histories of *critical* structural members, was then recorded and evaluated.

The *typical* truck pulse developed in Chapter 2 was used to simulate the loading scenario for a single truck "event." Once the appropriate pressure magnitudes were determined for each analytical model, dynamic time history analysis was performed. These analyses consisted of loading each structure with the typical truck-induced pressure pulse, modified accordingly, and then recording the structure's response. The time history analysis consisted of the following steps:

1.) The model was subjected to a gravitational acceleration, and then allowed to settle under its self-weight.
2.) Sign and catwalk elements were loaded with surface pressures to simulate a single truck "event."
3.) After the truck pulse, the model was allowed to oscillate in free-vibration, and the response was recorded for a five second period after truck passage.

The time history analysis solution algorithm requires a non-zero gravitational acceleration be applied to the model to simulate the effects of gravity on the structure (*i.e.* self-weight). However, this is an inertial loading applied to the structure can cause oscillations producing fictitious stress ranges in the supporting members and inaccurate fatigue results. Therefore, the mass (α) and stiffness (β) matrix multipliers for Rayleigh damping were adjusted to reflect a damping ratio of 100 % of critical. This forces the model to settle under its self-weight gradually without oscillation. Figure 3.19 contains two plots of the centerline deflection for the analytical model of S-40-404.

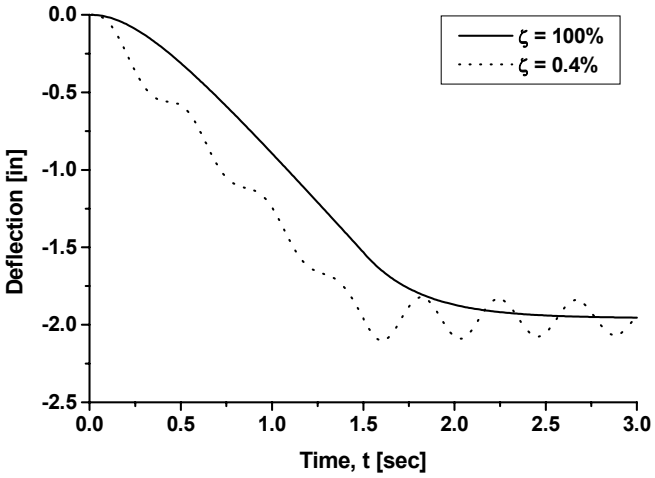

Figure 3.18: Gravity Loading Anomaly within ANSYS (Ginal 2003).

One curve shows the model ($\zeta = 0.004$) oscillating after the impulsive inertial acceleration due to gravity is applied, while the other shows the model with 100% of critical damping ($\zeta = 1.0$) gradually

approaching its centerline deflection under its self-weight. After the gravity load was applied in each analysis, the mass and stiffness matrix multipliers for damping were adjusted to reflect the actual damping of the structure.

Member forces extracted from ANSYS were then used to construct stress histories. The stress histories, $\sigma(t)_{total}$, consist of combined maximum axial and bending stresses. Axial stress, $\sigma(t)_{axial}$, and bending stress, $\sigma(t)_{bending}$, contributions were combined using simple superposition,

$$\sigma(t)_{total} = \sigma(t)_{axial} + \sigma(t)_{bending} = \frac{P(t)}{A} + \frac{M_r(t)y}{I} \tag{3.6}$$

where: $P(t)$ is the axial force on the cross-section, A is the cross-sectional area, $M_r(t) = \sqrt{M(t)_y^2 + M(t)_z^2}$ is the resultant bending moment, y is one half the outside pipe diameter, and I is the moment of inertia of the cross-section.

Stress histories were developed for *critical* members of each sign support structure. The stress histories generated for the analytical model of sign-bridge S-67-402 will be discussed in some detail. This structure supports a VMS, and the analytical model includes base plate and anchor rod modeling. This sign support structure has a relatively large volume of high-speed truck traffic passing beneath it. The stress histories of 14 *critical* members in S-67-402 were evaluated. Table 3.8 contains a brief description of these members and lists their corresponding finite element model number designations. The overhead truss chord and web members listed in Table 3.8 were selected based on their fatigue detail category (AASHTO 2001) and their large static tensile stresses relative to the other members in the model. The anchor rods were selected in order to evaluate the transfer of loading from the sign bridge superstructure to its supports.

Table 3.8: Elements Evaluated in Truck Pulse Analysis of Sign Bridge S-67-402 (Ginal 2003).

Element #'s	Description
45, 47, 48, 56	Overhead truss bottom chord members located at span centerline.
106, 124, 142	Overhead truss tension web members located near north uprights
123, 141, 159	Overhead truss tension web members located near south uprights
1815, 1817, 1818, 1820	North upright anchor rods

Figure 3.19 illustrates the location of the overhead truss web members in the analytical model. The locations of the *critical* web members in sign-bridge S-40-156 and S-40-404 are similar to those of S-67-402.

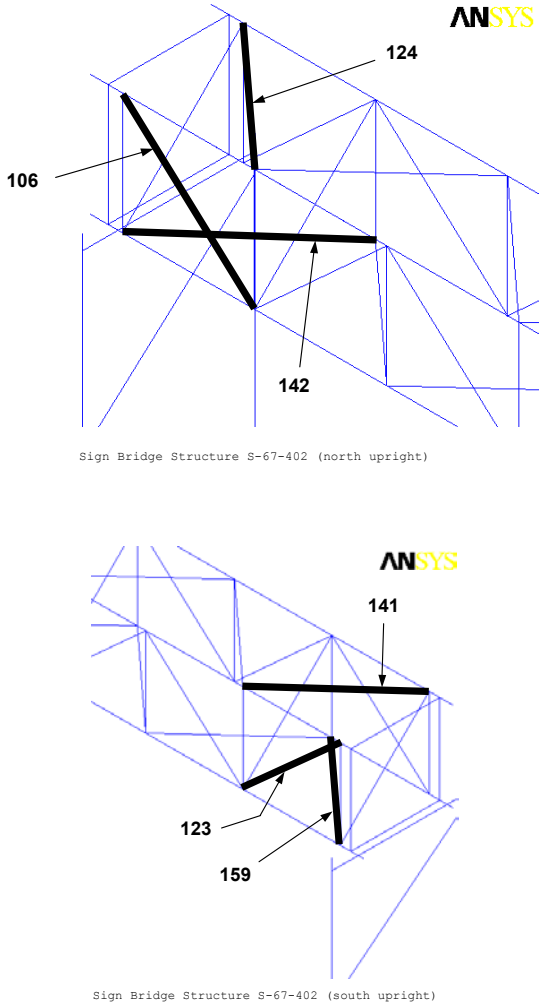

Figure 3.19: Critical Overhead Truss Web Members of Sign Bridge S-67-402 (Ginal 2003).

Figure 3.20 illustrates the anchor rods analyzed. In the truck pulse analytical study of S-67-402, equation (3.6) was used to generate stress histories for the 14 *critical* elements listed in Table 3.8 and illustrated in Figures 3.19 and 3.20. It should be noted that the stress histories generated by equation (3.6) are maximum combined normal stresses at a point along the member's cross-section at any time, t. However, the location along the perimeter of the member's cross-section where the maximum normal stress occurs depends on the relative magnitudes of the bending moment components, which vary with time. Therefore, these stress histories are not necessarily for a single point along the member's cross-section.

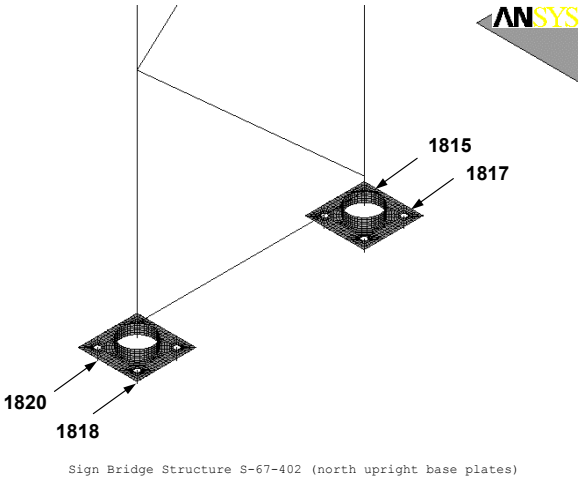

Figure 3.20: Anchor Rods in Analytical Model of Sign Bridge S-67-402 Analyzed for Truck Pulse Loading (Ginal 2003).

The location of maximum combined normal stress for each element was tracked in order to evaluate its variability. If the location varied considerably during the response, the resulting stress history would not be a valid record for evaluating fatigue life because the point of maximum tensile stress may "wander" around the perimeter of the member. Therefore, the location of maximum combined normal stress at any time was tracked using the element's local coordinate system and an angular reference. Since the members being analyzed all have circular cross-sections, the location of the maximum combined normal stress was referenced with an angle, θ. Figure 3.21 illustrates both the local coordinate system used as well as the angular reference for the pipe members and the anchor bolts.

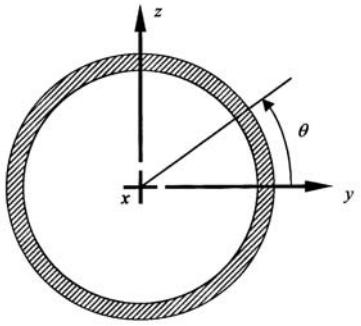

Figure 3.21: PIPE16 Local Coordinate System and Angular Reference θ (Ginal 2003).

The location of maximum combined stress normal to the cross-section was then tracked for each member by using the coordinate system in Figure 3.21 and the corresponding bending moments from the time history analyses. The location of maximum combined normal stress, $\theta(t)$, for each member was computed using the following relationships;

$$\theta(t) = \tan^{-1}\left(\frac{M(t)_z}{M(t)_y}\right) \qquad for \quad M(t)_z,\ M(t)_y\ >\ 0$$

$$\theta(t) = \tan^{-1}\left(\frac{M(t)_z}{M(t)_y}\right)\ +\ 180^\circ \qquad for \quad M(t)_z > 0,\ M(t)_y < 0 \quad or\ \ M(t)_z,\ M(t)_y\ <\ 0$$

$$\theta(t) = \tan^{-1}\left(\frac{M(t)_z}{M(t)_y}\right)\ +\ 360^\circ \qquad for \quad M(t)_z < 0,\ M(t)_y > 0$$

The above equations were used to generate frequency data for the location of maximum combined normal stress. A linear polar plot depicting the frequency count of this maximum stress at varying angles along the cross-section was then generated for each member. This plot, created for one end of element 106, is shown in Figure 3.22.

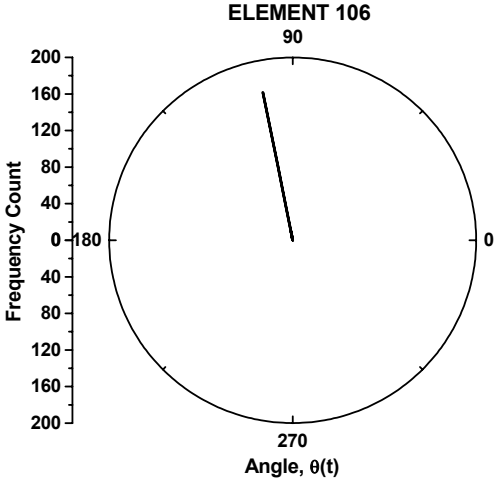

Figure 3.22: Frequency Count of Maximum Combined Normal Stress Along Cross-Section of Element 106 (Ginal 2003).

From this plot it is evident that the maximum combined normal stress occurs at virtually the same location along the cross-section perimeter during the entire stress history. Further evidence of this is shown in Figure 3.23, which is a plot of $\theta(t)$ versus time illustrating that the location of maximum combined normal stress occurs within a range of angles less than one half of a degree apart. Similar plots of the other 13 members analyzed for sign-bridge S-67-402, as well as plots made for structures S-40-156 and S-40-404, display comparable results. Therefore, the stress histories generated for each member were of a maximum state of normal stress at a single point along the cross-section perimeter and could be used to produce fatigue life predictions.

The stress histories for the *critical* members of each structure were then evaluated. A few observations were made regarding the resulting stress histories. Figure 3.24 is the recorded stress history for both ends (*i.e.* nodes i and j) of element 106 of sign bridge S-67-402 and stress history is typical of the those recorded for members in structures S-40-156 and S-40-404 as well.

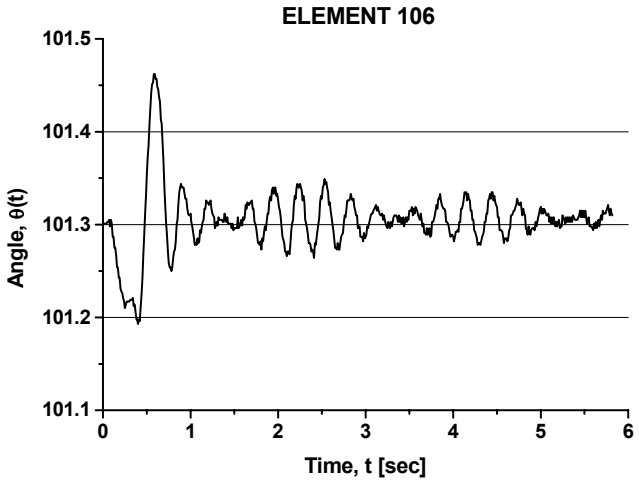

Figure 3.23: $\theta(t)$ Versus Time Plot for Element 106 (Ginal 2003).

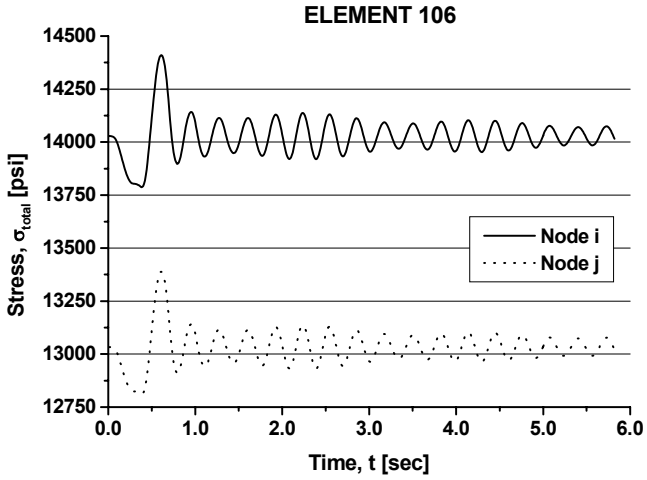

Figure 3.24: Single Truck Event Stress History for Element 106 (Ginal 2003).

A couple of general comments should be made regarding the stress history of element 106. The plot starts at a time, t, equal to zero. However, there is an additional five seconds of time preceding the data shown. During this time, gravity is applied to the structure and the structure is settling under its self-weight. The stress magnitude at the beginning of the stress history, shown above, is the static state of stress within the member. Therefore, the above stress history is oscillating about this mean stress level.

The period of time during which the truck impulse loading is applied to the structure is also obvious from the above stress history. During this loading, the member not only undergoes its largest stress range but its response is indicative of the shape of the forcing function. The frequency of the response during the loading is equal to the forcing frequency (*i.e.* $f = 1/T = 1/0.82\,\text{sec} = 1.22 Hz$), which is expected. After the load has been applied, the stress history shows evidence that the structure response begins to dampen out. As the structure oscillates in a damped free-vibration, the response takes on a new frequency. This frequency was calculated by taking the inverse of the time duration between successive peaks of the response. Using the stress history above for element 106, the frequency of the response was approximated as being equal to 3.3 Hz. This frequency is nearly equal to the natural frequency for the second modal vibration of Sign Bridge S-67-402, which was equal to 3.2013 Hz (Table 3.4). This makes sense since the truck-induced pressures are applied to the structure in a direction conducive to exciting the mode shape corresponding to this frequency.

The magnitude and quantity of the stress ranges experienced during these truck events directly affect the fatigue life of the structure. The stress history in Figure 3.24 has a large number of stress ranges. However, the magnitude of these stress ranges is relatively small. The maximum stress range for element 106 of sign bridge S-67-402 is approximately 620 psi for node i and 580 psi for node j. These maximum stress ranges occur when the load is being applied to the structure. The subsequent stress ranges are of a much lower magnitude (approximately 200 psi). Table 3.9 lists the largest, smallest, and average maximum stress ranges among the *critical* members of each of the test group sign support structures.

Table 3.9: Maximum Stress Ranges (in psi) in Test Group Structures From Truck-Induced Pressure Pulse (Ginal 2003).

Sign Bridge	Maximum Stress Range		
	Largest	**Smallest**	**Average**
S-40-156	180	30	95
S-40-404	1170	180	550
S-67-402	620	40	270

A single truck "event" produces relatively small stress ranges in the supporting members of the test group sign bridges. Consequently, a single truck pulse loading will most likely not be a source of fatigue damage for these sign support structures. However, if a sign support structure is subjected to consecutive truck-induced pressure pulses; it may produce significant stress ranges that cannot be ignored. Therefore, the present study performed time history analyses in which the test group analytical models were

subjected to 2 truck pulses back-to-back. The findings of this study and how they relate to the single truck "event" loading scenario are discussed in the next subsection.

3.2.5.2 Truck Pulse Comparative Study

The effects of consecutive truck pulse loadings were evaluated using time history analyses in which each analytical model was subjected to two consecutive pulses. After the load was applied, the structures were allowed to vibrate for a period of time while their response was recorded. As before, the results of the analysis performed on sign-bridge S-67-402 will be discussed in detail. The analysis procedure used to evaluate the structure's response to consecutive truck pulses was identical to that used for the single truck "event." Stress histories were again created for the *critical* members of the three sign bridges. Figure 3.26 illustrates both of these stress histories for each node of element 123 of Sign Bridge S-67-402.

Several observations were made regarding the typical element response plots characterized by Figure 3.25. The stress history from the consecutive truck pulse analysis shows the maximum stress ranges occur when the load is being applied to the structure. After the load is applied, the structure again oscillates with much smaller stress ranges as the vibration dampens out. A comparison between the two stress histories in Figure 3.25 shows a relationship between the number of truck pulses in the time history analysis and the number of maximum stress ranges in the response. The figures also illustrate that the stress histories resulting from a single truck "event" and multiple truck "events" do not affect the magnitudes of the largest stress ranges imparted to the structural components.

These findings were typical of the *critical* members of not only Sign Bridge S-67-402 but also structures S-40-156 and S-40-404. Therefore, the cumulative number of maximum stress ranges resulting from any number of consecutive truck "events" can be determined by multiplying the results from the single truck "event" analysis accordingly. This is useful when evaluating the fatigue performance of these structures based upon the truck-pulse loading scenario. For example, assume the maximum stress range from a truck "event" is damaging. Then, to determine the yearly damage accumulated by the structure based only on this loading, calculate the damage of one count of this maximum stress range and then multiply it by the number of truck "events" the structure is likely to see in a year.

3.2.5.3 Fatigue Damage Due to Truck-Induced Pressure

Results from the analytical study were used to assess the level of fatigue damage caused by truck traffic. Maximum stress ranges from the stress histories of each test structure's analytical model subjected to a single truck event were used to quantify fatigue damage.

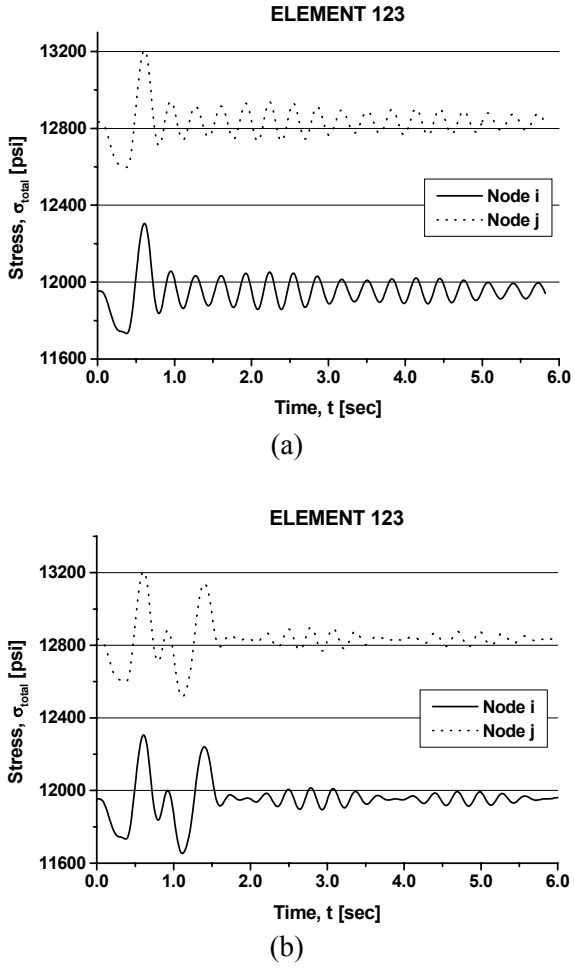

Figure 3.25: Stress Histories for Element 123 in Sign Bridge S-67-402: (a) A Single Truck "Event"; (b) Consecutive Truck "Events" (Ginal 2003).

The time history analyses for the truck-induced pulse loading facilitated computation of maximum stress ranges occurring at *critical* members in each structure. The largest, smallest, and average values of these maximum stress ranges were presented in Table 3.9. It was noted that the largest maximum stress range that occurred in any of the models was 1170 psi, and the next largest was 620 psi. The Constant Amplitude Fatigue Limit for an *ET* fatigue detail, which is the most fatigue sensitive detail in overhead sign support structures, is 1200 psi. Therefore, the largest maximum stress range recorded in this study that is attributed to truck-induced pressure pulses is below this limit. The average maximum stress range out of all the maximum stress ranges of the *critical* members from the three models was 310 psi.

Stress ranges below one half the CAFL, based on a 95% confidence level, are not considered damaging and can be excluded from any fatigue life analysis, regardless of the maximum stress range from the stress history (AASHTO 1998) If a structural detail undergoes a maximum stress range that is below the CAFL, fatigue would not govern the service life of that detail (AASHTO 1998). This

information, along with the maximum stress ranges listed in the previous paragraph; might suggest that truck-induced pressure pulses are not a source of fatigue damage in the full-span overhead sign support structures examined. However, one must recognize that truck-induced pressure pulses are not the only loadings that sign support structures are subjected to. Other sources of loading, such as natural wind, do cause stress ranges greater than the CAFL. Therefore, the only stress ranges that can be ignored in a fatigue life prediction, or that can be assumed to cause no damage, are those stress ranges below one half the CAFL.

Sign bridges S-40-156 and S-67-402 experience a maximum stress range, as a result of a truck-induced pressure, of 180 psi and 620 psi, respectively. These maximum stress ranges occurred in *critical* members of the corresponding structure, which are classified as category *ET* fatigue details and have a CAFL of 1200 psi. Therefore, in order for stress ranges resulting from truck-induced pressure pulses to be ignored for a fatigue life evaluation, they must be below one half the CAFL, which is 600 psi. The maximum stress range in Sign Bridge S-40-156 is clearly below this limit and, therefore, this particular loading scenario was not considered in this structure's fatigue assessment. The maximum stress range in S-67-402, resulting from a truck-induced pressure pulse, was just above the threshold limit of 600 psi. However, given the approximate nature of the present study as well as the method used to formulate the truck pulse loading, it was concluded that pressure pulses resulting from truck traffic are not a source of fatigue damage in S-67-402. Therefore, in the fatigue life predictions of sign bridges S-40-156 and S-67-402, stress ranges resulting from truck-induced pressure pulses were not considered damaging and were ignored.

Sign bridge S-40-404 will undergo a maximum stress range of 1,170 psi when loaded with a truck-induced pressure pulse. Similar to the aforementioned sign bridges, this maximum stress range occurs in a *critical* member that is classified as a category *ET* fatigue detail. However, unlike the test group sign bridges discussed above, the maximum stress range in S-40-404 is considerably greater than the cut-off limit of one half the CAFL for this particular detail. Therefore, in the fatigue evaluation of S-40-404, truck-induced pressure pulses should be considered. However, stress ranges resulting from truck-induced pressure pulses were ignored in the fatigue life predictions of this structure as well. The following discussion supports this decision.

Sign support structure S-40-404 is located over a roadway that does not experience high-speed truck traffic. This sign bridge is located over the westbound lanes of the "Airport Spur" near Milwaukee County's Mitchell Field, which has a posted speed limit well below highway limits, and very low truck traffic volume. Consequently, a relatively small number of trucks pass beneath this structure every year, and the ones that do are traveling at a speed well below that of the test trucks from Cook *et al.* (1996),

which were used to develop the typical truck pulse loading. Therefore, the truck-induced pressure pulse loading experienced by sign bridge S-40-404 will be of a much smaller magnitude than the loading for sign bridges S-40-156 and S-67-402. As a result of this smaller magnitude loading, stress ranges that will develop in *critical* members of sign bridge S-40-404 will likely fall below one half the CAFL and will not be considered damaging.

While ignoring stress ranges resulting from truck-induced pressure pulses in the fatigue evaluation of sign bridge S-40-404 is debatable, it is not correct to ignore this type of loading in sign bridges of a similar configuration, supported sign type, and span length, which may be located over roadways that have a high truck traffic volume and a posted speed limit of 55 mph or greater. Fatigue life predictions of such structures would need to include fatigue damage caused by truck-induced pressure pulses. Using Sign Bridge S-40-404 as an example, the following paragraphs describe one way to quantify the fatigue damage caused by truck-induced pressure pulse.

The structure's maximum response to the truck-induced pressure pulse loading is a stress range of 1,170 psi in a *critical* member that is an ET fatigue detail category. Truck traffic can be either visually counted or mechanically counted at the location of the structure for a given period of time. This data can then be used to estimate Average Daily Truck Traffic (ADTT) at the site, which can then be extrapolated to reflect population growth. The other method is to simply use ADTT values for bridges from the AASHTO Specification (AASHTO 1996). For this example, ADTT values will be taken from AASHTO since no available truck traffic data exists for Sign Bridge S-40-404.

ADTT is determined as a percentage of average daily traffic (ADT), which includes all vehicles. Under "normal conditions" the ADT for a single lane of traffic is physically limited to 20,000 vehicles (AASHTO 1996). This limiting value will be used to calculate the ADTT beneath S-40-404. Depending on the classification of the highway (*e.g.* urban), 10% to 20% of this value is considered truck traffic. In this example it will be assumed that the "highway" is classified as an "Urban Interstate". Therefore, 15% of the ADT value constitutes truck traffic, which is equal to 3,000 trucks per day. The yearly fatigue damage of Sign Bridge S-40-404 attributed to truck-induced pressure pulses can now be calculated as outlined below (Ginal 2003).

Given:
AASHTO Fatigue Detail Category ET with a 95% confidence level; $A = 1.30x10^{8}$ *;* $m = 3.0 ksi/cycle$ *;*

$$S = 1.17 ksi \;\&\; n = 3000\frac{cycles}{day}\cdot 365\frac{day}{year} = 1.095x10^{6}\frac{cycles}{year}.$$

Compute:
Yearly damage expected from truck traffic using linear damage accumulation..

Solution:

$$NS^m = A \qquad N = AS^{-m}$$

$$N = \left(1.30\,x10^8\right)\cdot\left(1.17\right)^{-3.0} = 8.117\,x10^7\,cycles$$

$$D = \frac{n}{N}$$

$$\therefore D = \frac{1.095\,x10^6}{8.117\,x10^7} = 0.013 = 1.3\%\ damage/year$$

From the above calculation it appears as though the truck-induced pressure pulse causes very little damage to the structure each year. To put it into perspective, if the truck-induced pressure pulse was the only loading applied to the structure over its entire service life, the structure would have a 5% chance of failing (*i.e.* 95% confidence level) after 77 years $\left(100\%/1.3\% = 76.9 \approx 77\right)$. As expected, for decreased confidence levels the yearly damage also decreases. For confidence levels of 70% and 50%, the yearly damage will be 0.79% and 0.62%, respectively. It should be noted that the CAFL for these decreased confidence levels was not adjusted but rather was left at the value corresponding to the 95% confidence level curve.

While it is obvious that these yearly damage percentages are rather small on their own, they become quite significant when considered in the entire fatigue assessment of the structure. For example, assume a sign bridge experiences a *total* yearly damage, including truck and wind loading, of 10% based on a 95% confidence level. This 10% yearly damage suggests that there is a 5% chance that the structure will have a fatigue life of 10 years $\left(100\%\ damage\cdot 1 year/10\%\ damage = 10 years\right)$, or less. Of this 10% yearly damage, the portion attributed to truck-induced pressure pulses is over 10% $\left(1.3\%/10\% = 0.13 = 13\%\right)$. Therefore, depending upon the anticipated *total* yearly damage of a structure, the truck-induced pressure pulse appears to be a significant loading scenario to be considered in the design of certain types of full-span overhead sign support structures. The short example provided outlines the process that may be used to predict damage accumulated by truck-induced gust pressures.

3.2.7 Susceptibility to Aero-Elastic Phenomena

There are two aero-elastic wind loading phenomena that may affect sign support structures: (a) galloping; and (b) vortex shedding. Galloping is a phenomenon caused by the aerodynamic instability of a structure and vortex shedding is a wind loading phenomenon that produces resonant oscillations of a structure perpendicular to the direction of flow. The current section of the Report addresses these aero-elastic phenomena as they relate to full-span overhead sign support structures. Detailed discussion of these phenomena and the derivation of all equations used to evaluate the sign structures studied can be found in Ginal (2003).

3.2.7.1 Galloping

Galloping vibrations are an important type of self-excited response of many structures subjected to natural wind. The theory used to study galloping is attributed to Den Hartog (1956) and a good engineering introduction to the theory can be found in Blevins (1990). When a structure vibrates in a fluid (in this case air) with a steady rate of flow, the flow begins to oscillate relative to the motion of the structure. The oscillating component of the flow produces a corresponding aerodynamic force on the structure. A structure is considered aerodynamically stable if this oscillating aerodynamic force helps to dampen out the vibrations of the structure. If this force increases the vibrations of the structure, the structure is considered aerodynamically unstable. In stability analysis, if the flow separates from the cross-section of the structure, the aerodynamic force becomes a nonlinear function of the angle of flow relative to the structure. The flow-induced vibration of such structures, which are termed "bluff" bodies, is referred to as galloping.

Galloping, or aerodynamic instability, was first associated with aerodynamic coefficients of a cross-section by Den Hartog (1956). From this work, came the Den Hartog criterion for aerodynamic stability. This criterion was used and refined by subsequent research to assess the stability of numerous cross-sectional shapes. The variable message sign (VMS), which is found on an increasing number of support structures, have cross-sections presented to the wind flow that are nearly rectangular. Past research related to galloping of rectangular cross-sections and the effects of wind turbulence on the galloping of these shapes (Novak 1969, 1972; Novak and Davenport 1970; Novak and Tanaka 1974) are directly applicable to the present study. The findings of this past research and their relation to the full-span overhead sign support structures in this study are the focus of the remainder of this section.

As mentioned previously, the galloping response of prismatic structures with rectangular cross-sections (Novak 1972; Novak and Tanaka 1974) will be used to evaluate the susceptibility of full-span overhead sign support structures to galloping oscillations. More specifically, the galloping of full-span structures supporting VMS will be addressed in the context of the test group structures supporting this sign type. The galloping response of a rectangular cross-section is used because of the nearly rectangular cross-section of the VMS box. Details of these calculations can be found in Ginal (2003).

"Universal" galloping response curves of prismatic structures with a side ratio *b/h* equal to 1/2 and 2/3 have been developed (Novak and Tanaka 1974). These curves include both smooth and turbulent flow and account for wind direction. Table 3.10 lists the relative magnitude of coefficient A_1 for each of these scenarios. These coefficients help to determine the necessary conditions for susceptibility of a bluff-body to galloping.

Table 3.10: Relative Magnitude of Coefficient A_1 for Smooth and Turbulent Flow of Rectangular Cross-Sections (Ginal 2003).

b/*h* ratio	Flow	Wind Direction	A_1
1/2	smooth	$\perp b, \perp h$	$> 0 , = 0$
	turbulent		$< 0 , > 0$
2/3	smooth	$\perp b, \perp h$	$> 0 , = 0$
	turbulent		$> 0 , > 0$

From the table it is evident that the nature of the flow (smooth or turbulent) has a direct impact on the magnitude of coefficient A_1 and, subsequently, the galloping response of a system. Cross-sections with a coefficient $A_1 \leq 0$ are generally more stable than cross-sections with $A_1 > 0$. The reason for this is that galloping of these cross-sections occurs at higher onset wind velocities and requires an initial disturbance in order for galloping oscillations to develop. Table 3.10 illustrates that rectangular cross-sections with a *b/h* ratio of 1/2 and wind direction $\perp h$ becomes more susceptible to galloping when the flow is turbulent, which is the opposite of what happens to the same cross-section with wind direction $\perp b$. It should be noted that *b* is the length of the prism parallel to the wind flow and *h* is the height of the prism perpendicular to the wind flow. Therefore, it is important that the correct scenario be utilized when determining the range of onset velocities, U_{cr}, for the test group.

The onset wind velocities for galloping oscillations of sign bridges S-40-404 and S-67-402 will now be discussed. The calculations used to determine these velocities were based on the following assumptions (Ginal 2003):

1. These structures are subjected to natural wind with a turbulence intensity of approximately 11%;
2. The aerodynamic characteristics of a VMS are similar to that of a rectangular cross-section with $b/h = 1/2$ and wind direction $\perp h$ (the actual cross-section of a VMS is trapezoidal with $b_1/b_2 = 1.19$ and $b_{avg}/h = 1/2.28$);
3. The vertical mode shape of these sign bridges can be modeled as a SDOF oscillator (the total mass of the VMS and catwalk and 50% of the mass of the overhead truss portion of the structure was assumed to participate in this mode).

With the sign bridge modeled as an SDOF oscillator, the onset wind velocity U_{crit} for galloping can be expressed as (Ginal 2003),

$$U_{crit} = \frac{8\pi m f \zeta \bar{U}}{\rho h l} \tag{3.1}$$

where: ρ is the density of air; h is the broad side (perpendicular to the wind stream) dimension of the prism (VMS); l is the length of the prism (VMS); m is the mass of the equivalent SDOF system; ζ is the damping ratio; f is the natural frequency (Hz); and $\bar{U}$ is the mean wind velocity.

Equation (3.1) was used to determine the onset wind velocities for galloping oscillations of sign bridges S-40-404 and S-67-402. From a modal analysis of these two structures, it was found that the third mode shape of Sign Bridge S-40-404 and the fourth mode shape of Sign Bridge S-67-402 are vertical modes of the overhead truss span. These mode shapes are illustrated in Figure 3.26. It should be noted that these mode shapes have a torsional component due to the eccentric mass of the VMS and catwalk. However, this coupling effect was not considered. Instead, it was assumed that these structures can be accurately modeled with a SDOF oscillator. The mass of the structure assumed to contribute in the modal vibrations being considered consisted of the total mass of the supported sign and catwalk and 50% of the mass of the overhead truss portion (Ginal 2003).

Table 3.11 lists all of the parameters used to calculate the onset wind velocities for both sign bridge S-40-404 and S-67-402. The following ranges for onset wind velocity of galloping were then calculated:

S-40-404: $219 \le U_{cr} \le 297$ (mph)

S-67-402: $475 \le U_{cr} \le 646$ (mph)

It should be noted that the lower bound velocities require initial amplitude to incite galloping. One might argue that a truck-induced gust pressure could "set off" galloping oscillations. However, the critical speeds are far above feasible wind speeds for anything, but tornado events.

A few comments regarding the onset wind velocities calculated above are in order. First, these values are an approximation of the wind speed required for aerodynamic instability (galloping) of these structures. From the previous discussion, it is apparent that galloping of prismatic structures is sensitive to very particular circumstances. A number of parameters need to be aligned in order for galloping to occur. Therefore, numerous assumptions were made in order to attain the above values for onset wind velocity, which can only be verified with a wind tunnel study of these structures. However, the above values provide a good estimate of the onset wind velocities for these structures as well as for similar full-span structures supporting VMS. It is obvious that wind speeds of these magnitudes are not probable.

Therefore, it was concluded that galloping does not need to be considered as a possible loading scenario for these structures.

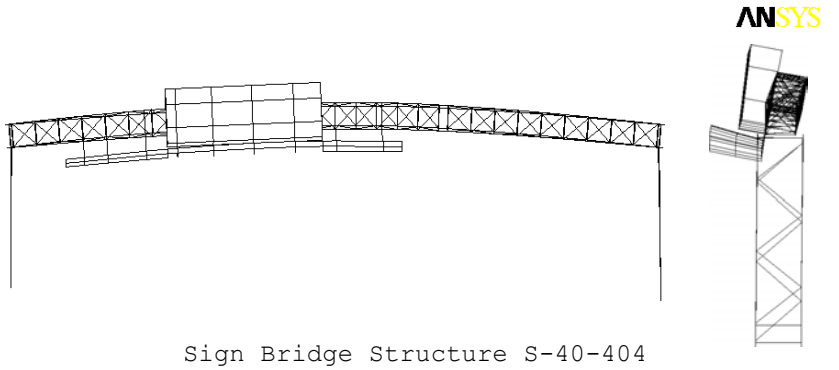

Sign Bridge Structure S-40-404

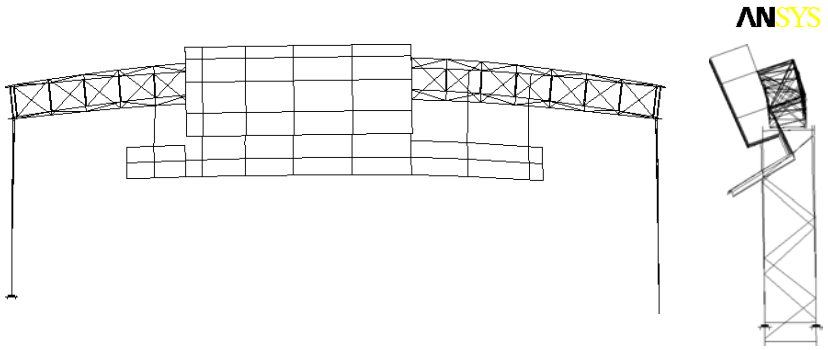

Sign Bridge Structure S-67-402

Figure 3.26: Mode Shape 3 of Sign Bridge S-40-404 (f = 2.355 Hz) and Mode Shape 4 of Sign Bridge S-67-402 (f = 6.289 Hz) (Ginal 2003).

Table 3.11: Parameters Used to Calculate Onset Wind Velocity U_{cr} for Sign Bridge S-40-404 and S-67-402 (Ginal 2003).

Structure	m $(slug)$	f (Hz)	ζ	ρ_{air} $(slug/ft^3)$	h (ft)	l (ft)
S-40-404	338.5	2.355	0.004	2.377 e-3	7.5	24.1
S-67-402	275.3	6.289	0.004	2.377 e-3	7.5	24.1

Before moving on to vortex shedding, the magnitude of the turbulence intensity assumed in the galloping sensitivity study (11%) should be qualified within the context of the natural environment in which the sign support structures reside. Turbulence intensity tends to vary with height above the earth's surface and can be defined as (Dyrbye and Hansen 1997),

$$I_u(z) = \frac{\sigma_u(z)}{U(z)} \tag{3.2}$$

where: $\sigma_u(z)$ is the standard deviation of the turbulent component of the wind, u, at height z; and $U(z)$ is the (smooth) mean wind velocity at height z. Thus, the turbulence intensity can be thought of simply as the magnitude of the variation in turbulent wind relative to the smooth (mean) wind. Higher turbulence intensity implies higher variation. A turbulence intensity of zero is smooth flow.

The turbulence intensity relationship can be simplified somewhat to allow values of turbulence intensity to be computed for (essentially) flat terrain with varying obstructions (*e.g.* buildings, trees). If flat terrain is assumed, the turbulence intensity can be written as (Dyrbye and Hansen 1997),

$$I_u(z) = \frac{1}{\ln\left(z/z_o\right)} \tag{3.3}$$

where: z_o is defined as the roughness length. The roughness length varies with the condition of the flat surface. For example, if the terrain is flat and open with no vertical obstructions, the surface roughness can be given by $z_o \approx 0.01$ m, while flat terrain with forested surface may give $z_o \approx 0.3$ m (Dyrbye and Hansen 1997).

These two extremes for surface roughness allow boundaries for turbulence intensity values to be computed. If we assume that the mid-height of the VMS "box" is located at 21.75 feet (6.63 m) above the earth's surface, the turbulence intensity can be expected to lie in the following range:

$$0.15 \text{ (smooth, flat)} \le I_u(z) \le 0.32 \text{ (rough, flat)}$$

The sign structures considered in this study are located over interstate highways, which can be considered as an open smooth corridor for wind flow. Therefore, these structures will tend to be subjected to wind turbulence intensity in the 15% range. This value is close to the 11% value assumed in the qualitative galloping study.

3.2.7.2 Vortex Shedding

Vortex shedding-induced vibrations of a structure occur when wind vortices are shed alternately from opposite sides of a "bluff" body presented to the wind flow. The shedding of these vortices is primarily dependent upon the cross-section of the structure. However, the motion of the structure and the nature of the flow (*i.e.* Reynolds number, Re) affect the shedding of vortices for certain cross-sectional shapes. Ginal (2003) contains detailed discussion of the factors that affect vortex shedding susceptibility. The present discussion will focus on applying the engineering theory of vortex shedding to evaluate a sign support structure's susceptibility to this aerodynamic phenomenon.

Lock-in wind velocities were determined for each of the three structures in the test group. These velocities were evaluated for the shedding of vortices off the structural members and/or supported sign. Since the structural members in the support trusses are circular tubes, the Strouhal number for a circular cross-section was used for these members. The VMS box was again modeled as a rectangular cross-section with a base-to-height ratio equal to 1:2. A Strouhal number for an appropriate rectangular section was used to study vortex shedding of the wind stream off of the VMS box.

Past research has found that the Strouhal number for a "bluff" body with a circular cross-section varies with Reynolds number. A Strouhal number equal to 0.20 was used to calculate "lock-in" velocities for the sign bridge structural members. This value is commonly accepted for circular cross-sections with a Reynolds number in the range of 10^3 to 10^5. When calculating "lock-in" velocities, the Reynolds number was checked to validate using the Strouhal number mentioned previously.

Research has also found that the relationship between Reynolds number and Strouhal number is not important for sharp-edged cross-sections (including rectangular bodies). The reason for this is that the "sharp" edges provide definitive points for flow separation from the "bluff" body, which is conducive for the shedding of vortices. Instead, the Strouhal number for a rectangular cross-section is a function of the ratio between the depth and width of the section. Figure 3.27 illustrates this relationship.

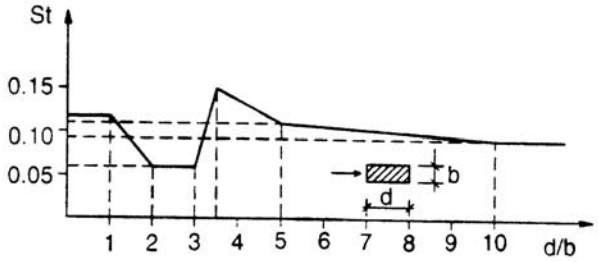

Figure 3.27: Strouhal Number for Rectangular Cross-Sections (Dyrbye and Hansen 1997).

The depth-to-width ratio of the rectangular cross-section representing the VMS is 1/2. Therefore, a Strouhal number of 0.12 was read from the plot in Figure 3.27 and used in the subsequent calculations.

Vortex shedding "lock-in" velocities were first calculated for the overhead truss members of each sign bridge. The parameters used to calculate "lock-in" velocities for each structure are listed in Table 3.12. The Reynolds numbers listed in Table 3.12 are within the appropriate range discussed previously to allow a Strouhal number of 0.20 to be used. It is apparent that the "lock-in" velocities are relatively small. These wind speeds can be converted to wind pressures using the following equation:

$$p = \frac{1}{2}\rho C_L U_{cr}^2 \tag{3.4}$$

where: ρ is the density of air; and C_L is the life coefficient. These wind pressures can then be converted to a force applied to the structure by multiplying by the projected area of the truss chord members. For example, Sign Bridge S-40-156 has three chords that are 67 feet in length and 0.46 feet in diameter. Therefore, with a lift coefficient equal to 1.0 (conservative), the pressure is calculated as,

$$p = \frac{1}{2}\left(0.00238\frac{\text{lb-s}^2}{\text{ft}^4}\right)(1.0)\left(19.2\frac{\text{ft}}{\text{s}}\right)^2 = 0.44\ psf$$

and, if one assumes that all three of the chord members are subjected to shedding vortices, the total resultant force is,

$$F_L = p \cdot A_{proj} = (0.44\ \text{psf})(3)(67\ \text{ft})(0.46\ \text{ft}) = 40.5\ lbs$$

This magnitude of force is much less than the self-weight of the structure itself. The above calculation and the small "lock-in" velocities listed in Table 3.12 are evidence that vortex shedding off of the support members for these sign bridges is not an issue for design.

Table 3.12: Vortex Shedding Parameters and "Lock-In" Velocities for Circular Tube Members of the Test Group Structures (Ginal 2003).

Structure	f (Hz)	St	D (ft)	ν ft/s	Re	U_{cr} (mph)
S-40-156	8.385	0.20	0.46	1.61 e-4	55,000	13.1
S-40-404	2.355	0.20	0.55	1.61 e-4	22,000	4.4
S-67-402	6.289	0.20	0.38	1.61 e-4	28,000	8.1

Next, "lock-in" velocities were calculated for the VMS of Sign Bridge S-40-404 and S-67-402. The parameters used to calculate these "lock-in" velocities, as well as the corresponding velocities, are listed in Table 3.13. It is obvious that the "lock-in" velocities are not in the range of probable wind speeds these structures will experience while in-service. Therefore, calculating a corresponding alternating force due to vortex shedding is not necessary for these types of structures.

3.2.8 Fatigue Damage Resulting from Natural Wind

This section discusses the analytical study of the test group structures subjected to wind pressures generated from simulated wind histories. In this study, dynamic time history analyses were conducted in which each analytical model was loaded with surface pressures generated by simulated wind records of

five seconds in duration. An in-depth discussion of the procedure used to conduct these analyses is provided as validation of the subsequent results of this study. Results for *critical* members in each structure are discussed so that they may be applied directly to the fatigue analysis. These results will also serve as indicators of the probable response of these and similar types of full span overhead sign support structures to natural wind loading.

Table 3.13: Vortex Shedding Parameters and "Lock-In" Velocities for VMS Supported by S-40-404 and S-67-402 (Ginal 2003).

Structure	f (Hz)	St	D (ft)	ν ft/s	Re	U_{cr} (mph)
S-40-404	2.355	0.12	7.5	1.61 e-4	6.9 e6	100.4
S-67-402	6.289	0.12	7.5	1.61 e-4	1.8 e7	268.0

ANSYS finite element (FE) software (SAS 2003a,b) was used to conduct time history analyses of the test group analytical models subjected to surface pressures from simulated wind histories. Each analytical model was subjected to 5-second simulations consisting of mean wind speeds ranging from 5 to 50 mph in 5 mph increments. The parameters used for each simulation were set to reflect the structure's actual in-service conditions. The range of mean wind speeds and the increment interval utilized in this analysis were determined using statistical data. Although there is a non-zero probability that all of the test group structures will experience wind speeds greater than 50 mph, the available statistical data indicates that these speeds constitute only a fraction of a percent of the in-service wind conditions. Therefore, it was felt that the above range of mean wind speeds enveloped the majority of probable wind loading scenarios for these structures and that it would be sufficiently accurate for the engineering analysis to assume that these wind speeds contributed the majority of damage to the fatigue-sensitive details.

Variable pressure loadings used in the time history analyses were established from the simulated wind records. Simulated wind speed histories were converted to pressures using (AASHTO 2001):

$$p(t) = \frac{1}{2}\rho C_d \left(U(t)\right)^2 \tag{3.5}$$

where, ρ is the density of air; C_d is the drag coefficient; and $U(t)$ is the combined mean and turbulent wind speed.

In the FE analyses, wind pressures were only applied to the sign elements. Pressures were not applied to the supporting structural members. This decision was based upon a comparison of the surface

area of the supported sign and the available surface area of the supporting structural members. For each of the three structures, the supported sign surface area constituted a much larger percentage of the total surface area available to wind loading. Therefore, in each analysis only the supported sign was loaded with wind pressures.

The drag coefficient, C_d, in equation (3.5) above is dependent upon the cross-section being loaded. The current design standards (AASHTO 2001) have tabulated values of the drag coefficient for various cross-sectional shapes. Since only the supported sign was loaded in the FE analyses, appropriate drag coefficients were determined based on the supported sign type and/or dimensions. Table 3.14 lists the drag coefficient used in the analysis of each test group sign support structure.

Table 3.14: Drag Coefficient, C_d, for Supported Sign of Test Group Structures.

Structure	Supported Sign Type	C_d
S-40-156	Type I	1.20
S-40-404	VMS	1.70
S-67-402	VMS	1.70

Once the appropriate drag coefficients were determined for each structure, wind pressure simulations were generated. Figure 3.28 illustrates time-varying wind pressures for the 10 wind simulations used in the analysis of S-40-404.

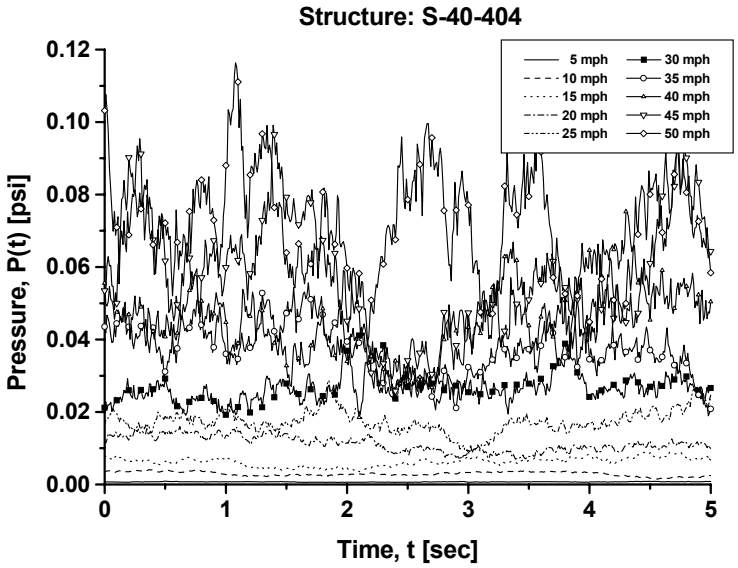

Figure 3.28: Pressure versus Time Plots used in Time History Analyses of Sign Bridge S-40-404 (Ginal 2003).

A few observations were made regarding these plots. First, the pressure magnitudes depicted in Figure 3.28 are reasonable for the range of wind speeds being simulated. Also, the wind simulations with higher mean wind speeds are qualitatively more turbulent than those simulations with lower mean wind speeds. This translates into larger pressure fluctuations in the higher mean wind speed simulations. This is also reasonable based on the specific wind spectrum being used in the simulations and observations of wind conditions at various speeds.

The time varying pressures computed using equation (3.5) can be incorporated into the previous discussed procedure for fatigue life predictions for the critical components of the sign support structures considered. The basic procedure described in chapter 2 of the report has some subtle modifications that will be discussed when each structure type (*e.g.* sign support, or high-mast luminaire support) is considered.

In the analytical wind load study discussed above, wind surface pressures were applied to the supported sign in only one direction (*i.e.* the front surface). However, the fatigue analysis considered wind applied to both the front and back surfaces of the supported sign. Ginal (2003) conducted a detailed study of the effect that wind direction had on the forces within the critical members in structures S-40-404 and S-67-402. The results of this study indicated that the wind pressures could be applied to the front of the sign structure and the number of stress-cycles resulting from this loading application could be used to account for wind loading from opposite directions (*e.g.* North and then South). Structure S-40-156 was shielded by a bridge structure and therefore only the front-face of the sign was loaded.

3.2.8.1 Structure S-40-156

The first structure for which a detailed fatigue analysis was performed was S-40-156 shown in Figure 3.9. This structure is a tri-chord support truss that has a significant signage area. A preliminary survey of the structure was undertaken to identify the important fatigue-critical details and the associated members that contained these details. Table 3.15 contains a listing of the elements deemed critical for future examination and consideration in the fatigue analysis.

The members contained in Table 3.15 include all fatigue detail categories found in Table 2.8. Figure 3.29 illustrates the locations of the critical members of Table 3.15 within the tri-chord truss structure. Members 41 and 65 are located near the mid-span of the truss structure and are located adjacent the flange-plate coupler connections used to splice segments of the truss together. Members 40 and 83 are chord members, with member 83 being the member subjected to the worst tensile stress due to wind loading on the sign and member 40 being subjected to the highest tensile stresses under gravity loading. The remaining members in the truss are diagonal members.

Table 3.15: Elements Evaluated in Wind Load Analysis of Sign Bridge S-40-156 (Ginal 2003).

Element Numbers	Description
40, 41, 65, 83	Overhead truss bottom and middle chord members located at span centerline
13, 94, 104	Overhead truss tension web members located near west uprights
30, 120, 128	Overhead truss tension web members located near east uprights

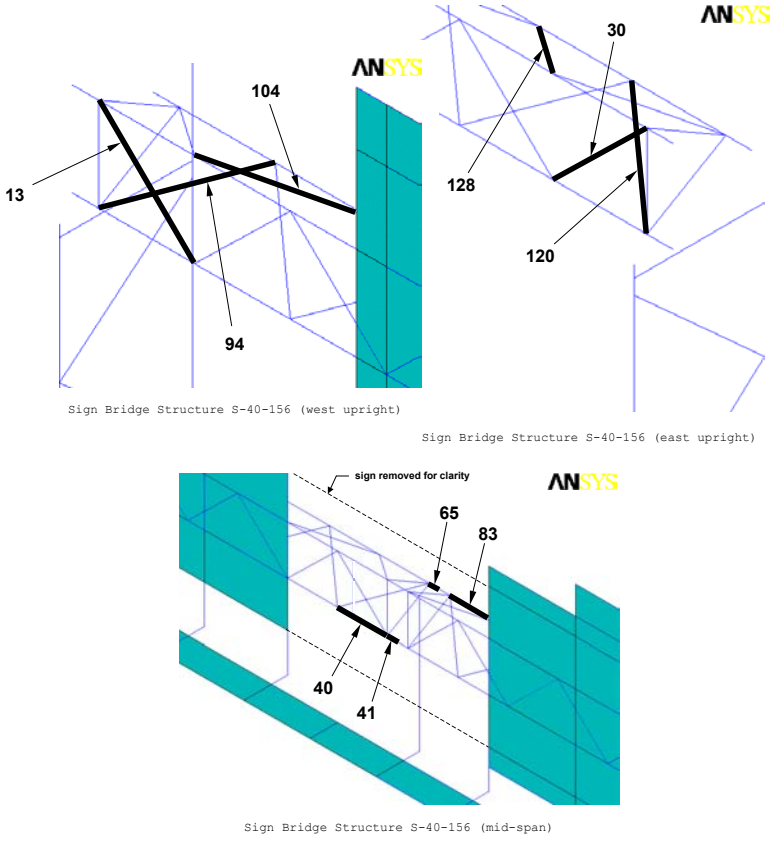

Figure 3.29: Critical Overhead Truss Web and Chord Members of sign Bridge S-40-156 (Ginal 2003).

Figure 3.30 illustrates the total stress histories for the elements that establish the lowest fatigue lives for structure S-40-156. Several very important items with regard to the response should be pointed out. First of all, the total response time is 10 seconds. The response begins immediately after allowance for the structure to come to rest under its own weight after the initial application of the acceleration due to

gravity at the supports. The gradual (linear) increase in stress from 0 to 5 seconds in the response is the application of the first pressure value in the time-varying pressure record over a 5-second interval with 100% of critical (Rayleigh) damping in the structure. This slow, fully-damped transient loading application was intended to simulate the graduate application of the "mean wind pressure" with subsequent turbulent loading. The application of the turbulent wind record occurs from 5 seconds to 10 seconds in the figure.

All elements undergo a constant state of stress when the structure is supporting its self-weight. This static stress magnitude depends upon the element. As expected, elements 13 and 30 are in a state of tension stress under the structure's self weight and this stress remains more or less unchanged under a 5 mph mean wind. However, the 25 and 50 mph mean winds cause significant cyclic tension stress in these elements. The reason for this is the fact that the sign is not "centered" on the tri-chord truss in the vertical direction. This causes the turbulent wind pressure to "twist" the truss structure thereby generating significant cyclical tension stresses in these members.

Member 65 is expected to have a state of near-zero stress under the gravity loading because the vertical truss composed of the two "front" chords are intended to carry a majority of the truss structure's self-weight. This result is clear in Figure 3.30(c). As the turbulent wind is applied the tensile stress becomes cyclic with significant stress-cycle magnitude. The 25-mph mean wind speed has relatively small stress range magnitudes when compared to the 50-mph wind. Therefore, it may be expected that 25 mph mean winds will cause a smaller portion of the fatigue damage.

Members 94 and 120 would likely be thought to have relatively small tensile stress in them when the structure carries its own weight. This is indeed seen in Figures 3.30(d) and 3.30(e). This tensile stress results from the "back chord" sagging under the trusses self-weight. The cyclical tension stress ranges in these members are significant for the 25-mph and 50-mph mean winds, but much greater damage might be expected for the 50-mph wind.

Fatigue life estimates can be generated for this structure using previously discussed procedures that included wind speed and direction combined probabilities as well as fatigue life statistics for critical details. Structure S-40-156 is in a rather unique location. Figure 3.9 illustrates that this structure is immediately adjacent to a vehicular bridge. Therefore, wind loading from the North is assumed to not affect the sign structure. Therefore, the fatigue analysis assumes loading from the South is all that is possible. Fatigue-life estimates were generated for the members and details in this structure for three confidence levels: 95%, 70%, and 50%. The results are included in Tables 3.16, 3.17, and 3.18.

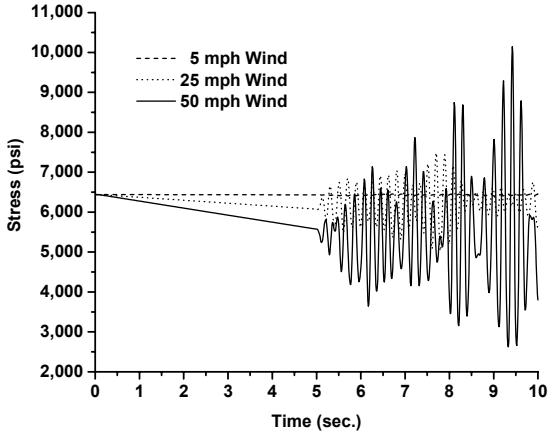

(a) Element 13 at Node 1

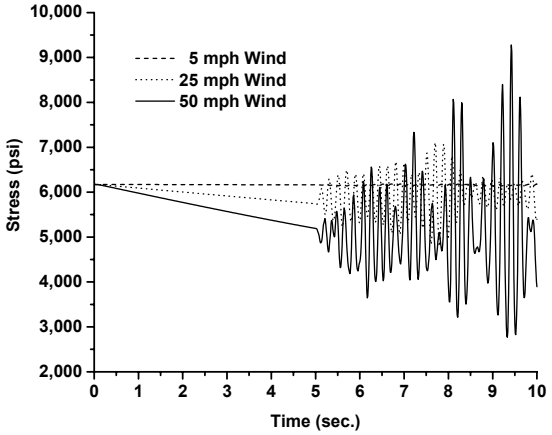

(b) Element 30 at Node 2

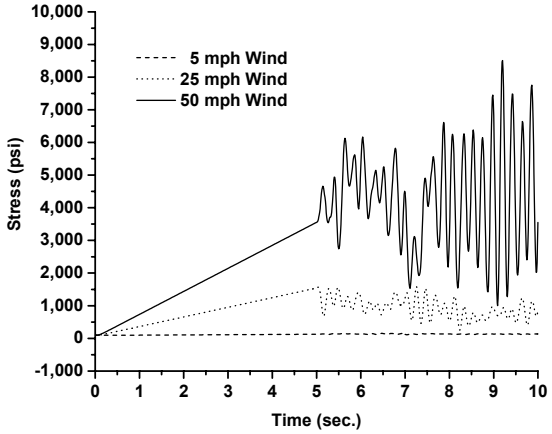

(c) Element 65 at Node 2

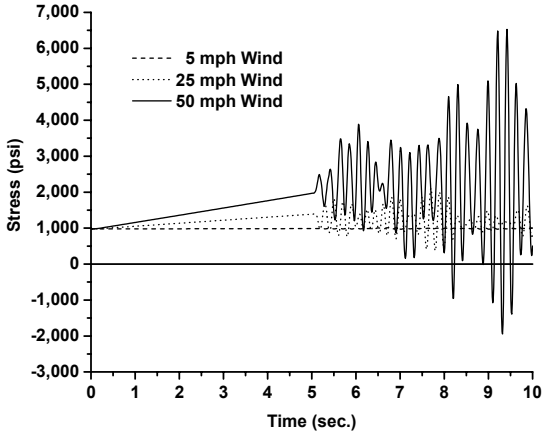

(d) Element 94 at Node 1

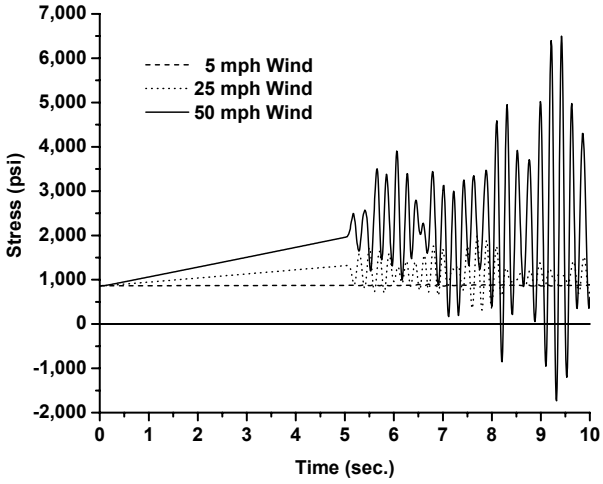

(e) Element 120 at Node 2

Figure 3.30: Stress Histories (Axial plus Bending) for Critical Elements within Sign Structure S-40-156 for a Variety of Mean Wind Speeds.

Table 3.16: Fatigue Life and Damage Estimates for Sign Structure S-40-156 for Critical Members and 95% Confidence Level (Wind Direction: South).

Element Number	Detail Category	Element Node (end)	Mean Wind Speed										SUM	Fatigue Life
			5 mph	10 mph	15 mph	20 mph	25 mph	30 mph	35 mph	40 mph	45 mph	50 mph		
13	ET	i	0.000000 (0.0 %)	0.000000 (0.0 %)	0.006438 (11.8 %)	0.006098 (11.2 %)	0.016290 (29.9 %)	0.009192 (16.8 %)	0.007676 (14.1 %)	0.006059 (11.1 %)	0.001278 (2.3 %)	0.001387 (2.5 %)	0.054421 (100 %)	18.4
		j	0.000000 (0.0 %)	0.000000 (0.0 %)	0.005669 (11.3 %)	0.006570 (13.1 %)	0.014641 (29.3 %)	0.008234 (16.5 %)	0.006898 (13.8 %)	0.005409 (10.8 %)	0.001132 (2.2 %)	0.001309 (2.6 %)	0.049865 (100 %)	20.1
30	ET	i	0.000000 (0.0 %)	0.000000 (0.0 %)	0.002897 (8.7 %)	0.003637 (11.0 %)	0.011075 (33.5 %)	0.006131 (18.5 %)	0.004422 (13.3 %)	0.003363 (10.1 %)	0.000737 (2.2 %)	0.000771 (2.3 %)	0.033037 (100 %)	30.3
		j	0.000000 (0.0 %)	0.000000 (0.0 %)	0.004935 (11.4 %)	0.004713 (10.9 %)	0.013982 (32.4 %)	0.007792 (18.1 %)	0.005609 (13.0 %)	0.004238 (9.8 %)	0.000929 (2.1 %)	0.000853 (1.9 %)	0.043055 (100 %)	23.2
40	E	i	0.000000 (0.0 %)	0.000000 (0.0 %)	0.000000 (0.0 %)	0.000000 (0.0 %)	0.000000 (0.0 %)	0.000000 (0.0 %)	0.000000 (0.0 %)	0.000000 (0.0 %)	0.000000 (0.0 %)	0.000000 (0.0 %)	0.000000 (100 %)	INFINITE
		j	0.000000 (0.0 %)	0.000000 (0.0 %)	0.000000 (0.0 %)	0.000000 (0.0 %)	0.000000 (0.0 %)	0.000000 (0.0 %)	0.000000 (0.0 %)	0.000000 (0.0 %)	0.000000 (0.0 %)	0.000000 (0.0 %)	0.000000 (100 %)	INFINITE
41	E	i	0.000000 (0.0 %)	0.000000 (0.0 %)	0.000000 (0.0 %)	0.000000 (0.0 %)	0.000000 (0.0 %)	0.000000 (0.0 %)	0.000000 (0.0 %)	0.000000 (0.0 %)	0.000000 (0.0 %)	0.000000 (0.0 %)	0.000000 (100 %)	INFINITE
	E'	j	0.000000 (0.0 %)	0.000000 (0.0 %)	0.000000 (0.0 %)	0.000000 (0.0 %)	0.000000 (0.0 %)	0.000000 (0.0 %)	0.000000 (0.0 %)	0.000000 (0.0 %)	0.000000 (0.0 %)	0.000000 (0.0 %)	0.000000 (100 %)	INFINITE
65	E	i	0.000000 (0.0 %)	0.000000 (0.0 %)	0.000000 (0.0 %)	0.000000 (0.0 %)	0.000000 (0.0 %)	0.000149 (10.8 %)	0.000564 (40.8 %)	0.000427 (30.9 %)	0.000051 (3.7 %)	0.000189 (13.7 %)	0.001383 (100 %)	722.8
	E'	j	0.000000 (0.0 %)	0.000000 (0.0 %)	0.000000 (0.0 %)	0.000000 (0.0 %)	0.000256 (4.4 %)	0.001219 (21.2 %)	0.002058 (35.7 %)	0.001456 (25.3 %)	0.000188 (3.2 %)	0.000571 (9.9 %)	0.005751 (100 %)	173.9
83	ET	i	0.000000 (0.0 %)	0.000000 (0.0 %)	0.000000 (0.0 %)	0.000000 (0.0 %)	0.000000 (0.0 %)	0.000176 (10.5 %)	0.000716 (42.8 %)	0.000496 (29.7 %)	0.000061 (3.7 %)	0.000218 (13.0 %)	0.001670 (100 %)	598.7
		j	0.000000 (0.0 %)	0.000000 (0.0 %)	0.000000 (0.0 %)	0.000000 (0.0 %)	0.000000 (0.0 %)	0.000000 (0.0 %)	0.000211 (33.8 %)	0.000245 (39.3 %)	0.000026 (4.2 %)	0.000141 (22.6 %)	0.000624 (100 %)	1601.3
94	ET	i	0.000000 (0.0 %)	0.000000 (0.0 %)	0.004321 (15.3 %)	0.003644 (12.9 %)	0.005002 (17.7 %)	0.003516 (12.4 %)	0.005949 (21.1 %)	0.004081 (14.4 %)	0.000478 (1.7 %)	0.001170 (4.1 %)	0.028163 (100 %)	35.5
		j	0.000000 (0.0 %)	0.000000 (0.0 %)	0.000000 (0.0 %)	0.000808 (10.1 %)	0.001228 (15.4 %)	0.001416 (17.7 %)	0.001946 (24.4 %)	0.001728 (21.6 %)	0.000204 (2.5 %)	0.000642 (8.0 %)	0.007974 (100 %)	125.4
104	ET	i	0.000000 (0.0 %)	0.000000 (0.0 %)	0.000000 (0.0 %)	0.000459 (9.1 %)	0.001275 (25.4 %)	0.001334 (26.5 %)	0.000708 (14.1 %)	0.000829 (16.5 %)	0.000229 (4.5 %)	0.000183 (3.6 %)	0.005019 (100 %)	199.2
		j	0.000000 (0.0 %)	0.000000 (0.0 %)	0.000000 (0.0 %)	0.000435 (8.7 %)	0.001284 (25.8 %)	0.001323 (26.6 %)	0.000695 (14.0 %)	0.000814 (16.3 %)	0.000233 (4.7 %)	0.000181 (3.6 %)	0.004968 (100 %)	201.3
120	ET	i	0.000000 (0.0 %)	0.000000 (0.0 %)	0.000000 (0.0 %)	0.000236 (3.9 %)	0.000806 (13.3 %)	0.001125 (18.6 %)	0.001614 (26.7 %)	0.001482 (24.6 %)	0.000177 (2.9 %)	0.000584 (9.6 %)	0.006029 (100 %)	165.9
		j	0.000000 (0.0 %)	0.000000 (0.0 %)	0.003205 (13.0 %)	0.003081 (12.5 %)	0.004439 (18.0 %)	0.003210 (13.0 %)	0.005392 (21.9 %)	0.003738 (15.1 %)	0.000436 (1.7 %)	0.001114 (4.5 %)	0.024620 (100 %)	40.6
128	ET	i	0.000000 (0.0 %)	0.000000 (0.0 %)	0.000000 (0.0 %)	0.000492 (8.2 %)	0.001596 (26.8 %)	0.001546 (26.0 %)	0.000832 (14.0 %)	0.000978 (16.4 %)	0.000275 (4.6 %)	0.000218 (3.6 %)	0.005939 (100 %)	168.4
		j	0.000000 (0.0 %)	0.000000 (0.0 %)	0.000000 (0.0 %)	0.000303 (6.6 %)	0.000784 (17.1 %)	0.001269 (27.7 %)	0.000754 (16.4 %)	0.000975 (21.2 %)	0.000269 (5.8 %)	0.000225 (4.9 %)	0.004581 (100 %)	218.3

Table 3.17: Fatigue Life and Damage Estimates for Sign Structure S-40-156 for Critical Members and 70% Confidence Level (Wind Direction: South).

Element Number	Detail Category	Element Node (end)	Mean Wind Speed										SUM	Fatigue Life
			5 mph	10 mph	15 mph	20 mph	25 mph	30 mph	35 mph	40 mph	45 mph	50 mph		
13	ET	i	0.000000 (0.0 %)	0.000000 (0.0 %)	0.003773 (11.8 %)	0.003574 (11.2 %)	0.009547 (29.9 %)	0.005387 (16.8 %)	0.004499 (14.1 %)	0.003551 (11.1 %)	0.000749 (2.3 %)	0.000813 (2.5 %)	0.031895 (100 %)	31.35
		j	0.000000 (0.0 %)	0.000000 (0.0 %)	0.003322 (11.3 %)	0.003850 (13.1 %)	0.008580 (29.3 %)	0.004826 (16.5 %)	0.004042 (13.8 %)	0.003170 (10.8 %)	0.000663 (2.2 %)	0.000767 (2.6 %)	0.029225 (100 %)	34.22
30	ET	i	0.000000 (0.0 %)	0.000000 (0.0 %)	0.001698 (8.7 %)	0.002131 (11.0 %)	0.006491 (33.5 %)	0.003593 (18.5 %)	0.002591 (13.3 %)	0.001971 (10.1 %)	0.000432 (2.2 %)	0.000452 (2.3 %)	0.019362 (100 %)	51.65
		j	0.000000 (0.0 %)	0.000000 (0.0 %)	0.002892 (11.4 %)	0.002762 (10.9 %)	0.008194 (32.4 %)	0.004566 (18.1 %)	0.003287 (13.0 %)	0.002484 (9.8 %)	0.000544 (2.1 %)	0.000500 (1.9 %)	0.025233 (100 %)	39.63
40	E	i	0.000000 (0.0 %)	0.000000 (0.0 %)	0.000000 (0.0 %)	0.000000 (0.0 %)	0.000000 (0.0 %)	0.000000 (0.0 %)	0.000000 (0.0 %)	0.000000 (0.0 %)	0.000000 (0.0 %)	0.000000 (0.0 %)	0.000000 (100 %)	INFINTE
		j	0.000000 (0.0 %)	0.000000 (0.0 %)	0.000000 (0.0 %)	0.000000 (0.0 %)	0.000000 (0.0 %)	0.000000 (0.0 %)	0.000000 (0.0 %)	0.000000 (0.0 %)	0.000000 (0.0 %)	0.000000 (0.0 %)	0.000000 (100 %)	INFINITE
41	E	i	0.000000 (0.0 %)	0.000000 (0.0 %)	0.000000 (0.0 %)	0.000000 (0.0 %)	0.000000 (0.0 %)	0.000000 (0.0 %)	0.000000 (0.0 %)	0.000000 (0.0 %)	0.000000 (0.0 %)	0.000000 (0.0 %)	0.000000 (100 %)	INFINITE
	E'	j	0.000000 (0.0 %)	0.000000 (0.0 %)	0.000000 (0.0 %)	0.000000 (0.0 %)	0.000000 (0.0 %)	0.000000 (0.0 %)	0.000000 (0.0 %)	0.000000 (0.0 %)	0.000000 (0.0 %)	0.000000 (0.0 %)	0.000000 (100 %)	INFINITE
65	E	i	0.000000 (0.0 %)	0.000000 (0.0 %)	0.000000 (0.0 %)	0.000000 (0.0 %)	0.000000 (0.0 %)	0.000108 (10.8 %)	0.000409 (40.8 %)	0.000310 (30.9 %)	0.000037 (3.7 %)	0.000137 (13.7 %)	0.001004 (100 %)	995.57
	E'	j	0.000000 (0.0 %)	0.000000 (0.0 %)	0.000000 (0.0 %)	0.000000 (0.0 %)	0.000168 (4.4 %)	0.000802 (21.2 %)	0.001353 (35.7 %)	0.000958 (25.3 %)	0.000123 (3.2 %)	0.000376 (9.9 %)	0.003782 (100 %)	264.36
83	ET	i	0.000000 (0.0 %)	0.000000 (0.0 %)	0.000000 (0.0 %)	0.000000 (0.0 %)	0.000000 (0.0 %)	0.000128 (10.5 %)	0.000520 (42.8 %)	0.000360 (29.7 %)	0.000045 (3.7 %)	0.000158 (13.0 %)	0.001212 (100 %)	824.64
		j	0.000000 (0.0 %)	0.000000 (0.0 %)	0.000000 (0.0 %)	0.000000 (0.0 %)	0.000000 (0.0 %)	0.000000 (0.0 %)	0.000153 (33.8 %)	0.000178 (39.3 %)	0.000019 (4.2 %)	0.000102 (22.6 %)	0.000453 (100 %)	2205.51
94	ET	i	0.000000 (0.0 %)	0.000000 (0.0 %)	0.002532 (15.3 %)	0.002135 (12.9 %)	0.002931 (17.7 %)	0.002061 (12.4 %)	0.003486 (21.1 %)	0.002391 (14.4 %)	0.000280 (1.7 %)	0.000686 (4.1 %)	0.016506 (100 %)	60.58
		j	0.000000 (0.0 %)	0.000000 (0.0 %)	0.000000 (0.0 %)	0.000473 (10.1 %)	0.000719 (15.4 %)	0.000829 (17.7 %)	0.001140 (24.4 %)	0.001013 (21.6 %)	0.000119 (2.5 %)	0.000376 (8.0 %)	0.004673 (100 %)	213.98
104	ET	i	0.000000 (0.0 %)	0.000000 (0.0 %)	0.000000 (0.0 %)	0.000269 (9.1 %)	0.000747 (25.4 %)	0.000782 (26.5 %)	0.000415 (14.1 %)	0.000485 (16.5 %)	0.000134 (4.5 %)	0.000107 (3.6 %)	0.002941 (100 %)	339.94
		j	0.000000 (0.0 %)	0.000000 (0.0 %)	0.000000 (0.0 %)	0.000255 (8.7 %)	0.000752 (25.8 %)	0.000775 (26.6 %)	0.000407 (14.0 %)	0.000477 (16.3 %)	0.000136 (4.7 %)	0.000106 (3.6 %)	0.002911 (100 %)	343.43
120	ET	i	0.000000 (0.0 %)	0.000000 (0.0 %)	0.000000 (0.0 %)	0.000138 (3.9 %)	0.000472 (13.3 %)	0.000659 (18.6 %)	0.000946 (26.7 %)	0.000869 (24.6 %)	0.000104 (2.9 %)	0.000342 (9.6 %)	0.003533 (100 %)	283
		j	0.000000 (0.0 %)	0.000000 (0.0 %)	0.001878 (13.0 %)	0.001805 (12.5 %)	0.002601 (18.0 %)	0.001881 (13.0 %)	0.003160 (21.9 %)	0.002191 (15.1 %)	0.000256 (1.7 %)	0.000653 (4.5 %)	0.014429 (100 %)	69.3
128	ET	i	0.000000 (0.0 %)	0.000000 (0.0 %)	0.000000 (0.0 %)	0.000288 (8.2 %)	0.000935 (26.8 %)	0.000906 (26.0 %)	0.000487 (14.0 %)	0.000573 (16.4 %)	0.000161 (4.6 %)	0.000127 (3.6 %)	0.003480 (100 %)	287.28
		j	0.000000 (0.0 %)	0.000000 (0.0 %)	0.000000 (0.0 %)	0.000177 (6.6 %)	0.000459 (17.1 %)	0.000743 (27.7 %)	0.000442 (16.4 %)	0.000571 (21.2 %)	0.000158 (5.8 %)	0.000132 (4.9 %)	0.002685 (100 %)	372.42

Table 3.18: Fatigue Life and Damage Estimates for Sign Structure S-40-156 for Critical Members and 50% Confidence Level (Wind Direction: South).

Element Number	Detail Category	Element Node (end)	Mean Wind Speed										SUM	Fatigue Life
			5 mph	10 mph	15 mph	20 mph	25 mph	30 mph	35 mph	40 mph	45 mph	50 mph		
13	ET	i	0.000000 (0.0 %)	0.000000 (0.0 %)	0.002938 (11.8 %)	0.002783 (11.2 %)	0.007434 (29.9 %)	0.004195 (16.8 %)	0.003503 (14.1 %)	0.002765 (11.1 %)	0.000583 (2.3 %)	0.000633 (2.5 %)	0.024837 (100 %)	40.26
		j	0.000000 (0.0 %)	0.000000 (0.0 %)	0.002587 (11.3 %)	0.002998 (13.1 %)	0.006682 (29.3 %)	0.003758 (16.5 %)	0.003148 (13.8 %)	0.002468 (10.8 %)	0.000517 (2.2 %)	0.000597 (2.6 %)	0.022758 (100 %)	43.94
30	ET	i	0.000000 (0.0 %)	0.000000 (0.0 %)	0.001322 (8.7 %)	0.001660 (11.0 %)	0.005054 (33.5 %)	0.002798 (18.5 %)	0.002018 (13.3 %)	0.001535 (10.1 %)	0.000336 (2.2 %)	0.000352 (2.3 %)	0.015077 (100 %)	66.32
		j	0.000000 (0.0 %)	0.000000 (0.0 %)	0.002252 (11.4 %)	0.002151 (10.9 %)	0.006381 (32.4 %)	0.003556 (18.1 %)	0.002560 (13.0 %)	0.001934 (9.8 %)	0.000424 (2.1 %)	0.000389 (1.9 %)	0.019650 (100 %)	50.89
40	E	i	0.000000 (0.0 %)	0.000000 (0.0 %)	0.000000 (0.0 %)	0.000000 (0.0 %)	0.000000 (0.0 %)	0.000000 (0.0 %)	0.000000 (0.0 %)	0.000000 (0.0 %)	0.000000 (0.0 %)	0.000000 (0.0 %)	0.000000 (100 %)	INFINITE
		j	0.000000 (0.0 %)	0.000000 (0.0 %)	0.000000 (0.0 %)	0.000000 (0.0 %)	0.000000 (0.0 %)	0.000000 (0.0 %)	0.000000 (0.0 %)	0.000000 (0.0 %)	0.000000 (0.0 %)	0.000000 (0.0 %)	0.000000 (100 %)	INFINITE
41	E	i	0.000000 (0.0 %)	0.000000 (0.0 %)	0.000000 (0.0 %)	0.000000 (0.0 %)	0.000000 (0.0 %)	0.000000 (0.0 %)	0.000000 (0.0 %)	0.000000 (0.0 %)	0.000000 (0.0 %)	0.000000 (0.0 %)	0.000000 (100 %)	INFINITE
	E'	j	0.000000 (0.0 %)	0.000000 (0.0 %)	0.000000 (0.0 %)	0.000000 (0.0 %)	0.000000 (0.0 %)	0.000000 (0.0 %)	0.000000 (0.0 %)	0.000000 (0.0 %)	0.000000 (0.0 %)	0.000000 (0.0 %)	0.000000 (100 %)	INFINITE
65	E	i	0.000000 (0.0 %)	0.000000 (0.0 %)	0.000000 (0.0 %)	0.000000 (0.0 %)	0.000000 (0.0 %)	0.000092 (10.8 %)	0.000349 (40.8 %)	0.000265 (30.9 %)	0.000031 (3.7 %)	0.000117 (13.7 %)	0.000857 (100 %)	1166.05
	E'	j	0.000000 (0.0 %)	0.000000 (0.0 %)	0.000000 (0.0 %)	0.000000 (0.0 %)	0.000133 (4.4 %)	0.000637 (21.2 %)	0.001076 (35.7 %)	0.000761 (25.3 %)	0.000098 (3.2 %)	0.000298 (9.9 %)	0.003006 (100 %)	332.57
83	ET	i	0.000000 (0.0 %)	0.000000 (0.0 %)	0.000000 (0.0 %)	0.000000 (0.0 %)	0.000000 (0.0 %)	0.000109 (10.5 %)	0.000444 (42.8 %)	0.000307 (29.7 %)	0.000038 (3.7 %)	0.000135 (13.0 %)	0.001035 (100 %)	965.85
		j	0.000000 (0.0 %)	0.000000 (0.0 %)	0.000000 (0.0 %)	0.000000 (0.0 %)	0.000000 (0.0 %)	0.000000 (0.0 %)	0.000131 (33.8 %)	0.000152 (39.3 %)	0.000016 (4.2 %)	0.000087 (22.6 %)	0.000387 (100 %)	2583.16
94	ET	i	0.000000 (0.0 %)	0.000000 (0.0 %)	0.001972 (15.3 %)	0.001663 (12.9 %)	0.002283 (17.7 %)	0.001604 (12.4 %)	0.002715 (21.1 %)	0.001862 (14.4 %)	0.000218 (1.7 %)	0.000534 (4.1 %)	0.012853 (100 %)	77.8
		j	0.000000 (0.0 %)	0.000000 (0.0 %)	0.000000 (0.0 %)	0.000368 (10.1 %)	0.000560 (15.4 %)	0.000646 (17.7 %)	0.000888 (24.4 %)	0.000788 (21.6 %)	0.000093 (2.5 %)	0.000293 (8.0 %)	0.003639 (100 %)	274.78
104	ET	i	0.000000 (0.0 %)	0.000000 (0.0 %)	0.000000 (0.0 %)	0.000209 (9.1 %)	0.000582 (25.4 %)	0.000609 (26.5 %)	0.000323 (14.1 %)	0.000378 (16.5 %)	0.000104 (4.5 %)	0.000083 (3.6 %)	0.002290 (100 %)	436.53
		j	0.000000 (0.0 %)	0.000000 (0.0 %)	0.000000 (0.0 %)	0.000198 (8.7 %)	0.000586 (25.8 %)	0.000604 (26.6 %)	0.000317 (14.0 %)	0.000371 (16.3 %)	0.000106 (4.7 %)	0.000082 (3.6 %)	0.002267 (100 %)	441.02
120	ET	i	0.000000 (0.0 %)	0.000000 (0.0 %)	0.000000 (0.0 %)	0.000108 (3.9 %)	0.000368 (13.3 %)	0.000513 (18.6 %)	0.000737 (26.7 %)	0.000676 (24.6 %)	0.000081 (2.9 %)	0.000266 (9.6 %)	0.002751 (100 %)	363.42
		j	0.000000 (0.0 %)	0.000000 (0.0 %)	0.001462 (13.0 %)	0.001406 (12.5 %)	0.002026 (18.0 %)	0.001465 (13.0 %)	0.002461 (21.9 %)	0.001706 (15.1 %)	0.000199 (1.7 %)	0.000508 (4.5 %)	0.011236 (100 %)	89
128	ET	i	0.000000 (0.0 %)	0.000000 (0.0 %)	0.000000 (0.0 %)	0.000224 (8.2 %)	0.000728 (26.8 %)	0.000705 (26.0 %)	0.000379 (14.0 %)	0.000446 (16.4 %)	0.000125 (4.6 %)	0.000099 (3.6 %)	0.002710 (100 %)	368.92
		j	0.000000 (0.0 %)	0.000000 (0.0 %)	0.000000 (0.0 %)	0.000138 (6.6 %)	0.000357 (17.1 %)	0.000579 (27.7 %)	0.000344 (16.4 %)	0.000445 (21.2 %)	0.000123 (5.8 %)	0.000102 (4.9 %)	0.002090 (100 %)	478.25

The fatigue-life estimates indicate that member 13 appears to control the fatigue life of the truss structure. Base upon the *ET* detail category fatigue details at each end of this member, one would have 95% confidence that the fatigue life would be 18.4 years. One could be 70% confident that the structure would last 31.4 years, and there would be a 50/50 chance that the structure would survive 40.3 years prior to fatigue failure. The fatigue life indicates that there is a 95% chance the structure will not achieve its desired service life of 50 years (Dexter and Ricker 2002). It should be noted that anything with a fatigue life over 10,000 years was considered infinite.

Furthermore, the fatigue analysis of these structures would indicate that initial failure would occur at the diagonals near the supports (on the vertical face of the tri-chord for this structure), then likely occur on the diagonals on the top face of the tri-chord near the supports, and then finally move toward the center of the truss. The significant sign area above the tri-chord truss (refer to Figure 3.9) results in twisting of the truss structure under turbulent wind and therefore, the diagonals on the front fact of the tri-chord truss are the controlling fatigue components.

The damage accumulation for all wind speeds is also a highly useful piece of information. Figure 3.31 is a histogram of cumulative damage for the most fatigue-sensitive members in the structure.

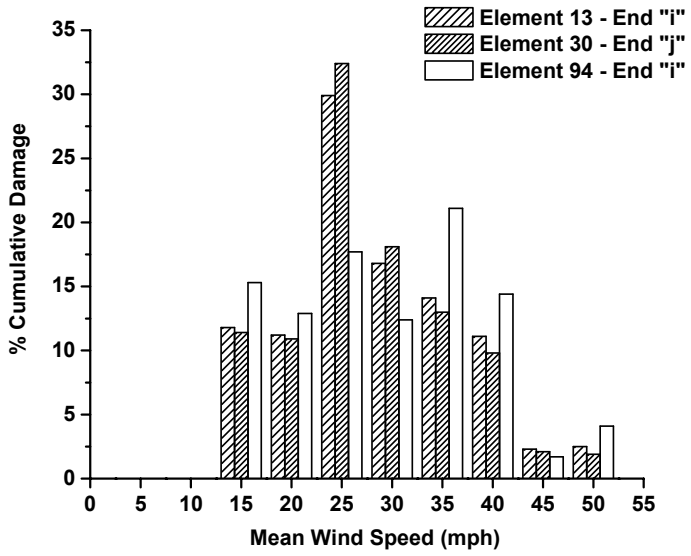

Figure 3.31: Histogram of Cumulative Damage for Critical Elements of S-40-156.

Figure 3.31 illustrates that element 13 receives the majority of fatigue damage under very frequently occurring winds (25 mph). Furthermore, the histogram illustrates that 95% of the fatigue damage to this element is created for winds less than or equal to 40 mph. The damage histogram for element 30 is very similar with 95% of the fatigue damage resulting from wind speeds less than or equal to 40 mph. The

damage distribution for element 94 is much more distributed and closer to uniform over wind speeds from 15 to 40 mph.

3.2.8.2 Structure S-40-404

Sign support structure S-40-404 is a four-chord box truss structure (see Figure 3.8). This structure can have the sign subjected to wind loading from the East and the West. Ginal (2003) conducted a detailed study that illustrated that the fatigue analysis for this structure can utilize a transient analysis for wind loading from one direction (*e.g.* wind from the West) to account for wind loading from both directions (*e.g.* wind from East and West). The number of stress cycles from the East and West can be based upon the stress cycles from the same analysis and appropriate probabilities. The number of cumulative cycles for winds from both directions can then be simply added together.

The critical elements for this structure were selected using a preliminary analysis effort (Ginal 2003). This analysis resulted in the elements found in Table 3.19 being considered as those elements that would control the fatigue life of the structure. Figure 3.32 illustrates where these elements are found within the structure's topology.

The stress histories of several of the critical elements within the structure have been plotted in Figures 3.33 through 3.36. Figure 3.33 illustrates the response history for element 301 within structure S-40-404. The total stress response as a function of time for this element indicates that there are significant stress ranges for 25 and 50 mph winds. The 5 mph loading cannot generate stress ranges in this element and therefore, 5 mph mean winds are expected to cause very little fatigue damage.

Element 328 is across the sign bridge at the North upright (refer to Figure 3.32). This element is a diagonal member in the lower truss of the box-chord structure. The orientation of the sign as shown in Figure 3.8 would suggest that the mean stress level for 328 would be less than that of element 301 when the VMS sign is subjected to wind pressure. Figure 3.34 illustrates the difference in stress response for these two elements (at each end) when a 50 mph mean wind loads the structure (element 301 has the higher overall stress state). As expected the mean stress for element 328 is less than that of element 301. Furthermore, the stress ranges found for element 301 (at both ends) are greater than those found in element 328. Therefore, one should expect that the fatigue life for element 301 would be less than that of element 328.

Element 211 is a diagonal element on the front face of the box-chord truss (see Figure 3.32). The mean stress in this member is expected to be high because this diagonal member acts to support the self-

weight of the truss structure and the weight of the VMS box and catwalk structure. Figure 3.35 illustrates the stress response history at each end of element 211.

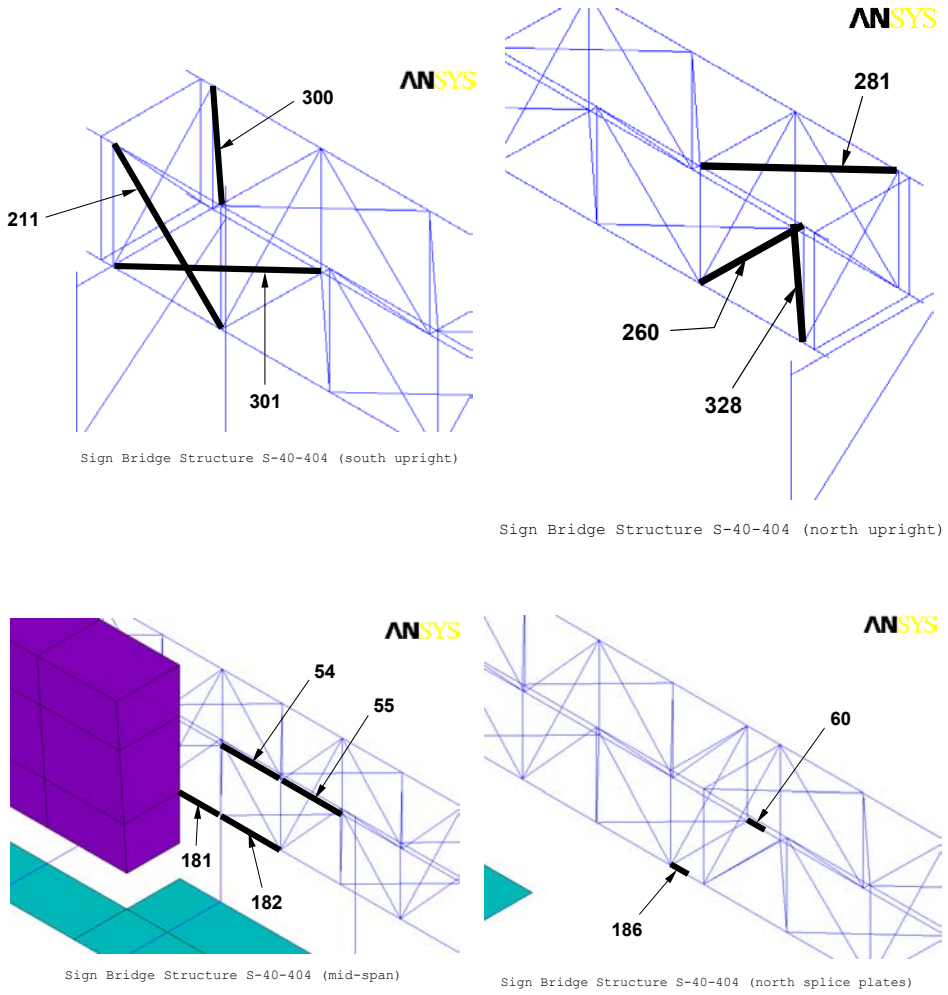

Figure 3.32: Critical Overhead Truss Web and Chord Members of Sign Bridge S-40-404 (Ginal 2003).

Table 3.19: Elements Evaluate in Wind Load Analysis of Sign Bridge S-40-404 (Ginal 2003).

Element #'s	Description
54, 55, 181, 182	Overhead truss bottom chord members located at span centerline
60, 186	Overhead truss bottom chord members located at northern splice
211, 300, 301	Overhead truss tension web members located near south uprights
260, 281, 328	Overhead truss tension web members located near north uprights

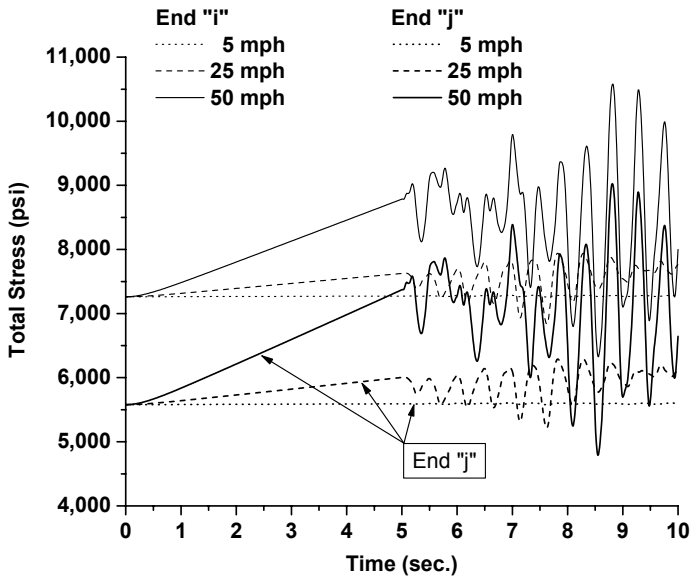

Figure 3.33: Total Stress History for Element 301 within S-40-404 for Various Mean Wind Speeds.

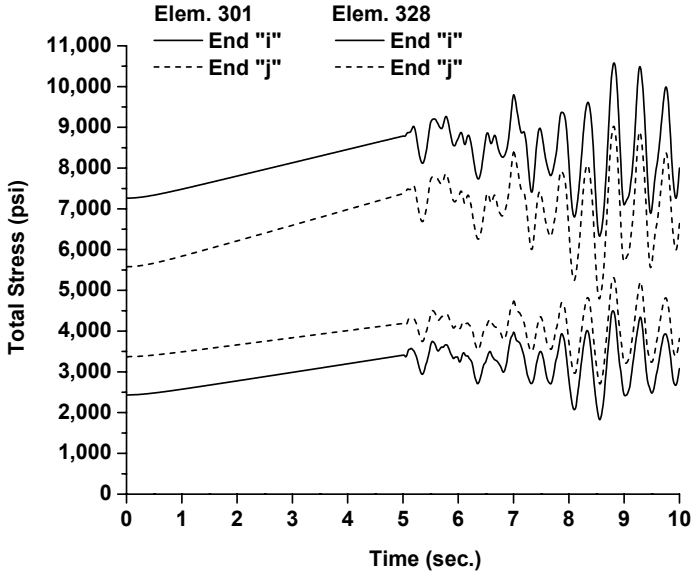

Figure 3.34: Stress Response History for Elements 301 and 328 for 50-mph Mean Wind Speed.

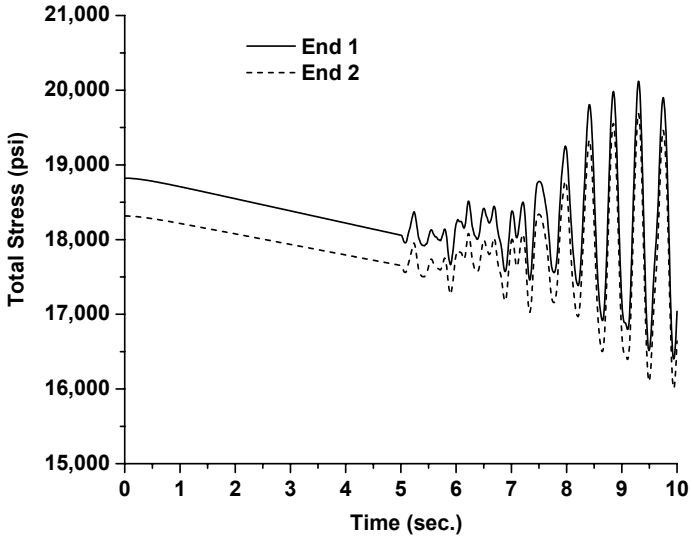

Figure 3.35: Stress History for Element 211 in Sign Support Structure S-40-404 During 50 mph Mean Wind Speed.

The maximum stress range seen by element 211 during the 50 mph wind is approximately 3,500 psi. This is a significant stress range considering that the welded details at the ends of this round HSS member are detail category *ET*. Thus, it is expected that the 50-mph mean wind speed will indeed cause damage to this element.

The impact of mean wind speed on the cyclic response of element 211 is illustrated in Figure 3.36. As one might expect, 5-mph mean winds are unable to move the sign support structure from its equilibrium position under its self-weight. Therefore, it certainly can be expected that 5-mph winds will cause no damage to this element within the structure.

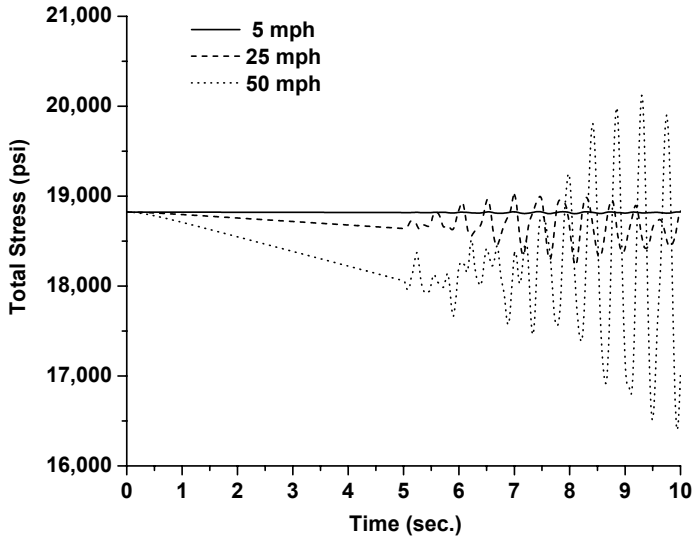

Figure 3.36: Stress History for Element 211 in Sign Support Structure S-40-404 During Various Mean Wind Speeds.

One could also argue that 25-mph winds will require many applications to generate fatigue damage given the 500 psi peak stress range magnitude. As discussed previously, the 50-mph mean winds will indeed cause damage to this component within the sign support structure.

Fatigue life and damage estimates for the various critical components of sign structure S-40-404 are given in Tables 3.20 through 3.22. The component that governs the fatigue life estimate for this structure is element 301. Table 3.20 indicates that this element as a limiting fatigue life of approximately 62.3 years. This estimate has a 95% confidence attached to it. The structure has a 70% likelihood that it will survive 106.3 years and a 50/50 chance it will last 136.5 years. The fatigue analysis conducted indicates that the structure has a 95% confidence that it will last the expected service life of 50 years suggested for ancillary highway structures (Dexter and Ricker 2002).

Table 3.20: Fatigue Life and Damage Estimates for Sign Structure S-40-404 for Critical Members and 95% Confidence Level (Wind Direction: East and West).

Element Number	Detail Category	Element Node (end)	Mean Wind Speed										SUM	Fatigue Life
			5 mph	10 mph	15 mph	20 mph	25 mph	30 mph	35 mph	40 mph	45 mph	50 mph		
54	E	i	0.000000 (0.0 %)	0.000000 (0.0 %)	0.000000 (0.0 %)	0.000000 (0.0 %)	0.000000 (0.0 %)	0.000000 (0.0 %)	0.000000 (0.0 %)	0.000000 (0.0 %)	0.000000 (0.0 %)	0.000123 (100.0 %)	0.000123 (100 %)	8078.5
		j	0.000000 (0.0 %)	0.000000 (0.0 %)	0.000000 (0.0 %)	0.000000 (0.0 %)	0.000000 (0.0 %)	0.000000 (0.0 %)	0.000000 (0.0 %)	0.000000 (0.0 %)	0.000000 (0.0 %)	0.000069 (100.0 %)	6.917999 (100 %)	INFINITE
55	E	i	0.000000 (0.0 %)	0.000000 (0.0 %)	0.000000 (0.0 %)	0.000000 (0.0 %)	0.000000 (0.0 %)	0.000000 (0.0 %)	0.000000 (0.0 %)	0.000000 (0.0 %)	0.000000 (0.0 %)	0.000065 (100.0 %)	6.593000 (100 %)	INFINITE
		j	0.000000 (0.0 %)	0.000000 (0.0 %)	0.000000 (0.0 %)	0.000000 (0.0 %)	0.000000 (0.0 %)	0.000000 (0.0 %)	0.000000 (0.0 %)	0.000000 (0.0 %)	0.000000 (0.0 %)	0.000146 (100.0 %)	0.000146 (100 %)	6810.0
60	E	i	0.000000 (0.0 %)	0.000000 (0.0 %)	0.000000 (0.0 %)	0.000000 (0.0 %)	0.000000 (0.0 %)	0.000000 (0.0 %)	0.000000 (0.0 %)	0.000000 (0.0 %)	0.000000 (0.0 %)	0.000132 (100.0 %)	0.000132 (100 %)	7527.4
	E'	j	0.000000 (0.0 %)	0.000000 (0.0 %)	0.000000 (0.0 %)	0.000000 (0.0 %)	0.000000 (0.0 %)	0.000000 (0.0 %)	0.000260 (37.4 %)	0.000153 (22.0 %)	0.000028 (4.1 %)	0.000254 (36.4 %)	0.000697 (100 %)	1433.7
181	E	i	0.000000 (0.0 %)	0.000000 (0.0 %)	0.000000 (0.0 %)	0.000000 (0.0 %)	0.000000 (0.0 %)	0.000000 (0.0 %)	0.000000 (0.0 %)	0.000000 (0.0 %)	0.000000 (0.0 %)	0.000024 (100.0 %)	2.415000 (100 %)	INFINITE
		j	0.000000 (0.0 %)	0.000000 (0.0 %)	0.000000 (0.0 %)	0.000000 (0.0 %)	0.000000 (0.0 %)	0.000000 (0.0 %)	0.000000 (0.0 %)	0.000000 (0.0 %)	0.000059 (32.4 %)	0.000123 (67.5 %)	0.000182 (100 %)	5481.3
182	E	i	0.000000 (0.0 %)	0.000000 (0.0 %)	0.000000 (0.0 %)	0.000000 (0.0 %)	0.000000 (0.0 %)	0.000000 (0.0 %)	0.000000 (0.0 %)	0.000000 (0.0 %)	0.000097 (31.1 %)	0.000215 (68.8 %)	0.000313 (100 %)	3191.4
		j	0.000000 (0.0 %)	0.000000 (0.0 %)	0.000000 (0.0 %)	0.000000 (0.0 %)	0.000000 (0.0 %)	0.000000 (0.0 %)	0.000000 (0.0 %)	0.000000 (0.0 %)	0.000000 (0.0 %)	0.000025 (100.0 %)	2.576000 (100 %)	INFINITE
186	E	i	0.000000 (0.0 %)	0.000000 (0.0 %)	0.000000 (0.0 %)	0.000000 (0.0 %)	0.000000 (0.0 %)	0.000000 (0.0 %)	0.000000 (0.0 %)	0.000000 (0.0 %)	0.000000 (0.0 %)	0.000000 (0.0 %)	0.000000 (100 %)	INFINITE
	E'	j	0.000000 (0.0 %)	0.000000 (0.0 %)	0.000000 (0.0 %)	0.000000 (0.0 %)	0.000000 (0.0 %)	0.000000 (0.0 %)	0.000000 (0.0 %)	0.000056 (20.8 %)	0.000057 (21.2 %)	0.000157 (57.8 %)	0.000271 (100 %)	3679.9
211	ET	i	0.000000 (0.0 %)	0.000000 (0.0 %)	0.000000 (0.0 %)	0.000000 (0.0 %)	0.001006 (11.8 %)	0.000586 (6.9 %)	0.002070 (24.3 %)	0.001899 (22.3 %)	0.000602 (7.1 %)	0.002330 (27.4 %)	0.008496 (100 %)	117.7
		j	0.000000 (0.0 %)	0.000000 (0.0 %)	0.000000 (0.0 %)	0.000000 (0.0 %)	0.000988 (12.1 %)	0.000452 (5.5 %)	0.002046 (25.0 %)	0.001862 (22.8 %)	0.000568 (6.9 %)	0.002242 (27.4 %)	0.008161 (100 %)	122.5
260	ET	i	0.000000 (0.0 %)	0.000000 (0.0 %)	0.000000 (0.0 %)	0.000000 (0.0 %)	0.000000 (0.0 %)	0.000000 (0.0 %)	0.000248 (27.9 %)	0.000264 (29.7 %)	0.000078 (8.8 %)	0.000297 (33.4 %)	0.000889 (100 %)	1123.7
		j	0.000000 (0.0 %)	0.000000 (0.0 %)	0.000000 (0.0 %)	0.000000 (0.0 %)	0.000000 (0.0 %)	0.000000 (0.0 %)	0.000275 (26.5 %)	0.000338 (32.6 %)	0.000089 (8.6 %)	0.000332 (32.0 %)	0.001037 (100 %)	964.2
281	ET	i	0.000000 (0.0 %)	0.000000 (0.0 %)	0.000000 (0.0 %)	0.000000 (0.0 %)	0.000000 (0.0 %)	0.000177 (21.6 %)	0.000198 (24.3 %)	0.000165 (20.2 %)	0.000112 (13.7 %)	0.000163 (19.9 %)	0.000817 (100 %)	1223.4
		j	0.000000 (0.0 %)	0.000000 (0.0 %)	0.000000 (0.0 %)	0.000000 (0.0 %)	0.000000 (0.0 %)	0.000166 (21.8 %)	0.000193 (25.4 %)	0.000152 (19.9 %)	0.000098 (12.9 %)	0.000151 (19.8 %)	0.000762 (100 %)	1311.7
300	ET	i	0.000000 (0.0 %)	0.000000 (0.0 %)	0.000000 (0.0 %)	0.000000 (0.0 %)	0.000404 (7.5 %)	0.001261 (23.6 %)	0.001026 (19.2 %)	0.001134 (21.2 %)	0.000611 (11.4 %)	0.000896 (16.8 %)	0.005335 (100 %)	187.4
		j	0.000000 (0.0 %)	0.000000 (0.0 %)	0.000000 (0.0 %)	0.000000 (0.0 %)	0.000393 (7.7 %)	0.001232 (24.3 %)	0.000997 (19.7 %)	0.001053 (20.8 %)	0.000565 (11.1 %)	0.000820 (16.2 %)	0.005063 (100 %)	197.5
301	ET	i	0.000000 (0.0 %)	0.000000 (0.0 %)	0.000000 (0.0 %)	0.000459 (2.8 %)	0.002290 (14.2 %)	0.001200 (7.4 %)	0.004510 (28.1 %)	0.003916 (24.4 %)	0.000767 (4.7 %)	0.002904 (18.1 %)	0.016048 (100 %)	62.3
		j	0.000000 (0.0 %)	0.000000 (0.0 %)	0.000000 (0.0 %)	0.000448 (2.8 %)	0.002059 (13.1 %)	0.001400 (8.9 %)	0.004645 (29.5 %)	0.003613 (22.9 %)	0.000770 (4.9 %)	0.002782 (17.7 %)	0.015720 (100 %)	63.6
328	ET	i	0.000000 (0.0 %)	0.000000 (0.0 %)	0.000000 (0.0 %)	0.000000 (0.0 %)	0.000209 (7.1 %)	0.000167 (5.7 %)	0.000972 (33.1 %)	0.000814 (27.7 %)	0.000121 (4.1 %)	0.000645 (22.0 %)	0.002931 (100 %)	341.1
		j	0.000000 (0.0 %)	0.000000 (0.0 %)	0.000000 (0.0 %)	0.000000 (0.0 %)	0.000209 (7.0 %)	0.000122 (4.1 %)	0.001099 (37.0 %)	0.000794 (26.8 %)	0.000122 (4.1 %)	0.000616 (20.7 %)	0.002964 (100 %)	337.4

Table 3.21: Fatigue Life and Damage Estimates for Sign Structure S-40-404 for Critical Members and 70% Confidence Level (Wind Direction: East and West).

Element Number	Detail Category	Element Node (end)	Mean Wind Speed										SUM	Fatigue Life
			5 mph	10 mph	15 mph	20 mph	25 mph	30 mph	35 mph	40 mph	45 mph	50 mph		
54	E	i	0.000000 (0.0 %)	0.000000 (0.0 %)	0.000000 (0.0 %)	0.000000 (0.0 %)	0.000000 (0.0 %)	0.000000 (0.0 %)	0.000000 (0.0 %)	0.000000 (0.0 %)	0.000000 (0.0 %)	0.000089 (100.0 %)	8.987000 (100 %)	INFINITE
		j	0.000000 (0.0 %)	0.000000 (0.0 %)	0.000000 (0.0 %)	0.000000 (0.0 %)	0.000000 (0.0 %)	0.000000 (0.0 %)	0.000000 (0.0 %)	0.000000 (0.0 %)	0.000000 (0.0 %)	0.000050 (100.0 %)	5.021999 (100 %)	INFINITE
55	E	i	0.000000 (0.0 %)	0.000000 (0.0 %)	0.000000 (0.0 %)	0.000000 (0.0 %)	0.000000 (0.0 %)	0.000000 (0.0 %)	0.000000 (0.0 %)	0.000000 (0.0 %)	0.000000 (0.0 %)	0.000047 (100.0 %)	4.787000 (100 %)	INFINITE
		j	0.000000 (0.0 %)	0.000000 (0.0 %)	0.000000 (0.0 %)	0.000000 (0.0 %)	0.000000 (0.0 %)	0.000000 (0.0 %)	0.000000 (0.0 %)	0.000000 (0.0 %)	0.000000 (0.0 %)	0.000106 (100.0 %)	0.000106 (100 %)	9379.8
60	E	i	0.000000 (0.0 %)	0.000000 (0.0 %)	0.000000 (0.0 %)	0.000000 (0.0 %)	0.000000 (0.0 %)	0.000000 (0.0 %)	0.000000 (0.0 %)	0.000000 (0.0 %)	0.000000 (0.0 %)	0.000096 (100.0 %)	9.645e-0 (100 %)	INFINITE
	E'	j	0.000000 (0.0 %)	0.000000 (0.0 %)	0.000000 (0.0 %)	0.000000 (0.0 %)	0.000000 (0.0 %)	0.000000 (0.0 %)	0.000171 (37.4 %)	0.000101 (22.0 %)	0.000018 (4.1 %)	0.000167 (36.4 %)	0.000458 (100 %)	2179.9
181	E	i	0.000000 (0.0 %)	0.000000 (0.0 %)	0.000000 (0.0 %)	0.000000 (0.0 %)	0.000000 (0.0 %)	0.000000 (0.0 %)	0.000000 (0.0 %)	0.000000 (0.0 %)	0.000000 (0.0 %)	0.000017 (100.0 %)	1.754000 (100 %)	INFINITE
		j	0.000000 (0.0 %)	0.000000 (0.0 %)	0.000000 (0.0 %)	0.000000 (0.0 %)	0.000000 (0.0 %)	0.000000 (0.0 %)	0.000000 (0.0 %)	0.000000 (0.0 %)	0.000042 (32.4 %)	0.000089 (67.5 %)	0.000132 (100 %)	7549.7
182	E	i	0.000000 (0.0 %)	0.000000 (0.0 %)	0.000000 (0.0 %)	0.000000 (0.0 %)	0.000000 (0.0 %)	0.000000 (0.0 %)	0.000000 (0.0 %)	0.000000 (0.0 %)	0.000070 (31.1 %)	0.000156 (68.8 %)	0.000227 (100 %)	4395.7
		j	0.000000 (0.0 %)	0.000000 (0.0 %)	0.000000 (0.0 %)	0.000000 (0.0 %)	0.000000 (0.0 %)	0.000000 (0.0 %)	0.000000 (0.0 %)	0.000000 (0.0 %)	0.000000 (0.0 %)	0.000018 (100.0 %)	1.870000 (100 %)	INFINITE
186	E	i	0.000000 (0.0 %)	0.000000 (0.0 %)	0.000000 (0.0 %)	0.000000 (0.0 %)	0.000000 (0.0 %)	0.000000 (0.0 %)	0.000000 (0.0 %)	0.000000 (0.0 %)	0.000000 (0.0 %)	0.000000 (0.0 %)	0.000000 (100 %)	INFINITE
	E'	j	0.000000 (0.0 %)	0.000000 (0.0 %)	0.000000 (0.0 %)	0.000000 (0.0 %)	0.000000 (0.0 %)	0.000000 (0.0 %)	0.000000 (0.0 %)	0.000037 (20.8 %)	0.000038 (21.2 %)	0.000103 (57.8 %)	0.000178 (100 %)	5595.3
211	ET	i	0.000000 (0.0 %)	0.000000 (0.0 %)	0.000000 (0.0 %)	0.000000 (0.0 %)	0.000590 (11.8 %)	0.000343 (6.9 %)	0.001213 (24.3 %)	0.001113 (22.3 %)	0.000353 (7.1 %)	0.001366 (27.4 %)	0.004979 (100 %)	200.8
		j	0.000000 (0.0 %)	0.000000 (0.0 %)	0.000000 (0.0 %)	0.000000 (0.0 %)	0.000579 (12.1 %)	0.000265 (5.5 %)	0.001199 (25.0 %)	0.001091 (22.8 %)	0.000333 (6.9 %)	0.001314 (27.4 %)	0.004783 (100 %)	209.1
260	ET	i	0.000000 (0.0 %)	0.000000 (0.0 %)	0.000000 (0.0 %)	0.000000 (0.0 %)	0.000000 (0.0 %)	0.000000 (0.0 %)	0.000145 (27.9 %)	0.000154 (29.7 %)	0.000046 (8.8 %)	0.000174 (33.4 %)	0.000521 (100 %)	1917.3
		j	0.000000 (0.0 %)	0.000000 (0.0 %)	0.000000 (0.0 %)	0.000000 (0.0 %)	0.000000 (0.0 %)	0.000000 (0.0 %)	0.000161 (26.5 %)	0.000198 (32.6 %)	0.000052 (8.6 %)	0.000195 (32.0 %)	0.000607 (100 %)	1645.1
281	ET	i	0.000000 (0.0 %)	0.000000 (0.0 %)	0.000000 (0.0 %)	0.000000 (0.0 %)	0.000000 (0.0 %)	0.000103 (21.6 %)	0.000116 (24.3 %)	0.000097 (20.2 %)	0.000065 (13.7 %)	0.000095 (19.9 %)	0.000479 (100 %)	2087.4
		j	0.000000 (0.0 %)	0.000000 (0.0 %)	0.000000 (0.0 %)	0.000000 (0.0 %)	0.000000 (0.0 %)	0.000097 (21.8 %)	0.000113 (25.4 %)	0.000089 (19.9 %)	0.000057 (12.9 %)	0.000088 (19.8 %)	0.000446 (100 %)	2238.1
300	ET	i	0.000000 (0.0 %)	0.000000 (0.0 %)	0.000000 (0.0 %)	0.000000 (0.0 %)	0.000236 (7.5 %)	0.000739 (23.6 %)	0.000601 (19.2 %)	0.000665 (21.2 %)	0.000358 (11.4 %)	0.000525 (16.8 %)	0.003126 (100 %)	319.8
		j	0.000000 (0.0 %)	0.000000 (0.0 %)	0.000000 (0.0 %)	0.000000 (0.0 %)	0.000230 (7.7 %)	0.000722 (24.3 %)	0.000584 (19.7 %)	0.000617 (20.8 %)	0.000331 (11.1 %)	0.000480 (16.2 %)	0.002967 (100 %)	337.0
301	ET	i	0.000000 (0.0 %)	0.000000 (0.0 %)	0.000000 (0.0 %)	0.000269 (2.8 %)	0.001342 (14.2 %)	0.000703 (7.4 %)	0.002643 (28.1 %)	0.002295 (24.4 %)	0.000449 (4.7 %)	0.001701 (18.1 %)	0.009405 (100 %)	106.3
		j	0.000000 (0.0 %)	0.000000 (0.0 %)	0.000000 (0.0 %)	0.000262 (2.8 %)	0.001206 (13.1 %)	0.000820 (8.9 %)	0.002722 (29.5 %)	0.002117 (22.9 %)	0.000451 (4.9 %)	0.001630 (17.7 %)	0.009213 (100 %)	108.5
328	ET	i	0.000000 (0.0 %)	0.000000 (0.0 %)	0.000000 (0.0 %)	0.000000 (0.0 %)	0.000122 (7.1 %)	0.000098 (5.7 %)	0.000570 (33.1 %)	0.000477 (27.7 %)	0.000071 (4.1 %)	0.000378 (22.0 %)	0.001718 (100 %)	582.0
		j	0.000000 (0.0 %)	0.000000 (0.0 %)	0.000000 (0.0 %)	0.000000 (0.0 %)	0.000122 (7.0 %)	0.000071 (4.1 %)	0.000644 (37.0 %)	0.000465 (26.8 %)	0.000071 (4.1 %)	0.000361 (20.7 %)	0.001737 (100 %)	575.6

Table 3.22: Fatigue Life and Damage Estimates for Sign Structure S-40-404 for Critical Members and 50% Confidence Level (Wind Direction: East and West).

Element Number	Detail Category	Element Node (end)	Mean Wind Speed										SUM	Fatigue Life
			5 mph	10 mph	15 mph	20 mph	25 mph	30 mph	35 mph	40 mph	45 mph	50 mph		
54	E	i	0.000000 (0.0 %)	0.000000 (0.0 %)	0.000000 (0.0 %)	0.000000 (0.0 %)	0.000000 (0.0 %)	0.000000 (0.0 %)	0.000000 (0.0 %)	0.000000 (0.0 %)	0.000000 (0.0 %)	0.000076 (100.0 %)	7.673000 (100 %)	INFINITE
		j	0.000000 (0.0 %)	0.000000 (0.0 %)	0.000000 (0.0 %)	0.000000 (0.0 %)	0.000000 (0.0 %)	0.000000 (0.0 %)	0.000000 (0.0 %)	0.000000 (0.0 %)	0.000000 (0.0 %)	0.000042 (100.0 %)	4.288000 (100 %)	INFINITE
55	E	i	0.000000 (0.0 %)	0.000000 (0.0 %)	0.000000 (0.0 %)	0.000000 (0.0 %)	0.000000 (0.0 %)	0.000000 (0.0 %)	0.000000 (0.0 %)	0.000000 (0.0 %)	0.000000 (0.0 %)	0.000040 (100.0 %)	4.087e-0 (100 %)	INFINITE
		j	0.000000 (0.0 %)	0.000000 (0.0 %)	0.000000 (0.0 %)	0.000000 (0.0 %)	0.000000 (0.0 %)	0.000000 (0.0 %)	0.000000 (0.0 %)	0.000000 (0.0 %)	0.000000 (0.0 %)	0.000091 (100.0 %)	9.103000 (100 %)	INFINITE
60	E	i	0.000000 (0.0 %)	0.000000 (0.0 %)	0.000000 (0.0 %)	0.000000 (0.0 %)	0.000000 (0.0 %)	0.000000 (0.0 %)	0.000000 (0.0 %)	0.000000 (0.0 %)	0.000000 (0.0 %)	0.000082 (100.0 %)	8.234999 (100 %)	INFINITE
	E'	j	0.000000 (0.0 %)	0.000000 (0.0 %)	0.000000 (0.0 %)	0.000000 (0.0 %)	0.000000 (0.0 %)	0.000000 (0.0 %)	0.000136 (37.4 %)	0.000080 (22.0 %)	0.000015 (4.1 %)	0.000132 (36.4 %)	0.000364 (100 %)	2742.4
181	E	i	0.000000 (0.0 %)	0.000000 (0.0 %)	0.000000 (0.0 %)	0.000000 (0.0 %)	0.000000 (0.0 %)	0.000000 (0.0 %)	0.000000 (0.0 %)	0.000000 (0.0 %)	0.000000 (0.0 %)	0.000014 (100.0 %)	1.497000 (100 %)	INFINITE
		j	0.000000 (0.0 %)	0.000000 (0.0 %)	0.000000 (0.0 %)	0.000000 (0.0 %)	0.000000 (0.0 %)	0.000000 (0.0 %)	0.000000 (0.0 %)	0.000000 (0.0 %)	0.000036 (32.4 %)	0.000076 (67.5 %)	0.000113 (100 %)	8842.4
182	E	i	0.000000 (0.0 %)	0.000000 (0.0 %)	0.000000 (0.0 %)	0.000000 (0.0 %)	0.000000 (0.0 %)	0.000000 (0.0 %)	0.000000 (0.0 %)	0.000000 (0.0 %)	0.000060 (31.1 %)	0.000133 (68.8 %)	0.000194 (100 %)	5148.3
		j	0.000000 (0.0 %)	0.000000 (0.0 %)	0.000000 (0.0 %)	0.000000 (0.0 %)	0.000000 (0.0 %)	0.000000 (0.0 %)	0.000000 (0.0 %)	0.000000 (0.0 %)	0.000000 (0.0 %)	0.000015 (100.0 %)	1.597000 (100 %)	INFINITE
186	E	i	0.000000 (0.0 %)	0.000000 (0.0 %)	0.000000 (0.0 %)	0.000000 (0.0 %)	0.000000 (0.0 %)	0.000000 (0.0 %)	0.000000 (0.0 %)	0.000000 (0.0 %)	0.000000 (0.0 %)	0.000000 (0.0 %)	0.000000 (100 %)	INFINITE
	E'	j	0.000000 (0.0 %)	0.000000 (0.0 %)	0.000000 (0.0 %)	0.000000 (0.0 %)	0.000000 (0.0 %)	0.000000 (0.0 %)	0.000000 (0.0 %)	0.000029 (20.8 %)	0.000030 (21.2 %)	0.000082 (57.8 %)	0.000142 (100 %)	7039.0
211	ET	i	0.000000 (0.0 %)	0.000000 (0.0 %)	0.000000 (0.0 %)	0.000000 (0.0 %)	0.000459 (11.8 %)	0.000267 (6.9 %)	0.000945 (24.3 %)	0.000866 (22.3 %)	0.000275 (7.1 %)	0.001063 (27.4 %)	0.003877 (100 %)	257.9
		j	0.000000 (0.0 %)	0.000000 (0.0 %)	0.000000 (0.0 %)	0.000000 (0.0 %)	0.000451 (12.1 %)	0.000206 (5.5 %)	0.000934 (25.0 %)	0.000849 (22.8 %)	0.000259 (6.9 %)	0.001023 (27.4 %)	0.003724 (100 %)	268.5
260	ET	i	0.000000 (0.0 %)	0.000000 (0.0 %)	0.000000 (0.0 %)	0.000000 (0.0 %)	0.000000 (0.0 %)	0.000000 (0.0 %)	0.000113 (27.9 %)	0.000120 (29.7 %)	0.000035 (8.8 %)	0.000135 (33.4 %)	0.000406 (100 %)	2462.1
		j	0.000000 (0.0 %)	0.000000 (0.0 %)	0.000000 (0.0 %)	0.000000 (0.0 %)	0.000000 (0.0 %)	0.000000 (0.0 %)	0.000125 (26.5 %)	0.000154 (32.6 %)	0.000040 (8.6 %)	0.000151 (32.0 %)	0.000473 (100 %)	2112.6
281	ET	i	0.000000 (0.0 %)	0.000000 (0.0 %)	0.000000 (0.0 %)	0.000000 (0.0 %)	0.000000 (0.0 %)	0.000080 (21.6 %)	0.000090 (24.3 %)	0.000075 (20.2 %)	0.000051 (13.7 %)	0.000074 (19.9 %)	0.000373 (100 %)	2680.5
		j	0.000000 (0.0 %)	0.000000 (0.0 %)	0.000000 (0.0 %)	0.000000 (0.0 %)	0.000000 (0.0 %)	0.000075 (21.8 %)	0.000088 (25.4 %)	0.000069 (19.9 %)	0.000044 (12.9 %)	0.000069 (19.8 %)	0.000347 (100 %)	2874.0
300	ET	i	0.000000 (0.0 %)	0.000000 (0.0 %)	0.000000 (0.0 %)	0.000000 (0.0 %)	0.000184 (7.5 %)	0.000575 (23.6 %)	0.000468 (19.2 %)	0.000517 (21.2 %)	0.000278 (11.4 %)	0.000409 (16.8 %)	0.002434 (100 %)	410.7
		j	0.000000 (0.0 %)	0.000000 (0.0 %)	0.000000 (0.0 %)	0.000000 (0.0 %)	0.000179 (7.7 %)	0.000562 (24.3 %)	0.000455 (19.7 %)	0.000480 (20.8 %)	0.000258 (11.1 %)	0.000374 (16.2 %)	0.002310 (100 %)	432.8
301	ET	i	0.000000 (0.0 %)	0.000000 (0.0 %)	0.000000 (0.0 %)	0.000209 (2.8 %)	0.001045 (14.2 %)	0.000547 (7.4 %)	0.002058 (28.1 %)	0.001787 (24.4 %)	0.000350 (4.7 %)	0.001325 (18.1 %)	0.007324 (100 %)	136.5
		j	0.000000 (0.0 %)	0.000000 (0.0 %)	0.000000 (0.0 %)	0.000204 (2.8 %)	0.000939 (13.1 %)	0.000639 (8.9 %)	0.002120 (29.5 %)	0.001649 (22.9 %)	0.000351 (4.9 %)	0.001270 (17.7 %)	0.007174 (100 %)	139.4
328	ET	i	0.000000 (0.0 %)	0.000000 (0.0 %)	0.000000 (0.0 %)	0.000000 (0.0 %)	0.000095 (7.1 %)	0.000076 (5.7 %)	0.000443 (33.1 %)	0.000371 (27.7 %)	0.000055 (4.1 %)	0.000294 (22.0 %)	0.001338 (100 %)	747.3
		j	0.000000 (0.0 %)	0.000000 (0.0 %)	0.000000 (0.0 %)	0.000000 (0.0 %)	0.000095 (7.0 %)	0.000055 (4.1 %)	0.000501 (37.0 %)	0.000362 (26.8 %)	0.000055 (4.1 %)	0.000281 (20.7 %)	0.001352 (100 %)	739.2

3.2.8.3 Structure S-67-402

Structure S-67-402 has several unique characteristics that make it highly interesting to study. Like S-40-404, it is a four-chord box truss. However, its span is significantly shorter. Furthermore, the anchor rod stand-off heights in the median-strip upright are severe (see Figure 3.16). Figure 3.7 contains a photograph of the structure in service.

An analytical study associated with truck-induced gust pressures (Ginal 2003) revealed several highly stressed, and therefore fatigue-critical, members and details within the structure. Table 3.23 includes a listing of these elements.

Table 3.23: Elements Evaluated in Truck Pulse Analysis of Sign Bridge S-67-402 (Ginal 2003).

Element #'s	Description
45, 47, 48, 56	Overhead truss bottom chord members located at span centerline.
106, 124, 142	Overhead truss tension web members located near north uprights
123, 141, 159	Overhead truss tension web members located near south uprights
1812, 1813	North upright round HSS members connecting to "plate" finite element rigid regions (Figure 3.17).
1815, 1817, 1818, 1820	North upright anchor rods

There are considerably more fatigue-critical components in this structure relative to the former structures analyzed. Part of the reason for this is the presence of the anchor rods being included in the analytical model. Figure 3.37 illustrates the critical element's positions within the complete analytical model for the sign support structure.

Following the recommendation of Dexter and Ricker (2002), the presence of the significant stand-off height results in anchor rod bending stresses being considered in the fatigue-life estimate. Furthermore, the compression portion of the stress cycle (if any) is included in the stress range counting algorithm (Dexter and Ricker 2002). The distance between the bottom of the leveling nut and the concrete pedestal surface is much greater than the anchor rod diameter. Furthermore, the base plate thickness at the north upright is very close to the anchor rod diameter. All this conspires to create a very interesting fatigue scenario for this structural component.

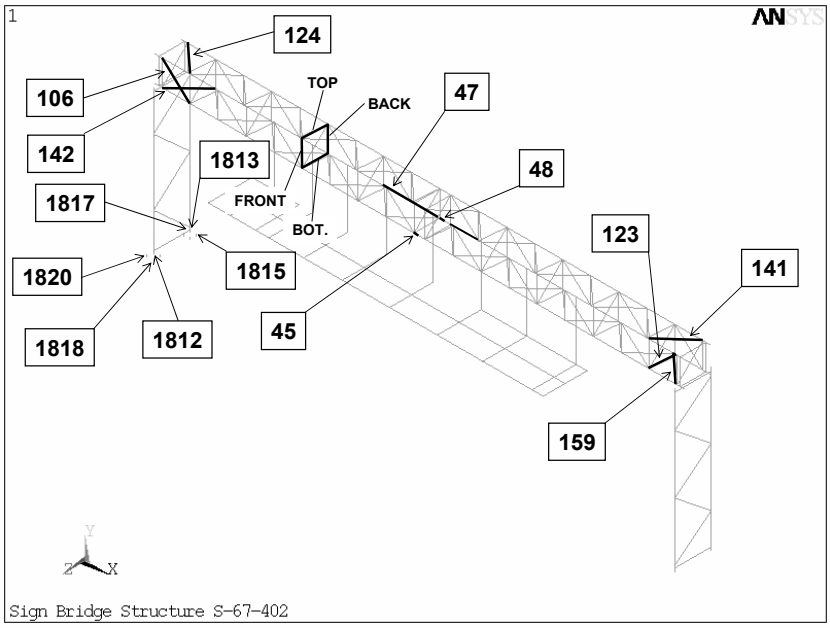

Figure 3.37: Sign Support Structure S-67-402 and Fatigue-Critical Elements.

A schematic of the anchor rod element is shown in Figure 3.38. It should be noted that bi-axial bending moments are present in the anchors within the analytical model.

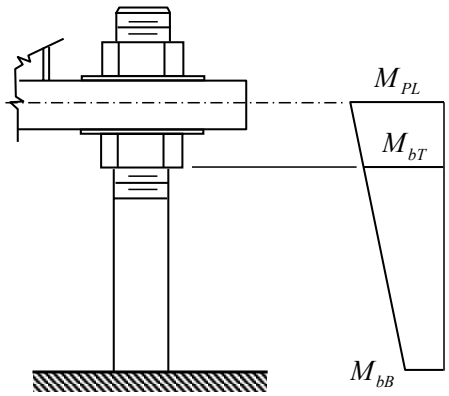

Figure 3.38: Anchor Rod Schematic and Resultant Vector Moment Diagram.

The analytical FE model assumes that the mid-plane thickness of the plate element is coincident with the node on the beam element modeling the anchor rod. The reality of the configuration requires that the anchor rod NOT generate curvature between the centerline of the base plate and the bottom of the leveling nut. Therefore, the bending moment, M_{PL}, is an aberration resulting from the analytical model. A more appropriate bending moment to consider in the analysis is that at the bottom of the leveling nut, M_{bT}.

The bending moments M_{PL} and M_{bB} are determined via finite element analysis. This results in a conservatively high bending moment in the anchor rod at the plate level. The leveling nut is not modeled. This can be easily appreciated through examination of the bending moment diagram in Figure 3.39 and comparing M_{bT} to M_{PL}. If the moment gradient over the anchor rod height is steep, then there will be a larger difference in these two moments. However, the "true" moment in the anchor rod at the top will be lower than M_{PL} reported by the software.

The total stress history (axial plus bending stress) for the anchor rods (element 1817) in structure S-67-402 are illustrated in Figures 3.39 and 3.40 (end "i" is M_{PL} in Figure 3.38).

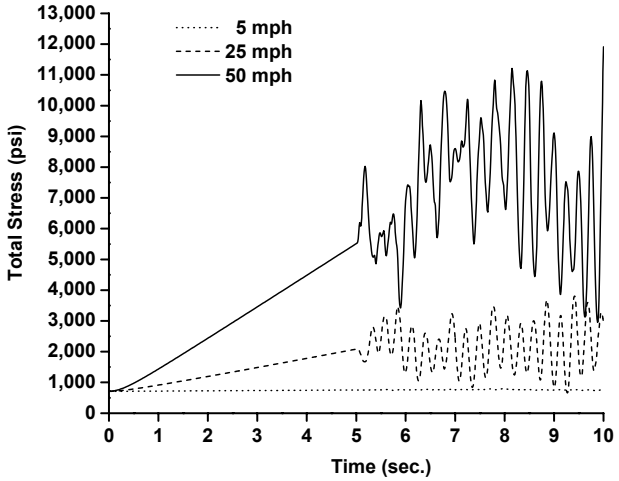

Figure 3.39: Stress History for Anchor Rod 1817 (at end "i") in Sign Support Structure S-67-402 During a Variety of Mean Wind Speeds.

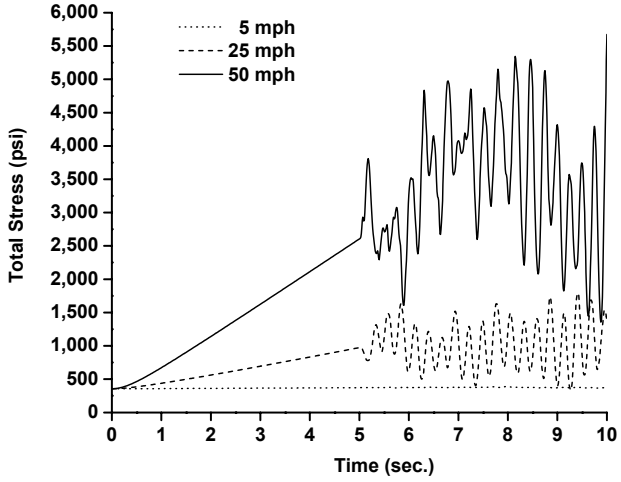

Figure 3.40: Stress History for Anchor Rod 1817 (at end "j") in Sign Support Structure S-67-402 During a Variety of Mean Wind Speeds.

The shape of the response at both ends is similar, but one can certainly see the significant difference in the magnitudes of the stress ranges. The stress ranges at the base of the anchor rod (embedment location into concrete pedestal) are much lower than those at the base plate centerline. It should be noted that the "stress area" and "stress moment of inertia" for the anchor rods are computed using recommendations of Dexter and Ricker (2002). This assumption extends to the cross section at the surface of the concrete pedestal even though the anchor rod threading may not extend into the concrete. The fatigue damage at the plate centerline is certainly expected to be much greater that at the anchor rod base, but the conservatism raised in the analytical model should not be discounted.

The stress response history of one of the diagonal members within the truss structure is shown in Figure 3.41.

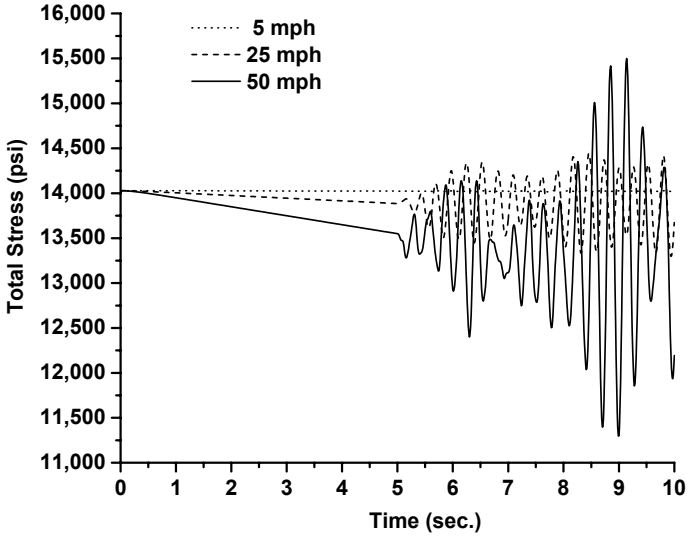

Figure 3.41: Stress History for Element 106 (at end "i") for Various Mean Wind Speeds.

Although the cyclic nature of the response is significant, the stress ranges are not the same magnitude as those for the anchor rods. However, the fatigue detail categories will determine the fatigue damage created by these cyclic loads.

Estimates for the fatigue life of this structure were determined using previously discussed methodologies. It should be noted that the anchor rods were considered non-pretensioned and in the "double-nut" configuration (see Figure 3.17). Therefore, the anchor rods can be considered as a fatigue detail category E' with CAFL consistent with category D (Dexter and Ricker 2002). The compression portion of the stress range (if any) was also included in a cycle count (Dexter and Ricker 2002). The fatigue lives were estimated for 95%, 70% and 50% confidence levels. The results are given in Tables 3.24 through 3.26.

Table 3.24: Fatigue Life and Damage Estimates for Sign Structure S-67-402 for Critical Members and 95% Confidence Level (Wind Direction: East and West).

Element Number	Detail Category	Element Node (end)	Mean Wind Speed										SUM	Fatigue Life
			5 mph	10 mph	15 mph	20 mph	25 mph	30 mph	35 mph	40 mph	45 mph	50 mph		
45	E	i	0.000000 (0.0 %)	0.000000 (0.0 %)	0.000000 (0.0 %)	0.000000 (0.0 %)	0.000000 (0.0 %)	0.000000 (0.0 %)	0.000000 (0.0 %)	0.000000 (0.0 %)	0.000000 (0.0 %)	0.000000 (0.0 %)	0.000000 (100 %)	INFINITE
	E'	j	0.000000 (0.0 %)	0.000000 (0.0 %)	0.000000 (0.0 %)	0.000000 (0.0 %)	0.000000 (0.0 %)	0.000000 (0.0 %)	0.000000 (0.0 %)	0.000000 (0.0 %)	0.000000 (0.0 %)	0.000000 (0.0 %)	0.000000 (100 %)	INFINITE
47	E	i	0.000000 (0.0 %)	0.000000 (0.0 %)	0.000000 (0.0 %)	0.000000 (0.0 %)	0.000000 (0.0 %)	0.000000 (0.0 %)	0.000000 (0.0 %)	0.000000 (0.0 %)	0.000000 (0.0 %)	0.000000 (0.0 %)	0.000000 (100 %)	INFINITE
		j	0.000000 (0.0 %)	0.000000 (0.0 %)	0.000000 (0.0 %)	0.000000 (0.0 %)	0.000000 (0.0 %)	0.000000 (0.0 %)	0.000000 (0.0 %)	0.000000 (0.0 %)	0.000000 (0.0 %)	0.000000 (0.0 %)	0.000000 (100 %)	INFINITE
48	E	i	0.000000 (0.0 %)	0.000000 (0.0 %)	0.000000 (0.0 %)	0.000000 (0.0 %)	0.000000 (0.0 %)	0.000000 (0.0 %)	0.000000 (0.0 %)	0.000000 (0.0 %)	0.000000 (0.0 %)	0.000000 (0.0 %)	0.000000 (100 %)	INFINITE
	E'	j	0.000000 (0.0 %)	0.000000 (0.0 %)	0.000000 (0.0 %)	0.000000 (0.0 %)	0.000000 (0.0 %)	0.000000 (0.0 %)	0.000000 (0.0 %)	0.000174 (50.9 %)	0.000082 (24.1 %)	0.000085 (24.9 %)	0.000342 (100 %)	2916.9
56	E	i	0.000000 (0.0 %)	0.000000 (0.0 %)	0.000000 (0.0 %)	0.000000 (0.0 %)	0.000000 (0.0 %)	0.000000 (0.0 %)	0.000000 (0.0 %)	0.000000 (0.0 %)	0.000038 (59.2 %)	0.000026 (40.7 %)	6.511000 (100 %)	INFINITE
		j	0.000000 (0.0 %)	0.000000 (0.0 %)	0.000000 (0.0 %)	0.000000 (0.0 %)	0.000000 (0.0 %)	0.000000 (0.0 %)	0.000000 (0.0 %)	0.000000 (0.0 %)	0.000000 (0.0 %)	0.000000 (0.0 %)	0.000000 (100 %)	INFINITE
106	ET	i	0.000000 (0.0 %)	0.000000 (0.0 %)	0.000000 (0.0 %)	0.000000 (0.0 %)	0.007004 (28.4 %)	0.002267 (9.2 %)	0.003917 (15.9 %)	0.004562 (18.5 %)	0.003542 (14.4 %)	0.003314 (13.4 %)	0.024609 (100 %)	40.6
		j	0.000000 (0.0 %)	0.000000 (0.0 %)	0.000000 (0.0 %)	0.000000 (0.0 %)	0.005408 (28.6 %)	0.001315 (6.9 %)	0.002997 (15.8 %)	0.003500 (18.5 %)	0.003049 (16.1 %)	0.002604 (13.8 %)	0.018875 (100 %)	53.0
123	ET	i	0.000000 (0.0 %)	0.000000 (0.0 %)	0.000000 (0.0 %)	0.000000 (0.0 %)	0.003515 (25.7 %)	0.000886 (6.4 %)	0.002305 (16.8 %)	0.002600 (19.0 %)	0.002305 (16.8 %)	0.002058 (15.0 %)	0.013671 (100 %)	73.2
		j	0.000000 (0.0 %)	0.000000 (0.0 %)	0.000000 (0.0 %)	0.000000 (0.0 %)	0.005503 (29.7 %)	0.001376 (7.4 %)	0.002976 (16.1 %)	0.003380 (18.3 %)	0.002660 (14.4 %)	0.002579 (13.9 %)	0.018477 (100 %)	54.1
124	ET	i	0.000000 (0.0 %)	0.000000 (0.0 %)	0.000000 (0.0 %)	0.000000 (0.0 %)	0.007294 (33.7 %)	0.001661 (7.6 %)	0.002836 (13.1 %)	0.004500 (20.8 %)	0.003511 (16.2 %)	0.001834 (8.4 %)	0.021639 (100 %)	46.2
		j	0.000000 (0.0 %)	0.000000 (0.0 %)	0.000000 (0.0 %)	0.000000 (0.0 %)	0.005806 (33.0 %)	0.001308 (7.4 %)	0.002342 (13.3 %)	0.003555 (20.2 %)	0.002955 (16.7 %)	0.001629 (9.2 %)	0.017597 (100 %)	56.8
141	ET	i	0.000000 (0.0 %)	0.000000 (0.0 %)	0.000000 (0.0 %)	0.000000 (0.0 %)	0.004119 (31.9 %)	0.000907 (7.0 %)	0.001703 (13.2 %)	0.002663 (20.6 %)	0.002240 (17.3 %)	0.001248 (9.6 %)	0.012883 (100 %)	77.6
		j	0.000000 (0.0 %)	0.000000 (0.0 %)	0.000000 (0.0 %)	0.000000 (0.0 %)	0.005045 (32.5 %)	0.001102 (7.1 %)	0.002022 (13.0 %)	0.003236 (20.8 %)	0.002653 (17.1 %)	0.001433 (9.2 %)	0.015494 (100 %)	64.5
142	ET	i	0.000000 (0.0 %)	0.000000 (0.0 %)	0.000000 (0.0 %)	0.000000 (0.0 %)	0.000000 (0.0 %)	0.000354 (9.2 %)	0.000486 (12.7 %)	0.001154 (30.1 %)	0.000627 (16.3 %)	0.001210 (31.5 %)	0.003834 (100 %)	260.8
		j	0.000000 (0.0 %)	0.000000 (0.0 %)	0.000000 (0.0 %)	0.000000 (0.0 %)	0.000206 (4.5 %)	0.000291 (6.4 %)	0.000503 (11.1 %)	0.001464 (32.3 %)	0.000845 (18.6 %)	0.001223 (26.9 %)	0.004535 (100 %)	220.5
159	ET	i	0.000000 (0.0 %)	0.000000 (0.0 %)	0.000000 (0.0 %)	0.000000 (0.0 %)	0.000000 (0.0 %)	0.000142 (4.8 %)	0.000352 (11.9 %)	0.000911 (30.7 %)	0.000579 (19.5 %)	0.000978 (32.9 %)	0.002965 (100 %)	337.3
		j	0.000000 (0.0 %)	0.000000 (0.0 %)	0.000000 (0.0 %)	0.000000 (0.0 %)	0.000000 (0.0 %)	0.000224 (7.0 %)	0.000452 (14.2 %)	0.000914 (28.6 %)	0.000500 (15.6 %)	0.001097 (34.4 %)	0.003188 (100 %)	313.6
1812	E'	i	0.000000 (0.0 %)	0.000000 (0.0 %)	0.000000 (0.0 %)	0.000000 (0.0 %)	0.000000 (0.0 %)	0.000000 (0.0 %)	0.000000 (0.0 %)	0.000000 (0.0 %)	0.000085 (42.5 %)	0.000116 (57.5 %)	0.000202 (100 %)	4942.8
		j	0.000000 (0.0 %)	0.000000 (0.0 %)	0.000000 (0.0 %)	0.000000 (0.0 %)	0.000000 (0.0 %)	0.000000 (0.0 %)	0.000000 (0.0 %)	0.000000 (0.0 %)	0.000056 (41.3 %)	0.000080 (58.7 %)	0.000137 (100 %)	7275.4
1813	E'	i	0.000000 (0.0 %)	0.000000 (0.0 %)	0.000000 (0.0 %)	0.000000 (0.0 %)	0.000000 (0.0 %)	0.000000 (0.0 %)	0.000000 (0.0 %)	0.000000 (0.0 %)	0.000000 (0.0 %)	0.000000 (0.0 %)	0.000000 (100 %)	INFINITE
		j	0.000000 (0.0 %)	0.000000 (0.0 %)	0.000000 (0.0 %)	0.000000 (0.0 %)	0.000000 (0.0 %)	0.000000 (0.0 %)	0.000000 (0.0 %)	0.000000 (0.0 %)	0.000000 (0.0 %)	0.000000 (0.0 %)	0.000000 (100 %)	INFINITE
1815	E'	i	0.000000 (0.0 %)	0.000000 (0.0 %)	0.000000 (0.0 %)	0.000000 (0.0 %)	0.000000 (0.0 %)	0.006407 (7.5 %)	0.010286 (12.1 %)	0.031690 (37.5 %)	0.021091 (24.9 %)	0.014967 (17.7 %)	0.084443 (100 %)	11.8
		j	0.000000 (0.0 %)	0.000000 (0.0 %)	0.000000 (0.0 %)	0.000000 (0.0 %)	0.000000 (0.0 %)	0.000000 (0.0 %)	0.000000 (0.0 %)	0.001375 (31.7 %)	0.001749 (40.3 %)	0.001207 (27.8 %)	0.004332 (100 %)	230.8
1817	E'	i	0.000000 (0.0 %)	0.000000 (0.0 %)	0.000000 (0.0 %)	0.000000 (0.0 %)	0.000000 (0.0 %)	0.007205 (7.5 %)	0.012867 (13.5 %)	0.034531 (36.3 %)	0.023853 (25.1 %)	0.016514 (17.3 %)	0.094972 (100 %)	10.5
		j	0.000000 (0.0 %)	0.000000 (0.0 %)	0.000000 (0.0 %)	0.000000 (0.0 %)	0.000000 (0.0 %)	0.000000 (0.0 %)	0.000000 (0.0 %)	0.001340 (31.4 %)	0.001744 (41.0 %)	0.001170 (27.5 %)	0.004255 (100 %)	235.0
1818	E'	i	0.000000 (0.0 %)	0.000000 (0.0 %)	0.000000 (0.0 %)	0.000000 (0.0 %)	0.000000 (0.0 %)	0.000000 (0.0 %)	0.005338 (19.7 %)	0.008200 (30.3 %)	0.006808 (25.2 %)	0.006672 (24.6 %)	0.027020 (100 %)	37.0
		j	0.000000 (0.0 %)	0.000000 (0.0 %)	0.000000 (0.0 %)	0.000000 (0.0 %)	0.000000 (0.0 %)	0.000000 (0.0 %)	0.000000 (0.0 %)	0.000000 (0.0 %)	0.000787 (65.1 %)	0.000421 (34.8 %)	0.001208 (100 %)	827.2
1820	E'	i	0.000000 (0.0 %)	0.000000 (0.0 %)	0.000000 (0.0 %)	0.000000 (0.0 %)	0.000000 (0.0 %)	0.000000 (0.0 %)	0.005636 (21.7 %)	0.010084 (38.9 %)	0.005734 (22.1 %)	0.004422 (17.0 %)	0.025878 (100 %)	38.6
		j	0.000000 (0.0 %)	0.000000 (0.0 %)	0.000000 (0.0 %)	0.000000 (0.0 %)	0.000000 (0.0 %)	0.000000 (0.0 %)	0.000000 (0.0 %)	0.000000 (0.0 %)	0.000757 (65.4 %)	0.000399 (34.5 %)	0.001156 (100 %)	864.8

Notes:

1.) It should be noted that the anchor bolts (elements 1815, 1817, 1818, and 1820) are considered to be non-pretensioned and are assumed to have a CAFL equal to that for category *D* details (*i.e.* 7,000 psi).

Table 3.25: Fatigue Life and Damage Estimates for Sign Structure S-67-402 for Critical Members and 70% Confidence Level (Wind Direction: East and West).

Element Number	Detail Category	Element Node (end)	Mean Wind Speed										SUM	Fatigue Life
			5 mph	10 mph	15 mph	20 mph	25 mph	30 mph	35 mph	40 mph	45 mph	50 mph		
45	E	i	0.000000 (0.0 %)	0.000000 (0.0 %)	0.000000 (0.0 %)	0.000000 (0.0 %)	0.000000 (0.0 %)	0.000000 (0.0 %)	0.000000 (0.0 %)	0.000000 (0.0 %)	0.000000 (0.0 %)	0.000000 (0.0 %)	0.000000 (100 %)	INFINITE
	E'	j	0.000000 (0.0 %)	0.000000 (0.0 %)	0.000000 (0.0 %)	0.000000 (0.0 %)	0.000000 (0.0 %)	0.000000 (0.0 %)	0.000000 (0.0 %)	0.000000 (0.0 %)	0.000000 (0.0 %)	0.000000 (0.0 %)	0.000000 (100 %)	INFINITE
47	E	i	0.000000 (0.0 %)	0.000000 (0.0 %)	0.000000 (0.0 %)	0.000000 (0.0 %)	0.000000 (0.0 %)	0.000000 (0.0 %)	0.000000 (0.0 %)	0.000000 (0.0 %)	0.000000 (0.0 %)	0.000000 (0.0 %)	0.000000 (100 %)	INFINITE
		j	0.000000 (0.0 %)	0.000000 (0.0 %)	0.000000 (0.0 %)	0.000000 (0.0 %)	0.000000 (0.0 %)	0.000000 (0.0 %)	0.000000 (0.0 %)	0.000000 (0.0 %)	0.000000 (0.0 %)	0.000000 (0.0 %)	0.000000 (100 %)	INFINITE
48	E	i	0.000000 (0.0 %)	0.000000 (0.0 %)	0.000000 (0.0 %)	0.000000 (0.0 %)	0.000000 (0.0 %)	0.000000 (0.0 %)	0.000000 (0.0 %)	0.000000 (0.0 %)	0.000000 (0.0 %)	0.000000 (0.0 %)	0.000000 (100 %)	INFINITE
	E'	j	0.000000 (0.0 %)	0.000000 (0.0 %)	0.000000 (0.0 %)	0.000000 (0.0 %)	0.000000 (0.0 %)	0.000000 (0.0 %)	0.000000 (0.0 %)	0.000114 (50.9 %)	0.000054 (24.1 %)	0.000056 (24.9 %)	0.000225 (100 %)	4435.2
56	E	i	0.000000 (0.0 %)	0.000000 (0.0 %)	0.000000 (0.0 %)	0.000000 (0.0 %)	0.000000 (0.0 %)	0.000000 (0.0 %)	0.000000 (0.0 %)	0.000000 (0.0 %)	0.000028 (59.2 %)	0.000019 (40.7 %)	4.727e-0 (100 %)	INFINITE
		j	0.000000 (0.0 %)	0.000000 (0.0 %)	0.000000 (0.0 %)	0.000000 (0.0 %)	0.000000 (0.0 %)	0.000000 (0.0 %)	0.000000 (0.0 %)	0.000000 (0.0 %)	0.000000 (0.0 %)	0.000000 (0.0 %)	0.000000 (100 %)	INFINITE
106	ET	i	0.000000 (0.0 %)	0.000000 (0.0 %)	0.000000 (0.0 %)	0.000000 (0.0 %)	0.004105 (28.4 %)	0.001329 (9.2 %)	0.002295 (15.9 %)	0.002673 (18.5 %)	0.002076 (14.4 %)	0.001942 (13.4 %)	0.014423 (100 %)	69.3
		j	0.000000 (0.0 %)	0.000000 (0.0 %)	0.000000 (0.0 %)	0.000000 (0.0 %)	0.003169 (28.6 %)	0.000771 (6.9 %)	0.001756 (15.8 %)	0.002051 (18.5 %)	0.001787 (16.1 %)	0.001526 (13.8 %)	0.011062 (100 %)	90.4
123	ET	i	0.000000 (0.0 %)	0.000000 (0.0 %)	0.000000 (0.0 %)	0.000000 (0.0 %)	0.002060 (25.7 %)	0.000519 (6.4 %)	0.001351 (16.8 %)	0.001523 (19.0 %)	0.001350 (16.8 %)	0.001206 (15.0 %)	0.008012 (100 %)	124.8
		j	0.000000 (0.0 %)	0.000000 (0.0 %)	0.000000 (0.0 %)	0.000000 (0.0 %)	0.003225 (29.7 %)	0.000806 (7.4 %)	0.001744 (16.1 %)	0.001981 (18.3 %)	0.001559 (14.4 %)	0.001511 (13.9 %)	0.010828 (100 %)	92.3
124	ET	i	0.000000 (0.0 %)	0.000000 (0.0 %)	0.000000 (0.0 %)	0.000000 (0.0 %)	0.004274 (33.7 %)	0.000973 (7.6 %)	0.001662 (13.1 %)	0.002637 (20.8 %)	0.002057 (16.2 %)	0.001075 (8.4 %)	0.012682 (100 %)	78.9
		j	0.000000 (0.0 %)	0.000000 (0.0 %)	0.000000 (0.0 %)	0.000000 (0.0 %)	0.003403 (33.0 %)	0.000767 (7.4 %)	0.001372 (13.3 %)	0.002083 (20.2 %)	0.001731 (16.7 %)	0.000955 (9.2 %)	0.010313 (100 %)	97.0
141	ET	i	0.000000 (0.0 %)	0.000000 (0.0 %)	0.000000 (0.0 %)	0.000000 (0.0 %)	0.002414 (31.9 %)	0.000531 (7.0 %)	0.000998 (13.2 %)	0.001561 (20.6 %)	0.001312 (17.3 %)	0.000731 (9.6 %)	0.007550 (100 %)	132.4
		j	0.000000 (0.0 %)	0.000000 (0.0 %)	0.000000 (0.0 %)	0.000000 (0.0 %)	0.002956 (32.5 %)	0.000646 (7.1 %)	0.001185 (13.0 %)	0.001897 (20.8 %)	0.001554 (17.1 %)	0.000840 (9.2 %)	0.009080 (100 %)	110.1
142	ET	i	0.000000 (0.0 %)	0.000000 (0.0 %)	0.000000 (0.0 %)	0.000000 (0.0 %)	0.000000 (0.0 %)	0.000208 (9.2 %)	0.000285 (12.7 %)	0.000676 (30.1 %)	0.000367 (16.3 %)	0.000709 (31.5 %)	0.002247 (100 %)	445.0
		j	0.000000 (0.0 %)	0.000000 (0.0 %)	0.000000 (0.0 %)	0.000000 (0.0 %)	0.000120 (4.5 %)	0.000171 (6.4 %)	0.000294 (11.1 %)	0.000858 (32.3 %)	0.000495 (18.6 %)	0.000717 (26.9 %)	0.002658 (100 %)	376.2
159	ET	i	0.000000 (0.0 %)	0.000000 (0.0 %)	0.000000 (0.0 %)	0.000000 (0.0 %)	0.000000 (0.0 %)	0.000083 (4.8 %)	0.000206 (11.9 %)	0.000534 (30.7 %)	0.000339 (19.5 %)	0.000573 (32.9 %)	0.001737 (100 %)	575.5
		j	0.000000 (0.0 %)	0.000000 (0.0 %)	0.000000 (0.0 %)	0.000000 (0.0 %)	0.000000 (0.0 %)	0.000131 (7.0 %)	0.000265 (14.2 %)	0.000535 (28.6 %)	0.000293 (15.6 %)	0.000643 (34.4 %)	0.001868 (100 %)	535.1
1812	E'	i	0.000000 (0.0 %)	0.000000 (0.0 %)	0.000000 (0.0 %)	0.000000 (0.0 %)	0.000000 (0.0 %)	0.000000 (0.0 %)	0.000000 (0.0 %)	0.000000 (0.0 %)	0.000056 (42.5 %)	0.000076 (57.5 %)	0.000133 (100 %)	7515.5
		j	0.000000 (0.0 %)	0.000000 (0.0 %)	0.000000 (0.0 %)	0.000000 (0.0 %)	0.000000 (0.0 %)	0.000000 (0.0 %)	0.000000 (0.0 %)	0.000000 (0.0 %)	0.000037 (41.3 %)	0.000053 (58.7 %)	9.040000 (100 %)	INFINITE
1813	E'	i	0.000000 (0.0 %)	0.000000 (0.0 %)	0.000000 (0.0 %)	0.000000 (0.0 %)	0.000000 (0.0 %)	0.000000 (0.0 %)	0.000000 (0.0 %)	0.000000 (0.0 %)	0.000000 (0.0 %)	0.000000 (0.0 %)	0.000000 (100 %)	INFINITE
		j	0.000000 (0.0 %)	0.000000 (0.0 %)	0.000000 (0.0 %)	0.000000 (0.0 %)	0.000000 (0.0 %)	0.000000 (0.0 %)	0.000000 (0.0 %)	0.000000 (0.0 %)	0.000000 (0.0 %)	0.000000 (0.0 %)	0.000000 (100 %)	INFINITE
1815	E'	i	0.000000 (0.0 %)	0.000000 (0.0 %)	0.000000 (0.0 %)	0.000000 (0.0 %)	0.000000 (0.0 %)	0.004213 (7.5 %)	0.006765 (12.1 %)	0.020841 (37.5 %)	0.013871 (24.9 %)	0.009843 (17.7 %)	0.055536 (100 %)	18.0
		j	0.000000 (0.0 %)	0.000000 (0.0 %)	0.000000 (0.0 %)	0.000000 (0.0 %)	0.000000 (0.0 %)	0.000000 (0.0 %)	0.000000 (0.0 %)	0.000904 (31.7 %)	0.001150 (40.3 %)	0.000794 (27.8 %)	0.002849 (100 %)	350.9
1817	E'	i	0.000000 (0.0 %)	0.000000 (0.0 %)	0.000000 (0.0 %)	0.000000 (0.0 %)	0.000000 (0.0 %)	0.004739 (7.5 %)	0.008462 (13.5 %)	0.022710 (36.3 %)	0.015687 (25.1 %)	0.010861 (17.3 %)	0.062461 (100 %)	16.0
		j	0.000000 (0.0 %)	0.000000 (0.0 %)	0.000000 (0.0 %)	0.000000 (0.0 %)	0.000000 (0.0 %)	0.000000 (0.0 %)	0.000000 (0.0 %)	0.000881 (31.4 %)	0.001147 (41.0 %)	0.000769 (27.5 %)	0.002798 (100 %)	357.3
1818	E'	i	0.000000 (0.0 %)	0.000000 (0.0 %)	0.000000 (0.0 %)	0.000000 (0.0 %)	0.000000 (0.0 %)	0.000000 (0.0 %)	0.003511 (19.7 %)	0.005393 (30.3 %)	0.004477 (25.2 %)	0.004388 (24.6 %)	0.017770 (100 %)	56.3
		j	0.000000 (0.0 %)	0.000000 (0.0 %)	0.000000 (0.0 %)	0.000000 (0.0 %)	0.000000 (0.0 %)	0.000000 (0.0 %)	0.000000 (0.0 %)	0.000000 (0.0 %)	0.000518 (65.1 %)	0.000276 (34.8 %)	0.000795 (100 %)	1257.7
1820	E'	i	0.000000 (0.0 %)	0.000000 (0.0 %)	0.000000 (0.0 %)	0.000000 (0.0 %)	0.000000 (0.0 %)	0.000000 (0.0 %)	0.003707 (21.7 %)	0.006632 (38.9 %)	0.003771 (22.1 %)	0.002908 (17.0 %)	0.017019 (100 %)	58.8
		j	0.000000 (0.0 %)	0.000000 (0.0 %)	0.000000 (0.0 %)	0.000000 (0.0 %)	0.000000 (0.0 %)	0.000000 (0.0 %)	0.000000 (0.0 %)	0.000000 (0.0 %)	0.000497 (65.4 %)	0.000262 (34.5 %)	0.000760 (100 %)	1314.9

Table 3.26: Fatigue Life and Damage Estimates for Sign Structure S-67-402 for Critical Members and 50% Confidence Level (Wind Direction: East and West).

Element Number	Detail Category	Element Node (end)	Mean Wind Speed										SUM	Fatigue Life
			5 mph	10 mph	15 mph	20 mph	25 mph	30 mph	35 mph	40 mph	45 mph	50 mph		
45	E	i	0.000000 (0.0 %)	0.000000 (0.0 %)	0.000000 (0.0 %)	0.000000 (0.0 %)	0.000000 (0.0 %)	0.000000 (0.0 %)	0.000000 (0.0 %)	0.000000 (0.0 %)	0.000000 (0.0 %)	0.000000 (0.0 %)	0.000000 (100 %)	INFINITE
	E'	j	0.000000 (0.0 %)	0.000000 (0.0 %)	0.000000 (0.0 %)	0.000000 (0.0 %)	0.000000 (0.0 %)	0.000000 (0.0 %)	0.000000 (0.0 %)	0.000000 (0.0 %)	0.000000 (0.0 %)	0.000000 (0.0 %)	0.000000 (100 %)	INFINITE
47	E	i	0.000000 (0.0 %)	0.000000 (0.0 %)	0.000000 (0.0 %)	0.000000 (0.0 %)	0.000000 (0.0 %)	0.000000 (0.0 %)	0.000000 (0.0 %)	0.000000 (0.0 %)	0.000000 (0.0 %)	0.000000 (0.0 %)	0.000000 (100 %)	INFINITE
		j	0.000000 (0.0 %)	0.000000 (0.0 %)	0.000000 (0.0 %)	0.000000 (0.0 %)	0.000000 (0.0 %)	0.000000 (0.0 %)	0.000000 (0.0 %)	0.000000 (0.0 %)	0.000000 (0.0 %)	0.000000 (0.0 %)	0.000000 (100 %)	INFINITE
48	E	i	0.000000 (0.0 %)	0.000000 (0.0 %)	0.000000 (0.0 %)	0.000000 (0.0 %)	0.000000 (0.0 %)	0.000000 (0.0 %)	0.000000 (0.0 %)	0.000000 (0.0 %)	0.000000 (0.0 %)	0.000000 (0.0 %)	0.000000 (100 %)	INFINITE
	E'	j	0.000000 (0.0 %)	0.000000 (0.0 %)	0.000000 (0.0 %)	0.000000 (0.0 %)	0.000000 (0.0 %)	0.000000 (0.0 %)	0.000000 (0.0 %)	0.000091 (50.9 %)	0.000043 (24.1 %)	0.000044 (24.9 %)	0.000179 (100 %)	5579.5
56	E	i	0.000000 (0.0 %)	0.000000 (0.0 %)	0.000000 (0.0 %)	0.000000 (0.0 %)	0.000000 (0.0 %)	0.000000 (0.0 %)	0.000000 (0.0 %)	0.000000 (0.0 %)	0.000023 (59.2 %)	0.000016 (40.7 %)	4.037000 (100 %)	INFINITE
		j	0.000000 (0.0 %)	0.000000 (0.0 %)	0.000000 (0.0 %)	0.000000 (0.0 %)	0.000000 (0.0 %)	0.000000 (0.0 %)	0.000000 (0.0 %)	0.000000 (0.0 %)	0.000000 (0.0 %)	0.000000 (0.0 %)	0.000000 (100 %)	INFINITE
106	ET	i	0.000000 (0.0 %)	0.000000 (0.0 %)	0.000000 (0.0 %)	0.000000 (0.0 %)	0.003197 (28.4 %)	0.001034 (9.2 %)	0.001787 (15.9 %)	0.002082 (18.5 %)	0.001616 (14.4 %)	0.001512 (13.4 %)	0.011231 (100 %)	89.0
		j	0.000000 (0.0 %)	0.000000 (0.0 %)	0.000000 (0.0 %)	0.000000 (0.0 %)	0.002468 (28.6 %)	0.000600 (6.9 %)	0.001367 (15.8 %)	0.001597 (18.5 %)	0.001391 (16.1 %)	0.001188 (13.8 %)	0.008614 (100 %)	116.1
123	ET	i	0.000000 (0.0 %)	0.000000 (0.0 %)	0.000000 (0.0 %)	0.000000 (0.0 %)	0.001604 (25.7 %)	0.000404 (6.4 %)	0.001052 (16.8 %)	0.001186 (19.0 %)	0.001052 (16.8 %)	0.000939 (15.0 %)	0.006239 (100 %)	160.3
		j	0.000000 (0.0 %)	0.000000 (0.0 %)	0.000000 (0.0 %)	0.000000 (0.0 %)	0.002511 (29.7 %)	0.000628 (7.4 %)	0.001358 (16.1 %)	0.001542 (18.3 %)	0.001214 (14.4 %)	0.001177 (13.9 %)	0.008432 (100 %)	118.6
124	ET	i	0.000000 (0.0 %)	0.000000 (0.0 %)	0.000000 (0.0 %)	0.000000 (0.0 %)	0.003328 (33.7 %)	0.000758 (7.6 %)	0.001294 (13.1 %)	0.002054 (20.8 %)	0.001602 (16.2 %)	0.000837 (8.4 %)	0.009876 (100 %)	101.3
		j	0.000000 (0.0 %)	0.000000 (0.0 %)	0.000000 (0.0 %)	0.000000 (0.0 %)	0.002650 (33.0 %)	0.000597 (7.4 %)	0.001068 (13.3 %)	0.001622 (20.2 %)	0.001348 (16.7 %)	0.000743 (9.2 %)	0.008031 (100 %)	124.5
141	ET	i	0.000000 (0.0 %)	0.000000 (0.0 %)	0.000000 (0.0 %)	0.000000 (0.0 %)	0.001880 (31.9 %)	0.000414 (7.0 %)	0.000777 (13.2 %)	0.001215 (20.6 %)	0.001022 (17.3 %)	0.000569 (9.6 %)	0.005879 (100 %)	170.1
		j	0.000000 (0.0 %)	0.000000 (0.0 %)	0.000000 (0.0 %)	0.000000 (0.0 %)	0.002302 (32.5 %)	0.000503 (7.1 %)	0.000923 (13.0 %)	0.001477 (20.8 %)	0.001210 (17.1 %)	0.000654 (9.2 %)	0.007071 (100 %)	141.4
142	ET	i	0.000000 (0.0 %)	0.000000 (0.0 %)	0.000000 (0.0 %)	0.000000 (0.0 %)	0.000000 (0.0 %)	0.000162 (9.2 %)	0.000222 (12.7 %)	0.000527 (30.1 %)	0.000286 (16.3 %)	0.000552 (31.5 %)	0.001750 (100 %)	571.4
		j	0.000000 (0.0 %)	0.000000 (0.0 %)	0.000000 (0.0 %)	0.000000 (0.0 %)	0.000094 (4.5 %)	0.000133 (6.4 %)	0.000229 (11.1 %)	0.000668 (32.3 %)	0.000385 (18.6 %)	0.000558 (26.9 %)	0.002069 (100 %)	483.1
159	ET	i	0.000000 (0.0 %)	0.000000 (0.0 %)	0.000000 (0.0 %)	0.000000 (0.0 %)	0.000000 (0.0 %)	0.000065 (4.8 %)	0.000161 (11.9 %)	0.000415 (30.7 %)	0.000264 (19.5 %)	0.000446 (32.9 %)	0.001353 (100 %)	739.0
		j	0.000000 (0.0 %)	0.000000 (0.0 %)	0.000000 (0.0 %)	0.000000 (0.0 %)	0.000000 (0.0 %)	0.000102 (7.0 %)	0.000206 (14.2 %)	0.000417 (28.6 %)	0.000228 (15.6 %)	0.000500 (34.4 %)	0.001455 (100 %)	687.1
1812	E'	i	0.000000 (0.0 %)	0.000000 (0.0 %)	0.000000 (0.0 %)	0.000000 (0.0 %)	0.000000 (0.0 %)	0.000000 (0.0 %)	0.000000 (0.0 %)	0.000000 (0.0 %)	0.000044 (42.5 %)	0.000060 (57.5 %)	0.000105 (100 %)	9454.6
		j	0.000000 (0.0 %)	0.000000 (0.0 %)	0.000000 (0.0 %)	0.000000 (0.0 %)	0.000000 (0.0 %)	0.000000 (0.0 %)	0.000000 (0.0 %)	0.000000 (0.0 %)	0.000029 (41.3 %)	0.000042 (58.7 %)	7.184999 (100 %)	INFINITE
1813	E'	i	0.000000 (0.0 %)	0.000000 (0.0 %)	0.000000 (0.0 %)	0.000000 (0.0 %)	0.000000 (0.0 %)	0.000000 (0.0 %)	0.000000 (0.0 %)	0.000000 (0.0 %)	0.000000 (0.0 %)	0.000000 (0.0 %)	0.000000 (100 %)	INFINITE
		j	0.000000 (0.0 %)	0.000000 (0.0 %)	0.000000 (0.0 %)	0.000000 (0.0 %)	0.000000 (0.0 %)	0.000000 (0.0 %)	0.000000 (0.0 %)	0.000000 (0.0 %)	0.000000 (0.0 %)	0.000000 (0.0 %)	0.000000 (100 %)	INFINITE
1815	E'	i	0.000000 (0.0 %)	0.000000 (0.0 %)	0.000000 (0.0 %)	0.000000 (0.0 %)	0.000000 (0.0 %)	0.003349 (7.5 %)	0.005377 (12.1 %)	0.016567 (37.5 %)	0.011026 (24.9 %)	0.007824 (17.7 %)	0.044146 (100 %)	22.7
		j	0.000000 (0.0 %)	0.000000 (0.0 %)	0.000000 (0.0 %)	0.000000 (0.0 %)	0.000000 (0.0 %)	0.000000 (0.0 %)	0.000000 (0.0 %)	0.000719 (31.7 %)	0.000914 (40.3 %)	0.000631 (27.8 %)	0.002265 (100 %)	441.5
1817	E'	i	0.000000 (0.0 %)	0.000000 (0.0 %)	0.000000 (0.0 %)	0.000000 (0.0 %)	0.000000 (0.0 %)	0.003767 (7.5 %)	0.006727 (13.5 %)	0.018052 (36.3 %)	0.012470 (25.1 %)	0.008633 (17.3 %)	0.049650 (100 %)	20.1
		j	0.000000 (0.0 %)	0.000000 (0.0 %)	0.000000 (0.0 %)	0.000000 (0.0 %)	0.000000 (0.0 %)	0.000000 (0.0 %)	0.000000 (0.0 %)	0.000700 (31.4 %)	0.000911 (41.0 %)	0.000611 (27.5 %)	0.002224 (100 %)	449.5
1818	E'	i	0.000000 (0.0 %)	0.000000 (0.0 %)	0.000000 (0.0 %)	0.000000 (0.0 %)	0.000000 (0.0 %)	0.000000 (0.0 %)	0.002791 (19.7 %)	0.004287 (30.3 %)	0.003559 (25.2 %)	0.003488 (24.6 %)	0.014125 (100 %)	70.8
		j	0.000000 (0.0 %)	0.000000 (0.0 %)	0.000000 (0.0 %)	0.000000 (0.0 %)	0.000000 (0.0 %)	0.000000 (0.0 %)	0.000000 (0.0 %)	0.000000 (0.0 %)	0.000411 (65.1 %)	0.000220 (34.8 %)	0.000632 (100 %)	1582.2
1820	E'	i	0.000000 (0.0 %)	0.000000 (0.0 %)	0.000000 (0.0 %)	0.000000 (0.0 %)	0.000000 (0.0 %)	0.000000 (0.0 %)	0.002946 (21.7 %)	0.005272 (38.9 %)	0.002997 (22.1 %)	0.002312 (17.0 %)	0.013529 (100 %)	73.9
		j	0.000000 (0.0 %)	0.000000 (0.0 %)	0.000000 (0.0 %)	0.000000 (0.0 %)	0.000000 (0.0 %)	0.000000 (0.0 %)	0.000000 (0.0 %)	0.000000 (0.0 %)	0.000395 (65.4 %)	0.000208 (34.5 %)	0.000604 (100 %)	1654.1

The fatigue life of these structures is limited by the anchor rods. The fatigue life estimate for this structure is 10.5 years with 95% confidence. This life-span is governed by the anchor rod 1817 at end "i", which is the bending moment at the plate centerline. This is expected to be a very conservative number (*i.e.* low estimate for fatigue life) because the bending moment at the plate centerline has been shown to be conservative. If stress cycles include this high bending moment, the fatigue life will be adversely affected and predictions will be of shorter duration than the "true life". The staggering difference in fatigue life when end "j" is considered should be noted. This emphasizes the importance of the bending moment contribution obtained from the hybrid FEA models in establishing fatigue damage for the anchor rods in this structure.

It is perhaps more important to note that there is significant bending in the anchor rods in this structure. It appears that current recommendations (AASHTO 2001; Dexter and Ricker 2002) do not have a thorough theoretical or experimental basis. For example, the bending in these anchors is much greater than that resulting from the 1:40 limitation assumed in the design provisions (AASHTO 2001). Further experimental and analytical work is needed to quantify the effect of bending on the double-nut anchor rod configuration with stand-off height and bending moment in the anchors.

The distribution of fatigue damage over the various wind speeds is found in Tables 3.24 through 3.26, but it is often useful to examine a histogram representation of damage for various elements. An example is shown in Figure 3.42.

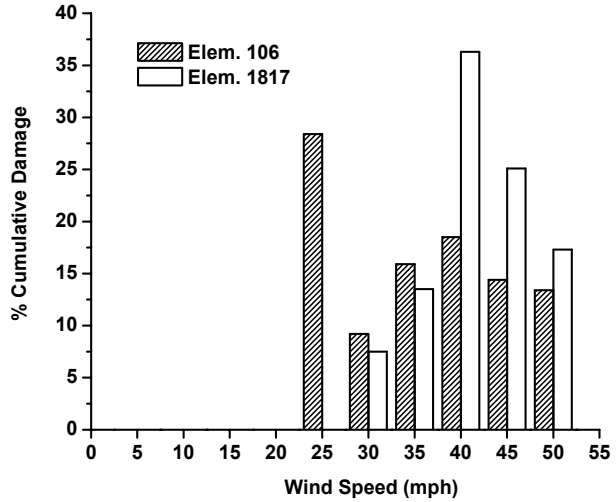

Figure 3.42: Damage Histograms for Elements 106 (end "i") and 1817 (end "i") within Structure S-67-402.

The damage in the anchor bolts is distributed for wind speeds in the upper-end of the spectrum. The "spike" in percentage of cumulative damage for 25-mph winds for element 106 should be noted. The

stress ranges shown in Figure 3.41 are not "large", but are definitely above 1/2 times the CAFL for the *ET* detail category. Therefore, the extremely frequent 25-mph wind out of the east and west directions have an ability to contribute significant damage. Figure 2.22 illustrates that there is a large portion of 25-mph winds coming from the easterly direction orthogonal to the VMS face. Figure 2.23 illustrates that less and less of the higher speed winds (*e.g.* 30, 40, 45, etc...) are coming from the East and therefore, damage will be reduced by the lessened likelihood that winds will be orthogonal to the VMS.

3.3 High-Mast Luminaire (HML) Support Structures

The Wisconsin Department of Transportation (WisDOT) is broken into six districts. The present study focuses on structures supervised by District 2 headquartered in Waukesha, Wisconsin. Luminaire support structures are designated as high-mast (HML) by WisDOT when the mast is greater than 100 feet in height. WisDOT District 2 maintains a database of 79 high-mast luminaire support structures that are located in the metro-Milwaukee area (usually located at interstate and U.S. highway interchanges).

These 79 HML structures are inspected on a regular cycle by WisDOT or Milwaukee County Highway Department (MCHD) personnel. Other than the Zoo Interchange failure and the material-deficiencies with the Core-Ten masts discussed in Chapter 1, the HML structures managed by WisDOT have been very reliable structures and have fulfilled their intended service lives quite admirably without incident. In fact, there have been many cases where a 13 year old HML support mast was replaced with a new superstructure using the existing anchor rods and foundation. However, if one were to track the design complexities for HML structures that have developed over the past 5 years and have been included in design specifications (AASHTO 2001), one would think that these structures have had very poor service records.

The HML structures erected by WisDOT all have very similar configurations that are efficient in resisting the intended wind loading. Therefore, choosing structures for detailed study centered on selecting HML configurations that were "unique" or those that had the possibility for extrapolation to a majority of HML structures currently under management by WisDOT. A database of luminaire support structures was obtained from WisDOT District 2 personnel. The 79 structures contained in this database have heights (to the luminaire assembly) ranging from 100 feet to 150 feet. The anchor rod arrangements were predominantly circular in pattern (with 6 to 8 anchor rods). However, there were instances where 100 foot tall HML structures were supported on square anchor rod patters with 4 anchor rods. It was decided to then study HML structures that had four anchor rod base conditions and those that were over 125 feet in height. It was felt that this would give sufficient breadth to the study (given the finite time

period for the effort) to yield the most information for establishing inspection intervals, identifying fatigue-life-limiting details, etc.

Two structures were chosen for detailed study. The first structure was HML-40-061 located in Milwaukee County at the Canal Street Interchange. This structure was erected in 2001 using the four-bolt anchor rod arrangement from the former structure erected in 1987. The structure has four luminaires in its lighting assembly and is 100 feet tall. The second structure, HML-67-006, is located in Waukesha County at the Main Street Interchange. It was erected in 1993. The structure contains an eight anchor rod arrangement and is 150 feet tall (the tallest height used by WisDOT). There are 6 luminaires in the lighting assembly. This section in the report will outline and discuss the detailed structural analysis of these two structures and will present fatigue life estimates generated using previously discussed methodologies.

3.3.1 Luminaire Support HML-40-061

Luminaire structure HML-40-061 is located in the Canal Street Interchange of Interstate Highway 94. The structure is shown in Figure 3.43. The Structure was put into service in late 2001/early 2002. The new structure was installed using existing anchor rods installed in 1987. The support mast has a 4-bolt anchor pattern as shown in Figure 3.44. Dimensional details are illustrated in Figures 3.45 and 3.46 (taken from WisDOT shop drawings).

(a) (b)

Figure 3.43: HML-40-061 Luminaire Assembly and Support Mast: (a) Luminaire Support Mast; and (b) Luminaire Assembly.

(a) (b)

Figure 3.44: Base Plate Arrangement for HML-40-061: (a) Exiting Anchor Rods and Pattern; (b) Hand-Hole and Mounting Plate.

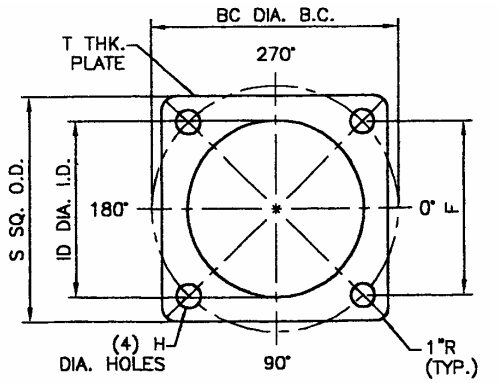

Figure 3.45: Anchor Rod Pattern Used for HML-40-061.

The anchor plate is square with 26-inch sides (S-dimension) and the bolt pattern diameter (BC-dimension) is 27 inches. The anchor rods used in the new installation were existing 2-1/4" diameter A615 Grade 70 material. The stand-off height on the bolts is approximately 2 inches (see Figure 3.44). The base plate is composed of A36 structural steel material. The weld at the base of the mast (to the base plate) was a full penetration groove weld (45-degree bevel) with fillet reinforcement and machining (see Figure 3.46). A backup ring was used and ultrasonic testing to ensure weld quality was specified.

The mast for the HML support structure is composed of ASTM A709 Grade 50 steel "round tubes" with 18 flat sides. The mast was assembled using two segments (approximately 51 feet long). The lap joint used was a male-female slip connection with full-penetration seam welds. Welds were specified to be ground smooth and the joints were specified to be a "snug fit with 1/16" maximum deviation. Longitudinal seam welds for the mast segments were specified to have 60% minimum penetration groove welds and were also specified to be low profile. The two mast segments tapered at a rate of 0.132 inches

per foot of height. Segment number 1 (the lower segment) had a bottom outer diameter equal to 19.25 inches and a top diameter equal to 12.5 inches. The wall thickness is 0.25 inches. Mast segment number two (the upper segment) had a bottom diameter of 13.25 inches (to accommodate the slip-over joint) and a top diameter of 6.5 inches. The wall thickness for this segment is 0.1875 inches.

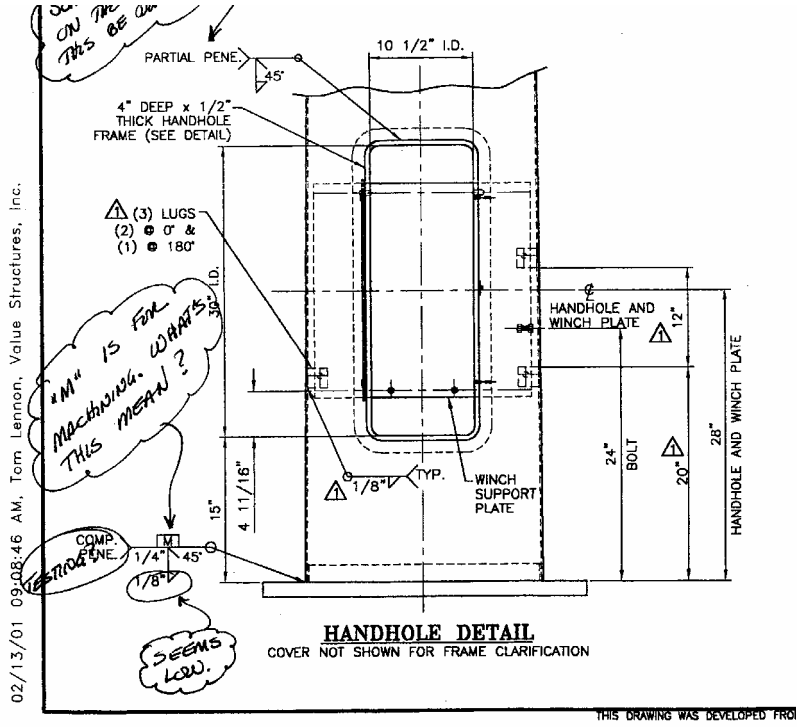

Figure 3.46: Hand-Hole Detail Illustrating Full Penetration Groove Weld at Mast Base.

All welding and quality control procedures were required to follow AWS 660.4.2. The finish on the mast and base plate was specified to be hot-dipped galvanizing following ASTM A123. No special reconditioning of the anchors was done with the new installation. According to WisDOT maintenance records the initial installation of a structure at this location was in 1987 and it is believed that the anchor rods installed in 1987 were the existing anchors used in the new installation.

At the time of initial reconnaissance, the mast, luminaire assembly welds and anchor rods appeared to be in very good condition (see Figure 3.47). All anchor rod nuts were tight. Only cursory visual inspection was performed. The intent of the inspection was to determine if any "glaring" irregularities in the structural configuration existed relative to the WisDOT shop drawings for the structure. The base plate alignment with respect to direction is shown in Figure 3.48.

(a) (b)

Figure 3.47: Initial Condition of HML-40-061 Luminaire Support: (a) Base Plate Weld; and (b) Anchor Rod Condition.

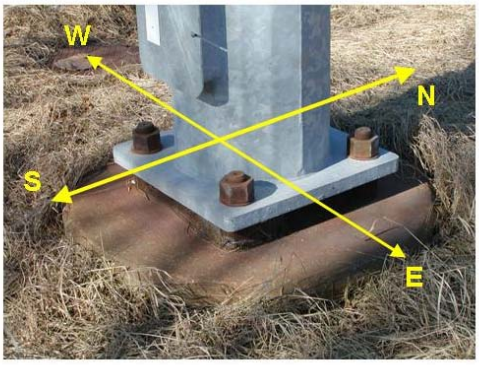

Figure 3.48: HML Base Plate Directional Orientation for Later Wind Direction Analysis and FE Analysis.

This alignment was used to make a correlation between the loading direction applied in the FEA model and the actual wind direction relative to the structure.

3.3.1.1 Finite Element Analysis (FEA) Modeling

The ANSYS finite element analysis system SAS (2000a;b) was used to generate a finite element model for the HML support structure. Two important phases were covered with the FE model. The first was the development of the analytical model itself, and the second was the loading. This portion of the discussion will focus on the analytical model (*e.g.* element types, configuration) and a second discussion (in another section of this chapter) will focus in on the generation of the loading for the FEA.

The FE model was generated using PIPE16 elastic elements for the HML mast (assuming that the 18-sided tubular configuration could be assigned as an equivalent round pipe. The base plate was modeled using SHELL63 (four-node shell) elements. Elastic behavior was assumed. A short segment of SHELL63 elements was used to model a portion of the HML mast. Again, an equivalent "round" configuration was assumed. The anchor bolts were also modeled. These components of the structure were modeled using three-dimensional beam elements (BEAM4).

In order to "marry" the shell elements used to model a portion of the mast and base plate with the pipe elements in the mast and the beam elements used to model the anchor bolts, "rigid-regions" or constraint equations were used. The rigid region forces compatibility of deformations between nodes in the model. For example, the rigid region enforced compatibility of deformations between the nodes at the shell edges in the HML mast with the pipe elements used to continue the FE model 100 feet up from the base plate. The concept of rigid regions in the FE models used for this HML structure is shown in Figures 3.49 and 3.50.

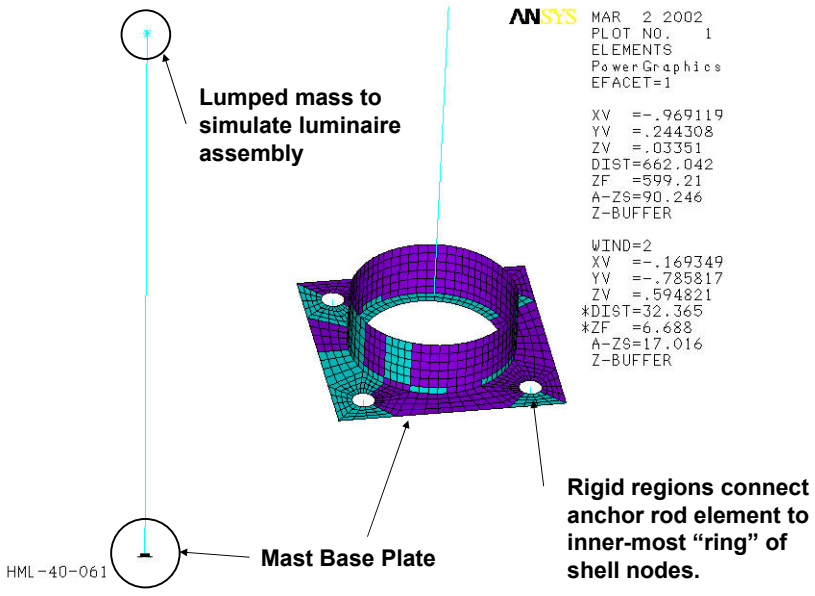

Figure 3.49: Schematic Illustrating Overall Finite Element Model for HML Structure.

As can be seen, the 3D pipe elements, 3D beam elements and shell elements are all contained in the model. The mass of the lumiaire assembly at the top of the mast was modeled using the "lumped mass" element available in ANSYS. The luminaire assembly for this structure was assumed to weight 775 pounds, which equates to a mass of $2.0\, lb \cdot s^2/in$.

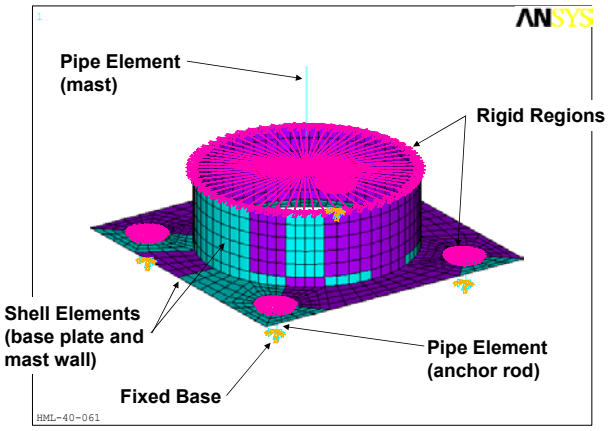

Figure 3.50: Rigid Regions Used in FE Model to Simulate Compatible Deformations.

The rigid regions (shown in Figure 3.50) allow much more efficient use of computational resources. The analyst can model the "important" regions using more complicated shell elements and allow less complicated regions (*e.g.* the mast region) to be modeled using more efficient beam elements. Furthermore, the rigid regions at the anchor bolt base plate interface allowed the interaction of the base plate and its natural flexibility to be modeled along with the flexural characteristics of the anchor rods. The anchor rods were modeled assuming that their base was analytically "fixed" to the concrete foundation. It should be noted that the effect of the washer and nut on the flexural characteristics of the base plate was not modeled. The impact of this omission was discussed with S-67-402 and will be re-visited later in this section.

3.3.1.2 General FE Model Evaluations

The finite element model for HML-40-061 was subjected to a series of "controlled" analyses. The first was conducted to study the effect of base plate stand-off height on the modal frequencies of the HML structure. The reason that this was done is that it would allow evaluation of the impact of anchor rod stand-off heights on the structure's natural frequencies of vibration. This has significant impact when one considers the tendency for vortex shedding behavior for the HML structure.

Three stand-off heights of the anchor rods considered were: 2-1/2", 4", and 6" and the first seven modal vibrational shapes were considered important. The FE model was copied and modified to remove the detailed FE modeling of the base plate, mast, and anchor rods. These elements were replaced with a segment of pipe finite element that had all displacements and rotations restrained at its base. The natural

frequencies of vibration for this configuration then became the "normalizing" frequencies for the stand-off analyses. The base plate thickness used in the analysis was 1.75 inches.

Figure 3.51 illustrates that anchor rod stand-off height has an effect on the natural frequencies of vibration for the HML structure. The presence of base plate stand-off height ensures that the natural frequencies will not coincide with the fixed base condition, but there is very small error (less than 5%). The actual numbers associated with these vibrational frequencies are shown in Table 3.27. All frequencies for the first seven modes are within 5% of the fixed base assumption as indicated in Figure 3.51. Furthermore, the natural frequencies differ very little for all seven modes considered. The fixed-base assumption has the least error when the fundamental mode is considered and the error increases ever so slightly for the higher modes. The actual structure has a stand-off height of approximately 2-1/2 inches (relative to base plate centerline). Four and six inch stand-off heights are believed to be excessive, but results for these were deemed to be useful for characterizing behavior. The shapes of the first seven modes of vibration are shown in Figure 3.52.

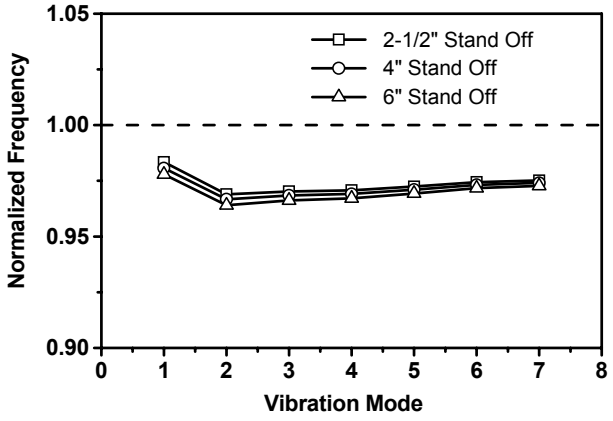

Figure 3.51: Natural Frequency of Vibration Variation with Anchor Bolt Stand-Off Height.

Table 3.27: Variation in Natural Frequencies for Dominant Modes of Vibration with Anchor Rod Stand-Off Height Variation (1-3/4" base plate used).

Vibration Mode	Vibration Frequency (Hz)			
	2-1/2" Stand-Off	4" Stand-Off	6" Stand-Off	Fixed Base
1	0.356	0.355	0.354	0.362
2	1.777	1.773	1.768	1.834
3	4.825	4.816	4.805	4.973
4	9.691	9.675	9.655	9.983
5	16.164	16.140	16.112	16.622
6	24.519	24.488	24.451	25.163
7	34.368	34.329	34.282	35.243

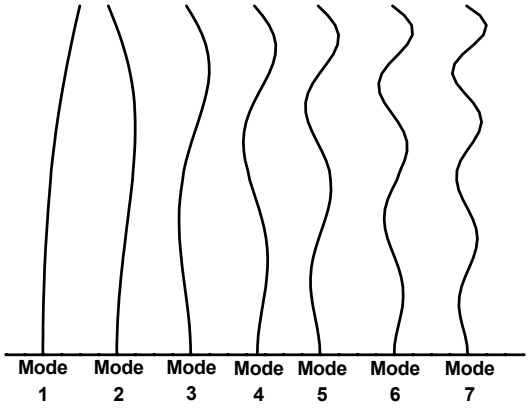

Figure 3.52: First Seven Vibrational Mode Shapes for HML-40-061.

The base plate thickness was also thought to have an effect on the modal frequencies of vibration for the HML support structure. As a result, a short study was undertaken to evaluate the effect of variation in base plate thickness had on the vibrational frequencies. As with the stand-off height study, the fixed base HML FE model was used to generate the normalized response. The base plate thicknesses chosen were: 7/8", 1-3/4", and 3-1/2". This variation encompassed the thickness used in the actual structure and represents the span the thicknesses most commonly used.

Figure 3.53 illustrates the effect of base plate thickness on the normalized modal vibration frequency for the seven mode shapes shown in Figure 3.52. Table 3.28 contains numerical values for the modal vibration frequencies for each case considered.

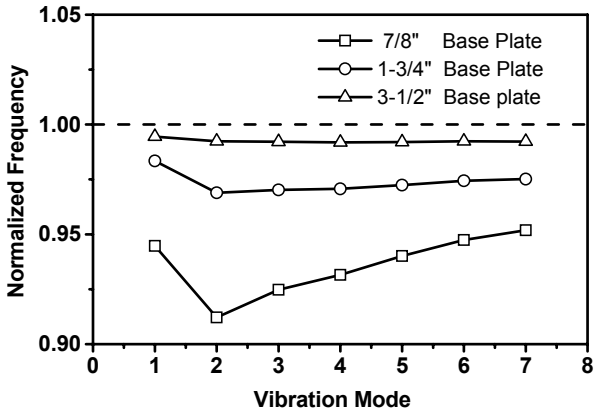

Figure 3.53: Variation in Natural Frequency of Modal Vibration Shapes with Variation in HML Base Plate Thickness.

Table 3.28: Variation in Natural Frequencies for Dominant Modes of Vibration with Base Plate Thickness (constant 2-1/2" stand-off height used).

Vibration Mode	Vibration Frequency (Hz)			
	7/8" Plate	1-3/4" Plate	3-1/2" Plate	Fixed Base
1	0.342	0.356	0.360	0.362
2	1.673	1.777	1.820	1.834
3	4.599	4.825	4.934	4.973
4	9.300	9.691	9.902	9.983
5	15.627	16.164	16.490	16.622
6	23.840	24.159	24.971	25.163
7	33.547	34.368	34.970	35.243

The fixed base vibration frequencies are included again for convenience. As illustrated, the largest variation from the fixed base condition arises for the thin base plate configuration. One should have expected that as the base plate thickens, the vibrational mode shapes and corresponding frequencies should approach those of the fixed base condition. This is certainly demonstrated. The thickest base plate does indeed approach the fixed base condition much more closely than the short stand off height for the 1-3/4" base plate condition. This suggests that the base plate thickness is more important for approaching the fixed base condition than the anchor rod stand off height. In all but the thinnest base plate, the analytical error in assuming the fixed base condition is less than 5%.

The limited study of modal response characteristics of this HML support structure illustrates that the usual designer assumptions of fixed base condition (in conflict with the reality of a relatively thin base plate with significant anchor bolt stand-off height) will cause negligible error in estimating modal frequencies for these structures.

The second evaluation of the FE model paralleled that done with comparison to the experimental reports generated previously (Kaczinski *et al.* 1998) and controlled concentrated loading at the mast top. In the controlled loading study, the HML structure was subjected to a concentrated loading at the luminaire assembly level. The first loading condition considered employed a 1,000-lb force parallel to the x-direction (*i.e.* aligned with the base plate sides). The second loading condition incorporated a 1,000-lb "quartering force". This resulted in two orthogonal components (oriented parallel to the x- and y-directions) of magnitude 707 lbs. The goal of these loading conditions was to evaluate the stress and internal force response of the mast base, the base plate, and the anchor rods to these controlled static forces.

The first loading condition studied was the 1,000-lb quartering force. The state of stress in the HML mast near the base plate is shown in the contour plot of Figure 3.54. Upon examination of this stress contour, the concentration of stress near the anchor rod should stand out. The quartering wind direction approaches diagonally across the base plate configuration. Thus, two anchor rods have small (near zero) force and two (diagonally opposing) anchor rods have the largest axial forces. The principal stress trajectories shown in Figure 3.55 also clearly illustrate the concentration of stress near the resisting anchor rods.

The stress distribution makes physical sense because the stress field must seek the most effective support. These supports are the two anchor rods parallel to the line of action of the force. In the fixed base condition, the stress field can seek effective support around the entire circumference of the mast wall. Therefore, if this mechanics hypothesis holds, one would certainly expect that the stress field for the non-quartering force direction would cause a more nearly uniform state of principal stress around the mast circumference. Of course, it could not match the fixed base condition because the base plate is still supported on discrete anchor rods. Figures 3.56 and 3.57 illustrate that the stress fields follow the predicted behavior.

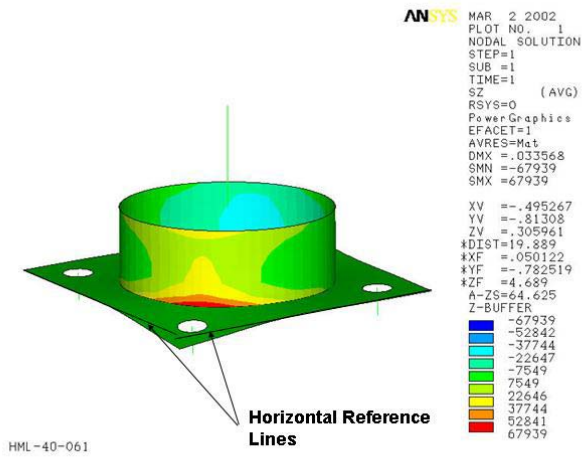

Figure 3.54: Stress Contour for Quartering Force Applied to Top of HML Mast.

The principal stress trajectories shown in Figure 3.57 show a slight angle as the stress field seeks the anchor rod supports. Comparison of Figures 3.54 and 3.56 illustrates the significant concentration of stress that occurs for the quartering force condition. This quartering-force phenomenon is only present for the four-bolt anchor arrangement. As shown later in this report, the eight bolt arrangement exhibits near fixed base behavior. This result is very important because there is no published fatigue data on the

quartering force condition in the Literature. As will be shown in the wind loading analysis, depending upon the base plate orientation, there is a high likelihood that large wind force magnitudes will generate stresses of the form shown in Figures 3.54 and 3.55. Of course, there is also a high likelihood that stress states such as that shown in Figures 3.56 and 3.57 will also exist. However, the direction of winds may coincide with the "quartering direction" and therefore, can cause more damage in the four-bolt configuration when compared to others. This was the motivation for study of the fixed base condition and normalization of these other two directions with respect to this case.

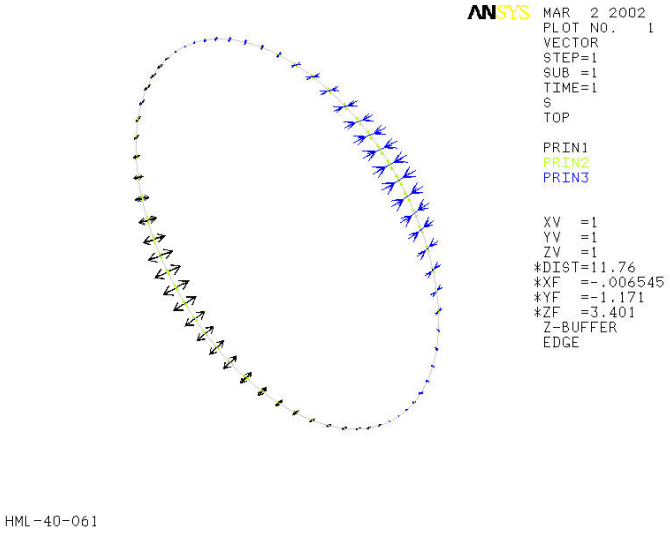

Figure 3.55: Principal Stress Trajectories for Quartering Wind Force.

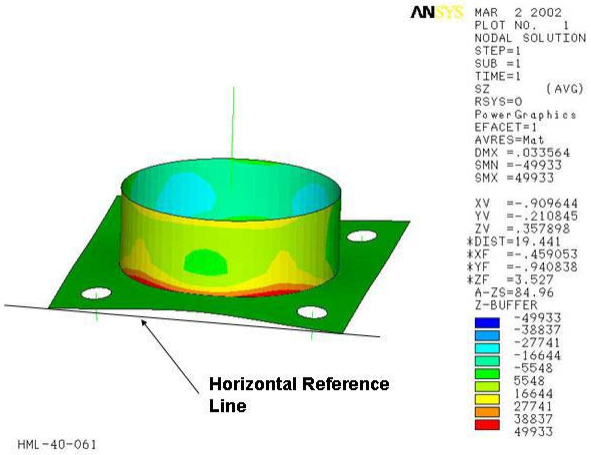

Figure 3.56: Stress Contour for Non-Quartering Force Applied at Top of Mast.

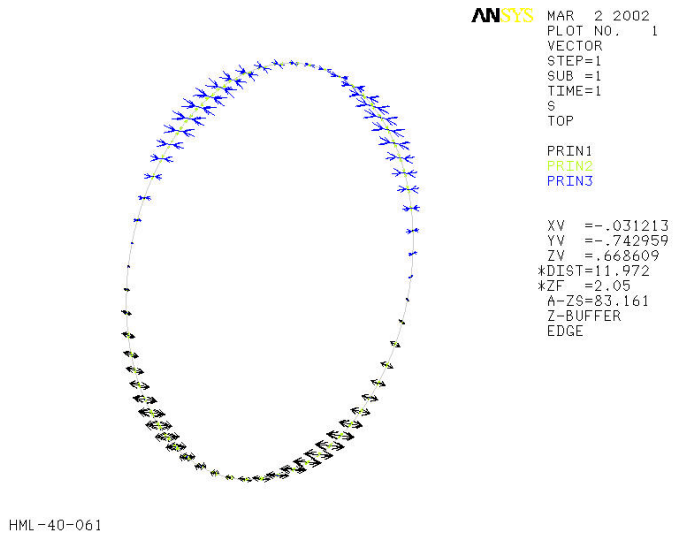

Figure 3.57: Principal Stress Trajectories at Base of HML Mast for Non-Quartering Force.

Designers most likely would be using a fixed base condition in their design analysis and the fixed base condition was used as a normalization state for the stress in the mast wall. The principal stress contour and trajectory are shown in Figure 3.58. The usual "smooth" stress contour around the circumference of the mast base is indeed exhibited in the FE model for the fixed mast base and the magnitude of the stresses is much less than the previous two configurations (Figures 3.53 and 3.56).

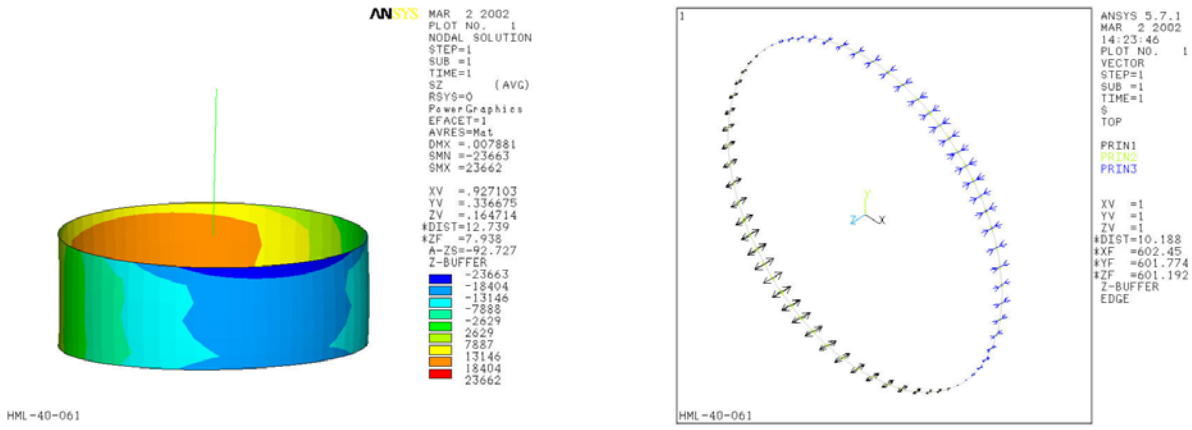

(a) (b)

Figure 3.58: Stress Contours and Principal Stress Trajectories for Fixed Base HML condition: (a) Stress Contour; and (b) Principal Stress Trajectory.

Since the fatigue analysis would employ the FE model with anchor rod stand-off and base plate, a comparison to fatigue data that included stress concentrations normally found in mast base plate connections was needed. It should be noted that the concentrations of stress in Figure 3.54 are not present in the fatigue data provided by Kaczinski *et al.* (1998), but are mentioned in Fisher *et al.* (1983).

The following rationale was used to develop stress states that were consistent with the fatigue data currently contained in the sign and luminaire specifications (AASHTO 2001). First of all, the FE modeling gives a stress state at the centerline of the base plate that is analytically possible, but physically not present. The procedure usually used to determine stress concentrations at right-angle welded connections employs "extrapolation" of stress states in the mast wall to the base plate. This extrapolation accounts for the physically improbable state of stress at the mid-thickness of the base plate.

The results of fatigue testing (Kaczinski *et al.* 1998) does include the concentration of stress at the fillet or groove weld at the base of the mast. However, this testing did not include the concentration of stress that results from the anchor rod stand-off in concert with the relatively thin base plate condition. Therefore, the procedure used in this study to determine stress ranges compatible with the fatigue testing data is as follows. First of all, examine the state of tensile stress along the outer surface of the mast wall around its circumference. This is shown in Figures 3.54 through 3.58. Account for the base plate thickness (ignored in the shell FE model) and move up the wall to a location where the stress interference due to the base-plate to mast connection is removed. Compare the state of tensile stress at this location to that for the fixed base mast. Develop a stress concentration factor (SCF) that accounts for the "lifted" base plate condition and quartering wind effect.

The result of this normalization process is shown in Figure 3.59. As illustrated in the figure, the quartering force direction causes a significant concentration of stress in the outer surface of the mast wall as the stress field seeks the anchor bolt support. This concentration of stress is not accounted for in the detail categories used for the mast-to-base-plate welded connection. This concentration of stress is not present in the non-quartering force direction. The results shown in Figure 3.59 illustrate that there is a significant rise in stress in the mast wall when quartering force is applied. This rise in stress is certainly present in the stress contours and the principal stress trajectories for this loading condition.

The concentration of stress present at the top of the base plate and adjacent mast wall is present in the fatigue testing that supports the fatigue detail category for the mast base weld region. Therefore, if the analysis can determine the stress state at the base of the mast for the fixed base condition, a stress concentration factor must be applied to the tensile stress resulting from bending,

$$\sigma_{tens} = \sigma_{direct} + SCF \cdot \sigma_{bend} \tag{3.1}$$

Figure 3.59 suggests that the stress concentration factor for the quartering force direction can be taken as 1.40 and the concentration factor for non-quartering direction wind can be taken as 1.00. Therefore, an estimate for the stress at the surface of the mast wall for quartering direction wind can be determined using,

$$\begin{aligned}\sigma_{tens} &= \sigma_{direct} + SCF \cdot \sigma_{bend} \\ &= \frac{P}{A} + 1.40 \cdot \left(\frac{M_{base} \cdot d}{2 \cdot I_{mast}} \right)\end{aligned} \tag{3.2}$$

where: M_{base} is the bending moment at the top of the rigid region (Figure 3.59). The tensile stress given in equation (3.2) can then be used to define stress ranges and evaluate the fatigue life of the weld at the mast to base plate connection.

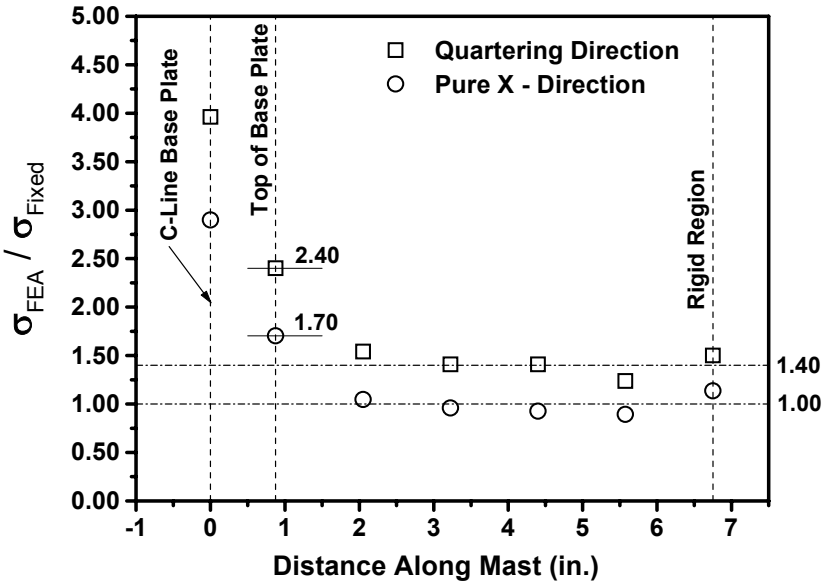

Figure 3.59: Non-Dimensional Stress at Mast Surface Along Mast Height.

The deformed shapes of the base plate shown in Figures 3.54 and 3.56 illustrate that there is a significant amount of bending that will be generated in the anchor rods. A small study was undertaken to determine the feasibility of thickening the base plate to remove bending moment in the anchor rods. The base plate for this FE model of HML-40-061 was increased to 6 inches and the bending in the anchor rods remained significant although significantly lessened from the 1-1/2 inch base plate thickness condition. The 6 inch base plate configuration can be considered impractical for typical HML structures. In most cases, if the plate were needed to be that thick for base fixity consideration, this can more effectively be accomplished through the use of stiffeners.

3.3.1.3 Vortex-Shedding Susceptibility

High-mast luminaire assembly support structures have sufficient height and slenderness to warrant consideration of vortex-shedding effects in the fatigue performance evaluation. The mast configuration used for HML-40-061 is typical of the HML structures used in Wisconsin and it tapers at a rather significant rate (0.132 in/ft). This tapering rate, coupled with the non-deterministic nature of lift coefficients thought to be important for vortex-shedding-induced vibrations, makes quantification of the susceptibility of HML structures to across-wind vibrations difficult. This section of the Report will evaluate the susceptibility of HML-40-061 to vortex-shedding induced vibrations using accepted wind-engineering theory.

When a bluff-body (such as the 16-sided HML shape) is presented to a free wind stream, there is the possibility of both along-wind and across-wind vibrations. The along-wind vibrations can be modeled using turbulent wind-pressure simulation techniques used previously for the sign support structures. The across-wind vibrations are considerably more difficult to quantify. We will begin with the assumption that the 16-sided bluff-body shape can be adequately modeled as a circular cross-section. The vortex shedding response of bluff bodies is well documented in wind engineering and vibration literature (Buchholdt 1997; Dyrbye and Hansen 1997; Simiu and Scanlon 1996), and will only be briefly outlined in the present discussion.

When the wind stream is interrupted by a bluff body, streamlines form around its circumference as the wind stream moves around the obstruction in the flow. The adherence of the streamlines to the surface of the bluff-body depends upon the kinematic viscosity of the fluid (in the present case – air), the dimension of the body perpendicular to the wind stream, the surface roughness of the body, and the velocity of the wind. Wind tunnel studies have been used to develop non-dimensional relationships using these basic parameters to describe the manner in which the streamlines separate from the bluff body and the tendency for the formation of periodic and regularly shed vortices resulting in across-wind vibrations. A dimensionless number quantifying the formation of vortices is called the *Reynolds Number*, and it is computed using,

$$\mathrm{Re} = \frac{U \cdot D}{\upsilon} \tag{3.3}$$

where: υ is the kinematic viscosity of air ($1.615 \times 10^{-4}\ ft^2/s$); U is the mean (or constant) velocity of the wind stream; and D is the dimension of the bluff body presented to the wind stream. Surface roughness is not addressed in the present analysis because the painted surface of the mast is not contradictory with the wind tunnel experiments upon which equation (3.3) is based.

The Reynolds number is used to determine the tendency for periodically shed (*i.e.* organized) vortices behind the bluff body. Periodically shed vortices form what is often called a von Karman vortex street. These types of vortices can cause across-wind vibration of the bluff body. The tendency for the across-wind vibration is a function of where the streamlines separate from the bluff body (Buchholdt 1997; Dyrbye and Hansen 1997; Liu 1991; Simiu and Scanlon 1996). If the separation occurs in the range of 80-115 degrees from the stagnation pressure point at the leading "tip" of the circular section, vortices within a relatively narrow band of frequencies are shed in a regular pattern. When the streamlines adhere to the bluff body and separate on the leeward side, the wake is relatively narrow and the vortices are shed in a "random" fashion. The tendency for regularly shed vortices is quantified using the Reynolds number (Dyrbye and Hansen 1997; Liu 1991);

Subcritical Flow ($300 \le \mathrm{Re} \le 10^5$):	Periodically shed vortices
Supercritical Flow ($10^5 \le \mathrm{Re} \le 3.5 \times 10^6$)	Irregular (unorganized) vortex shedding.
Transcritical (hypercritical) Flow ($3.5 \times 10^6 < \mathrm{Re}$)	Regularly shed vortices.

Therefore, the dimension of the bluff body, the velocity of the flow, and the kinematic viscosity of the fluid must "align" themselves properly to create the conditions suitable for the formation for periodic and regularly shed vortices and lock-in. If supercritical flow exists, these vortices will have a low probability of forming in an organized manner.

If the flow conditions are right, the frequency at which vortices are shed can be computed using the following expression (Liu 1991),

$$n_s = \frac{St \cdot U}{D} \tag{3.4}$$

where: *St* is a non-dimensional constant called the Strouhal number. For circular cross-sections, this number can be taken to be 0.20 (Buchholdt 1997; Dyrbye and Hansen 1997; Simiu and Scanlon 1996). If the frequency at which vortices are shed is near the natural frequency of a vibration mode for the HML structure, a condition called *lock-in* can occur. When this situation arises, large amplitude and self-perpetuating across-wind vibrations can develop. It should be noted that the mean wind speed in equation (3.4) is constant, whereas "real" wind is turbulent.

Wind speeds (using NCDC procedures) are measured at a standard height of 10 meters (approximately 33 feet). As discussed in chapter 2 of the report, the power law can be used to modify this wind speed to account for height above the boundary layer surface (*i.e.* the earth's surface) accounting for surface roughness variability.

The formation of vortex shedding loads is a very complex phenomenon. However, there are several aspects to these loads that are known and are incorporated into the evaluation of the HML structure's susceptibility to this phenomenon. Assuming that vortices are shed in a regular manner, and that the frequency of the shedding coincides with a natural modal frequency of the structure, a *lift load* (orthogonal to the direction of the wind stream) is created (Buchholdt 1997; Dyrbye and Hansen 1997; Liu 1991; Simiu and Scanlon 1996),

$$P_L(t) = \frac{1}{2} \cdot \rho \cdot D \cdot U^2 \cdot C_L(t) \tag{3.5}$$

where: ρ is the density of air; U is the mean wind speed considered and $C_L(t)$ is lift coefficient (often assumed as a zero-mean normally distributed random variable).

The random nature of the lift coefficient is what makes evaluating vortex shedding response so difficult. There have been numerous studies attempting to define lift coefficients for chimneys and stacks in both steel and concrete (Simiu and Scanlon 1996). Difficulty in defining the lift coefficient is enhanced by the fact that vortices tend to have *correlation lengths* along the bluff-body's length (Dyrbye and Hansen 1997; Simiu and Scanlon 1996) over which the vortices are assumed to act in phase. These two issues conspire to make definition of the across-wind loading and prediction of across-wind deformations caused by vortex shedding loads relatively inaccurate when compared to along-wind deformations (Dyrbye and Hansen 1997; Simiu and Scanlon 1996).

There have been several simplified approaches that can be used for determining the lift coefficient and correlation lengths for vortex-shedding. The Canadian Highway Bridge Design Code (CSA 2000) has a relatively concise approach to consideration of vortex-shedding deformations and the corresponding stresses. The lift coefficient was previously described as a zero-mean random variable. Therefore, one could estimate the RMS (root mean squared) value of the lift coefficient and use it to define lift force magnitudes that correspond to various confidence intervals. CSA (2000) suggests the following root mean square values for circular cross-sections;

Subcritical Flow ($\mathrm{Re} \le 3 \times 10^5$): $\left(C_L\right)_{RMS} = 0.50$

Supercritical and Transcritical Flow ($\mathrm{Re} > 3 \times 10^5$): $\left(C_L\right)_{RMS} = 0.20$

A very common model for loading resulting from vortex shedding assumes a sinusoidal variation with amplitude defined using equation (3.5), frequency set equal to the natural frequency of the structure (multiple modes should be considered), and a stationary lift coefficient set at a design magnitude. The loading (load per linear foot of mast length) then takes the form below (Buchholdt 1997; Dyrbye and Hansen 1997; Liu 1991; Simiu and Scanlon 1996).

$$P_L(t) = \frac{1}{2} \cdot \rho \cdot D \cdot U^2 \cdot C_L \cdot \sin\left(2\pi n_{struc} t\right) \tag{3.6}$$

where: n_{struc} is the natural frequency of the structure; and C_L can be defined for a variety of confidence levels.

Equation (3.6) implicitly subscribes to the theory of "lock-in" velocities (Dyrbye and Hansen 1997; Liu 1991; Simiu and Scanlon 1996) whereby it is assumed that there is a range of wind speeds over which the vortex shedding frequency and the natural frequency of the structure "lock-in" with one another and large across-wind vibrations result. The loading used to simulate these across-wind deformations is given by equation (3.6). The difficulty with "lock-in" arises from the knowledge that there is a *range* of natural frequencies of the structure over which lock-in can occur (Dyrbye and Hansen 1997). It has been recommended that the tendency for vortex-shedding to cause across-wind vibrations be computed using a *range* of frequencies around the shedding frequency and comparison to modal vibration frequencies of the structure. Mathematically, this can be described as,

$$n_s^L \le n_s \le n_s^U \tag{3.7}$$

where: n_s^L and n_s^U are lower and upper bounds on the vortex shedding frequency computed using (Dyrbye and Hansen 1997),

$$n_s^L = n_s - n_s' = \frac{St \cdot \bar{U}_z}{D} - \frac{St \cdot u_z'}{D} = n_s\left[1 - \frac{u_z'}{\bar{U}_z}\right] \tag{3.8}$$

$$n_s^U = n_s + n_s' = \frac{St \cdot \bar{U}_z}{D} + \frac{St \cdot u_z'}{D} = n_s\left[1 + \frac{u_z'}{\bar{U}_z}\right] \tag{3.9}$$

where: $\bar{U}_z$ is the mean component of the wind at height z; and u_z' is the turbulent component at height z (above or below the means wind speed). Thus, if the structure's natural frequency in any mode of vibration lies within these lower- and upper-bounds; vortex shedding could excite that mode of vibration.

The turbulent component of the wind speed is often assumed to be zero-mean random variable with Gaussian distribution (Dyrbye and Hansen 1997; Levy 1996; Simiu and Scanlon 1996) and its magnitude depends upon height above the earth's surface. As a result, a roughness length, z_o, is often utilized to estimate this effect. Typical roughness coefficient magnitudes for various terrain topologies are given below (Dyrbye and Hansen 1997):

$z_o = 0.033$ ft for open land with little vegetation and houses;

$z_o = 0.164$ ft for agricultural areas with few houses and wind breaks;

$z_o = 0.984$ ft for villages and agricultural areas with many wind breaks.

The HML structures considered in this study are located in areas that may be considered to have few wind breaks and trees. Therefore, a roughness length of $z_o = 0.164$ feet was assumed for computations.

Experimental results have allowed the empirical definition of the standard deviation for turbulent horizontal wind component to be determined. An expression for the standard deviation that has been validated through experiment is (Dyrbye and Hansen 1997);

$$\sigma_u = A \cdot u_* \tag{3.10}$$

where $A \approx 2.5$ for a roughness length, $z_o = 0.164$ ft . The friction velocity can be computed as (Dyrbye and Hansen 1997);

$$u_* = \frac{\bar{U}_z \kappa}{\ln\left(z/z_o\right)} \tag{3.11}$$

where von Karman's constant, κ , can be approximated as 0.4; and z is the height above the surface of the earth. An estimate for the standard deviation of the turbulent wind component at any height, z , can therefore be written as,

$$\left(\sigma_u\right)_z = \frac{A \cdot \bar{U}_z \cdot \kappa}{\ln\left(z/z_o\right)} \tag{3.12}$$

It will be assumed that the frequency boundaries given by equations (3.8) and (3.9) can be based upon the maximum turbulent wind speed variation from the mean speed, $\bar{U}_z$. This maximum can be defined as $u'_{z,\max}$. It will be assumed that the peak variation in turbulent component from the mean will be $1\sigma_u$ (above or below). Therefore, the upper and lower bounds on shedding frequencies can be computed using,

$$n_s^L = n_s\left[1 - \frac{u'_{z,\max}}{\bar{U}_z}\right] = n_s\left[1 - \frac{1\left(\sigma_u\right)_z}{\bar{U}_z}\right] \tag{3.13}$$

$$n_s^U = n_s\left[1 + \frac{u'_{z,\max}}{\bar{U}_z}\right] = n_s\left[1 + \frac{1\left(\sigma_u\right)_z}{\bar{U}_z}\right] \tag{3.14}$$

where the standard deviation of the turbulent component is computed using equation (3.12) at the given height above the ground.

In addition to the complications previously described, there is also the complexity that arises from the vortices needing to act in phase with one another over lengths of the HML mast. This is often approximated using a correlation length (Dyrbye and Hansen 1997). For a circular cross-section the following has been recommended for the correlation lengths (CSA 2000);

Subcritical Flow ($\mathrm{Re} \le 3 \times 10^5$): $L_{corr} = 2.5 \cdot D$

Supercritical and Transcritical Flow ($\mathrm{Re} > 3\times10^5$): $L_{corr} = 1.0 \cdot D$

Thus, in subcritical flow, a 16 inch diameter mast can be expected to have vortices acting in phase over a length of 40 inches. It should be noted that a tapered shafts of the HML structures studied will disrupt this simplistic correlation length computation.

The present HML structure is 100 feet tall. Therefore, in order to fully assess the tendency for vortex-shedding-induced vibrations to form, the wind speed, Reynolds number, and shedding frequency of the vortices along the structure height require evaluation. In the present structure, the situation is somewhat complicated because the diameter of the mast changes with vertical rise. Therefore, the following procedure was developed to evaluate the tendency for vortex shedding loads to develop on the HML structure considered.

1. Determine the wind speeds at the reference height (33 feet) that will be used for fatigue loading study. In the present case, wind speeds in the range of 5 through 50 mph are used.
2. Discretize the mast height into intervals suitable for wind speed evaluation. Compute an "average" mast diameter over each of these intervals. In the present study, the average length of the intervals was 33 inches.
3. Compute the wind velocity at the centerline of each interval using the power law for each of the wind speeds considered.
4. For each of the velocities computed, use equation (3.3) to compute the Reynolds numbers for the wind flow. If the Reynolds number at the location considered is in the supercritical flow regime, then a regular shedding frequency will not occur and vortex shedding load need not be considered at this level.
5. For each velocity computed, use equation (3.4) to compute the shedding frequency of the vortices when formed in subcritical flow.
6. For each velocity defined in step 1 and vortex shedding frequency defined in step 5, compute an upper- and lower-range for the vortex shedding frequencies using equations (3.13) and (3.14).
7. Locate segments along the mast where Reynolds numbers are conducive to periodic and regular shedding of vortices at each of the velocities considered.
8. For each velocity and location where regular vortices can be shed from step 7, determine if the natural frequency of any mode of vibration for the support mast falls within the lower- and upper-bounds set using equations (3.13) and (3.14). These locations are those in which a sinusoidal loading described using equation (3.6) should be applied.

The sequential evaluation process described above was applied to this HML structure and the results are given in Tables 3.29 through 3.32.

Table 3.29: Wind Speeds at Various Elevations for HML-40-061 as a Function of Reference Height , h_{ref} , Wind Speeds.

Level (in.)	Outside Diameter	Average Diameter	Wall Thickness	Kin. Vis	H (ft)	V (ft/s) at H 5 mph	10 mph	15 mph	20 mph	25 mph	30 mph	35 mph	40 mph	45 mph	50 mph
6.75	19.19														
		19.14	0.25	1.615E-04	0.91	4.4	8.8	13.2	17.6	21.9	26.3	30.7	35.1	39.5	43.9
15.00	19.09														
		18.92	0.25	1.615E-04	2.54	5.1	10.2	15.2	20.3	25.4	30.5	35.6	40.7	45.7	50.8
45.88	18.75														
		18.57	0.25	1.615E-04	5.24	5.6	11.3	16.9	22.6	28.2	33.8	39.5	45.1	50.7	56.4
79.85	18.38														
		18.19	0.25	1.615E-04	8.07	6.0	12.0	18.0	24.0	30.0	36.0	42.0	48.0	54.0	60.0
113.82	18.01														
		17.82	0.25	1.615E-04	10.90	6.3	12.5	18.8	25.0	31.3	37.6	43.8	50.1	56.3	62.6
147.79	17.63														
		17.45	0.25	1.615E-04	13.73	6.5	12.9	19.4	25.9	32.3	38.8	45.3	51.8	58.2	64.7
181.76	17.26														
		17.07	0.25	1.615E-04	16.56	6.6	13.3	19.9	26.6	33.2	39.9	46.5	53.2	59.8	66.5
215.73	16.89														
		16.70	0.25	1.615E-04	19.39	6.8	13.6	20.4	27.2	34.0	40.8	47.6	54.4	61.2	68.0
249.70	16.51														
		16.33	0.25	1.615E-04	22.22	6.9	13.9	20.8	27.7	34.7	41.6	48.5	55.4	62.4	69.3
283.67	16.14														
		15.95	0.25	1.615E-04	25.05	7.1	14.1	21.2	28.2	35.3	42.3	49.4	56.4	63.5	70.5
317.64	15.77														
		15.58	0.25	1.615E-04	27.89	7.2	14.3	21.5	28.6	35.8	43.0	50.1	57.3	64.4	71.6
351.61	15.39														
		15.20	0.25	1.615E-04	30.72	7.3	14.5	21.8	29.0	36.3	43.6	50.8	58.1	65.3	72.6
385.58	15.02														
		14.83	0.25	1.615E-04	33.55	7.4	14.7	22.1	29.4	36.8	44.1	51.5	58.8	66.2	73.5
419.55	14.64														
		14.46	0.25	1.615E-04	36.38	7.4	14.9	22.3	29.7	37.2	44.6	52.1	59.5	66.9	74.4
453.52	14.27														
		14.08	0.25	1.615E-04	39.21	7.5	15.0	22.5	30.1	37.6	45.1	52.6	60.1	67.6	75.2
487.49	13.90														
		13.71	0.25	1.615E-04	42.04	7.6	15.2	22.8	30.4	38.0	45.5	53.1	60.7	68.3	75.9
521.46	13.52														
		13.34	0.25	1.615E-04	44.87	7.7	15.3	23.0	30.6	38.3	46.0	53.6	61.3	69.0	76.6
555.43	13.15														
		12.96	0.25	1.615E-04	47.70	7.7	15.5	23.2	30.9	38.6	46.4	54.1	61.8	69.6	77.3
589.40	12.78														
		12.89	0.19	1.615E-04	50.07	7.8	15.6	23.4	31.1	38.9	46.7	54.5	62.3	70.1	77.8
612.40	13.00														
		12.81	0.19	1.615E-04	52.48	7.8	15.7	23.5	31.3	39.2	47.0	54.9	62.7	70.5	78.4
647.01	12.62														
		12.43	0.19	1.615E-04	55.36	7.9	15.8	23.7	31.6	39.5	47.4	55.3	63.2	71.1	79.0
681.63	12.24														
		12.04	0.19	1.615E-04	58.25	8.0	15.9	23.9	31.8	39.8	47.7	55.7	63.6	71.6	79.5
716.25	11.85														
		11.66	0.19	1.615E-04	61.13	8.0	16.0	24.0	32.0	40.0	48.1	56.1	64.1	72.1	80.1
750.87	11.47														
		11.28	0.19	1.615E-04	64.01	8.1	16.1	24.2	32.2	40.3	48.4	56.4	64.5	72.6	80.6
785.49	11.09														
		10.90	0.19	1.615E-04	66.90	8.1	16.2	24.3	32.4	40.6	48.7	56.8	64.9	73.0	81.1
820.11	10.71														
		10.52	0.19	1.615E-04	69.78	8.2	16.3	24.5	32.6	40.8	49.0	57.1	65.3	73.5	81.6
854.73	10.33														
		10.14	0.19	1.615E-04	72.67	8.2	16.4	24.6	32.8	41.0	49.3	57.5	65.7	73.9	82.1
889.35	9.95														
		9.76	0.19	1.615E-04	75.55	8.3	16.5	24.8	33.0	41.3	49.5	57.8	66.0	74.3	82.5
923.96	9.57														
		9.38	0.19	1.615E-04	78.44	8.3	16.6	24.9	33.2	41.5	49.8	58.1	66.4	74.7	83.0
958.58	9.19														
		9.00	0.19	1.615E-04	81.32	8.3	16.7	25.0	33.4	41.7	50.1	58.4	66.7	75.1	83.4
993.20	8.81														
		8.62	0.19	1.615E-04	84.21	8.4	16.8	25.2	33.5	41.9	50.3	58.7	67.1	75.5	83.8
1027.82	8.43														
		8.24	0.19	1.615E-04	87.09	8.4	16.8	25.3	33.7	42.1	50.5	59.0	67.4	75.8	84.2
1062.44	8.05														
		7.86	0.19	1.615E-04	89.98	8.5	16.9	25.4	33.9	42.3	50.8	59.2	67.7	76.2	84.6
1097.06	7.67														
		7.48	0.19	1.615E-04	92.86	8.5	17.0	25.5	34.0	42.5	51.0	59.5	68.0	76.5	85.0
1131.68	7.28														
		7.09	0.19	1.615E-04	95.75	8.5	17.1	25.6	34.2	42.7	51.2	59.8	68.3	76.8	85.4
1166.30	6.90														
		6.71	0.19	1.615E-04	98.63	8.6	17.1	25.7	34.3	42.9	51.4	60.0	68.6	77.2	85.7
1200.91	6.52														

Table 3.30: Frequencies of Vortex Shedding at Various Elevations for HML-40-061 as a Function of Reference Height, h_{ref} , Wind Speeds.

Level (in.)	Outside Diameter	Average Diameter	Wall Thickness	Kin. Vis	H (ft)	n_s (Hz) 5 mph	10 mph	15 mph	20 mph	25 mph	30 mph	35 mph	40 mph	45 mph	50 mph
6.75	19.19	19.14	0.25	1.615E-04	0.91	0.55	1.10	1.65	2.20	2.75	3.30	3.85	4.40	4.95	5.50
15.00	19.09	18.92	0.25	1.615E-04	2.54	0.64	1.29	1.93	2.58	3.22	3.87	4.51	5.16	5.80	6.45
45.88	18.75	18.57	0.25	1.615E-04	5.24	0.73	1.46	2.19	2.91	3.64	4.37	5.10	5.83	6.56	7.29
79.85	18.38	18.19	0.25	1.615E-04	8.07	0.79	1.58	2.37	3.16	3.96	4.75	5.54	6.33	7.12	7.91
113.82	18.01	17.82	0.25	1.615E-04	10.90	0.84	1.69	2.53	3.37	4.22	5.06	5.90	6.74	7.59	8.43
147.79	17.63	17.45	0.25	1.615E-04	13.73	0.89	1.78	2.67	3.56	4.45	5.34	6.23	7.12	8.01	8.90
181.76	17.26	17.07	0.25	1.615E-04	16.56	0.93	1.87	2.80	3.74	4.67	5.61	6.54	7.47	8.41	9.34
215.73	16.89	16.70	0.25	1.615E-04	19.39	0.98	1.95	2.93	3.91	4.88	5.86	6.84	7.81	8.79	9.77
249.70	16.51	16.33	0.25	1.615E-04	22.22	1.02	2.04	3.06	4.08	5.09	6.11	7.13	8.15	9.17	10.19
283.67	16.14	15.95	0.25	1.615E-04	25.05	1.06	2.12	3.18	4.24	5.30	6.36	7.43	8.49	9.55	10.61
317.64	15.77	15.58	0.25	1.615E-04	27.89	1.10	2.21	3.31	4.41	5.51	6.62	7.72	8.82	9.93	11.03
351.61	15.39	15.20	0.25	1.615E-04	30.72	1.15	2.29	3.44	4.58	5.73	6.87	8.02	9.17	10.31	11.46
385.58	15.02	14.83	0.25	1.615E-04	33.55	1.19	2.38	3.57	4.76	5.95	7.14	8.33	9.52	10.71	11.89
419.55	14.64	14.46	0.25	1.615E-04	36.38	1.23	2.47	3.70	4.94	6.17	7.41	8.64	9.88	11.11	12.34
453.52	14.27	14.08	0.25	1.615E-04	39.21	1.28	2.56	3.84	5.12	6.40	7.68	8.97	10.25	11.53	12.81
487.49	13.90	13.71	0.25	1.615E-04	42.04	1.33	2.66	3.99	5.32	6.64	7.97	9.30	10.63	11.96	13.29
521.46	13.52	13.34	0.25	1.615E-04	44.87	1.38	2.76	4.14	5.52	6.89	8.27	9.65	11.03	12.41	13.79
555.43	13.15	12.96	0.25	1.615E-04	47.70	1.43	2.86	4.29	5.72	7.16	8.59	10.02	11.45	12.88	14.31
589.40	12.78	12.89	0.19	1.615E-04	50.07	1.45	2.90	4.35	5.80	7.25	8.70	10.15	11.60	13.05	14.50
612.40	13.00	12.81	0.19	1.615E-04	52.48	1.47	2.94	4.41	5.87	7.34	8.81	10.28	11.75	13.22	14.68
647.01	12.62	12.43	0.19	1.615E-04	55.36	1.53	3.05	4.58	6.10	7.63	9.15	10.68	12.20	13.73	15.25
681.63	12.24	12.04	0.19	1.615E-04	58.25	1.58	3.17	4.75	6.34	7.92	9.51	11.09	12.68	14.26	15.85
716.25	11.85	11.66	0.19	1.615E-04	61.13	1.65	3.30	4.94	6.59	8.24	9.89	11.53	13.18	14.83	16.48
750.87	11.47	11.28	0.19	1.615E-04	64.01	1.71	3.43	5.14	6.86	8.57	10.29	12.00	13.72	15.43	17.15
785.49	11.09	10.90	0.19	1.615E-04	66.90	1.79	3.57	5.36	7.14	8.93	10.71	12.50	14.29	16.07	17.86
820.11	10.71	10.52	0.19	1.615E-04	69.78	1.86	3.72	5.58	7.45	9.31	11.17	13.03	14.89	16.75	18.62
854.73	10.33	10.14	0.19	1.615E-04	72.67	1.94	3.89	5.83	7.77	9.71	11.66	13.60	15.54	17.48	19.43
889.35	9.95	9.76	0.19	1.615E-04	75.55	2.03	4.06	6.09	8.12	10.15	12.18	14.21	16.24	18.27	20.30
923.96	9.57	9.38	0.19	1.615E-04	78.44	2.12	4.25	6.37	8.49	10.62	12.74	14.86	16.99	19.11	21.24
958.58	9.19	9.00	0.19	1.615E-04	81.32	2.22	4.45	6.67	8.90	11.12	13.35	15.57	17.80	20.02	22.25
993.20	8.81	8.62	0.19	1.615E-04	84.21	2.33	4.67	7.00	9.34	11.67	14.01	16.34	18.68	21.01	23.35
1027.82	8.43	8.24	0.19	1.615E-04	87.09	2.45	4.91	7.36	9.82	12.27	14.73	17.18	19.64	22.09	24.54
1062.44	8.05	7.86	0.19	1.615E-04	89.98	2.59	5.17	7.76	10.34	12.93	15.51	18.10	20.68	23.27	25.85
1097.06	7.67	7.48	0.19	1.615E-04	92.86	2.73	5.46	8.19	10.92	13.65	16.38	19.11	21.84	24.57	27.29
1131.68	7.28	7.09	0.19	1.615E-04	95.75	2.89	5.78	8.67	11.55	14.44	17.33	20.22	23.11	26.00	28.89
1166.30	6.90	6.71	0.19	1.615E-04	98.63	3.07	6.13	9.20	12.26	15.33	18.39	21.46	24.52	27.59	30.65
1200.91	6.52														

Table 3.31: Reynolds Numbers for Wind Flow at Various Elevations for HML-40-061 as a Function of Reference Height, h_{ref} , Wind Speeds.

Level (in.)	Outside Diameter	Average Diameter	Wall Thickness	Kin. Vis	H (ft)	Re 5 mph	10 mph	15 mph	20 mph	25 mph	30 mph	35 mph	40 mph	45 mph	50 mph
6.75	19.19														
		19.14	0.25	1.615E-04	0.91	**4.33E+04**	**8.67E+04**	1.30E+05	1.73E+05	2.17E+05	2.60E+05	3.03E+05	3.47E+05	3.90E+05	4.33E+05
15.00	19.09														
		18.92	0.25	1.615E-04	2.54	**4.96E+04**	**9.93E+04**	1.49E+05	1.99E+05	2.48E+05	2.98E+05	3.47E+05	3.97E+05	4.47E+05	4.96E+05
45.88	18.75														
		18.57	0.25	1.615E-04	5.24	**5.40E+04**	1.08E+05	1.62E+05	2.16E+05	2.70E+05	3.24E+05	3.78E+05	4.32E+05	4.86E+05	5.40E+05
79.85	18.38														
		18.19	0.25	1.615E-04	8.07	**5.63E+04**	1.13E+05	1.69E+05	2.25E+05	2.81E+05	3.38E+05	3.94E+05	4.50E+05	5.07E+05	5.63E+05
113.82	18.01														
		17.82	0.25	1.615E-04	10.90	**5.76E+04**	1.15E+05	1.73E+05	2.30E+05	2.88E+05	3.45E+05	4.03E+05	4.60E+05	5.18E+05	5.76E+05
147.79	17.63														
		17.45	0.25	1.615E-04	13.73	**5.82E+04**	1.16E+05	1.75E+05	2.33E+05	2.91E+05	3.49E+05	4.08E+05	4.66E+05	5.24E+05	5.82E+05
181.76	17.26														
		17.07	0.25	1.615E-04	16.56	**5.85E+04**	1.17E+05	1.76E+05	2.34E+05	2.93E+05	3.51E+05	4.10E+05	4.68E+05	5.27E+05	5.85E+05
215.73	16.89														
		16.70	0.25	1.615E-04	19.39	**5.86E+04**	1.17E+05	1.76E+05	2.34E+05	2.93E+05	3.51E+05	4.10E+05	4.69E+05	5.27E+05	5.86E+05
249.70	16.51														
		16.33	0.25	1.615E-04	22.22	**5.84E+04**	1.17E+05	1.75E+05	2.34E+05	2.92E+05	3.50E+05	4.09E+05	4.67E+05	5.25E+05	5.84E+05
283.67	16.14														
		15.95	0.25	1.615E-04	25.05	**5.80E+04**	1.16E+05	1.74E+05	2.32E+05	2.90E+05	3.48E+05	4.06E+05	4.64E+05	5.22E+05	5.80E+05
317.64	15.77														
		15.58	0.25	1.615E-04	27.89	**5.75E+04**	1.15E+05	1.73E+05	2.30E+05	2.88E+05	3.45E+05	4.03E+05	4.60E+05	5.18E+05	5.75E+05
351.61	15.39														
		15.20	0.25	1.615E-04	30.72	**5.69E+04**	1.14E+05	1.71E+05	2.28E+05	2.85E+05	3.42E+05	3.99E+05	4.56E+05	5.13E+05	5.69E+05
385.58	15.02														
		14.83	0.25	1.615E-04	33.55	**5.63E+04**	1.13E+05	1.69E+05	2.25E+05	2.81E+05	3.38E+05	3.94E+05	4.50E+05	5.06E+05	5.63E+05
419.55	14.64														
		14.46	0.25	1.615E-04	36.38	**5.55E+04**	1.11E+05	1.66E+05	2.22E+05	2.77E+05	3.33E+05	3.88E+05	4.44E+05	4.99E+05	5.55E+05
453.52	14.27														
		14.08	0.25	1.615E-04	39.21	**5.46E+04**	1.09E+05	1.64E+05	2.18E+05	2.73E+05	3.28E+05	3.82E+05	4.37E+05	4.92E+05	5.46E+05
487.49	13.90														
		13.71	0.25	1.615E-04	42.04	**5.37E+04**	1.07E+05	1.61E+05	2.15E+05	2.69E+05	3.22E+05	3.76E+05	4.30E+05	4.83E+05	5.37E+05
521.46	13.52														
		13.34	0.25	1.615E-04	44.87	**5.27E+04**	1.05E+05	1.58E+05	2.11E+05	2.64E+05	3.16E+05	3.69E+05	4.22E+05	4.75E+05	5.27E+05
555.43	13.15														
		12.96	0.25	1.615E-04	47.70	**5.17E+04**	1.03E+05	1.55E+05	2.07E+05	2.59E+05	3.10E+05	3.62E+05	4.14E+05	4.65E+05	5.17E+05
589.40	12.78														
		12.89	0.19	1.615E-04	50.07	**5.18E+04**	1.04E+05	1.55E+05	2.07E+05	2.59E+05	3.11E+05	3.62E+05	4.14E+05	4.66E+05	5.18E+05
612.40	13.00														
		12.81	0.19	1.615E-04	52.48	**5.18E+04**	1.04E+05	1.55E+05	2.07E+05	2.59E+05	3.11E+05	3.62E+05	4.14E+05	4.66E+05	5.18E+05
647.01	12.62														
		12.43	0.19	1.615E-04	55.36	**5.06E+04**	1.01E+05	1.52E+05	2.03E+05	2.53E+05	3.04E+05	3.54E+05	4.05E+05	4.56E+05	5.06E+05
681.63	12.24														
		12.04	0.19	1.615E-04	58.25	**4.94E+04**	**9.89E+04**	1.48E+05	1.98E+05	2.47E+05	2.97E+05	3.46E+05	3.95E+05	4.45E+05	4.94E+05
716.25	11.85														
		11.66	0.19	1.615E-04	61.13	**4.82E+04**	**9.64E+04**	1.45E+05	1.93E+05	2.41E+05	2.89E+05	3.37E+05	3.86E+05	4.34E+05	4.82E+05
750.87	11.47														
		11.28	0.19	1.615E-04	64.01	**4.69E+04**	**9.39E+04**	1.41E+05	1.88E+05	2.35E+05	2.82E+05	3.29E+05	3.75E+05	4.22E+05	4.69E+05
785.49	11.09														
		10.90	0.19	1.615E-04	66.90	**4.56E+04**	**9.13E+04**	1.37E+05	1.83E+05	2.28E+05	2.74E+05	3.19E+05	3.65E+05	4.11E+05	4.56E+05
820.11	10.71														
		10.52	0.19	1.615E-04	69.78	**4.43E+04**	**8.86E+04**	1.33E+05	1.77E+05	2.22E+05	2.66E+05	3.10E+05	3.54E+05	3.99E+05	4.43E+05
854.73	10.33														
		10.14	0.19	1.615E-04	72.67	**4.30E+04**	**8.59E+04**	1.29E+05	1.72E+05	2.15E+05	2.58E+05	3.01E+05	3.44E+05	3.87E+05	4.30E+05
889.35	9.95														
		9.76	0.19	1.615E-04	75.55	**4.16E+04**	**8.31E+04**	1.25E+05	1.66E+05	2.08E+05	2.49E+05	2.91E+05	3.33E+05	3.74E+05	4.16E+05
923.96	9.57														
		9.38	0.19	1.615E-04	78.44	**4.02E+04**	**8.03E+04**	1.20E+05	1.61E+05	2.01E+05	2.41E+05	2.81E+05	3.21E+05	3.61E+05	4.02E+05
958.58	9.19														
		9.00	0.19	1.615E-04	81.32	**3.87E+04**	**7.75E+04**	1.16E+05	1.55E+05	1.94E+05	2.32E+05	2.71E+05	3.10E+05	3.49E+05	3.87E+05
993.20	8.81														
		8.62	0.19	1.615E-04	84.21	**3.73E+04**	**7.46E+04**	1.12E+05	1.49E+05	1.86E+05	2.24E+05	2.61E+05	2.98E+05	3.36E+05	3.73E+05
1027.82	8.43														
		8.24	0.19	1.615E-04	87.09	**3.58E+04**	**7.16E+04**	1.07E+05	1.43E+05	1.79E+05	2.15E+05	2.51E+05	2.86E+05	3.22E+05	3.58E+05
1062.44	8.05														
		7.86	0.19	1.615E-04	89.98	**3.43E+04**	**6.86E+04**	1.03E+05	1.37E+05	1.72E+05	2.06E+05	2.40E+05	2.74E+05	3.09E+05	3.43E+05
1097.06	7.67														
		7.48	0.19	1.615E-04	92.86	**3.28E+04**	**6.56E+04**	**9.84E+04**	1.31E+05	1.64E+05	1.97E+05	2.30E+05	2.62E+05	2.95E+05	3.28E+05
1131.68	7.28														
		7.09	0.19	1.615E-04	95.75	**3.13E+04**	**6.25E+04**	**9.38E+04**	1.25E+05	1.56E+05	1.88E+05	2.19E+05	2.50E+05	2.81E+05	3.13E+05
1166.30	6.90														
		6.71	0.19	1.615E-04	98.63	**2.97E+04**	**5.94E+04**	**8.91E+04**	1.19E+05	1.49E+05	1.78E+05	2.08E+05	2.38E+05	2.67E+05	2.97E+05
1200.91	6.52														

Note: The **shaded regions** indicate wind speeds and locations along the HML structure where $300 \le \mathrm{Re} \le 10^5$ or $\mathrm{Re} > 3.5\times10^6$.

Table 3.32: Shedding Frequency (Hz) Boundaries at Various Elevations for HML-40-061 as a Function of Reference Height, h_{ref}, Wind Speeds.

	Outside	Average	Wall		H	5 mph		10 mph		15 mph		20 mph		25 mph		30 mph		35 mph		40 mph		45 mph		50 mph	
Level (in.)	Diameter	Diameter	Thickness	Kin. Vis	(ft)	n_low (Hz)	n_hgh (Hz)	n_low (Hz)	n_hgh (Hz)	n_low (Hz)	n_hgh (Hz)	n_low (Hz)	n_hgh (Hz)	n_low (Hz)	n_hgh (Hz)	n_low (Hz)	n_hgh (Hz)	n_low (Hz)	n_hgh (Hz)	n_low (Hz)	n_hgh (Hz)	n_low (Hz)	n_hgh (Hz)	n_low (Hz)	n_hgh (Hz)
6.75	19.19	19.14	0.25	1.615E-04	0.91	**0.23**	**0.87**	0.46	1.74	**0.69**	**2.62**	**0.91**	**3.49**	**1.14**	**4.36**	**1.37**	**5.23**	**1.60**	**6.10**	1.83	6.98	**2.06**	**7.85**	**2.28**	**8.72**
15.00	19.09	18.92	0.25	1.615E-04	2.54	0.41	0.88	0.82	1.76	**1.23**	**2.64**	**1.64**	**3.52**	2.05	4.40	**2.46**	**5.28**	**2.86**	**6.16**	**3.27**	**7.04**	**3.68**	**7.92**	**4.09**	**8.80**
45.88	18.75	18.57	0.25	1.615E-04	5.24	0.52	0.94	**1.04**	**1.88**	**1.56**	**2.82**	2.07	3.76	2.59	4.70	**3.11**	**5.63**	**3.63**	**6.57**	**4.15**	**7.51**	**4.67**	**8.45**	5.18	9.39
79.85	18.38	18.19	0.25	1.615E-04	8.07	0.59	0.99	**1.18**	**1.99**	**1.76**	**2.98**	2.35	3.98	**2.94**	**4.97**	**3.53**	**5.96**	**4.12**	**6.96**	**4.70**	**7.95**	5.29	8.95	5.88	9.94
113.82	18.01	17.82	0.25	1.615E-04	10.90	0.64	1.04	**1.28**	**2.09**	1.93	3.13	2.57	4.18	**3.21**	**5.22**	**3.85**	**6.26**	**4.50**	**7.31**	5.14	8.35	5.78	9.40	**6.42**	**10.44**
147.79	17.63	17.45	0.25	1.615E-04	13.73	0.69	1.09	**1.38**	**2.18**	2.07	3.27	2.76	4.36	**3.44**	**5.46**	**4.13**	**6.55**	**4.82**	**7.64**	5.51	8.73	6.20	9.82	**6.89**	**10.91**
181.76	17.26	17.07	0.25	1.615E-04	16.56	0.73	1.14	**1.46**	**2.27**	2.20	3.41	2.93	4.55	**3.66**	**5.68**	**4.39**	**6.82**	5.12	7.96	5.85	9.09	**6.59**	**10.23**	**7.32**	**11.37**
215.73	16.89	16.70	0.25	1.615E-04	19.39	0.77	1.18	**1.54**	**2.36**	2.32	3.54	3.09	4.73	**3.86**	**5.91**	**4.63**	**7.09**	5.41	8.27	6.18	9.45	**6.95**	**10.63**	**7.72**	**11.82**
249.70	16.51	16.33	0.25	1.615E-04	22.22	0.81	1.23	**1.62**	**2.45**	2.43	3.68	**3.25**	**4.91**	**4.06**	**6.13**	4.87	7.36	5.68	8.58	6.49	9.81	**7.30**	**11.04**	**8.11**	**12.26**
283.67	16.14	15.95	0.25	1.615E-04	25.05	0.85	1.27	**1.70**	**2.54**	2.55	3.81	**3.40**	**5.09**	**4.25**	**6.36**	5.10	7.63	5.95	8.90	**6.80**	**10.17**	**7.65**	**11.44**	**8.50**	**12.72**
317.64	15.77	15.58	0.25	1.615E-04	27.89	0.89	1.32	1.78	2.64	2.66	3.95	**3.55**	**5.27**	**4.44**	**6.59**	5.33	7.91	6.22	9.22	**7.11**	**10.54**	**7.99**	**11.86**	**8.88**	**13.18**
351.61	15.39	15.20	0.25	1.615E-04	30.72	0.93	1.36	1.85	2.73	2.78	4.09	**3.71**	**5.46**	**4.63**	**6.82**	5.56	8.19	6.49	9.55	**7.41**	**10.92**	**8.34**	**12.28**	**9.27**	**13.65**
385.58	15.02	14.83	0.25	1.615E-04	33.55	0.97	1.41	1.93	2.83	2.90	4.24	**3.86**	**5.65**	**4.83**	**7.07**	5.80	8.48	6.76	9.89	**7.73**	**11.30**	**8.69**	**12.72**	**9.66**	**14.13**
419.55	14.64	14.46	0.25	1.615E-04	36.38	1.01	1.46	2.01	2.93	3.02	4.39	**4.02**	**5.85**	5.03	7.31	6.04	8.78	**7.04**	**10.24**	**8.05**	**11.70**	**9.05**	**13.17**	10.06	14.63
453.52	14.27	14.08	0.25	1.615E-04	39.21	1.05	1.51	2.09	3.03	3.14	4.54	**4.19**	**6.06**	5.23	7.57	6.28	9.09	**7.33**	**10.60**	**8.38**	**12.12**	**9.42**	**13.63**	10.47	15.15
487.49	13.90	13.71	0.25	1.615E-04	42.04	1.09	1.57	2.18	3.14	3.27	4.71	**4.36**	**6.27**	5.45	7.84	6.54	9.41	**7.63**	**10.98**	**8.71**	**12.55**	**9.80**	**14.12**	10.89	15.68
521.46	13.52	13.34	0.25	1.615E-04	44.87	1.13	1.62	2.27	3.25	**3.40**	**4.87**	**4.53**	**6.50**	5.67	8.12	6.80	9.75	**7.93**	**11.37**	**9.07**	**13.00**	10.20	14.62	**11.33**	**16.25**
555.43	13.15	12.96	0.25	1.615E-04	47.70	1.18	1.68	2.36	3.37	**3.54**	**5.05**	**4.72**	**6.73**	5.89	8.42	**7.07**	**10.10**	**8.25**	**11.78**	**9.43**	**13.47**	10.61	15.15	**11.79**	**16.83**
589.40	12.78	12.89	0.19	1.615E-04	50.07	1.20	1.70	2.39	3.41	**3.59**	**5.11**	**4.78**	**6.81**	5.98	8.51	**7.18**	**10.22**	**8.37**	**11.92**	**9.57**	**13.62**	10.77	15.33	**11.96**	**17.03**
612.40	13.00	12.81	0.19	1.615E-04	52.48	1.21	1.72	2.43	3.45	**3.64**	**5.17**	4.86	6.89	6.07	8.62	**7.28**	**10.34**	**8.50**	**12.06**	**9.71**	**13.78**	10.92	15.51	**12.14**	**17.23**
647.01	12.62	12.43	0.19	1.615E-04	55.36	**1.26**	**1.79**	2.53	3.57	**3.79**	**5.36**	5.05	7.15	6.32	8.94	**7.58**	**10.72**	**8.84**	**12.51**	10.10	14.30	11.37	16.08	**12.63**	**17.87**
681.63	12.24	12.04	0.19	1.615E-04	58.25	**1.31**	**1.85**	2.63	3.71	**3.94**	**5.56**	5.26	7.42	6.57	9.27	**7.89**	**11.13**	**9.20**	**12.98**	10.52	14.84	**11.83**	**16.69**	**13.15**	**18.55**
716.25	11.85	11.66	0.19	1.615E-04	61.13	**1.37**	**1.93**	2.74	3.85	**4.11**	**5.78**	5.48	7.70	6.85	9.63	**8.22**	**11.56**	**9.59**	**13.48**	10.96	15.41	**12.33**	**17.34**	**13.70**	**19.26**
750.87	11.47	11.28	0.19	1.615E-04	64.01	**1.43**	**2.00**	2.85	4.00	**4.28**	**6.01**	5.71	8.01	**7.14**	**10.01**	**8.56**	**12.01**	9.99	14.01	11.42	16.02	**12.85**	**18.02**	**14.27**	**20.02**
785.49	11.09	10.90	0.19	1.615E-04	66.90	**1.49**	**2.08**	2.98	4.17	**4.47**	**6.25**	5.95	8.33	**7.44**	**10.41**	**8.93**	**12.50**	10.42	14.58	**11.91**	**16.66**	**13.40**	**18.75**	**14.89**	**20.83**
820.11	10.71	10.52	0.19	1.615E-04	69.78	**1.55**	**2.17**	3.11	4.34	**4.66**	**6.51**	6.22	8.68	**7.77**	**10.85**	**9.32**	**13.01**	10.88	15.18	**12.43**	**17.35**	**13.99**	**19.52**	**15.54**	**21.69**
854.73	10.33	10.14	0.19	1.615E-04	72.67	**1.62**	**2.26**	3.25	4.52	4.87	6.78	6.50	9.05	**8.12**	**11.31**	**9.74**	**13.57**	11.37	15.83	**12.99**	**18.09**	**14.62**	**20.35**	16.24	22.62
889.35	9.95	9.76	0.19	1.615E-04	75.55	**1.70**	**2.36**	3.40	4.72	5.10	7.08	6.80	9.44	**8.49**	**11.80**	10.19	14.16	**11.89**	**16.53**	**13.59**	**18.89**	**15.29**	**21.25**	16.99	23.61
923.96	9.57	9.38	0.19	1.615E-04	78.44	1.78	2.47	**3.56**	**4.94**	5.34	7.40	7.12	9.87	**8.90**	**12.34**	10.68	14.81	**12.46**	**17.27**	**14.23**	**19.74**	**16.01**	**22.21**	**17.79**	**24.68**
958.58	9.19	9.00	0.19	1.615E-04	81.32	1.87	2.58	**3.73**	**5.17**	5.60	7.75	**7.47**	**10.33**	**9.33**	**12.92**	11.20	15.50	**13.06**	**18.08**	**14.93**	**20.67**	16.80	23.25	**18.66**	**25.83**
993.20	8.81	8.62	0.19	1.615E-04	84.21	1.96	2.71	**3.92**	**5.42**	5.88	8.13	**7.84**	**10.84**	**9.80**	**13.54**	11.76	16.25	**13.72**	**18.96**	**15.69**	**21.67**	17.65	24.38	**19.61**	**27.09**
1027.82	8.43	8.24	0.19	1.615E-04	87.09	2.06	2.85	**4.13**	**5.69**	6.19	8.54	**8.25**	**11.38**	10.32	14.23	**12.38**	**17.07**	**14.44**	**19.92**	16.51	22.77	**18.57**	**25.61**	**20.63**	**28.46**
1062.44	8.05	7.86	0.19	1.615E-04	89.98	2.18	3.00	**4.35**	**5.99**	6.53	8.99	**8.70**	**11.98**	10.88	14.98	**13.05**	**17.97**	**15.23**	**20.97**	17.40	23.96	**19.58**	**26.96**	**21.76**	**29.95**
1097.06	7.67	7.48	0.19	1.615E-04	92.86	2.30	3.16	**4.60**	**6.32**	6.90	9.48	**9.20**	**12.64**	11.49	15.80	**13.79**	**18.96**	**16.09**	**22.12**	**18.39**	**25.28**	**20.69**	**28.44**	**22.99**	**31.60**
1131.68	7.28	7.09	0.19	1.615E-04	95.75	2.44	3.34	4.87	6.68	**7.31**	**10.03**	**9.74**	**13.37**	**12.18**	**16.71**	**14.61**	**20.05**	17.05	23.39	**19.48**	**26.74**	**21.92**	**30.08**	**24.35**	**33.42**
1166.30	6.90	6.71	0.19	1.615E-04	98.63	2.59	3.54	5.17	7.09	**7.76**	**10.63**	10.35	14.18	**12.93**	**17.72**	**15.52**	**21.27**	**18.10**	**24.81**	**20.69**	**28.36**	**23.28**	**31.90**	25.86	35.44
1200.91	6.52																								

Note: The **shaded regions** indicate wind speeds and locations along the HML structure where $n_s^L \le n_{struc}^k \le n_s^U$ where *k* indicates any mode.

As expected, the wind speeds increase with elevation. It should be noted that the values in the table are expressed in 'ft/s'. Table 3.30 shows the frequencies of vortices shed over the *average diameter* mast segments. These frequencies are computed using equation (3.4). The expected increase in shedding frequency with wind speed (height) and reduction in diameter is seen in the values. The Reynolds numbers conducive to regularly shed vortices are shown in Table 3.31 (shaded regions). The shaded values in the table illustrate Reynolds numbers for flow in subcritical or transcritical critical regions. As reference wind speeds increase, less of the mast encounters flow with Reynolds numbers conducive to periodic and regular shedding of vortices. At 5 mph, the entire mast will shed periodic vortices and as the mean wind speed increases, segments where periodic vortices may be expected migrate towards the top of the mast. It should be noted that mean wind speeds above 20 mph result in Reynolds numbers for the flow in the super-critical region where irregular vortices tend to form.

Table 3.32 contains values for the upper- and lower-bound shedding frequencies for vortices at each wind speed considered. The shaded values in the Table correspond to mast segments where the natural frequency of any of the 6 vibrational mode shapes considered (see Table 3.27 with 2-1/2" stand off height) fall within the upper and lower bounds for the vortex shedding frequencies defined in equation (3.7). As shown by the shaded regions of the Table, there are many locations along the HML mast where the structure's natural frequencies fall within the upper and lower boundaries of shedding frequencies. However, mean wind speeds above 20 mph do not have Reynolds numbers that are conducive to periodic vortex shedding and therefore, vortex shedding loading for these wind speed above 20 mph can be ignored for this mast.

At mean wind speeds below 20 mph, there are segments of the mast where flow is conducive to periodically shed vortices (5 mph – full height; 10 mph – 57 to 100 ft; 15 mph – 91 to 100 ft). Therefore, one could compute periodic loading over the mast at levels 54 ft. to 77 ft above the ground using equation (3.6) and the frequency for the second mode of vibration for 5 mph mean wind. At 10 mph mean wind speed, the overlap occurs at levels 77 ft. through 94 ft. above the ground. Therefore, sinusoidal loading at a frequency corresponding to the third vibrational mode could be applied. At 15 mph mean wind speeds, the overlap in Reynolds number and frequency boundaries occurs at the top of the mast over a 5.7 foot segment. This location would contain sinusoidal loading corresponding to the 4th vibrational mode.

Wind speeds in the range of 5-15 mph will cause sinusoidal loading magnitudes that are very low relative to the along-wind stress magnitudes (lift coefficients are much less than drag). Furthermore, the segments over which the sinusoidal loading would act are limited (when compared to the length of mast over which loading is applied when evaluating along-wind response). As a result, vortex-shedding need not be considered in the fatigue life evaluation of this HML mast.

The lack of these structures exhibiting vortex-shedding response was supported with visual observation during 30-40 mph winds. Figure 3.60 illustrates the observed along-wind response for an HML structure (HML-67-006). Unfortunately, visual observations of HML-40-061 were not made during this high-wind event (wind speeds dropped by the time HML-40-061 was visited). As shown, the along-wind deformations are significant. The lateral sway under the wind event (approximately 30 mph sustained winds) is over one diameter at the mast top. Along-wind oscillations about a mean positive deformed position were observed. There was no across-wind oscillation of the mast. The lack of vortex shedding deformations in the visual observations along with the results shown in Tables 3.29 through 3.32 justify the omission of across-wind response and its impact on HML structure fatigue life.

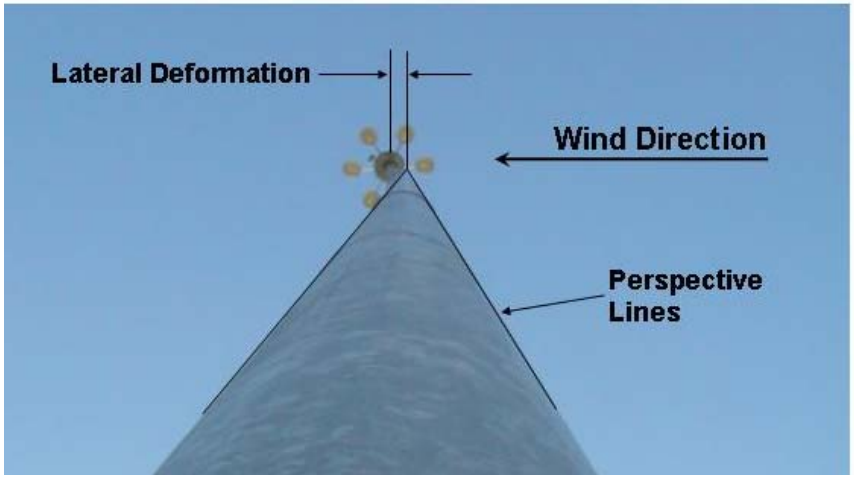

Figure 3.60: Along-Wind Response of HML-67-006 Illustrating Lack of Vortex-Shedding Deformations.

3.3.1.4 Response to Natural Wind

Simulated wind speeds and pressures were generated using the procedures discussed in chapter 2 of the report. Example wind speed simulations for five levels over the height of the HML mast are shown in Figure 3.61. For computational simplicity, the luminaire mast length was broken down into 4 (nearly equal) segments and the wind velocity was assumed to be established at the mid-height: 11.82 feet; 34.96 feet; 61.64 feet; and 88.54 feet above the base. The wind speeds at each of these heights were computed using the power law with $U_{ref} = 50\,mph$ and open terrain. The luminaire assembly was set at 100.0 feet above the base.

A time-varying wind pressure was determined using the equation below (Simiu and Scanlon 1996),

$$p_z(t) = \frac{1}{2} \cdot \rho \cdot U_z(t)^2 \cdot C_{d,z} \tag{3.15}$$

where: $C_{d,z}$ is the drag coefficient for the 16-sided bluff body at a defined mast location z, $U_z(t)$ is the simulated wind velocity as a function of time at a defined height location z; and ρ is the density of air.

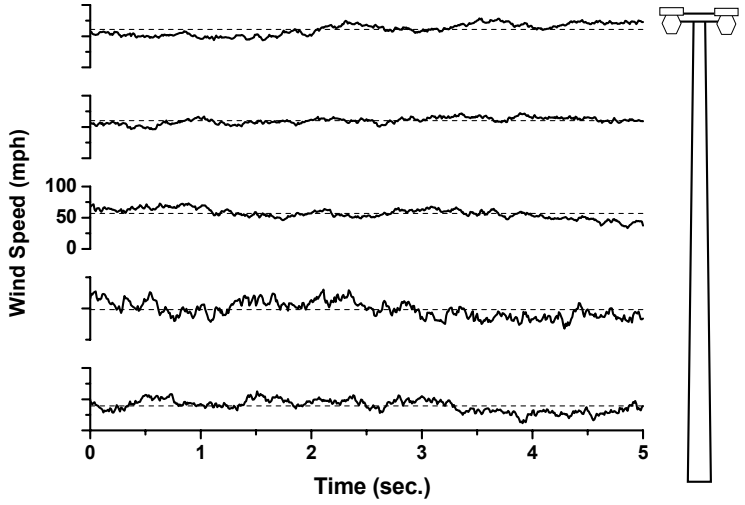

Figure 3.61: Simulated Wind Speeds Over Height of HML-40-061 Assuming a Mean Wind Speed at 33-feet Equal to 50 mph.

The drag coefficients depend upon the diameter of the mast and the wind speed velocity chosen (AASHTO 2001). Assuming that the distance between parallel faces exceeds 8 times the corner radius on dodecagonal shape, the drag coefficients are (AASHTO 2001);

$$C_d = 1.20 \qquad \text{for } C_v V \cdot d \le 39 \quad mph \cdot ft \tag{3.16}$$

$$C_d = \frac{10.8}{\left(C_v V \cdot d\right)^{0.6}} \qquad \text{for } \; 39 \le C_v V \cdot d \le \; 78 \quad mph \cdot ft \tag{3.17}$$

$$C_d = 0.79 \qquad \text{for } \; C_v V \cdot d > 78 \quad mph \cdot ft \tag{3.18}$$

where: C_v is a velocity conversion factor intended to allow conversion of wind speeds to a variety of mean recurrence interval winds; V is the mean wind speed (in mph for 3-second averaging time); and d is the dimension of the dodecagonal shape mast (between flat sides in feet). The metro-Milwaukee area falls within a 90-mph 50-year MRI wind assuming a 3-second gust. The specifications allow the 50-year wind speed to be adjusted using the velocity conversion factor. Its magnitude ranges from 1.07 for 100-year MRI to 0.84 for 10-year MRI.

This led to a dilemma in developing wind loading simulations for subsequent fatigue life simulations because the drag coefficients in the specifications (AASHTO 2001) were intended to be used in conjunction with strength and/or deflection analysis. Fatigue life prediction cannot be realistically done for wind speeds on the order of,

100-year MRI wind: $1.07(90\ mph) = 96.3\ mph\ (3-\text{sec}) = 95.1\ mph\ (5-\text{sec})$

10-year MRI wind: $0.84(90\ mph) = 75.6\ mph\ (3-\text{sec}) = 74.6\ mph\ (5-\text{sec})$

These wind speeds are far above the 99.6% mean wind speed of 50 mph (5-second gust) measured at Mitchell International Airport (Ginal 2003). One could argue that the 10-year MRI wind is more appropriate for fatigue-life predictions even though the resulting 5-second mean wind speed exceeds the 99.6% wind for Milwaukee over the time period examined.

The average diameters of the HML mast at each of the four segment heights are approximately: 18 inches; 14 inches; 11 inches; and 8 inches as one rises from the bottom to the top. Using equations (3.16) through (3.18), this implies that the drag coefficient varies over the height of the mast. The upper-limit on wind speed assumed in the present study was 50 mph. This speed is less than the 10-year MRI wind assumed in the Specifications. Thus, using the Durst curve approach, the 50-year 3-second gust can be converted to a 5-second gust consistent with the present averaging time assumed,

$$V_5 = (90)\left(\frac{1}{1.55}\right)\left(\frac{1.53}{1}\right) = 88.84\ mph$$

The 10-year MRI wind was converted previously (74.6 mph).

The four HML mast diameters and the 10-year MRI wind were used to study the variation in drag coefficient for each of these four segments. Table 3.33 contains drag coefficient values for these four heights computed using equations (3.16) through (3.18).

Table 3.33: Drag Coefficient Variation with Height for 10-Year MRI Wind

Segment	Diameter (ft)	10-Year MRI		50-Year MRI	
		C_vVd	C_d	C_vVd	C_d
1	1.50	111.9	0.79	133.2	0.79
2	1.17	87.3	0.79	103.9	0.79
3	0.92	68.6	0.85	81.7	0.79
4	0.67	50	1.03	59.5	0.92

Although slightly unconservative, the 50-year MRI drag coefficients were used in the definition of wind pressures over the height of the luminaire mast. In reality, the drag coefficient will likely be *higher* for lower wind speeds (Recall, wind speeds from 5 mph to 50 mph was used in this study). If C_vV were assumed to be 50 mph, the resulting drag coefficients for segments 1 and 4 would be; 0.81 and 1.20. As the wind speeds are reduced toward the 5-mph level, all drag coefficients would approach 1.20. The upper-limit of 1.20 appears excessive since the cylindrical upper-limit is 1.10 (19% higher than the upper limit of 0.92 used here). Therefore, the drag coefficient approximation used was felt to be acceptable.

The luminaire assembly was assumed to have a drag coefficient equal to 1.20 on a projected area of 12 square feet.

The time varying wind pressures at each of the five heights computed using equation (3.15) are shown in Figure 3.62. As expected, the luminaire assembly has the largest "average" pressure resulting from the largest mean wind speed and the largest drag coefficient. Allowing the wind speeds to be constant over segments of the mast length was felt to be an acceptable approximation for the following reasons. First of all, the wind speed and pressure do increase with height. However, the diameter of the mast will get smaller with height. Therefore, even though the velocity and pressure increase with height, the small diameter will tend toward reducing the line loading applied to the mast. Having a uniform pressure over 8-9 finite elements (a mast segment) will result in slightly larger pressure being applied to lower finite elements in a mast segment and slightly lower pressures to be applied to higher finite elements in a mast segment. This approximation was tolerated to preclude the need for 36 time histories (one for each of the 36 finite elements used to discretize the HML mast).

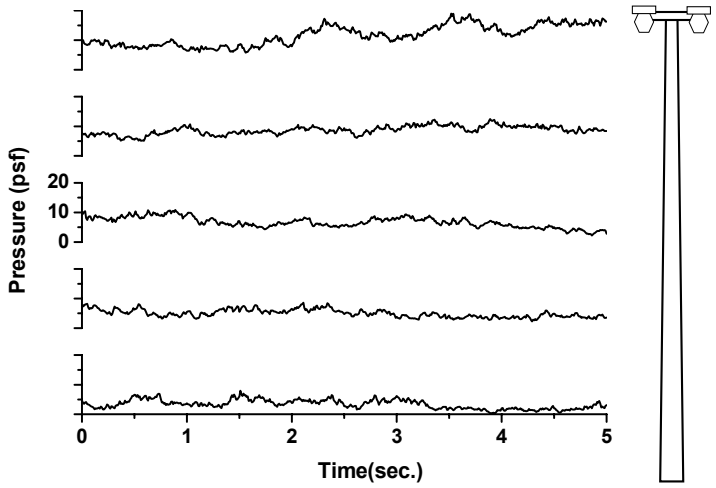

Figure 3.62: Simulated Wind Pressures Over Height of HML-40-061 Assuming a Mean Wind Speed at 33-feet Equal to 50 mph.

There is a three-phase loading protocol used in the transient analysis upon which the fatigue life predictions are based. The first phase of loading involves the application of acceleration due to gravity over a time frame of 5 seconds. This transient loading is applied with Rayleigh damping coefficients designed to provide 100% of the critical damping ratio averaged over vibration modes expected to be significant in the response (modes 1 through 4 – frequencies shown in Table 3.27). The combination of 100% damping and gradual acceleration application serves to prevent the HML structure from

"bouncing" after the acceleration due to gravity is applied (Ginal 2003). The second loading phase is application of the first pressure in the 5-second turbulent record with 100% damping over a 5-second interval. This simulates the quasi-static application of the mean wind pressure in the turbulent record. The third phase in the loading protocol is application of the transient turbulent wind pressure of 5-second duration. Rayleigh damping coefficients corresponding to 0.1% of critical damping averaged over modes 1 through 4 were used in the transient analysis for this third phase. As a result, the wind loading is applied over 10 seconds and the gravity loading is applied over 5 seconds. The total duration of the loading record is 15 seconds.

The simulated wind loading discussed in the previous section was first used to study the anchor rod response in the base of the luminaire structure. Two wind loading directions were applied. The first was defined as FX and the second was defined as FX/FY. Figure 3.63 will clarify these designations with respect to the loading orientation relative to the anchor rod pattern.

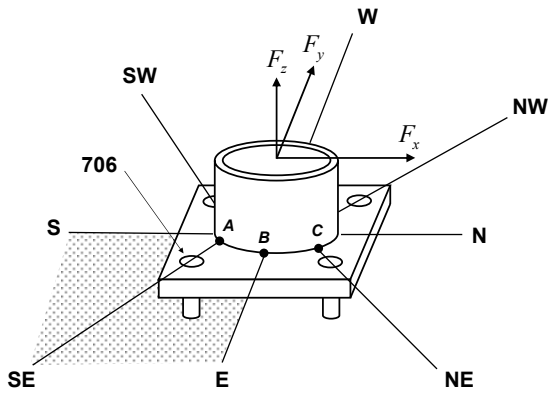

Figure 3.63: HML-40-061 Anchor Rod Orientation and Wind Direction Orientation.

The anchor rod diameters are 2-1/2 inches. Assuming that 8 UNC course threads exist, the "stress area" for the anchor rods can be taken as 4.0 square inches (Dexter and Ricker 2002). The diameter of the anchor rod used for stress computations can then be taken as 2.26 inches. The second moment of area then can be computed as $1.27\ in^4$.

Figure 3.64 illustrates the anchor bolt axial stress variation (anchor bolt 706 – see Figure 3.63) for varying wind speeds and directions. The loading protocol discussed previously can be seen in the axial stress record shown in Figure 3.64. The HML structure's self-weight is applied (with critical damping) over the first 5 seconds. Therefore, at 5 seconds, the there is compressive stress in the anchor rods. From 5 seconds to 10 seconds the first pressure in the 5-second turbulent record is applied using critical

damping. This is analogous to application of the climatic component of natural wind (Dyrbye and Hansen 1997), or the slow variation in mean wind speed over days accounting for weather system movement. As with the gravity loading, the near linear response as this pressure is applied exhibits the effect of 100% of critical damping used in the transient analysis. The 5-second turbulent wind record is applied from 10 seconds to 15 seconds. One can see that the 50-mph mean wind creates axial stress cycles of much greater magnitude than the 25-mph, which is to be expected. Furthermore, it can be seen that the 5-mph mean wind is not capable of generating tensile stresses in anchor bolt 706 (*i.e.* the wind loading stress cannot reverse the built-in stress due to the HML self weight). One also should appreciate the difference in axial stress resulting from wind pressures in the FX/FY direction.

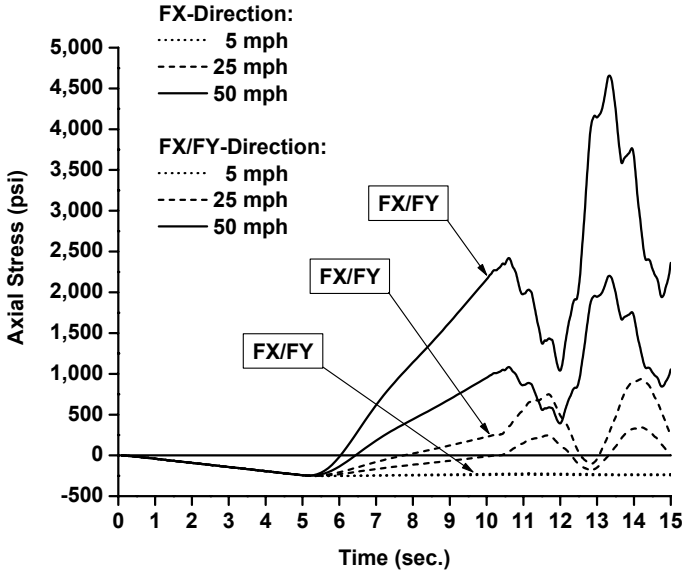

Figure 3.64: Anchor Rod 706 Axial Stress Variations with Wind Speed and Wind Direction.

The HML structure is a natural filter seeking out frequency characteristics in the naturally turbulent wind and responding to those frequencies. Furthermore, Figure 3.62 illustrates that the pressure at the height of the luminaire assembly is (on average) higher than that at the other segments up the mast. The projected area of the luminaire assembly was assumed to be 12 square feet for this structure. Therefore, there will be a significant loading at the top of the mast with the tendency to have the HML structure respond to the turbulent wind with first-mode characteristics. One can see that the response of HML-40-061 to wind speeds of 25 mph and 50 mph (both directions) has a period of approximately 2.5-2.8 seconds, which is close to the first mode of vibration period of 2.81 seconds given in Table 3.27. Other higher-frequency components are present for 50-mph winds, but the response is indeed first-mode dominant at lower wind speeds (*e.g.* 25-mph). Thus, one could say that the response of this structure to wind will indeed be first-mode dominant (mainly due to the luminaire assembly projected area).

Previous discussion alluded to the fact that bending stresses may be very important in characterizing the response of the anchor rods of HML-40-061 to natural wind. Figure 3.65 illustrates the bending stress history for anchor rod 706 for two wind directions and 3 wind speeds. It is apparent that the bending stresses are significant. Figures 3.47 and 3.48 illustrates that the exposed length of the anchor rod below the leveling nut is approximately equal to the diameter of the anchor rod. This is the criteria for omitting bending stresses in the fatigue computations (Dexter and Ricker 2002). However, one should certainly appreciate the magnitude of the bending stresses even though they will be omitted from the fatigue computations. It is recommended that this issue be studied in more detail (especially with respect to anchor rod stand off heights). The bending stress reported in Figure 3.65 is based upon a vector resultant of the bi-axial moments acting at the "bottom" of the anchor rod (*i.e.* at the top surface of the concrete).

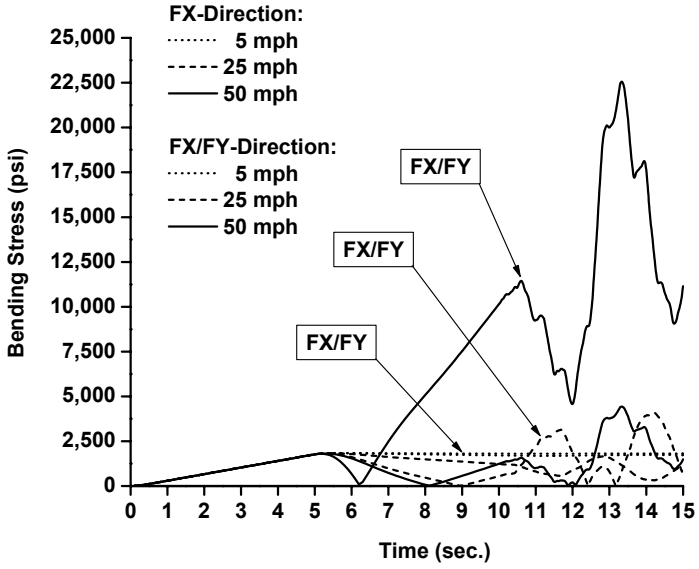

Figure 3.65: Anchor Rod 706 Bending Stress Variations with Wind Speed and Wind Direction.

The mast-to-base-plate weld is a fatigue-critical detail and it is prudent to examine the stress history at this connection during various wind speeds from multiple directions. Figure 3.66 illustrates the stress-response history for the base of the mast. The stress concentration factor discussed previously, equation (3.2), should be pointed out in the response. This is the difference between the FX and FX/FY stress magnitudes.

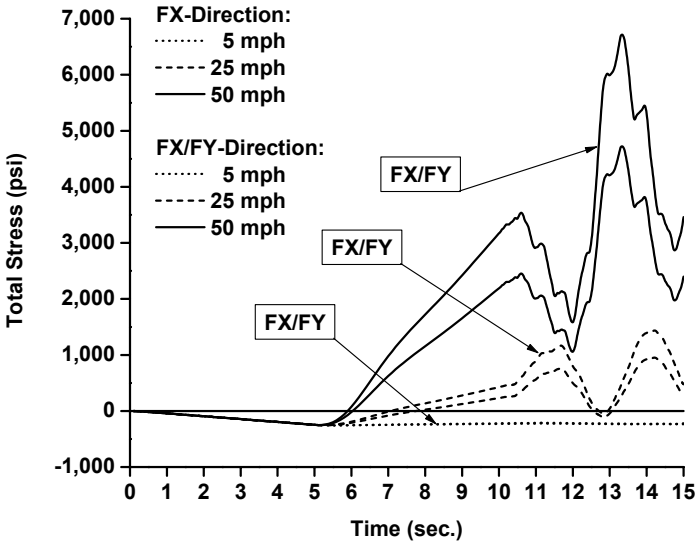

Figure 3.66: Mast Wall Stress History (Bending Plus Axial Stress) Variation with Wind Speed and Direction.

3.3.1.5 Fatigue Life Prediction

Predicting fatigue lives for the HML structures in the absence of a full-year wind loading simulation is approximate in nature. However, provisions have been taken with loading records, mean wind speed probability, and mean wind speed directional probability to ensure that good fatigue life predictions can be made for the HML structures. The procedure outlined in chapter 2 for generating fatigue life estimates has been used to generate fatigue life estimates for the critical components of HML-40-061. It should be noted that the entire stress history is used when counting stress-range cycles. This will allow for a portion of the climatic component of the wind speed variation to be included in the stress cycle counting. In other words, the slowly varying rise and fall of the mean wind speed will be included in the fatigue life prediction (in an appropriate manner).

One very important item of note in the fatigue-life computations is that the anchor rods are considered as E' details with a CAFL that corresponds to detail category D. Furthermore, compression portions of the stress cycle are included in the rainflow counting algorithm. This was done only for the anchor rods. The mast base and hand-hole stress ranges did not include the compression portion of the stress range.

As shown by Ginal (2003), wind speeds of 50 mph and less account for 99.6% of all mean (5-second) wind speeds measured at Mitchell International Airport for the five-plus contiguous years of wind data considered. Ginal (2003) also provided a statistical study of wind direction and mean velocity for winds measured at Mitchell International Airport. The probabilistic data generated in this study were used in the fatigue life predictions for the HML support structures.

Mean wind speed, its turbulent nature, and its direction are all critical to determining the fatigue life of an HML support structure. Figure 3.63 illustrated a schematic of the base of HML-40-061 and overlays wind directions assumed for the fatigue life estimate of anchor rods, the mast base, and the hand hole. The figure illustrates anchor rod 706 will be subject to tensile stresses when wind is out of the east (E), southeast (SE) and south (S). Similar statements can be made for other anchor rods being subjected to tensile stresses for winds out of the E-NE-N, N-NW-W, and W-SW-S directions. The mast base and hand-hole stress computations are based upon the maximum distance from the neutral axis of bending.

Fatigue life predictions for all four rods in the base arrangement can be made if an analysis for anchor rod 706 is made for wind coming from the FX and FX/FY directions is used. For example, the axial stress history for anchor rod 706 for wind from the FX direction can be used to generate stress cycle counts for wind coming from the East. The axial stress history for anchor rod 706 for wind coming from the FX/FY direction can be used to generate stress cycle counts for wind coming from the Southeast and Northeast direction. These three cycle counts can then be used to generate total stress range counts for anchor rod 706 for winds causing the maximum possible stress ranges.

Three components were used to characterize the fatigue life of HML-40-061: (a) the anchor rods; (b) the mast-to-base plate fillet weld; and (c) the fillet welds located at the hand hole reinforcing plates. Fatigue damage accumulation histograms for these three components are shown in Figures 3.67 through 3.69.

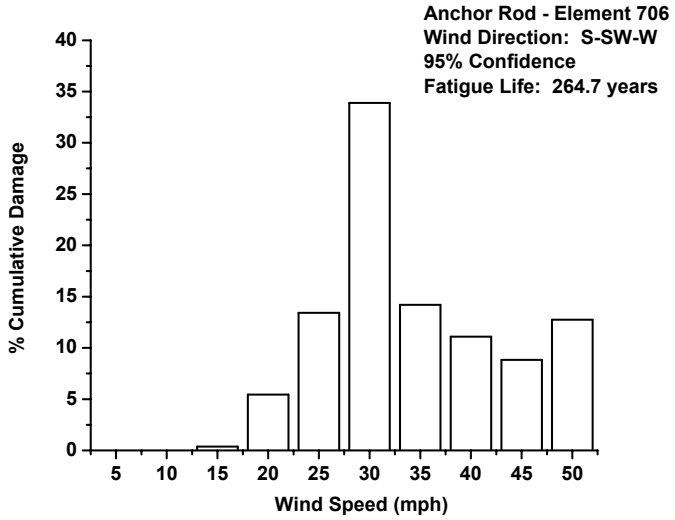

Figure 3.67: Fatigue Damage Accumulation in Anchor Rods for HML-40-061 for Mean Wind Speeds Ranging from 5 to 50-mph.

The confidence levels for all three of the fatigue life estimates are 95%. This means that the fatigue lives listed in the figures have a 95% chance of occurring during service. Of course, there are other

confidence levels associated with fatigue life estimates and these have been provided as well and these will be discussed.

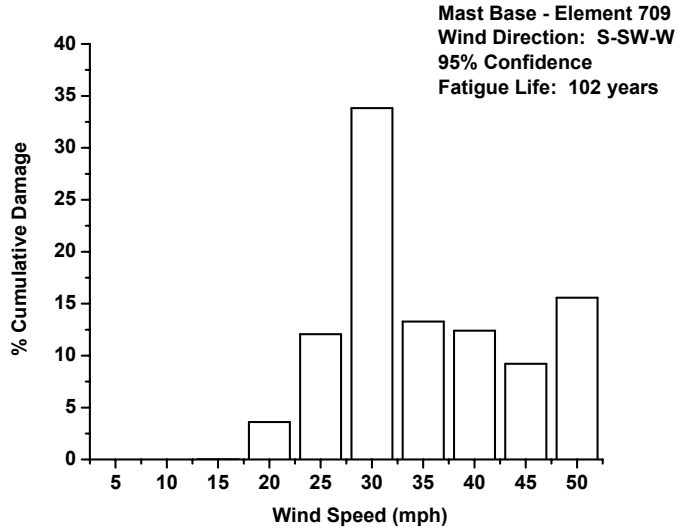

Figure 3.68: Fatigue Damage Accumulation in Mast Base Fillet Weld for HML-40-061 for Mean Wind Speeds Ranging from 5 to 50-mph.

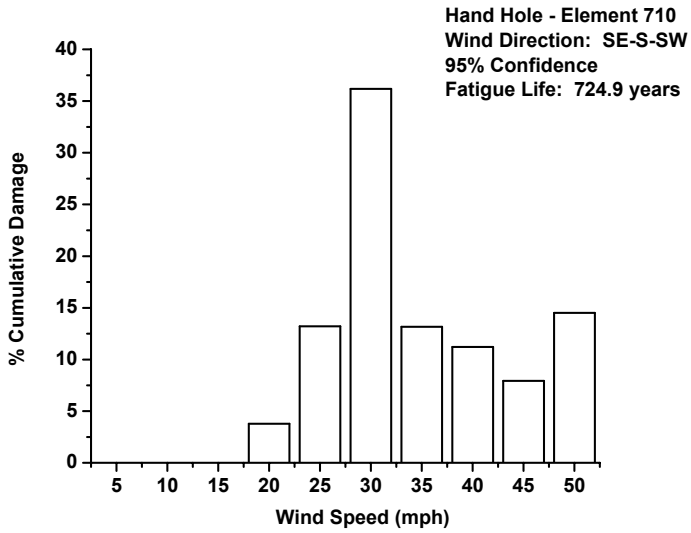

Figure 3.69: Fatigue Damage Accumulation at Hand-Hole Fillet Welds for HML-40-061 for Mean Wind Speeds Ranging from 5 to 50-mph.

The damage accumulation is very similar for all three components. One could likely surmise this given the response histories shown in Figures 3.64 through 3.66. The 95% confidence fatigue lives are very interesting. All three exceed the expected service life of 50 years (AASHTO 2001; Dexter and Ricker 2002). In fact, if the structure were to arrive in the field in "perfect" condition, there would be no inspection required during the structure's 50-year service life. This, of course, assumes that there is no

degradation (*e.g.* cross-section loss due to corrosion) during the service life. From the photographs shown in Figures 3.44 and 3.47, degradation certainly seems non-existent in this 2 year old structure. The anchor rods do have slight surface corrosion and this has been omitted in the analysis.

"Staged" loss of cross-section due to corrosion over yearly intervals could be included in revised fatigue life estimates. However, time limitations of the study did not allow for staged section loss assessments to be made and included in the fatigue life estimates. Furthermore, there appears to be very little information in the Literature regarding anchor bolt section loss in natural environments. It is expected that loss of cross-section due to corrosion will reduce the fatigue lives for the anchor rods from the 265 years currently estimated. However, the lengthy fatigue life computed without section loss does have "room" to allow for 200+ years to be expended through corrosion degradation (assuming a 50-year service life target).

A summary of the fatigue lives for these three critical components is given in Table 3.34. The fatigue lives listed in Figures 3.67 through 3.69 and in Table 3.34 correspond to 95% confidence levels. An infinite life is assigned to any component that has an expected fatigue life of 75 years or more. The position of the hand-hole dictated that winds from the Southeast, South, and Southwest should be considered in the fatigue-life estimate.

Table 3.34: Component Fatigue Life Estimates (years) for HML-40-061 for 95% Confidence Level.

Location (Element)	Wind Direction Span									Life (years)
	N	NE	E	SE	S	SW	W	NW	N	
Anchor Bolt							351.5			264 (Infinite)
					264.7					
	485.2									
			770.7							
Mast Base	168.6				102.1					102 (Infinite
			272.8				122.3			
Hand Hole				724.9						725 (Infinite)

Table 3.34 illustrates that the anchor bolts, mast base, and hand holes have essentially infinite fatigue life. Although other confidence levels could be computed, the minimum 95% confidence level (102 years) for the mast base suggests that the 70% and 50% confidence levels would not yield additional information useful for establishing inspection intervals.

The fatigue life study for HML-40-061 suggests that the mast base detail is the critical component that determines the fatigue life. The severe (E') category for this detail would suggest this as well. However, to the authors' knowledge there has never been a base plate to mast weld failure in these type of HML structures in Wisconsin. These failures have been experienced in other states, however. The 102-year fatigue life for this component should be tempered with the understanding that the mast-base-plate fillet weld detail has not been experimentally studied with anchor rod stand-off heights and base plate thicknesses typical of these types of structures. This research would significantly improve the fatigue life estimates.

The present analytical study for HML-40-061 indicates that if a "perfect" structure leaves the fabricating shop and is erected, the structure will easily meet its expected service life of 50 years. A properly executed galvanized coating will preserve the cross-section integrity and therefore, the analysis indicates that structures similar to HML-40-061 need not be inspected during their service lives. There is 95% confidence that the 102 year fatigue life will be achieved.

Loss of cross-sectional area resulting from corrosion will serve to move the mean stress during the response upward. However, it is expected that the stress range is not expected to change. Therefore, if one assumes that the mean stress does not affect the fatigue life (only the stress-range is important), it is expected that section loss due to corrosion will not impact the fatigue life, unless it reduces to a level that inelastic stress cycles are induced (this is unlikely).

3.3.2 Luminaire Support HML-67-006

This high-mast luminaire support structure studied is located in Menomonee Falls, Wisconsin. This structure, designated HML-67-006 is shown in Figure 3.70 and was erected in 1993. Shaft material has been specified as ASTM A-607 Grade 50 and the base plate material was specified as ASTM A-36. The hand-hole frame material was specified to be ASTM A-572 Grade 50. The threaded portions of the anchor rods were required to be "galvanized per ASTM A153 Class C" with a special note regarding over tapping. The anchor rod material was specified as AASHTO M314-90 Grade 55. Minimum CVN numbers for the material were also specified.

The structure is 150 feet tall and includes an 8 anchor rod arrangement at the base. There is an octagonal base plate (thickness 1-1/2 inches). The anchor rods were specified to be 2 inches in diameter. The mast was fabricated in four segments. The first segment was 43'-9" long, the second segment was 43'-3" long; the third was 35'-0" long; and the final segment was 35'-0" long. Slip (overlapping) splices were utilized between the segments.

(a) (b)

Figure 3.70: Luminaire Support Structure HML-67-006: (a) Full-Height View of Structure; (b) Detailed View of Base Plate and Anchor Rod Arrangement.

The splice overlaps ranged from 33 inches at the base, 27 inches at mid-mast-height, and 24 inches at the top splice. A reconnaissance visit was conducted to examine the condition of the mast and anchor rods. Photographs illustrating the anchor rod arrangement, mast to base plate welds, and hand-hole reinforcement welds are shown in Figure 3.71. This figure illustrates that the HML structure is in excellent condition. The galvanizing on the anchor rods is in good condition and the welding done on the structure is first-rate. This structure was put into service in 1993 and it has very little (if any) degradation during its nearly ten year service life (at the time the photos were taken).

The anchor rod pattern and welding details at critical locations in the HML structure are given in Figure 3.72. These were taken from WisDOT shop drawings for HML-67-006. As with HML-40-061 the mast to base plate connection is a full-penetration groove weld with back-up plate and reinforcing fillet weld. A similar detail exists for the hand-hole reinforcing plate. From Figure 3.71, it can be seen that the anchor rod stand off height (below the leveling nut) is much smaller than the diameter of the anchor rod. This will allow bending stresses to be omitted in the fatigue computations (Dexter and Ricker 2002).

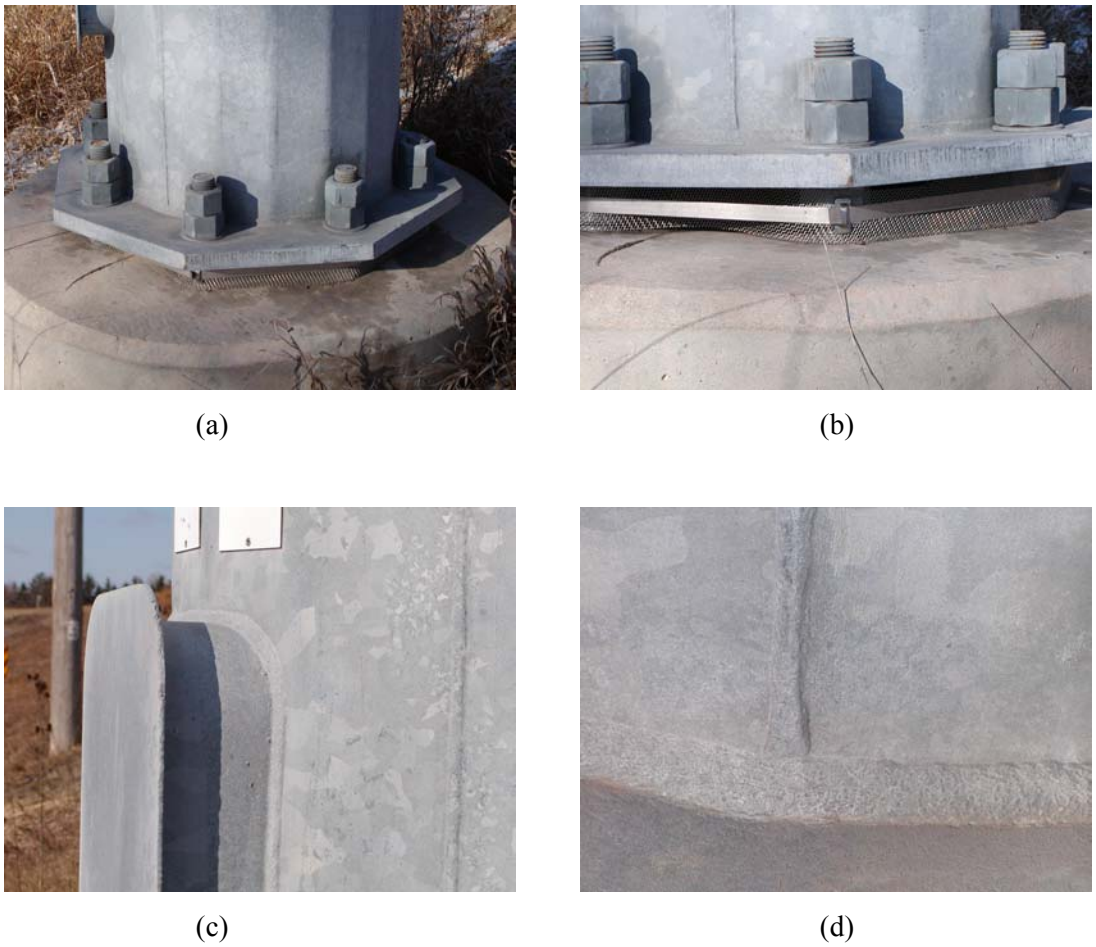

(a) (b)

(c) (d)

Figure 3.71: Critical Details for HML-67-006: (a) Anchor Rod Arrangement; (b) Stand-Off Height; (c) Hand-Hole Reinforcing Plate; (d) Mast-to-Base Plate Weld.

The first two mast segments were spliced in the shop using full-penetration groove welds with back-up plates. The first mast segment had a wall thickness of 5/16 inches and had an outer diameter tapering from 27.5 inches at the base to 21.22 inches at the top over the 43'-9" length. The second segment had a wall thickness of 5/16 inches and tapered from 22.42 inches at the base to 16.21 inches at the top. The third segment tapered from 17.21 inches at the base to 12.18 inches at the top. The final mast segment tapered from 13.03 inches at the base to 8.0 inches at the top. The wall thicknesses for the top two segments were 0.25 inches.

There are 6 luminaires in the lighting assembly for the structure. It was assumed that the lighting assembly weighed 910 pounds. This equated to a concentrated mass at the top of the FEA model of $2.36\, lb \cdot s^2/in$.

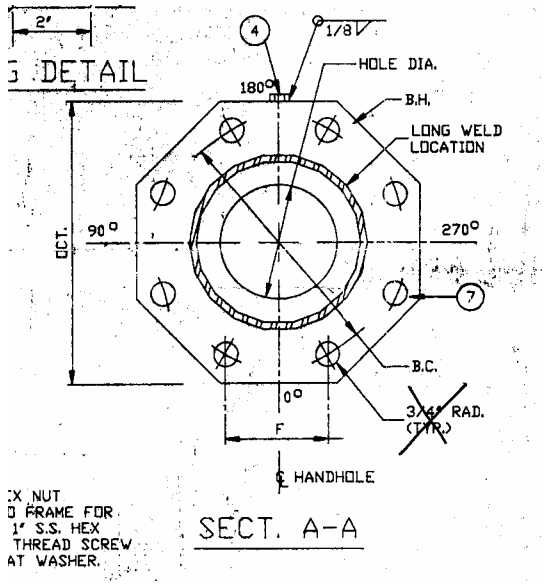

(a)

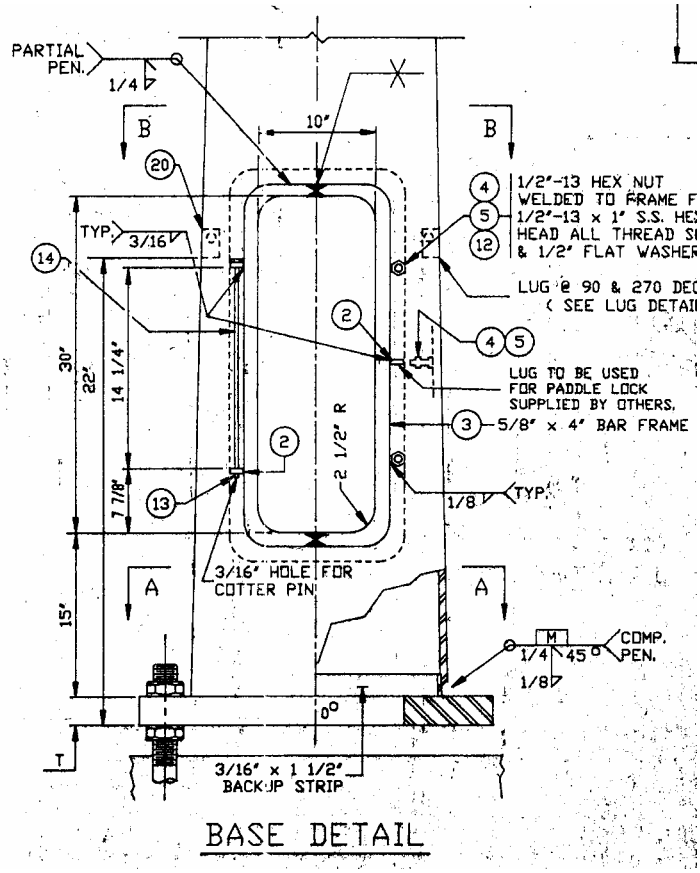

(b)

Figure 3.72: Excerpts from Shop Drawings for HML-67-006: (a) Anchor Rod Pattern; and (b) Welding Details at Critical Components.

3.3.2.1 Finite Element (FE) Modeling

The finite element modeling for HML-67-006 was conducted in much the same way as HML-40-061. An overall schematic of the model is shown in Figure 3.73.

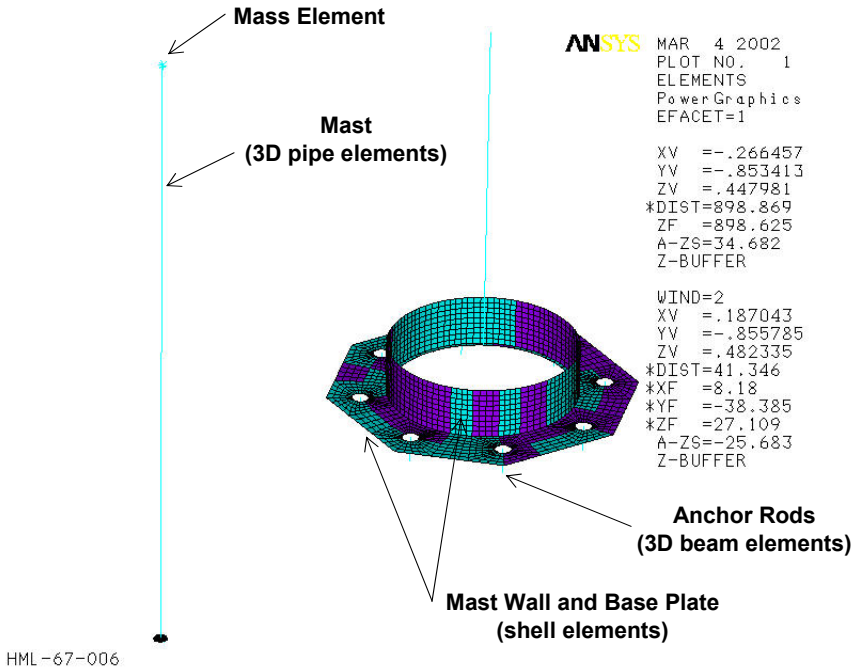

Figure 3.73: Schematic of Finite Element Model for HML-67-006.

The same finite elements were used for this structure as were used in the analysis of HML-40-061. The 18-sided mast was modeled as an equivalent circular cross-section. The 3D beam elements were again "married" to the shell elements using the concept of rigid regions. The rigid region modeling and support conditions on the anchor rods are shown in Figure 3.74.

The stand-off height assumed for the anchor rods was 3.5 inches to the bottom of the base plate. From Figures 3.71, it appears that this may be too large. However, given the 8 anchor arrangement, this was expected to affect the axial loading in the anchors by an insignificant amount. The FE model assumed the cross-sectional area was based upon full (gross) cross-sectional properties, while the stresses used in the fatigue life estimation were based upon the "stress areas" for the 2 inch diameter (8 UNC Coarse Thread) anchor rod (Dexter and Ricker 2002).

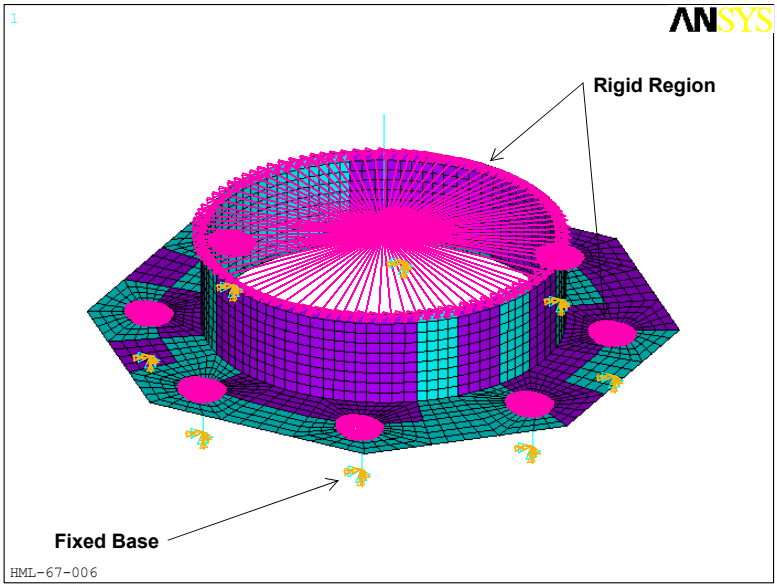

Figure 3.74: Rigid Region Modeling for HML-67-006.

3.3.2.2 General Finite Element (FE) Model Evaluations

A general FE analysis was undertaken with concentrated loading of 1,000 lbs applied at the top of the HML mast. This analysis was geared toward quantifying any stress raisers that result from the anchor rod stand off height. The vibration characteristics of the structure were also desired.

The first analysis conducted placed a 1,000 pound (resultant in some cases) loading at the top of the HML mast. This was done using three scenarios: (a) loading perpendicular to two anchor rods on one side; and (b) loading applied parallel to diagonal line through opposing anchor rods in the arrangement. The stress contours in the mast wall and the deformed shape of the base plate for the three loading conditions considered are shown in Figures 3.75 and 3.76. There appears to be a lack of stress raiser resulting from anchor rod pattern that was present in HML-40-061. The peak stress in the mast wall is independent of loading direction for all intents and purposes. This makes the analysis for the response under natural wind much easier to carry out.

The variation in shell element membrane stress (stress in the mast wall) with height above the centerline of the base plate is shown in Figure 3.77. This figure confirms that a stress concentration (raiser) does not exist in the mast wall for this anchor rod arrangement. Therefore, it certainly appears that the 8 anchor arrangement is closest to the fixed base condition and is a good candidate for HML structures. Furthermore, since the stress raiser is not present, the bending stresses in the mast do not need to be increased to account for the increased stress using stress concentration factors (as with HML-40-

061). Finally, if one would require the mast wall stresses for design, one could certainly use a fixed base analysis for this structure.

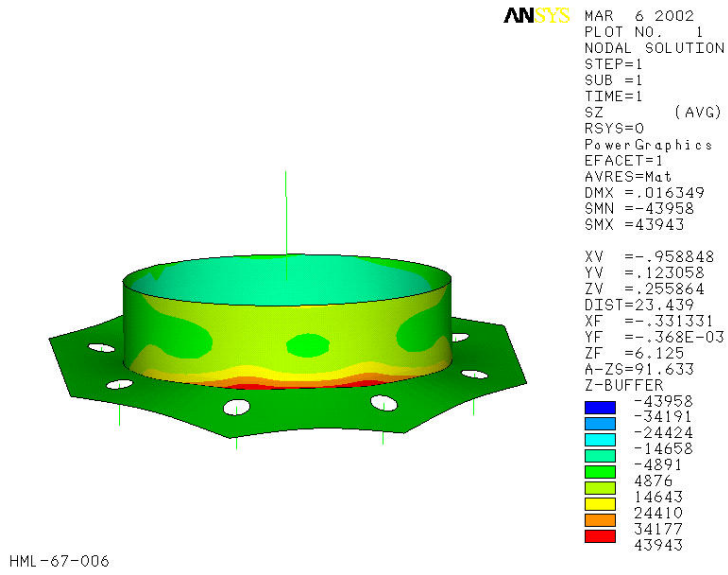

Figure 3.75: Stress Contour (SZ-direction tension face) for Concentrated Loading with the Following Magnitudes and Directions at Tip of the Mast: $F_x = 1{,}000\ lbs$ and also $F_x = F_y = 707.2\ lbs$.

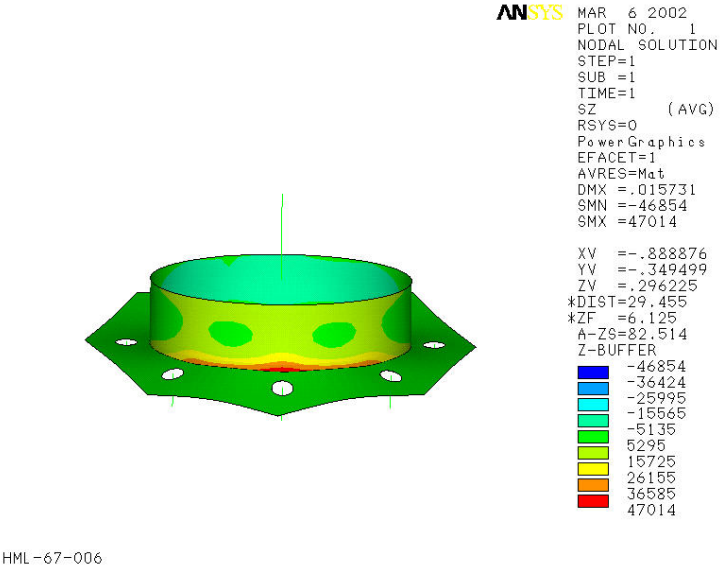

Figure 3.76: Stress Contour (SZ-direction compression face) for Concentrated Loading Combination of $F_x = 923.8\ lbs$ and $F_y = 382.8\ lbs$ at Tip of Mast.

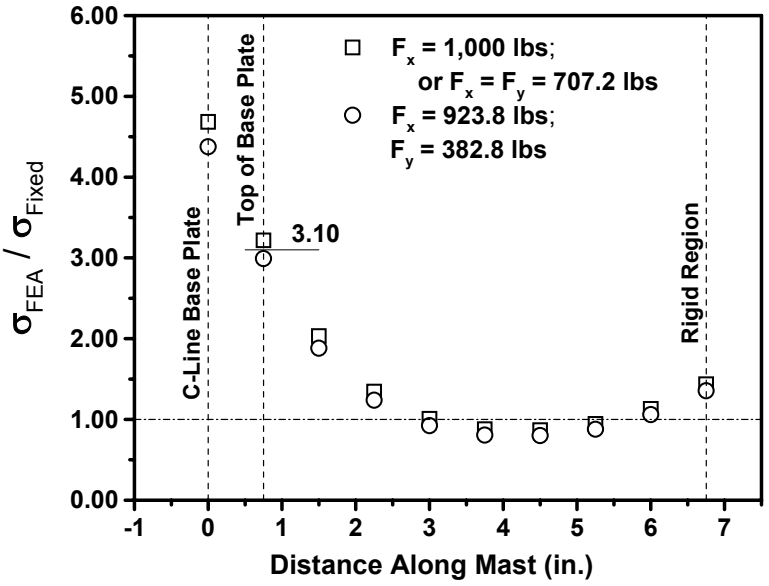

Figure 3.77: Normalized Bending Stress at Extreme Fiber in Mast. (Distance is measured from centerline of base plate to centerline of rigid region.)

Evaluating the susceptibility of the structure to vortex-shedding induced vibrations requires that the natural frequencies of vibration be quantified. Furthermore, understanding how the natural frequencies for all important modes of vibration vary with base plate thickness is important as well. Table 3.35 contains natural frequencies computed from modal analysis of HML-67-006 for three base plate thicknesses. From the analysis of HML-40-061 and the results shown in Figure 3.77, it appears that the 1-1/2 base plate is very close to the fixed base condition. Increasing or decreasing the base plate thickness does not affect the first 7 modal frequencies appreciably. There appears to be more sensitivity in the eighth mode of vibration. Therefore, susceptibility to aeroelastic instability can certainly be done assuming a fixed base condition.

3.3.2.3 Vortex Shedding Susceptibility

The susceptibility of HML-67-006 to aeroelastic instability (specifically vortex shedding) can be evaluated using the same procedure as that for HML-40-061. Tables 3.36 through 3.39 contain the necessary data to quantify the susceptibility of this structure to vortex shedding.

Table 3.38 illustrates that the segments of mast over which vortices are likely to form in regularly shed patterns are significant at wind speeds of 5 mph and 10 mph. However, these wind speeds cannot generate pressures that are of sufficient magnitude to "drive" large deformations of the mast thereby creating large enough stresses to cause damage. At wind speeds greater than 10 mph, there are no

locations along the mast where vortices are likely to be shed in regular patterns. In the regions where regularly shed vortices are likely to form (*i.e.* the shaded regions in Table 3.38), there is only a 34 foot segment in the 5 mph mean wind speed range where both the Reynolds number is conducive to lock in and a natural frequency of vibration for the HML falls within the lower and upper bounds. Therefore, the 5 mph wind is not capable of generating damaging stress ranges. The remaining locations along the HML mast do not have Reynolds numbers conducive to lock-in.

The present study provides evidence to support the omission of vortex shedding as a consideration in design for structures similar in configuration to HML-67-006. This recommendation has informal experimental support. The senior author visited HML-67-006 on a Sunday when 30-40 mph (peak) gusts were measured at General Mitchell Field. The displaced shape of the HML structure on this day is shown in Figure 3.78. This photograph is also shown with perspective lines in Figure 3.60.

The response during these winds was exclusively in the along-wind direction (using the naked eye and zoom lens of digital camera). The luminaire assembly simply oscillated back and forth in the along-wind direction never crossing back over the "neutral position". The turbulent wind simply "pushed" the assembly in oscillating fashion to one side of the vertical (first-mode dominant behavior). This response will be referenced again when the stresses in the structure are discussed.

Table 3.35: Variation in Natural Frequencies for Dominate Modes of Vibration with Base Plate Thickness Variation for HML-67-006.

Vibration Mode	Vibration Frequency (Hz)		
	3/4" Base Plate	1-1/2" Base Plate	3" Base Plate
1	0.293	0.297	0.300
2	1.118	1.139	1.155
3	2.982	3.036	3.079
4	5.905	6.007	6.092
5	9.819	9.966	10.095
6	14.793	14.993	15.179
7	20.843	21.093	21.335
8	27.880	28.184	28.491

Table 3.36: Wind Speeds at Various Elevations for HML-67-006 as a Function of Reference Height Wind Speeds.

	Outside	Average	Wall		H	V (ft/s) at H									
Level (in.)	Diameter	Diameter	Thickness	Kin. Vis	(ft)	5 mph	10 mph	15 mph	20 mph	25 mph	30 mph	35 mph	40 mph	45 mph	50 mph
6.75	27.4280	27.3740	0.3125	1.615E-04	0.94	4.4	8.8	13.2	17.6	22.0	26.5	30.9	35.3	39.7	44.1
15.75	27.3200	27.1400	0.3125	1.615E-04	2.56	5.1	10.2	15.3	20.4	25.5	30.5	35.6	40.7	45.8	50.9
45.75	26.9600	26.7365	0.3125	1.615E-04	5.36	5.7	11.3	17.0	22.6	28.3	33.9	39.6	45.3	50.9	56.6
83.00	26.5130	26.2895	0.3125	1.615E-04	8.47	6.0	12.1	18.1	24.2	30.2	36.2	42.3	48.3	54.3	60.4
120.25	26.0660	25.8425	0.3125	1.615E-04	11.57	6.3	12.6	18.9	25.3	31.6	37.9	44.2	50.5	56.8	63.1
157.50	25.6190	25.3955	0.3125	1.615E-04	14.68	6.5	13.1	19.6	26.1	32.7	39.2	45.7	52.3	58.8	65.3
194.75	25.1720	24.9485	0.3125	1.615E-04	17.78	6.7	13.4	20.1	26.9	33.6	40.3	47.0	53.7	60.4	67.1
232.00	24.7250	24.5015	0.3125	1.615E-04	20.89	6.9	13.7	20.6	27.5	34.3	41.2	48.1	55.0	61.8	68.7
269.25	24.2780	24.0545	0.3125	1.615E-04	23.99	7.0	14.0	21.0	28.0	35.0	42.0	49.0	56.1	63.1	70.1
306.50	23.8310	23.6075	0.3125	1.615E-04	27.09	7.1	14.3	21.4	28.5	35.6	42.8	49.9	57.0	64.2	71.3
343.75	23.3840	23.1605	0.3125	1.615E-04	30.20	7.2	14.5	21.7	29.0	36.2	43.4	50.7	57.9	65.2	72.4
381.00	22.9370	22.7135	0.3125	1.615E-04	33.30	7.3	14.7	22.0	29.4	36.7	44.1	51.4	58.7	66.1	73.4
418.25	22.4900	22.2665	0.3125	1.615E-04	36.41	7.4	14.9	22.3	29.7	37.2	44.6	52.1	59.5	66.9	74.4
455.50	22.0430	22.0335	0.3125	1.615E-04	39.51	7.5	15.0	22.6	30.1	37.6	45.1	52.7	60.2	67.7	75.2
492.75	22.0240	22.0240	0.3125	1.615E-04	42.44	7.6	15.2	22.8	30.4	38.0	45.6	53.2	60.8	68.4	76.0
525.75	22.0240	21.8121	0.3125	1.615E-04	45.28	7.7	15.3	23.0	30.7	38.4	46.0	53.7	61.4	69.1	76.7
561.06	21.6003	21.3884	0.3125	1.615E-04	48.23	7.7	15.5	23.2	31.0	38.7	46.5	54.2	61.9	69.7	77.4
596.37	21.1766	20.9648	0.3125	1.615E-04	51.17	7.8	15.6	23.4	31.2	39.0	46.8	54.7	62.5	70.3	78.1
631.67	20.7530	20.5411	0.3125	1.615E-04	54.11	7.9	15.7	23.6	31.5	39.4	47.2	55.1	63.0	70.8	78.7
666.98	20.3292	20.1174	0.3125	1.615E-04	57.05	7.9	15.9	23.8	31.7	39.6	47.6	55.5	63.4	71.4	79.3
702.29	19.9055	19.6937	0.3125	1.615E-04	60.00	8.0	16.0	24.0	31.9	39.9	47.9	55.9	63.9	71.9	79.9
737.60	19.4818	19.2700	0.3125	1.615E-04	62.94	8.0	16.1	24.1	32.2	40.2	48.3	56.3	64.3	72.4	80.4
772.90	19.0582	18.8463	0.3125	1.615E-04	65.88	8.1	16.2	24.3	32.4	40.5	48.6	56.7	64.8	72.9	80.9
808.21	18.6345	18.4226	0.3125	1.615E-04	68.82	8.1	16.3	24.4	32.6	40.7	48.9	57.0	65.2	73.3	81.5
843.52	18.2108	17.9989	0.3125	1.615E-04	71.76	8.2	16.4	24.6	32.8	41.0	49.2	57.4	65.6	73.7	81.9
878.83	17.7870	17.5752	0.3125	1.615E-04	74.71	8.2	16.5	24.7	33.0	41.2	49.4	57.7	65.9	74.2	82.4
914.13	17.3634	17.1516	0.3125	1.615E-04	77.65	8.3	16.6	24.9	33.1	41.4	49.7	58.0	66.3	74.6	82.9
949.44	16.9397	16.9132	0.3125	1.615E-04	80.59	8.3	16.7	25.0	33.3	41.7	50.0	58.3	66.6	75.0	83.3
984.75	16.8866	16.8866	0.3125	1.615E-04	83.19	8.4	16.7	25.1	33.5	41.8	50.2	58.6	67.0	75.3	83.7
1011.75	16.8866	16.6853	0.25	1.615E-04	85.71	8.4	16.8	25.2	33.6	42.0	50.4	58.8	67.2	75.6	84.0
1045.30	16.4840	16.2828	0.25	1.615E-04	88.51	8.4	16.9	25.3	33.8	42.2	50.7	59.1	67.5	76.0	84.4
1078.84	16.0815	15.8802	0.25	1.615E-04	91.30	8.5	17.0	25.4	33.9	42.4	50.9	59.4	67.8	76.3	84.8
1112.39	15.6789	15.4777	0.25	1.615E-04	94.10	8.5	17.0	25.6	34.1	42.6	51.1	59.6	68.1	76.7	85.2
1145.93	15.2764	15.0751	0.25	1.615E-04	96.89	8.6	17.1	25.7	34.2	42.8	51.3	59.9	68.4	77.0	85.5
1179.48	14.8738	14.6726	0.25	1.615E-04	99.69	8.6	17.2	25.8	34.4	42.9	51.5	60.1	68.7	77.3	85.9
1213.02	14.4714	14.2701	0.25	1.615E-04	102.48	8.6	17.2	25.9	34.5	43.1	51.7	60.4	69.0	77.6	86.2
1246.57	14.0688	13.8675	0.25	1.615E-04	105.28	8.7	17.3	26.0	34.6	43.3	51.9	60.6	69.2	77.9	86.6
1280.11	13.6663	13.4650	0.25	1.615E-04	108.07	8.7	17.4	26.1	34.8	43.4	52.1	60.8	69.5	78.2	86.9
1313.66	13.2637	13.0624	0.25	1.615E-04	110.87	8.7	17.4	26.2	34.9	43.6	52.3	61.0	69.8	78.5	87.2
1347.20	12.8612	12.8006	0.25	1.615E-04	113.66	8.8	17.5	26.3	35.0	43.8	52.5	61.3	70.0	78.8	87.5
1380.75	12.7400	12.7400	0.25	1.615E-04	116.06	8.8	17.6	26.3	35.1	43.9	52.7	61.4	70.2	79.0	87.8
1404.75	12.7400	12.5423	0.1875	1.615E-04	118.44	8.8	17.6	26.4	35.2	44.0	52.8	61.6	70.4	79.2	88.0
1437.75	12.3447	12.1470	0.1875	1.615E-04	121.19	8.8	17.7	26.5	35.3	44.2	53.0	61.8	70.6	79.5	88.3
1470.75	11.9493	11.7517	0.1875	1.615E-04	123.94	8.9	17.7	26.6	35.4	44.3	53.2	62.0	70.9	79.7	88.6
1503.75	11.5540	11.3563	0.1875	1.615E-04	126.69	8.9	17.8	26.7	35.5	44.4	53.3	62.2	71.1	80.0	88.9
1536.75	11.1586	10.9610	0.1875	1.615E-04	129.44	8.9	17.8	26.7	35.7	44.6	53.5	62.4	71.3	80.2	89.1
1569.75	10.7633	10.5656	0.1875	1.615E-04	132.19	8.9	17.9	26.8	35.8	44.7	53.6	62.6	71.5	80.5	89.4
1602.75	10.3680	10.1703	0.1875	1.615E-04	134.94	9.0	17.9	26.9	35.9	44.8	53.8	62.8	71.7	80.7	89.7
1635.75	9.9726	9.7750	0.1875	1.615E-04	137.69	9.0	18.0	27.0	36.0	45.0	54.0	63.0	71.9	80.9	89.9
1668.75	9.5773	9.3796	0.1875	1.615E-04	140.44	9.0	18.0	27.1	36.1	45.1	54.1	63.1	72.2	81.2	90.2
1701.75	9.1819	8.9843	0.1875	1.615E-04	143.19	9.0	18.1	27.1	36.2	45.2	54.3	63.3	72.4	81.4	90.4
1734.75	8.7866	8.5889	0.1875	1.615E-04	145.94	9.1	18.1	27.2	36.3	45.3	54.4	63.5	72.5	81.6	90.7
1767.75	8.3913	8.1936	0.1875	1.615E-04	148.69	9.1	18.2	27.3	36.4	45.5	54.6	63.6	72.7	81.8	90.9
1800.75	7.9959														

Table 3.37: Frequencies of Vortex Shedding at Various Elevations for HML-67-006 as a Function of Reference Height Wind Speeds.

Level (in.)	Outside Diameter	Average Diameter	Wall Thickness	Kin. Vis	H (ft)	n_s (Hz) 5 mph	10 mph	15 mph	20 mph	25 mph	30 mph	35 mph	40 mph	45 mph	50 mph
6.75	27.4280	27.3740	0.3125	1.615E-04	0.94	0.39	0.77	1.16	1.55	1.93	2.32	2.71	3.09	3.48	3.87
15.75	27.3200	27.1400	0.3125	1.615E-04	2.56	0.45	0.90	1.35	1.80	2.25	2.70	3.15	3.60	4.05	4.50
45.75	26.9600	26.7365	0.3125	1.615E-04	5.36	0.51	1.02	1.52	2.03	2.54	3.05	3.55	4.06	4.57	5.08
83.00	26.5130	26.2895	0.3125	1.615E-04	8.47	0.55	1.10	1.65	2.20	2.76	3.31	3.86	4.41	4.96	5.51
120.25	26.0660	25.8425	0.3125	1.615E-04	11.57	0.59	1.17	1.76	2.35	2.93	3.52	4.10	4.69	5.28	5.86
157.50	25.6190	25.3955	0.3125	1.615E-04	14.68	0.62	1.23	1.85	2.47	3.09	3.70	4.32	4.94	5.56	6.17
194.75	25.1720	24.9485	0.3125	1.615E-04	17.78	0.65	1.29	1.94	2.58	3.23	3.87	4.52	5.17	5.81	6.46
232.00	24.7250	24.5015	0.3125	1.615E-04	20.89	0.67	1.35	2.02	2.69	3.36	4.04	4.71	5.38	6.06	6.73
269.25	24.2780	24.0545	0.3125	1.615E-04	23.99	0.70	1.40	2.10	2.80	3.50	4.19	4.89	5.59	6.29	6.99
306.50	23.8310	23.6075	0.3125	1.615E-04	27.09	0.72	1.45	2.17	2.90	3.62	4.35	5.07	5.80	6.52	7.25
343.75	23.3840	23.1605	0.3125	1.615E-04	30.20	0.75	1.50	2.25	3.00	3.75	4.50	5.25	6.00	6.75	7.50
381.00	22.9370	22.7135	0.3125	1.615E-04	33.30	0.78	1.55	2.33	3.10	3.88	4.66	5.43	6.21	6.98	7.76
418.25	22.4900	22.2665	0.3125	1.615E-04	36.41	0.80	1.60	2.40	3.21	4.01	4.81	5.61	6.41	7.21	8.02
455.50	22.0430	22.0335	0.3125	1.615E-04	39.51	0.82	1.64	2.46	3.28	4.10	4.92	5.74	6.56	7.38	8.20
492.75	22.0240	22.0240	0.3125	1.615E-04	42.44	0.83	1.66	2.49	3.31	4.14	4.97	5.80	6.63	7.46	8.28
525.75	22.0240	21.8121	0.3125	1.615E-04	45.28	0.84	1.69	2.53	3.38	4.22	5.07	5.91	6.75	7.60	8.44
561.06	21.6003	21.3884	0.3125	1.615E-04	48.23	0.87	1.74	2.61	3.47	4.34	5.21	6.08	6.95	7.82	8.69
596.37	21.1766	20.9648	0.3125	1.615E-04	51.17	0.89	1.79	2.68	3.58	4.47	5.36	6.26	7.15	8.04	8.94
631.67	20.7530	20.5411	0.3125	1.615E-04	54.11	0.92	1.84	2.76	3.68	4.60	5.52	6.44	7.36	8.28	9.20
666.98	20.3292	20.1174	0.3125	1.615E-04	57.05	0.95	1.89	2.84	3.78	4.73	5.68	6.62	7.57	8.51	9.46
702.29	19.9055	19.6937	0.3125	1.615E-04	60.00	0.97	1.95	2.92	3.89	4.87	5.84	6.81	7.79	8.76	9.73
737.60	19.4818	19.2700	0.3125	1.615E-04	62.94	1.00	2.00	3.00	4.01	5.01	6.01	7.01	8.01	9.01	10.02
772.90	19.0582	18.8463	0.3125	1.615E-04	65.88	1.03	2.06	3.09	4.12	5.15	6.18	7.22	8.25	9.28	10.31
808.21	18.6345	18.4226	0.3125	1.615E-04	68.82	1.06	2.12	3.18	4.24	5.31	6.37	7.43	8.49	9.55	10.61
843.52	18.2108	17.9989	0.3125	1.615E-04	71.76	1.09	2.19	3.28	4.37	5.46	6.56	7.65	8.74	9.83	10.93
878.83	17.7870	17.5752	0.3125	1.615E-04	74.71	1.13	2.25	3.38	4.50	5.63	6.75	7.88	9.00	10.13	11.25
914.13	17.3634	17.1516	0.3125	1.615E-04	77.65	1.16	2.32	3.48	4.64	5.80	6.96	8.12	9.28	10.44	11.60
949.44	16.9397	16.9132	0.3125	1.615E-04	80.59	1.18	2.36	3.55	4.73	5.91	7.09	8.28	9.46	10.64	11.82
984.75	16.8866	16.8866	0.3125	1.615E-04	83.19	1.19	2.38	3.57	4.76	5.95	7.14	8.33	9.52	10.70	11.89
1011.75	16.8866	16.6853	0.25	1.615E-04	85.71	1.21	2.42	3.63	4.84	6.04	7.25	8.46	9.67	10.88	12.09
1045.30	16.4840	16.2828	0.25	1.615E-04	88.51	1.24	2.49	3.73	4.98	6.22	7.47	8.71	9.96	11.20	12.44
1078.84	16.0815	15.8802	0.25	1.615E-04	91.30	1.28	2.56	3.85	5.13	6.41	7.69	8.97	10.25	11.54	12.82
1112.39	15.6789	15.4777	0.25	1.615E-04	94.10	1.32	2.64	3.96	5.28	6.60	7.92	9.25	10.57	11.89	13.21
1145.93	15.2764	15.0751	0.25	1.615E-04	96.89	1.36	2.72	4.09	5.45	6.81	8.17	9.53	10.89	12.26	13.62
1179.48	14.8738	14.6726	0.25	1.615E-04	99.69	1.40	2.81	4.21	5.62	7.02	8.43	9.83	11.24	12.64	14.05
1213.02	14.4714	14.2701	0.25	1.615E-04	102.48	1.45	2.90	4.35	5.80	7.25	8.70	10.15	11.60	13.05	14.50
1246.57	14.0688	13.8675	0.25	1.615E-04	105.28	1.50	3.00	4.49	5.99	7.49	8.99	10.49	11.98	13.48	14.98
1280.11	13.6663	13.4650	0.25	1.615E-04	108.07	1.55	3.10	4.65	6.19	7.74	9.29	10.84	12.39	13.94	15.48
1313.66	13.2637	13.0624	0.25	1.615E-04	110.87	1.60	3.20	4.81	6.41	8.01	9.61	11.21	12.82	14.42	16.02
1347.20	12.8612	12.8006	0.25	1.615E-04	113.66	1.64	3.28	4.92	6.56	8.20	9.84	11.48	13.13	14.77	16.41
1380.75	12.7400	12.7400	0.25	1.615E-04	116.06	1.65	3.31	4.96	6.61	8.27	9.92	11.57	13.23	14.88	16.53
1404.75	12.7400	12.5423	0.1875	1.615E-04	118.44	1.68	3.37	5.05	6.74	8.42	10.11	11.79	13.47	15.16	16.84
1437.75	12.3447	12.1470	0.1875	1.615E-04	121.19	1.74	3.49	5.23	6.98	8.72	10.47	12.21	13.96	15.70	17.45
1470.75	11.9493	11.7517	0.1875	1.615E-04	123.94	1.81	3.62	5.43	7.24	9.05	10.86	12.67	14.47	16.28	18.09
1503.75	11.5540	11.3563	0.1875	1.615E-04	126.69	1.88	3.76	5.63	7.51	9.39	11.27	13.15	15.03	16.90	18.78
1536.75	11.1586	10.9610	0.1875	1.615E-04	129.44	1.95	3.90	5.86	7.81	9.76	11.71	13.66	15.62	17.57	19.52
1569.75	10.7633	10.5656	0.1875	1.615E-04	132.19	2.03	4.06	6.09	8.12	10.16	12.19	14.22	16.25	18.28	20.31
1602.75	10.3680	10.1703	0.1875	1.615E-04	134.94	2.12	4.23	6.35	8.46	10.58	12.70	14.81	16.93	19.05	21.16
1635.75	9.9726	9.7750	0.1875	1.615E-04	137.69	2.21	4.42	6.62	8.83	11.04	13.25	15.46	17.67	19.87	22.08
1668.75	9.5773	9.3796	0.1875	1.615E-04	140.44	2.31	4.62	6.92	9.23	11.54	13.85	16.15	18.46	20.77	23.08
1701.75	9.1819	8.9843	0.1875	1.615E-04	143.19	2.42	4.83	7.25	9.66	12.08	14.50	16.91	19.33	21.74	24.16
1734.75	8.7866	8.5889	0.1875	1.615E-04	145.94	2.53	5.07	7.60	10.14	12.67	15.20	17.74	20.27	22.81	25.34
1767.75	8.3913	8.1936	0.1875	1.615E-04	148.69	2.66	5.33	7.99	10.65	13.32	15.98	18.64	21.31	23.97	26.63
1800.75	7.9959														

Table 3.38: Reynolds Numbers for Wind Flow at Various Elevations for HML-67-006 as a Function of Reference Height Wind Speeds.

Level (in.)	Outside Diameter	Average Diameter	Wall Thickness	Kin. Vis	H (ft)	Re									
						5 mph	10 mph	15 mph	20 mph	25 mph	30 mph	35 mph	40 mph	45 mph	50 mph
6.75	27.4280	27.3740	0.3125	1.615E-04	0.94	**6.23E+04**	1.25E+05	1.87E+05	2.49E+05	3.11E+05	3.74E+05	4.36E+05	4.98E+05	5.61E+05	6.23E+05
15.75	27.3200	27.1400	0.3125	1.615E-04	2.56	**7.13E+04**	1.43E+05	2.14E+05	2.85E+05	3.56E+05	4.28E+05	4.99E+05	5.70E+05	6.42E+05	7.13E+05
45.75	26.9600	26.7365	0.3125	1.615E-04	5.36	**7.80E+04**	1.56E+05	2.34E+05	3.12E+05	3.90E+05	4.68E+05	5.46E+05	6.24E+05	7.02E+05	7.80E+05
83.00	26.5130	26.2895	0.3125	1.615E-04	8.47	**8.19E+04**	1.64E+05	2.46E+05	3.28E+05	4.10E+05	4.91E+05	5.73E+05	6.55E+05	7.37E+05	8.19E+05
120.25	26.0660	25.8425	0.3125	1.615E-04	11.57	**8.42E+04**	1.68E+05	2.53E+05	3.37E+05	4.21E+05	5.05E+05	5.89E+05	6.74E+05	7.58E+05	8.42E+05
157.50	25.6190	25.3955	0.3125	1.615E-04	14.68	**8.56E+04**	1.71E+05	2.57E+05	3.42E+05	4.28E+05	5.14E+05	5.99E+05	6.85E+05	7.70E+05	8.56E+05
194.75	25.1720	24.9485	0.3125	1.615E-04	17.78	**8.64E+04**	1.73E+05	2.59E+05	3.46E+05	4.32E+05	5.19E+05	6.05E+05	6.91E+05	7.78E+05	8.64E+05
232.00	24.7250	24.5015	0.3125	1.615E-04	20.89	**8.68E+04**	1.74E+05	2.61E+05	3.47E+05	4.34E+05	5.21E+05	6.08E+05	6.95E+05	7.82E+05	8.68E+05
269.25	24.2780	24.0545	0.3125	1.615E-04	23.99	**8.70E+04**	1.74E+05	2.61E+05	3.48E+05	4.35E+05	5.22E+05	6.09E+05	6.96E+05	7.83E+05	8.70E+05
306.50	23.8310	23.6075	0.3125	1.615E-04	27.09	**8.68E+04**	1.74E+05	2.61E+05	3.47E+05	4.34E+05	5.21E+05	6.08E+05	6.95E+05	7.82E+05	8.68E+05
343.75	23.3840	23.1605	0.3125	1.615E-04	30.20	**8.65E+04**	1.73E+05	2.60E+05	3.46E+05	4.33E+05	5.19E+05	6.06E+05	6.92E+05	7.79E+05	8.65E+05
381.00	22.9370	22.7135	0.3125	1.615E-04	33.30	**8.61E+04**	1.72E+05	2.58E+05	3.44E+05	4.30E+05	5.16E+05	6.02E+05	6.88E+05	7.75E+05	8.61E+05
418.25	22.4900	22.2665	0.3125	1.615E-04	36.41	**8.54E+04**	1.71E+05	2.56E+05	3.42E+05	4.27E+05	5.13E+05	5.98E+05	6.84E+05	7.69E+05	8.54E+05
455.50	22.0430	22.0335	0.3125	1.615E-04	39.51	**8.55E+04**	1.71E+05	2.57E+05	3.42E+05	4.28E+05	5.13E+05	5.99E+05	6.84E+05	7.70E+05	8.55E+05
492.75	22.0240	22.0240	0.3125	1.615E-04	42.44	**8.64E+04**	1.73E+05	2.59E+05	3.46E+05	4.32E+05	5.18E+05	6.05E+05	6.91E+05	7.77E+05	8.64E+05
525.75	22.0240	21.8121	0.3125	1.615E-04	45.28	**8.64E+04**	1.73E+05	2.59E+05	3.45E+05	4.32E+05	5.18E+05	6.04E+05	6.91E+05	7.77E+05	8.64E+05
561.06	21.6003	21.3884	0.3125	1.615E-04	48.23	**8.54E+04**	1.71E+05	2.56E+05	3.42E+05	4.27E+05	5.13E+05	5.98E+05	6.84E+05	7.69E+05	8.54E+05
596.37	21.1766	20.9648	0.3125	1.615E-04	51.17	**8.45E+04**	1.69E+05	2.53E+05	3.38E+05	4.22E+05	5.07E+05	5.91E+05	6.76E+05	7.60E+05	8.45E+05
631.67	20.7530	20.5411	0.3125	1.615E-04	54.11	**8.34E+04**	1.67E+05	2.50E+05	3.34E+05	4.17E+05	5.00E+05	5.84E+05	6.67E+05	7.51E+05	8.34E+05
666.98	20.3292	20.1174	0.3125	1.615E-04	57.05	**8.23E+04**	1.65E+05	2.47E+05	3.29E+05	4.12E+05	4.94E+05	5.76E+05	6.59E+05	7.41E+05	8.23E+05
702.29	19.9055	19.6937	0.3125	1.615E-04	60.00	**8.12E+04**	1.62E+05	2.43E+05	3.25E+05	4.06E+05	4.87E+05	5.68E+05	6.49E+05	7.30E+05	8.12E+05
737.60	19.4818	19.2700	0.3125	1.615E-04	62.94	**8.00E+04**	1.60E+05	2.40E+05	3.20E+05	4.00E+05	4.80E+05	5.60E+05	6.40E+05	7.20E+05	8.00E+05
772.90	19.0582	18.8463	0.3125	1.615E-04	65.88	**7.87E+04**	1.57E+05	2.36E+05	3.15E+05	3.94E+05	4.72E+05	5.51E+05	6.30E+05	7.08E+05	7.87E+05
808.21	18.6345	18.4226	0.3125	1.615E-04	68.82	**7.74E+04**	1.55E+05	2.32E+05	3.10E+05	3.87E+05	4.65E+05	5.42E+05	6.19E+05	6.97E+05	7.74E+05
843.52	18.2108	17.9989	0.3125	1.615E-04	71.76	**7.61E+04**	1.52E+05	2.28E+05	3.04E+05	3.81E+05	4.57E+05	5.33E+05	6.09E+05	6.85E+05	7.61E+05
878.83	17.7870	17.5752	0.3125	1.615E-04	74.71	**7.47E+04**	1.49E+05	2.24E+05	2.99E+05	3.74E+05	4.48E+05	5.23E+05	5.98E+05	6.73E+05	7.47E+05
914.13	17.3634	17.1516	0.3125	1.615E-04	77.65	**7.33E+04**	1.47E+05	2.20E+05	2.93E+05	3.67E+05	4.40E+05	5.13E+05	5.87E+05	6.60E+05	7.33E+05
949.44	16.9397	16.9132	0.3125	1.615E-04	80.59	**7.27E+04**	1.45E+05	2.18E+05	2.91E+05	3.64E+05	4.36E+05	5.09E+05	5.82E+05	6.54E+05	7.27E+05
984.75	16.8866	16.8866	0.3125	1.615E-04	83.19	**7.29E+04**	1.46E+05	2.19E+05	2.92E+05	3.65E+05	4.38E+05	5.10E+05	5.83E+05	6.56E+05	7.29E+05
1011.75	16.8866	16.6853	0.25	1.615E-04	85.71	**7.24E+04**	1.45E+05	2.17E+05	2.89E+05	3.62E+05	4.34E+05	5.07E+05	5.79E+05	6.51E+05	7.24E+05
1045.30	16.4840	16.2828	0.25	1.615E-04	88.51	**7.09E+04**	1.42E+05	2.13E+05	2.84E+05	3.55E+05	4.26E+05	4.97E+05	5.68E+05	6.38E+05	7.09E+05
1078.84	16.0815	15.8802	0.25	1.615E-04	91.30	**6.95E+04**	1.39E+05	2.08E+05	2.78E+05	3.47E+05	4.17E+05	4.86E+05	5.56E+05	6.25E+05	6.95E+05
1112.39	15.6789	15.4777	0.25	1.615E-04	94.10	**6.80E+04**	1.36E+05	2.04E+05	2.72E+05	3.40E+05	4.08E+05	4.76E+05	5.44E+05	6.12E+05	6.80E+05
1145.93	15.2764	15.0751	0.25	1.615E-04	96.89	**6.65E+04**	1.33E+05	2.00E+05	2.66E+05	3.33E+05	3.99E+05	4.66E+05	5.32E+05	5.99E+05	6.65E+05
1179.48	14.8738	14.6726	0.25	1.615E-04	99.69	**6.50E+04**	1.30E+05	1.95E+05	2.60E+05	3.25E+05	3.90E+05	4.55E+05	5.20E+05	5.85E+05	6.50E+05
1213.02	14.4714	14.2701	0.25	1.615E-04	102.48	**6.35E+04**	1.27E+05	1.90E+05	2.54E+05	3.17E+05	3.81E+05	4.44E+05	5.08E+05	5.71E+05	6.35E+05
1246.57	14.0688	13.8675	0.25	1.615E-04	105.28	**6.19E+04**	1.24E+05	1.86E+05	2.48E+05	3.10E+05	3.72E+05	4.34E+05	4.95E+05	5.57E+05	6.19E+05
1280.11	13.6663	13.4650	0.25	1.615E-04	108.07	**6.04E+04**	1.21E+05	1.81E+05	2.41E+05	3.02E+05	3.62E+05	4.23E+05	4.83E+05	5.43E+05	6.04E+05
1313.66	13.2637	13.0624	0.25	1.615E-04	110.87	**5.88E+04**	1.18E+05	1.76E+05	2.35E+05	2.94E+05	3.53E+05	4.11E+05	4.70E+05	5.29E+05	5.88E+05
1347.20	12.8612	12.8006	0.25	1.615E-04	113.66	**5.78E+04**	1.16E+05	1.73E+05	2.31E+05	2.89E+05	3.47E+05	4.05E+05	4.62E+05	5.20E+05	5.78E+05
1380.75	12.7400	12.7400	0.25	1.615E-04	116.06	**5.77E+04**	1.15E+05	1.73E+05	2.31E+05	2.88E+05	3.46E+05	4.04E+05	4.62E+05	5.19E+05	5.77E+05
1404.75	12.7400	12.5423	0.1875	1.615E-04	118.44	**5.70E+04**	1.14E+05	1.71E+05	2.28E+05	2.85E+05	3.42E+05	3.99E+05	4.56E+05	5.13E+05	5.70E+05
1437.75	12.3447	12.1470	0.1875	1.615E-04	121.19	**5.54E+04**	1.11E+05	1.66E+05	2.21E+05	2.77E+05	3.32E+05	3.87E+05	4.43E+05	4.98E+05	5.54E+05
1470.75	11.9493	11.7517	0.1875	1.615E-04	123.94	**5.37E+04**	1.07E+05	1.61E+05	2.15E+05	2.69E+05	3.22E+05	3.76E+05	4.30E+05	4.83E+05	5.37E+05
1503.75	11.5540	11.3563	0.1875	1.615E-04	126.69	**5.21E+04**	1.04E+05	1.56E+05	2.08E+05	2.60E+05	3.12E+05	3.65E+05	4.17E+05	4.69E+05	5.21E+05
1536.75	11.1586	10.9610	0.1875	1.615E-04	129.44	**5.04E+04**	1.01E+05	1.51E+05	2.02E+05	2.52E+05	3.03E+05	3.53E+05	4.03E+05	4.54E+05	5.04E+05
1569.75	10.7633	10.5656	0.1875	1.615E-04	132.19	**4.87E+04**	**9.75E+04**	1.46E+05	1.95E+05	2.44E+05	2.92E+05	3.41E+05	3.90E+05	4.39E+05	4.87E+05
1602.75	10.3680	10.1703	0.1875	1.615E-04	134.94	**4.71E+04**	**9.41E+04**	1.41E+05	1.88E+05	2.35E+05	2.82E+05	3.29E+05	3.76E+05	4.24E+05	4.71E+05
1635.75	9.9726	9.7750	0.1875	1.615E-04	137.69	**4.54E+04**	**9.07E+04**	1.36E+05	1.81E+05	2.27E+05	2.72E+05	3.18E+05	3.63E+05	4.08E+05	4.54E+05
1668.75	9.5773	9.3796	0.1875	1.615E-04	140.44	**4.37E+04**	**8.73E+04**	1.31E+05	1.75E+05	2.18E+05	2.62E+05	3.06E+05	3.49E+05	3.93E+05	4.37E+05
1701.75	9.1819	8.9843	0.1875	1.615E-04	143.19	**4.19E+04**	**8.39E+04**	1.26E+05	1.68E+05	2.10E+05	2.52E+05	2.93E+05	3.35E+05	3.77E+05	4.19E+05
1734.75	8.7866	8.5889	0.1875	1.615E-04	145.94	**4.02E+04**	**8.04E+04**	1.21E+05	1.61E+05	2.01E+05	2.41E+05	2.81E+05	3.22E+05	3.62E+05	4.02E+05
1767.75	8.3913	8.1936	0.1875	1.615E-04	148.69	**3.84E+04**	**7.69E+04**	1.15E+05	1.54E+05	1.92E+05	2.31E+05	2.69E+05	3.08E+05	3.46E+05	3.84E+05
1800.75	7.9959														

Note: The **shaded regions** indicate wind speeds and locations along the HML structure where $300 \le \mathrm{Re} \le 10^5$ or $\mathrm{Re} > 3.5 \times 10^6$.

Table 3.39: Shedding Frequency (Hz) Boundaries at Various Elevations for HML-67-006 as a Function of Reference Height Wind Speeds.

	Outside	Average	Wall		H	5 mph		10 mph		15 mph		20 mph		25 mph	
Level (in.)	Diameter	Diameter	Thickness	Kin. Vis	(ft)	n_low (Hz)	n_hgh (Hz)	n_low (Hz)	n_hgh (Hz)	n_low (Hz)	n_hgh (Hz)	n_low (Hz)	n_hgh (Hz)	n_low (Hz)	n_hgh (Hz)
6.75	27.4280	27.3740	0.3125	1.615E-04	0.94	**0.16**	**0.61**	**0.33**	**1.22**	**0.49**	**1.82**	**0.66**	**2.43**	**0.82**	**3.04**
15.75	27.3200	27.1400	0.3125	1.615E-04	2.56	**0.29**	**0.61**	**0.57**	**1.23**	**0.86**	**1.84**	1.15	2.46	**1.43**	**3.07**
45.75	26.9600	26.7365	0.3125	1.615E-04	5.36	0.36	0.65	**0.72**	**1.31**	**1.09**	**1.96**	1.45	2.61	**1.81**	**3.27**
83.00	26.5130	26.2895	0.3125	1.615E-04	8.47	0.41	0.69	**0.82**	**1.38**	1.23	2.07	1.65	2.76	**2.06**	**3.46**
120.25	26.0660	25.8425	0.3125	1.615E-04	11.57	0.45	0.72	**0.90**	**1.45**	1.35	2.17	1.79	2.90	**2.24**	**3.62**
157.50	25.6190	25.3955	0.3125	1.615E-04	14.68	0.48	0.75	**0.96**	**1.51**	1.44	2.26	1.92	3.02	**2.40**	**3.77**
194.75	25.1720	24.9485	0.3125	1.615E-04	17.78	0.51	0.78	**1.02**	**1.57**	1.52	2.35	**2.03**	**3.13**	**2.54**	**3.92**
232.00	24.7250	24.5015	0.3125	1.615E-04	20.89	0.53	0.81	**1.07**	**1.62**	1.60	2.44	**2.14**	**3.25**	**2.67**	**4.06**
269.25	24.2780	24.0545	0.3125	1.615E-04	23.99	0.56	0.84	**1.12**	**1.68**	1.68	2.52	**2.24**	**3.36**	**2.79**	**4.20**
306.50	23.8310	23.6075	0.3125	1.615E-04	27.09	0.58	0.87	1.17	1.73	1.75	2.60	**2.33**	**3.47**	**2.91**	**4.33**
343.75	23.3840	23.1605	0.3125	1.615E-04	30.20	0.61	0.89	1.21	1.79	1.82	2.68	**2.43**	**3.58**	**3.03**	**4.47**
381.00	22.9370	22.7135	0.3125	1.615E-04	33.30	0.63	0.92	1.26	1.84	1.89	2.77	**2.52**	**3.69**	3.15	4.61
418.25	22.4900	22.2665	0.3125	1.615E-04	36.41	0.65	0.95	1.31	1.90	1.96	2.85	**2.61**	**3.80**	3.27	4.75
455.50	22.0430	22.0335	0.3125	1.615E-04	39.51	0.67	0.97	1.34	1.94	2.01	2.91	**2.68**	**3.88**	3.35	4.85
492.75	22.0240	22.0240	0.3125	1.615E-04	42.44	0.68	0.98	1.36	1.95	2.04	2.93	**2.72**	**3.91**	3.40	4.89
525.75	22.0240	21.8121	0.3125	1.615E-04	45.28	0.69	0.99	1.39	1.99	2.08	2.98	**2.78**	**3.98**	3.47	4.97
561.06	21.6003	21.3884	0.3125	1.615E-04	48.23	0.72	1.02	1.43	2.04	**2.15**	**3.06**	**2.86**	**4.09**	3.58	5.11
596.37	21.1766	20.9648	0.3125	1.615E-04	51.17	0.74	1.05	1.48	2.10	**2.21**	**3.15**	**2.95**	**4.20**	3.69	5.25
631.67	20.7530	20.5411	0.3125	1.615E-04	54.11	0.76	1.08	1.52	2.16	**2.28**	**3.23**	3.04	4.31	3.80	5.39
666.98	20.3292	20.1174	0.3125	1.615E-04	57.05	0.78	1.11	1.57	2.22	**2.35**	**3.32**	3.14	4.43	3.92	5.54
702.29	19.9055	19.6937	0.3125	1.615E-04	60.00	**0.81**	**1.14**	1.62	2.28	**2.43**	**3.41**	3.23	4.55	4.04	5.69
737.60	19.4818	19.2700	0.3125	1.615E-04	62.94	**0.83**	**1.17**	1.67	2.34	**2.50**	**3.51**	3.33	4.68	4.17	5.85
772.90	19.0582	18.8463	0.3125	1.615E-04	65.88	**0.86**	**1.20**	1.72	2.41	**2.58**	**3.61**	3.44	4.81	**4.29**	**6.01**
808.21	18.6345	18.4226	0.3125	1.615E-04	68.82	**0.89**	**1.24**	1.77	2.47	**2.66**	**3.71**	3.54	4.95	**4.43**	**6.18**
843.52	18.2108	17.9989	0.3125	1.615E-04	71.76	**0.91**	**1.27**	1.83	2.54	**2.74**	**3.82**	3.65	5.09	**4.56**	**6.36**
878.83	17.7870	17.5752	0.3125	1.615E-04	74.71	**0.94**	**1.31**	1.88	2.62	**2.82**	**3.93**	3.77	5.24	**4.71**	**6.55**
914.13	17.3634	17.1516	0.3125	1.615E-04	77.65	**0.97**	**1.35**	1.94	2.70	**2.91**	**4.04**	3.89	5.39	**4.86**	**6.74**
949.44	16.9397	16.9132	0.3125	1.615E-04	80.59	**0.99**	**1.37**	1.98	2.75	**2.97**	**4.12**	3.97	5.49	**4.96**	**6.86**
984.75	16.8866	16.8866	0.3125	1.615E-04	83.19	**1.00**	**1.38**	2.00	2.76	**3.00**	**4.14**	3.99	5.52	**4.99**	**6.90**
1011.75	16.8866	16.6853	0.25	1.615E-04	85.71	**1.02**	**1.40**	2.03	2.80	3.05	4.21	4.06	5.61	**5.08**	**7.01**
1045.30	16.4840	16.2828	0.25	1.615E-04	88.51	**1.05**	**1.44**	2.09	2.88	3.14	4.33	4.19	5.77	**5.23**	**7.21**
1078.84	16.0815	15.8802	0.25	1.615E-04	91.30	**1.08**	**1.48**	2.16	2.97	3.24	4.45	4.32	5.94	**5.39**	**7.42**
1112.39	15.6789	15.4777	0.25	1.615E-04	94.10	**1.11**	**1.53**	**2.23**	**3.06**	3.34	4.59	**4.45**	**6.11**	**5.56**	**7.64**
1145.93	15.2764	15.0751	0.25	1.615E-04	96.89	1.15	1.58	**2.30**	**3.15**	3.44	4.73	**4.59**	**6.30**	**5.74**	**7.88**
1179.48	14.8738	14.6726	0.25	1.615E-04	99.69	1.19	1.62	**2.37**	**3.25**	3.56	4.87	**4.74**	**6.50**	**5.93**	**8.12**
1213.02	14.4714	14.2701	0.25	1.615E-04	102.48	1.22	1.68	**2.45**	**3.35**	3.67	5.03	**4.90**	**6.70**	6.12	8.38
1246.57	14.0688	13.8675	0.25	1.615E-04	105.28	1.27	1.73	**2.53**	**3.46**	3.80	5.19	**5.06**	**6.92**	6.33	8.65
1280.11	13.6663	13.4650	0.25	1.615E-04	108.07	1.31	1.79	**2.62**	**3.57**	3.93	5.36	**5.24**	**7.15**	6.55	8.94
1313.66	13.2637	13.0624	0.25	1.615E-04	110.87	1.36	1.85	**2.71**	**3.70**	4.07	5.54	**5.42**	**7.39**	6.78	9.24
1347.20	12.8612	12.8006	0.25	1.615E-04	113.66	1.39	1.89	**2.78**	**3.78**	4.17	5.67	**5.56**	**7.57**	6.95	9.46
1380.75	12.7400	12.7400	0.25	1.615E-04	116.06	1.40	1.91	**2.80**	**3.81**	4.20	5.72	**5.61**	**7.62**	7.01	9.53
1404.75	12.7400	12.5423	0.1875	1.615E-04	118.44	1.43	1.94	**2.86**	**3.88**	4.29	5.82	**5.71**	**7.76**	7.14	9.70
1437.75	12.3447	12.1470	0.1875	1.615E-04	121.19	1.48	2.01	**2.96**	**4.02**	**4.44**	**6.03**	**5.92**	**8.04**	**7.40**	**10.04**
1470.75	11.9493	11.7517	0.1875	1.615E-04	123.94	1.54	2.08	3.07	4.16	**4.61**	**6.25**	6.15	8.33	**7.68**	**10.41**
1503.75	11.5540	11.3563	0.1875	1.615E-04	126.69	1.60	2.16	3.19	4.32	**4.79**	**6.48**	6.38	8.64	**7.98**	**10.80**
1536.75	11.1586	10.9610	0.1875	1.615E-04	129.44	1.66	2.24	3.32	4.49	**4.98**	**6.73**	6.64	8.98	**8.30**	**11.22**
1569.75	10.7633	10.5656	0.1875	1.615E-04	132.19	1.73	2.33	3.46	4.67	**5.18**	**7.00**	6.91	9.34	**8.64**	**11.67**
1602.75	10.3680	10.1703	0.1875	1.615E-04	134.94	1.80	2.43	3.60	4.86	**5.40**	**7.29**	7.20	9.73	**9.00**	**12.16**
1635.75	9.9726	9.7750	0.1875	1.615E-04	137.69	1.88	2.54	3.76	5.07	**5.64**	**7.61**	**7.52**	**10.14**	9.40	12.68
1668.75	9.5773	9.3796	0.1875	1.615E-04	140.44	1.97	2.65	3.93	5.30	**5.90**	**7.95**	**7.86**	**10.60**	9.83	13.25
1701.75	9.1819	8.9843	0.1875	1.615E-04	143.19	2.06	2.77	4.12	5.55	6.18	8.32	**8.24**	**11.09**	10.30	13.86
1734.75	8.7866	8.5889	0.1875	1.615E-04	145.94	2.16	2.91	4.32	5.81	6.48	8.72	**8.64**	**11.63**	10.80	14.54
1767.75	8.3913	8.1936	0.1875	1.615E-04	148.69	**2.27**	**3.05**	**4.54**	**6.11**	6.82	9.16	**9.09**	**12.22**	**11.36**	**15.27**
1800.75	7.9959														

Note: The **shaded regions** indicate wind speeds and locations along the HML structure where $n_s^L \le n_{struc}^k \le n_s^U$ where *k* indicates any mode.

Table 3.39: Shedding Frequency (Hz) Boundaries at Various Elevations for HML-67-006 as a Function of Reference Height Wind Speeds. (CONTINUED).

Level (in.)	Outside Diameter	Average Diameter	Wall Thickness	Kin. Vis	H (ft)	30 mph		35 mph		40 mph		45 mph		50 mph	
						n_low (Hz)	n_hgh (Hz)	n_low (Hz)	n_hgh (Hz)	n_low (Hz)	n_hgh (Hz)	n_low (Hz)	n_hgh (Hz)	n_low (Hz)	n_hgh (Hz)
6.75	27.4280	27.3740	0.3125	1.615E-04	0.94	**0.99**	**3.65**	**1.15**	**4.26**	**1.32**	**4.87**	**1.48**	**5.47**	**1.65**	**6.08**
15.75	27.3200	27.1400	0.3125	1.615E-04	2.56	**1.72**	**3.68**	**2.00**	**4.30**	**2.29**	**4.91**	**2.58**	**5.53**	**2.86**	**6.14**
45.75	26.9600	26.7365	0.3125	1.615E-04	5.36	**2.17**	**3.92**	**2.54**	**4.57**	**2.90**	**5.23**	3.26	5.88	**3.62**	**6.53**
83.00	26.5130	26.2895	0.3125	1.615E-04	8.47	**2.47**	**4.15**	**2.88**	**4.84**	3.29	5.53	**3.70**	**6.22**	**4.11**	**6.91**
120.25	26.0660	25.8425	0.3125	1.615E-04	11.57	**2.69**	**4.34**	3.14	5.07	3.59	5.79	**4.04**	**6.52**	**4.49**	**7.24**
157.50	25.6190	25.3955	0.3125	1.615E-04	14.68	**2.88**	**4.53**	3.36	5.28	**3.84**	**6.04**	**4.32**	**6.79**	**4.80**	**7.55**
194.75	25.1720	24.9485	0.3125	1.615E-04	17.78	3.05	4.70	3.56	5.49	**4.06**	**6.27**	**4.57**	**7.05**	**5.08**	**7.84**
232.00	24.7250	24.5015	0.3125	1.615E-04	20.89	3.20	4.87	3.74	5.68	**4.27**	**6.49**	**4.81**	**7.31**	**5.34**	**8.12**
269.25	24.2780	24.0545	0.3125	1.615E-04	23.99	3.35	5.04	3.91	5.88	**4.47**	**6.71**	**5.03**	**7.55**	**5.59**	**8.39**
306.50	23.8310	23.6075	0.3125	1.615E-04	27.09	3.50	5.20	**4.08**	**6.07**	**4.66**	**6.93**	**5.25**	**7.80**	**5.83**	**8.67**
343.75	23.3840	23.1605	0.3125	1.615E-04	30.20	3.64	5.37	**4.25**	**6.26**	**4.85**	**7.15**	**5.46**	**8.05**	6.06	8.94
381.00	22.9370	22.7135	0.3125	1.615E-04	33.30	3.78	5.53	**4.41**	**6.45**	**5.04**	**7.38**	**5.67**	**8.30**	6.30	9.22
418.25	22.4900	22.2665	0.3125	1.615E-04	36.41	3.92	5.70	**4.57**	**6.65**	**5.23**	**7.60**	**5.88**	**8.55**	6.53	9.50
455.50	22.0430	22.0335	0.3125	1.615E-04	39.51	4.02	5.81	**4.69**	**6.78**	**5.36**	**7.75**	6.03	8.72	6.70	9.69
492.75	22.0240	22.0240	0.3125	1.615E-04	42.44	4.08	5.86	**4.75**	**6.84**	**5.43**	**7.82**	6.11	8.80	6.79	9.77
525.75	22.0240	21.8121	0.3125	1.615E-04	45.28	4.16	5.97	**4.86**	**6.96**	**5.55**	**7.96**	6.25	8.95	6.94	9.94
561.06	21.6003	21.3884	0.3125	1.615E-04	48.23	**4.30**	**6.13**	**5.01**	**7.15**	**5.73**	**8.17**	6.44	9.19	**7.16**	**10.22**
596.37	21.1766	20.9648	0.3125	1.615E-04	51.17	**4.43**	**6.30**	**5.17**	**7.35**	**5.91**	**8.40**	6.64	9.44	**7.38**	**10.49**
631.67	20.7530	20.5411	0.3125	1.615E-04	54.11	**4.57**	**6.47**	**5.33**	**7.55**	6.09	8.62	6.85	9.70	**7.61**	**10.78**
666.98	20.3292	20.1174	0.3125	1.615E-04	57.05	**4.71**	**6.65**	**5.49**	**7.75**	6.27	8.86	7.06	9.97	**7.84**	**11.08**
702.29	19.9055	19.6937	0.3125	1.615E-04	60.00	**4.85**	**6.83**	**5.66**	**7.97**	6.47	9.11	**7.28**	**10.24**	**8.08**	**11.38**
737.60	19.4818	19.2700	0.3125	1.615E-04	62.94	**5.00**	**7.02**	**5.83**	**8.19**	6.67	9.36	**7.50**	**10.53**	**8.33**	**11.70**
772.90	19.0582	18.8463	0.3125	1.615E-04	65.88	**5.15**	**7.22**	6.01	8.42	6.87	9.62	**7.73**	**10.82**	**8.59**	**12.03**
808.21	18.6345	18.4226	0.3125	1.615E-04	68.82	**5.31**	**7.42**	6.20	8.66	7.08	9.89	**7.97**	**11.13**	**8.85**	**12.37**
843.52	18.2108	17.9989	0.3125	1.615E-04	71.76	**5.48**	**7.63**	6.39	8.91	**7.30**	**10.18**	**8.22**	**11.45**	**9.13**	**12.72**
878.83	17.7870	17.5752	0.3125	1.615E-04	74.71	**5.65**	**7.86**	6.59	9.16	**7.53**	**10.47**	**8.47**	**11.78**	**9.42**	**13.09**
914.13	17.3634	17.1516	0.3125	1.615E-04	77.65	**5.83**	**8.09**	6.80	9.43	**7.77**	**10.78**	**8.74**	**12.13**	**9.71**	**13.48**
949.44	16.9397	16.9132	0.3125	1.615E-04	80.59	**5.95**	**8.24**	6.94	9.61	**7.93**	**10.98**	**8.92**	**12.36**	**9.91**	**13.73**
984.75	16.8866	16.8866	0.3125	1.615E-04	83.19	**5.99**	**8.28**	6.99	9.66	**7.99**	**11.04**	**8.99**	**12.42**	9.98	13.80
1011.75	16.8866	16.6853	0.25	1.615E-04	85.71	6.09	8.41	7.11	9.81	**8.13**	**11.22**	9.14	12.62	10.16	14.02
1045.30	16.4840	16.2828	0.25	1.615E-04	88.51	6.28	8.65	**7.33**	**10.10**	**8.37**	**11.54**	9.42	12.98	10.47	14.42
1078.84	16.0815	15.8802	0.25	1.615E-04	91.30	6.47	8.91	**7.55**	**10.39**	**8.63**	**11.88**	9.71	13.36	10.79	14.84
1112.39	15.6789	15.4777	0.25	1.615E-04	94.10	6.68	9.17	**7.79**	**10.70**	**8.90**	**12.23**	10.02	13.76	**11.13**	**15.29**
1145.93	15.2764	15.0751	0.25	1.615E-04	96.89	6.89	9.45	**8.04**	**11.03**	**9.19**	**12.60**	10.33	14.18	**11.48**	**15.75**
1179.48	14.8738	14.6726	0.25	1.615E-04	99.69	7.11	9.74	**8.30**	**11.37**	**9.48**	**12.99**	10.67	14.61	**11.86**	**16.24**
1213.02	14.4714	14.2701	0.25	1.615E-04	102.48	**7.35**	**10.05**	**8.57**	**11.73**	**9.80**	**13.40**	**11.02**	**15.08**	**12.25**	**16.75**
1246.57	14.0688	13.8675	0.25	1.615E-04	105.28	**7.60**	**10.38**	**8.86**	**12.11**	10.13	13.84	**11.40**	**15.57**	**12.66**	**17.30**
1280.11	13.6663	13.4650	0.25	1.615E-04	108.07	**7.86**	**10.72**	**9.17**	**12.51**	10.48	14.30	**11.79**	**16.08**	**13.10**	**17.87**
1313.66	13.2637	13.0624	0.25	1.615E-04	110.87	**8.14**	**11.09**	**9.49**	**12.94**	10.85	14.78	**12.21**	**16.63**	**13.56**	**18.48**
1347.20	12.8612	12.8006	0.25	1.615E-04	113.66	**8.34**	**11.35**	**9.73**	**13.24**	**11.12**	**15.13**	**12.51**	**17.02**	**13.90**	**18.91**
1380.75	12.7400	12.7400	0.25	1.615E-04	116.06	**8.41**	**11.43**	**9.81**	**13.34**	**11.21**	**15.24**	**12.61**	**17.15**	**14.01**	**19.05**
1404.75	12.7400	12.5423	0.1875	1.615E-04	118.44	**8.57**	**11.64**	10.00	13.58	**11.43**	**15.52**	**12.86**	**17.46**	**14.28**	**19.40**
1437.75	12.3447	12.1470	0.1875	1.615E-04	121.19	**8.88**	**12.05**	10.36	14.06	**11.85**	**16.07**	**13.33**	**18.08**	**14.81**	**20.09**
1470.75	11.9493	11.7517	0.1875	1.615E-04	123.94	**9.22**	**12.49**	10.75	14.58	**12.29**	**16.66**	**13.83**	**18.74**	15.36	20.82
1503.75	11.5540	11.3563	0.1875	1.615E-04	126.69	**9.57**	**12.96**	**11.17**	**15.12**	**12.77**	**17.28**	**14.36**	**19.45**	15.96	21.61
1536.75	11.1586	10.9610	0.1875	1.615E-04	129.44	**9.96**	**13.47**	**11.62**	**15.71**	**13.27**	**17.96**	**14.93**	**20.20**	16.59	22.44
1569.75	10.7633	10.5656	0.1875	1.615E-04	132.19	10.37	14.01	**12.09**	**16.34**	**13.82**	**18.68**	15.55	21.01	17.28	23.35
1602.75	10.3680	10.1703	0.1875	1.615E-04	134.94	10.81	14.59	**12.61**	**17.02**	**14.41**	**19.45**	16.21	21.88	18.01	24.31
1635.75	9.9726	9.7750	0.1875	1.615E-04	137.69	**11.28**	**15.22**	**13.16**	**17.75**	15.04	20.29	16.92	22.82	18.80	25.36
1668.75	9.5773	9.3796	0.1875	1.615E-04	140.44	**11.80**	**15.90**	**13.76**	**18.55**	15.73	21.20	17.69	23.85	19.66	26.49
1701.75	9.1819	8.9843	0.1875	1.615E-04	143.19	**12.36**	**16.64**	**14.41**	**19.41**	16.47	22.18	18.53	24.95	20.59	27.73
1734.75	8.7866	8.5889	0.1875	1.615E-04	145.94	**12.97**	**17.44**	15.13	20.35	17.29	23.26	19.45	26.16	21.61	29.07
1767.75	8.3913	8.1936	0.1875	1.615E-04	148.69	**13.63**	**18.33**	15.91	21.38	18.18	24.44	20.45	27.49	22.72	30.54
1800.75	7.9959														

Note: The **shaded regions** indicate wind speeds and locations along the HML structure where $n_s^L \le n_{struc}^k \le n_s^U$ where *k* indicates any mode.

Figure 3.78: Displaced Shape of HML-67-006 During 20-30 mph Peak Gusts.

3.3.2.4 Response to Natural Wind

Turbulent wind pressure records of 5-second duration were generated for this structure using previously discussed procedures. The mast was broken down into 4 segments where the mid-height of each segment was utilized as the reference height for wind speed computations. The heights for wind speed simulation and the corresponding drag coefficients for wind pressure simulations are given in Table 3.40.

Table 3.40: Mast Segment Reference Heights for Wind Speed Determination and Drag Coefficients for Pressure Simulations.

Mast Segment	Reference Height (ft.)	Drag Coefficient
1	20.53	0.79
2	61.56	0.79
3	98.56	0.79
4	132.56	0.82
Luminaire	150.0	1.20

The drag coefficients included in Table 3.40 are the 50-year mean recurrence interval drag coefficients.

Procedures previously discussed for generation of turbulent wind pressures were again used (along with the data in Table 3.40) to generate loading protocols for the mast and luminaire in the structure. An example of the transient pressure records at each segment of the mast and the luminaire level are shown in Figure 3.79. There is significant variation in mean pressure from the base of the mast to the level of the luminaire assembly. It is interesting to note that with 6 luminaires, an equivalent projected area of the assembly was assumed to be 16 square feet. Figure 3.79 illustrates that the mean pressure at the luminaire

level is approximately 0.08 pounds per square inch. Therefore, the projected area of the luminaire assembly assumed results a mean concentrated loading of nearly 200 pounds with significant transient variation.

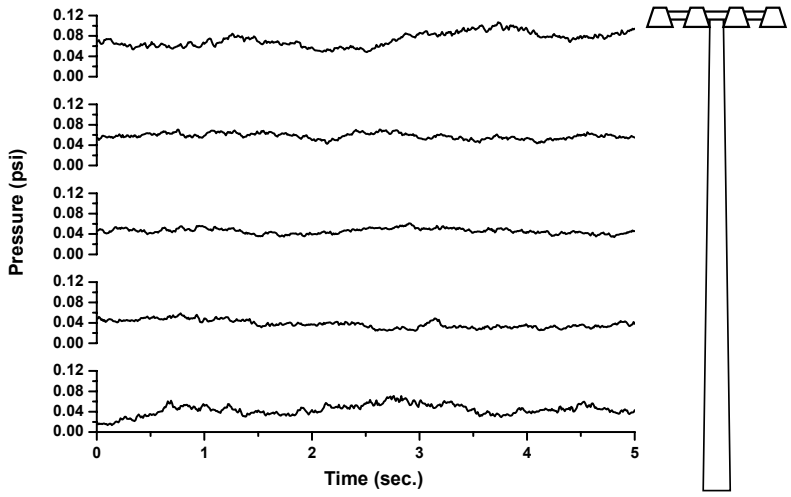

Figure 3.79: Transient Wind Pressure Records for 50-mph Mean Winds and HML-67-006.

This helps to explain the first-mode dominant response shown in Figure 3.78. Figure 3.79 also illustrates that the turbulence in the pressure records seems to decrease slightly with height until the luminaire assembly height is reached. The mean wind speed at the luminaire assembly level is nearly 91 mph when the speed is 50 mph at 33 feet.

The transient stress response for various components in HML-67-006 can be discussed with reference to Figure 3.80. The FEA force directions are indicated (x- and y-directions) along with wind-speed directions and anchor rod designations. The hand-hole is located on the mast wall projecting outward in the Southeast direction (not shown in the figure). Figure 3.80 is the basis for all discussion regarding wind response history and fatigue estimates.

Figure 3.81 illustrates the axial stress response history for anchor rod 8 for wind in the x-direction at a variety of wind speeds. The cyclic nature of the response for 50-mph wind appears to have a period of approximately 3.5 seconds, which is very close to the first mode frequency found in Table 3.35. The lack of cyclical response for the 45 mph mean wind speed is very interesting as well. Lower mean wind speeds are not capable of generating enough force to vary the axial stress in the anchor rod above the compressive stress present under the self weight.

Figure 3.82 illustrates the bending stress in anchor rod 8 (at its base) for three wind speeds. The cyclical nature of the response at 50 mph is similar to that for the axial stress, but the 25-mph and 5-mph mean wind speeds have a lack of significant cyclical behavior. One very important difference with regard to behavior when compared to HML-40-061 is the magnitude of bending stresses at the base. HML-40-061 had a four-anchor arrangement and bending stresses ranged from 6,000 psi to 20,500 psi when wind came from the FX/FY direction. The bending stresses in the anchor rods of HML-67-006 are much lower with a peak of approximately 4,500 psi under 50-mph mean winds.

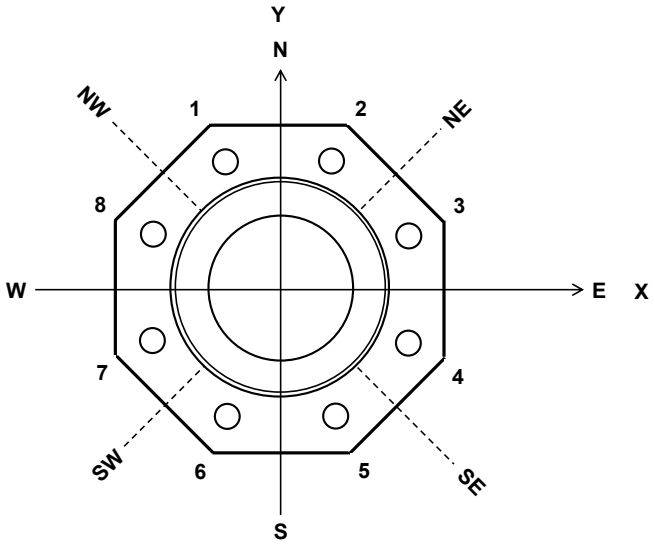

Figure 3.80: Anchor Rod Layout, FEA Force Directions, and Wind Directions for HML-67-006.

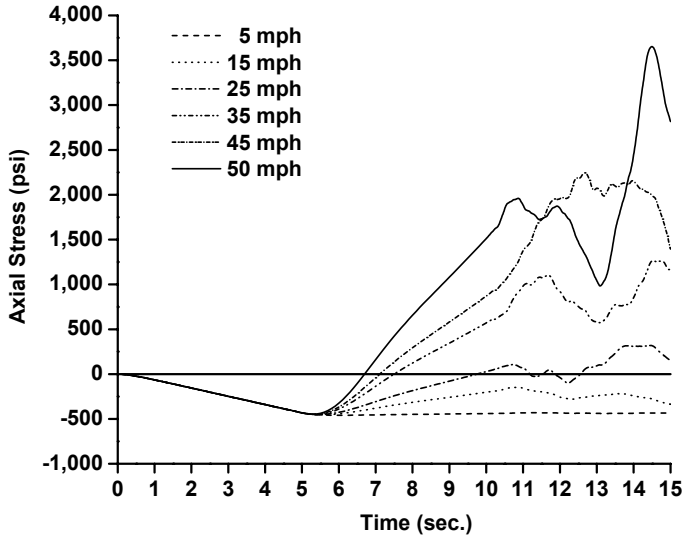

Figure 3.81: Transient Axial Stress Response of Anchor Rod 8 at Various Wind Speeds.

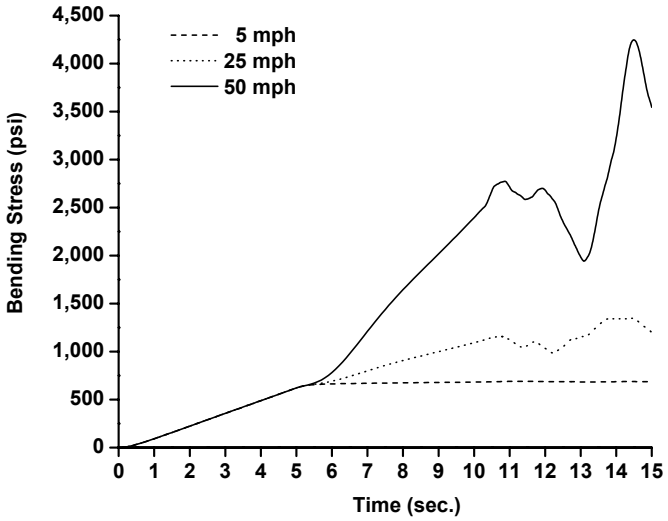

Figure 3.82: Transient Bending Stress Response of Anchor Rod 8 at Various Wind Speeds.

The stark difference in bending stresses between the 4-anchor and 8-anchor arrangement suggests that it is likely that the 8-anchor arrangement will experience better in-service behavior and reliability. The increased redundancy in the anchor arrangement is also advantageous. More importantly, research must begin to address the impact that bending of the anchor rods has on the fatigue life. HML-40-061 has stress peaks that are near 50% of the ultimate stress specified.

The membrane stress response in the mast wall at the base of the HML is shown in Figure 3.83. The membrane stress response history is similar to that of the anchor rod axial stress. The largest cyclic response is again at the highest mean wind speed (50 mph).

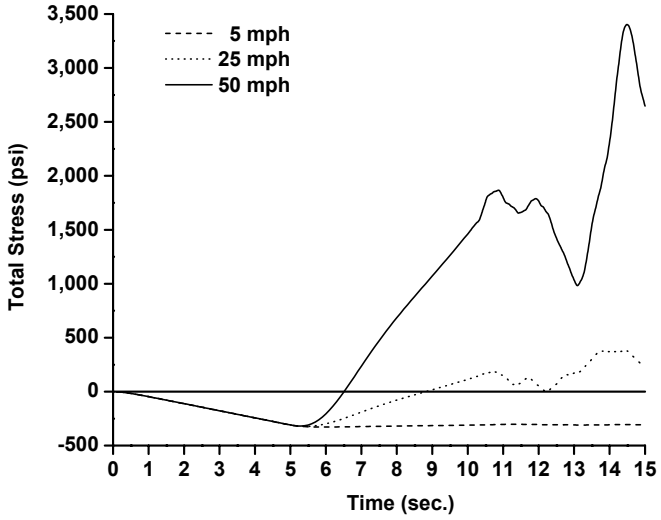

Figure 3.83: Stress Response at Base of HML-67-006 in Mast Wall for Various Wind Speeds.

The response at the level of the hand-hole reinforcement is very similar to that at the base in both cyclic nature and stress magnitude.

3.3.2.5 Fatigue Life Prediction

The fatigue life prediction of HML-67-006 was conducted in the same manner as HML-40-061. Computing the number of stress cycles from each wind direction was not as simple, however. Figure 3.84 illustrates the wind directions (shaded N through SW counterclockwise) that will result in tension stresses in anchor rod number 8.

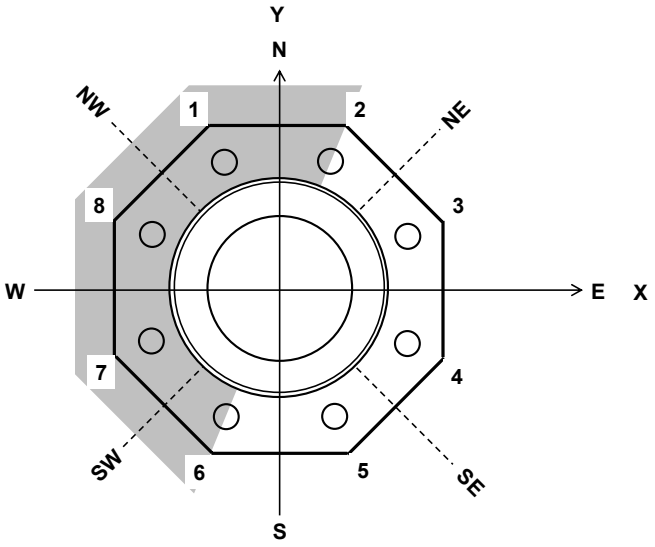

Figure 3.84: Wind Directions Contributing to Tension Stress Ranges in Anchor Rod 8 of HML-67-006.

Only one transient FE analysis was conducted (wind in the x-direction). This analysis results in stress histories being available for all anchor rods. If one focuses on anchor rod 8 for the moment, the methodology used for generating stress histories for all wind directions will be illustrated. First of all, wind loading from the x-direction was used to compute the stress history for anchor rod 8 and 1. The stress history for anchor rod 8 provided stress ranges for this anchor rod when wind is from the west. The stress history for anchor rod 1 was used to simulate the effect of wind from the southwest and north on anchor rod 8. Wind from the northwest will cause the same stress history in anchor rod 8 as the case of wind from the west. In this manner, stress histories and stress-range cycles for all pertinent wind directions can be developed for each anchor rod. If one rotates counterclockwise around the anchor rod pattern, four wind directions will contribute to the stress history in anchor rod 7 (NW-W-SW-S). The process can continue all the way around the anchor arrangement.

Figure 3.85 provides cumulative damage histograms for anchor rod 8. The cumulative damage distribution for this anchor rod and that of HML-40-061 should be immediately compared. HML-67-006 has remarkably consistent damage across all wind speeds. This would be consistent with first-mode dominant response. The results in Figure 3.81 illustrate progressively increasing stress ranges with wind speed and this would indicate the cumulative damage seen.

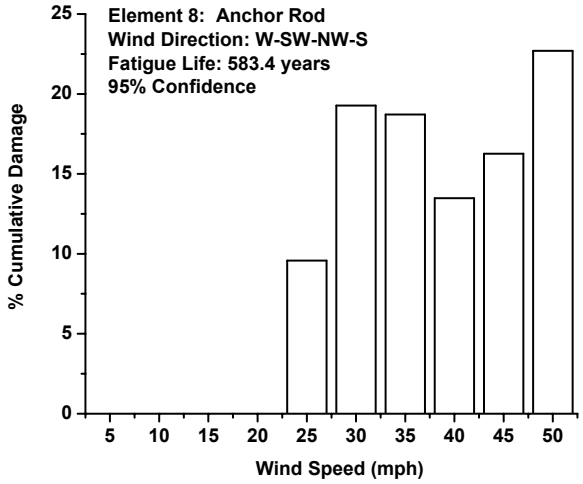

Figure 3.85: Cumulative Damage Histogram for Anchor Rod 8 in HML-67-006 for Critical Wind Directions: W-SW-NW-S.

HML-40-061 accumulated significant damage over several mean wind speeds in the range of 20 to 35 mph with smaller damage accumulation on the ends. The behavioral difference in fatigue damage accumulation is significant.

The 95% confidence level fatigue life is well beyond any expected service life required for this type of structure. Therefore, it could be stated that if HML-67-006 arrives on site and is erected without defect, its fatigue life will be infinite and no inspection is required. If the double-nut configuration on top of the base plate is utilized, it is highly unlikely that the anchors will loosen and no inspection would be required for this structure during service.

Figures 3.86 and 3.87 illustrate cumulative damage histograms for the mast base and the hand-hole bottom. In these cases, the damage progressively increases with wind speed. The reason for the difference when compared to Figure 3.85 is that four wind directions can cause appreciable damage to the anchor rod where only three directions cause appreciable damage to the hand-hole region and the mast base. In both cases the expected fatigue lives are well-beyond expected service lives and can be considered infinite.

The fatigue lives of all components have been made with 95% confidence levels. Therefore, as mentioned previously, if HML-67-006 is delivered to the site and erected without flaw, there is a 95% confidence that the fatigue life will be infinite. Therefore, HML-67-006 will not require inspection during its service lifetime. The galvanizing on the anchor rods have given even more confidence to the statement that the fatigue life will be infinite for this structure because degradation due to corrosion of the anchors will be severely limited or eliminated altogether.

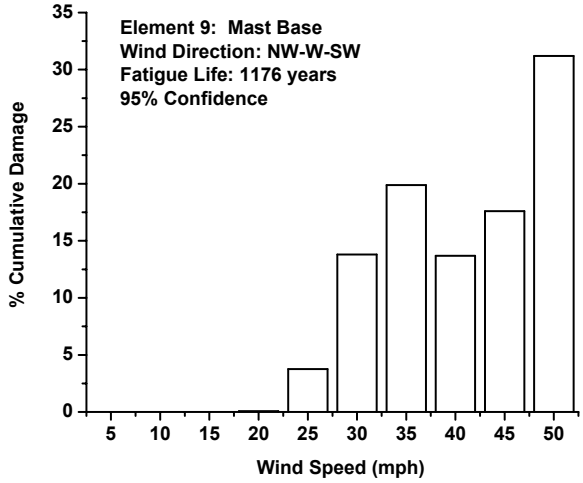

Figure 3.86: Cumulative Damage Histogram for Mast Base in HML-67-006.

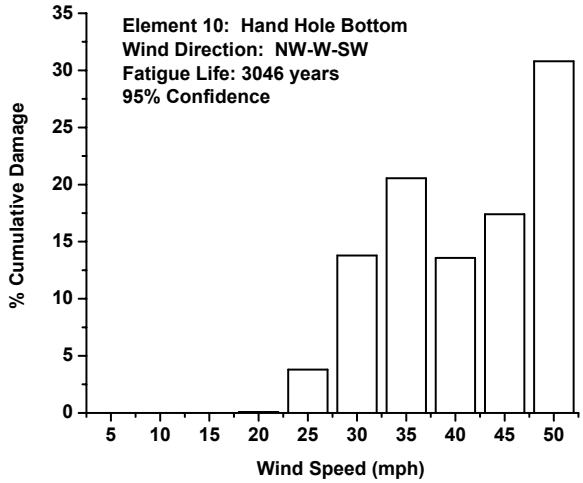

Figure 3.87: Cumulative Damage Histogram for Hand-Hole Bottom in HML-67-006.

Chapter 4

Conclusions and Suggested Research

4.1 Summary of Work Conducted

The present research effort focused on detailed structural analysis (including modal and membrane stress analysis), susceptibility to aerodynamic instability, and fatigue life prediction of high-mast luminaire support structures and full-span steel sign support structures within the State of Wisconsin. The objectives of the research study were:

1.) Develop realistic loading models for truck-induced gust pressures and natural turbulent wind that can be used as part of transient finite element analysis of sign and luminaire support structures.

2.) Thoroughly evaluate (analytically) the susceptibility of full-span sign and high-mast luminaire support structures to excessive vibration resulting from aeroelastic instability (*e.g.* vortex-shedding and galloping).

3.) Generate detailed finite element models capable of capturing all important phenomenological aspects to structure response for HML and sign support structures including; bending and axial stresses in the anchor rods; eccentric mass of VMS and catwalk supports on sign structures; uplift and suction pressures on catwalk and sign elements for full-span overhead structures from passing trucks; concentration of stress at the base plate/ring welded connections in HML structures; and bending of base plates and anchor rods for HML and sign support structures that include significant anchor rod stand off heights.

4.) Assemble statistical information needed to generate probabilistically-based loading scenarios suitable for generating fatigue life estimates for these structures.

5.) Gather and develop (as required) the necessary statistical information related to the fatigue performance of pertinent fatigue-critical details needed to generate fatigue lives with varying levels of confidence.

6.) Develop a methodology for predicting fatigue life estimates for various levels of confidence and generate fatigue life estimates for sign and luminaire support structures for these confidence levels. These estimates can then be used to address the fabrication/design dichotomy as well as establish rational inspection protocols for these structures.

The research effort succeeded in meeting these objectives. Applications of the results of the effort may foster better use of public funds for ancillary structure inspection and reduce inconvenience to the motoring public through establishing rational inspection intervals for these structures.

The research effort provided a literature review and synthesis of all pertinent information related to the state-of-the-art design and analysis methodologies for sign and luminaire support structures. The literature survey ended with a synthesis outlining research needs (some of which have been accomplished via this research effort). A probabilistic analysis was undertaken to provide data necessary to predict wind speed and direction probabilities for the metro-Milwaukee area. This analysis set the stage for generating fatigue-life predictions for full-span sign and luminaire support structures. An experimental effort was undertaken to generate statistical variability measures for the *ET* detail category suitable for developing fatigue life predictions with confidence levels other than 95%, which is assumed by AASHTO (2001). A procedure was described whereby natural wind can be simulated. This simulated wind was then used as loading in a finite element analysis for the structures considered with subsequent rainflow counting and fatigue life predictions. An analytical model for a truck-induced gust pressure pulse was developed for subsequent use in FEA and damage estimates for sign support structures resulting from passing trucks were computed.

Three full-span sign support structures were selected from those managed by WisDOT District 2. These structures were S-40-156, S-40-404, and S-67-402. The first was a tri-chord structure with Type 1 aluminum printed sign and the remaining two were four-chord box trusses supporting VMS. Detailed discussions of the finite element models and modal analysis of these structures were provided. Vibration characteristics of the structures were studied including the effect of base fixity on the modal vibration shapes. The susceptibility of these three structures to the aerodynamic instability phenomena of galloping and vortex-shedding was evaluated. Fatigue lives for these structures were computed and critical components that governed the fatigue lives were pointed out. The susceptibility of full-span sign support structures to damage resulting from truck-induced pressure pulses was also evaluated.

Two high-mast luminaire support structures were selected from the database of structures managed by WisDOT District 2. These structures were HML-40-061 and HML-67-006. The first was a 100 foot tall mast with four-anchor-rod base condition supporting a lighting assembly with 4 luminiares. The second was a 150 tall mast with eight anchor-rod base configuration and 6 luminaires in the lighting assembly. A detailed stress analysis of the base conditions and a study of the stress distribution in the mast wall at the base were provided including recommendations for stress-concentration factors for both base conditions. Modal analysis for both HML structures was conducted and the impact of base plate thickness and anchor rod stand off height was evaluated. The susceptibility of the HML structures to

vortex-shedding induced vibrations was evaluated in great detail. Finally, fatigue life predictions were made and critical components that limit the fatigue life of the HML structures considered were identified.

4.2 Conclusions Regarding Sign Support Structures

There are several conclusions that can be drawn from the completed study with regard to full-span sign support structures. The study illustrated that design of full-span sign support structures of the configuration examined need not consider galloping vibrations. The mean wind speeds necessary to cause "plunge-instability" and self-perpetuating galloping vibrations are outside the realm of reality. Therefore, it is suggested that this loading criteria, albeit its presence in the design specifications (AASHTO 2001), be ignored for these structures.

Truck-induced pressure pulses were found to cause very little damage to structure S-40-156. The stress ranges due to trucks passing beneath (using the proposed analytical model) were very small (180 psi). These are far below the CAFL for all details within the structure and therefore, truck-induced gust pressures can be ignored for the design of this structure (and other similar structures). Structure S-67-402 was also found to have peak stress ranges resulting from truck-gust pressures on the order of 620 psi. This peak stress range is also less than 1/2 the lowest 95% confidence CAFL (*ET* detail category) and therefore truck-induced gust pressures need not be considered in the design of this structure (and others of similar configuration).

Structure S-40-404, however, was found to have a peak tensile stress range in a member equal to 1,170 psi. This stress range exceeds the $1/2 \cdot CAFL$ threshold and could be considered damaging. If the $ADTT = 3,000$, truck-induced gust pressures could expend 1.3% of the *ET* detail's fatigue life each year. While taken alone, this may not be much, but in conjunction with natural wind, truck-induced gust pressures may be required as a design consideration. The difference between S-67-402 and S-40-404 is the span length. S-40-404 is a little over 36 feet longer than S-67-402 (see Appendix A). Therefore, truck-induced pressures may be required as a design consideration for "longer spans" in the four-chord "box-truss" configuration. Time prohibited detailed evaluation of this aspect, but it may be prudent to conduct future research in this arena.

Vortex shedding induced vibrations need not be considered in the design of full-span sign support structures. The senior author has personally observed vortex-shedding induced vibrations for a cantilevered (single arm) VMS support over an arterial roadway. Therefore, this statement should be limited to full-span structures only.

Tri-chord sign support structures (*e.g.* S-40-156) are likely to have service lives that are less than the 50-year target (AASHTO 2001; Dexter and Ricker 2002). Diagonal web members in the front face of the truss are likely to be the controlling members when determining the fatigue life of the structure. These structures can be subjected to significant cyclic twisting deformations (with associated tensile stress ranges).

Four-chord box trusses with VMS and grouted base plates are likely to attain their 50-year target service life. However, the fatigue life of 4-chord box trusses with stand-off heights in the anchor rods is likely to be less than the 50-year target. The analytical study conducted showed that the anchor rods for this configuration (S-67-402) are the fatigue-critical component and therefore, control the fatigue life of this structure. It is surmised that if the anchor rods did not have such a severe stand-off (*e.g.* less than one anchor rod diameter), the ability to omit bending stresses in the anchor rods when considering fatigue would likely have improved the fatigue life to the extent that it would extend into the target range of 50-years or more.

The detailed finite element analysis using probabilistically based turbulent wind simulations conducted on the structures considered indicates that the fatigue life for these structures is on the order of 18 years for the tri-chord truss structures; 10 years for four-chord box sign support structures with anchor rod stand off heights; and 60 years for four-chord box structures with grouted base plates. In general, all sign support structures should be inspected in detail during fabrication and once after erection. After the erection inspection, the structures should be inspected on a five year cycle. For tri-chord structures, this inspection cycle should drop to 2 years after the 15-year inspection. The inspections for these structures should focus on the diagonal web members. For four-chord structures with anchor rod stand-off, the inspection of the anchor rods should drop to two years after the 10-year inspection. Inspection intervals for the diagonal web members can continue on a 10-year cycle for these structures. However, after the 40-year inspection, it is recommended that the inspection interval drop to a 2-year cycle. For four-chord sign support structures with grouted bases, the inspection cycle can be 10 years for the first 40 years. After the 40-year inspection, the interval should drop to 2 years. The inspections for these structures should be focused on the diagonal web members in the overhead truss.

4.3 High-Mast-Luminaire Support Structures

There are several conclusions that one can draw regarding the analysis of the high-mast luminaire support structures considered in this study. Anchor bolt stand off heights have very little impact on the natural frequencies of the first five modes of vibration for both structures evaluated. Variation in base plate thickness has a greater impact than anchor rod stand-off height in causing the modal frequency (first five

modes) to deviate significantly from that of the fixed base condition. In general, computing modal frequencies using the fixed base assumption would cause very little error for the structures studied. If base plate thicknesses are 1-1/2 inches or greater, there is no concern. If base plate thicknesses become thinner than this threshold, higher-mode frequencies may differ considerably from the fixed base condition.

The four bolt anchor rod arrangement seen in HML-40-061 causes a 40% increase in the stress in the wall of the mast when bending is considered. This stress concentration should be considered when establishing stress ranges for the mast base fatigue detail as the 40% increase in tensile stress due to bending may cause damaging tensile stress cycles at lower wind loading. The reason for this is that it is likely that it will be easier for the bending stresses due to wind to overcome the compression stress at the base due to self-weight. The eight-anchor rod arrangement does not have a stress raiser condition and can simply be treated as a fixed base for stress computations.

The analytical study on the two structures considered suggests that vortex-shedding need not be considered for HML structures. The senior author personally watched HML-67-006 for nearly one hour in 25-35 mph measured winds. There was no across-wind vibration of the mast indicative of vortex-shedding vibrations. The equivalent projected area of the luminaire assembly and the ever decreasing shaft diameter makes first-mode vibration shapes dominant in the response.

The four-anchor-rod arrangement at the base of HML-40-061 results in significant bending stresses in the anchor rods. The magnitude of bending stress is significantly reduced in the eight anchor arrangement seen in HML-67-006. Therefore, it is suggested that the 4-anchor rod arrangements be avoided in HML structures. The 8-rod arrangement has a much smoother stress distribution at the base of the mast and the bending stresses in the anchor rods are alleviated.

Both HML structures studied have no difficulty in attaining their 50-year target service life with 95% confidence. The analysis of both structures ignored degradation of cross-section through corrosion. However, the 264 year fatigue life (in the case of HML-40-061) of the “perfect” anchor rod does leave some buffer.

It appears that the static design of the welds at the base of the HML should consider the stress concentration factor at the top of the plate when bending moments are applied to the base. This appears to be very important when checking the strength of welds and mast at the base. The study of HML-40-061 (four anchor rods) and HML-67-006 (eight anchor rods) suggest that this static stress concentration factor should be 2.4 and 3.1, respectively. A conservative value of 3.0 seems applicable to all HML structures.

4.4 General Conclusions and Recommendations for Future Research

There are some general conclusions that can be made regarding the results of this study. Of course, some must be refined with future research to solidify thinking, but the statements will hopefully provide direction for new research into these structures resulting in greater understanding of their behavior, greater understanding with regard to their design (*e.g.* required loading conditions), greater economy in their design, greater economy in their construction, and a reduced need for inspection leading to greater fiscal efficiency with public funding.

The bending of anchor rods in base plates with stand-off heights of both HML and sign support structures needs further study. It would be very useful to have experimental work done on anchors with significant bending in them (beyond the 1:40 out-of-plumb currently assumed). Furthermore, having statistical information regarding the fatigue life of these anchor conditions would also go a long way to improving design methodologies.

It appears that the fatigue design loading of 5.2 psf (assuming $C_d = 1.0$ and $I_F = 1.0$) found in (AASHTO 2001) is satisfactory for the metro-Milwaukee area. There is only a 1% chance that the wind speed will exceed a 50-mph mean wind (5-second averaging time) in Milwaukee, Wisconsin. Using equation (3-1) in the specifications (AASHTO 2001), the 50-mph mean wind equates to an approximate pressure of 6.4 psf with $C_d = K_z = I_r = 1.0$. Considering this loading magnitude as that required for infinite life with allowable stress ranges less than $1/2 \cdot CAFL$ for category *ET* and E' details, may result in details being very difficult to successfully design. A more detailed study of the infinite life fatigue design approach for sign and luminaire support structures needs to be undertaken.

The research team strongly believes that if a structure is inspected with great detail during fabrication (*e.g.* immediately after galvanizing) and immediately after erection with no flaws being found, the structure can likely be put into service with inspection intervals much longer than 2-year cycles. This statement holds for both full-span and high-mast luminaire support structures. If galvanizing of anchor rods is conducted with every structure and the bending stresses in the anchor rods are minimized, degradation of cross-section through corrosion would be minimized and attaining and inspection-free structure is truly possible. The tri-chord configuration has been shown to have a reduced fatigue life when compared to the four-chord configuration and therefore, it should be utilized with less sign area that that of S-40-156 considered in this study.

One could likely tailor a standard design to more closely match the intended 50-year service life rather than arbitrarily designing for infinite life. This would likely lead to more economy and greater

efficiency. Of course this would require statistical information specific to the details used in these structures rather than the blanket AASHTO (one-size-fits-all) detail categories.

In general, a better understanding of the statistical variability in the fatigue life of typical details found in sign and luminaire support structures would go a long way to more fully understanding why these structures have had questionable in-service performance and more importantly, why others have had stellar in-service performance records.

Last, but certainly not least, a better understanding of the galvanizing process and its effect on high-strength steels, welded connections, and the impact of partial dip galvanizing on welded truss structures is required. This wil help in understanding exactly why poor in-service performance has been obtained for some structures and the apparent link to the galvanizing process and fabrication.

This Page Intentionally Left Blank

References

1.) AASHTO. (1985). *Standard Specifications for Structural Supports for Highway Signs, Luminaires and Traffic Signals*, American Association of State Highway Transportation Officials, Washington, D.C.

2.) AASHTO. (1994). *Standard Specifications for Structural Supports for Highway Signs, Luminaires and Traffic Signals*, American Association of State Highway and Transportation Officials, Washington, D.C.

3.) AASHTO. (1996). *Standard Specifications for Highway Bridges*, American Association of State Highway and Transportation Officials, Washington, D.C.

4.) AASHTO. (1998). *LRFD Specifications for Highway Bridges*, American Association of State Highway and Transportation Officials, Washington, D.C.

5.) AASHTO. (2000). *Standard Specifications for Structural Supports for Highway Signs, Luminaires and Traffic Signals*, American Association of State Highway and Transportation Officials, Washington, D.C.

6.) AASHTO. (2001). *Standard Specifications for Structural Supports for Highway Signs, Luminaires and Traffic Signals, 4th Edition*, American Association of State Highway and Transportation Officials, Washington, D.C.

7.) AGA. (2000a). *The Design of Products to be Hot-Dip Galvanized After Fabrication*, American Galvanizers Association, Englewood, CO.

8.) AGA. (2000b). *Hot-Dip Galvanizing for Corrosion Protection of Steel Products*, American Galvanizers Association, Englewood, CO.

9.) AGA. (2001). *The Inspection of Products to be Hot-Dip Galvanized After Fabrication: Including a New Section on Touch-Up and Repair*, American Galvanizers Association, Englewood, CO.

10.) ASCE. (1998). *Minimum Design Loads for Buildings and Other Structures (ASCE 7-98)*, American Society of Civil Engineers, Reston, VA.

11.) ASTM. (1998). “Standard Practice for Verification fo Constant Amplitude Dynamic Forces in Axial Fatigue Testing System - ASTM Standard E 467-98a.”, ASTM, West Conshohocken, PA, 10.

12.) ASTM. (1999). “Standard Practice for Verification of Specimen Alignment Under Tensile Loading - ASTM Standard E 1012-99.”, ASTM, West Conshohocken, PA, 8.

13.) ASTM. (2002). “Standard Practice for Conducting Force Controlled Constant Amplitude Axial Fatigue Testing of Metallic Materials - ASTM Standard E 466-06.”, ASTM, West Conshohocken, PA, 8.

14.) AWS. (1999). *Structural Welding Code - Steel, 17th Edition (ANSI/AWS D1.1-98)*, American Welding Society, Miami, FL.

15.) Bannantine, J.A., Comer, J.J., and Handrock, J.L. (1990). *Fundamentals of Metal Fatigue Analysis*, Prentice Hall, New Jersey.

16.) Bigot, R., and Iost, A. (1999). “Residual Stresses in Galvanizing.” *Materials and Manufacturing Processes*, 14 (3), Marcel Dekker, Inc., 413-426.

17.) Blevins, R. (1990). *Flow Induced Vibrations, 2nd Edition*, Van Nostrand Reinhold, New York, NY.

18.) Buchholdt, H. (1997). *Structural Dynamics for Engineers*, Thomas Telford Publications, London, U.K.

19.) Chavez, J.W., Gilani, A.S., and Whittaker, A.S. (1997). “Fatigue-Life Evaluation of Changeable Message Sign Structures, Volume 2 - Retrofitted Structures.” *Report No. UCB/EERC-97/10*, Earthquake Engineering Research Center, University of California, Berkeley, CA.

20.) Cook, R.A., Bloomquist, D., Agosta, A.M., and Taylor, K.F. (1996). “Wind Load Data for Variable Message Signs.” *FL/DOT/RMC/0728-9488*, Florida Department of Transportation.

21.) Creamer, B.M., Frank, K.H., and Klingner, R.E. (1979). “Fatigue Loading of Cantilever Sign Structures from Truck Wind Gusts.” *FHWA/TX-79/10+209-1F*, Center for Highway Research, University of Texas - Austin, Austin, TX.

22.) Cresdee, R.B., Edwards, W.J., Thomas, P.J., and Voss, G.F. (1993). "Analysis of Beam Distortion During Hot Dip Galvanizing." *Materials Science and Technology*, 9 (February), Institute of Metals, London, 161-167.

23.) Davenport, A.G. (1961a). "Applications of Statistical Concepts to the Wind Loading of Structures." *Proceedings of the Institute of Civil Engineers*, 19, 449-472.

24.) Davenport, A.G. (1961b). "The Spectrum of Horizontal Gustiness Near the Ground in High Winds." *Journal of the Royal Meteorological Society*, 87, 194-211.

25.) Den Hartog, J.P. (1956). *Mechanical Vibrations, 4th Edition*, McGraw-Hill, Inc. (now Dover Publications 1985), New York, NY.

26.) DeSantis, P.V., and Haig, P.E. (1996) "Unanticipated Loading Causes Highway Sign Failure." *ANSYS Convention*, ANSYS Inc., 3.99-3.108.

27.) Dexter, R.J., and Ricker, M.J. (2002). *Fatigue-Resistant Design of Cantilevered Signal, Sign, and Light Supports*, NCHRP Report 469, Transportation Research Board - National Research Council, Washington, D.C.

28.) Durst, C.S. (1960). "Wind Speeds Over Short Periods of Time." *The Meteorological Magazine* (608), 181-186.

29.) Dusel, J.P. (1984). "Determination of Fatigue Characteristics of Hot-Dipped Galvanized A307 and A449 Anchor Bars and A325 Cap Screws.", State of California Department of Transportation Division of Engineering Services, Sacramento.

30.) Dyrbye, C., and Hansen, S.O. (1997). *Wind Loads on Structures*, John Wiley & Sons Ltd., Chichester.

31.) Edwards, J.A., and Bingham, W.L. (1984). "Deflection Criteria for Wind Induced Vibrations in Cantilever Highway Sign Structures." *North Carolina Department of Transporation FHWA/NC/84-001*, Center for Transportation Engineering Studies, North Carolina State University, Rayleigh, NC.

32.) Engtsrom, M. 2003. Cracking in Coped Beam Flange Region, (personal communication with) Foley, C.M.

33.) Fish, P.E. (1994) "NDT Applications in a Successful Fracture Critical Bridge Inspection Program." *Structural Materials Technology - An NDT Conference*, 219-227.

34.) Fish, P.E. (1995) "NDT Applications in a Successful Fracture Critical Bridge Inspection Program and Anchor Bolt Inspection Program." *Proceedings of the SPIE*, Society Photo-Optical and Instrumentation Engineering, 149-165.

35.) Fish, P.E. (1997a). "Inspection Report: S-40-189.", Wisconsin Department of Transportation, Madison, WI.

36.) Fish, P.E. (1997b). "Sign Bridge Inspection Report: S-18-44.", Wisconsin Department of Transportation, Madison, WI.

37.) Fish, P.E. (1998). "Evaluation of Cor-Ten Steel Lightpoles with Addendum A.", Wisconsin Department of Transportation, Madison, WI.

38.) Fish, P.E. (1999). "NDT Applications in a Successful Fracture Critical Bridge Inspection Program.", Wisconsin Department of Transportation.

39.) Fisher, J. 2003. Sign Support Cracking in Connecticut, (personal communication with) Foley, C.M.

40.) Fisher, J.W. (1981). "Fatigue Behavior of Steel Light Poles." *FHWA/CA/SD-81-82*, California Department of Transportation, Sacramento, CA.

41.) Fisher, J.W., Kulak, G.W., and Smith, I.F.C. (1998). *A Fatigue Primer for Structural Engineers*, American Institute of Steel Constrution, National Steel Bridge Alliance, Chicago, IL.

42.) Fisher, J.W., Miki, C., Slutter, R.G., Mertz, D.R., and Frank, W. (1983). "Fatigue Strength of Steel Pipe-Base Plate Connections." *Engineering Structures*, 5 (April), 90-96.

43.) Fouad, F.H., Calvert, E.A., and Nunez, E. (1998). "Structural Supports for Highway Signs, Luminaires, and Traffic Signals." *National Cooperative Highway Research Program, Report 411*, Transportation Research Board, National Research Council, Washington, D.C.

44.) Frank, K.H. (1980). "Fatigue Strength of Anchor Bolts." *Journal of Structural Division, ASCE*, 106 (ST6).

45.) Fuchs, H.O., and Stephens, R.I. (1980). *Metal Fatigue in Engineering*, John Wiley & Sons, Inc., New York, NY.

46.) Gilani, A., and Whittaker, A. (2000a). "Fatigue-Life Evaluation of Steel Post Structures. I: Background and Analysis." *Journal of Structural Engineering*, 126 (3), 322-330.

47.) Gilani, A., and Whittaker, A. (2000b). "Fatigue-Life Evaluation of Steel Post Structures. II: Experimentation." *Journal of Structural Engineering*, 126 (3), 331-340.

48.) Gilani, A.S., Chavez, J.W., and Whittaker, A.S. (1997). "Fatigue-Life Evaluation of Changeable Message Sign Structures, Volume 1 - As Built Structures." *Report No. UCB/EERC-97/10*, Earthquake Engineering Research Center, University of California, Berkeley, CA.

49.) Ginal, S.J. (2003). "Fatigue Performance of Full-Span Sign Support Structures Considering Truck-Induced Gust and Natural Wind Pressures," MS Thesis, Marquette University, Milwaukee, WI.

50.) Iannuzzi, A., and Spinelli, P. (1987). "Artificial Wind Generation and Structural Response." *Journal of Structural Engineering*, 113 (12), ASCE, 2382-2398.

51.) Irvine, T. (1999a). "Schock and Vibration Response Spectra Course: Unit 6A - The Fourier Transform.", Vibration Data Publications.

52.) Irvine, T. (1999b). "Schock and Vibration Response Spectra Course: Unit 7A - Power Spectral Density Function.", Vibration Data Publications.

53.) Irvine, T. (1999c). "Schock and Vibration Response Spectra Course: Unit 12 - Synthesizing a Time History to Satisfy a Power Spectral Density Using Sinusoids.", Vibration Data Publications.

54.) Irwin, H.P., and Peeters, M. (1980). "An Investigation of the Aerodynamic Stability of Slender Sign Bridges, Calgary." *LTR-LA-246*, National Research Council Canada - Aeronautical Establishment.

55.) Johns, K., and Dexter, R. (1998a). "Fatigue Testing and Failure Analysis of Aluminum Luminaire Support Structures." *98-06*, Center for Advanced Technology for Large Structural Systems, Lehigh University, Bethlehem, PA.

56.) Johns, K., and Dexter, R.J. (1998b). "Fatigue Related Wind Loads on Highway Support Structures." *98-03*, Center for Advanced Technology for Large Structural Systems, Lehigh University, Bethlehem, PA.

57.) Johns, K.W., and Dexter, R.J. (1998c). "The Development of Fatigue Design Load Ranges for Cantilevered Sign and Signal Support Structures." *Journal of Wind Engineering and Industrial Aerodynamics*, 77 & 78 (Sep-Dec), 315-326.

58.) Johns, K.W., and Dexter, R.J. (1999) "Truck Induced Wind Loads on Highway Sign Support Structures." *Structural Engineering in the 21st Century, Proceedings of the 1999 Structures Congress*, Avent, R.R. and Alawady, M.,Ed., New Orleans, LA, April 18-21, American Society of Civil Engineers - Structural Engineering Institute, 1103-1106.

59.) Kaczinski, M.R., Dexter, R.J., and Van Dien, J.P. (1998). "Fatigue Resistance Design of Cantilevered Signal, Sign and Light Supports." *(NCHRP Report 412 - Project 10-38)*, ATLSS Engineering Research Center, Bethlehem, PA.

60.) Kaimal, J.C. (1972). "Spectral Characteristics of Surface-Layer Turbulence." *Journal of the Royal Meteorological Society*, 98, 563-589.

61.) Kashar, L., Nester, M.R., Johns, J.W., Hariri, M., and Freizner, S. (1999) "Analysis of the Catastrophic Failure of the Support Structure of a Changeable Message Sign." *Structural Engineering in the 21st Century, Proceedings of the 1999 Structures Congress*, Avent, R.R. and Alawady, M.,Ed., New Orleans, LA, April 18-21, American Society of Civil Engineers - Structural Engineering Institute, 1115-1118.

62.) Keating, P.B., and Fisher, J.W. (1986a). "Evaluation of Fatigue Tests and Design Criteria on Welded Details." *NCHRP Report 286*, National Cooperative Highway Research Program, Washington, DC.

63.) Keating, P.B., and Fisher, J.W. (1986b). "Fatigue Resistance Design of Cantilevered Signal, Sign and Light Supports." *(NCHRP Report 286 - Project xx-xx)*, ATLSS Engineering Research Center, Bethlehem, PA.

64.) Kwok, K.C.S. (1985). "Dynamics of a Freestanding Steel Lighting Tower." *Engineering Structures*, 7 (Jan.), 46-50.

65.) Levy, R. (1996). *Structural Engineering of Microwave Antennas*, Institute of Electrical and Electronic Engineers, Inc., New York, NY.

66.) Liu, H. (1991). *Wind Engineering: A Handbook for Structural Engineers*, Prentice Hall, Inc., Englewood Cliffs, NJ.

67.) McDonald, J.R., Mehta, K.C., Oler, W., and Pulipaka, N. (1995). "Wind Load Effects on Signs, Luminaires and Traffic Signal Structures." *Texas Department of Transportation Report No. 1303-1F*, Wind Engineering Research Center - Texas Tech University, Lubbock, TX.

68.) Milford, R.V. (1989). "Gust Loading Factors for Lighting Masts." *Engineering Structures*, 11 (April), 62-67.

69.) Miner, M.A. (1945). "Cumulative Damage in Fatigue." *Transaction of the ASME, Journal of Applied Mechanics*, 67, A159-A164.

70.) Moses, F., Schilling, C.G., and Raju, K.S. (1987). "Fatigue Evaluation Procedures for Steel Bridges." *NCHRP Report 299*, National Cooperative Highway Research Program, Washington, DC.

71.) Novak, M. (1969). "Aeroelastic Galloping of Prismatic Bodies." *Journal of the Engineering Mechanics Division*, 95 (EM1), ASCE, 115-142.

72.) Novak, M. (1972). "Galloping Oscillations of Prismatic Structures." *Journal of the Engineering Mechanics Division*, 98 (EM1), ASCE, 27-46.

73.) Novak, M., and Davenport, A.G. (1970). "Aeroelastic Instability of Prisms in Turbulent Flow." *Journal of the Engineering Mechanics Division*, 96 (EM1), ASCE, 17-39.

74.) Novak, M., and Tanaka, H. (1974). "Effect of Turbulence on Galloping Instability." *Journal of the Engineering Mechanics Division*, 100 (EM1), ASCE, 27-47.

75.) Nowak, A.S., and Collins, K.R. (2000). *Reliability of Structures*, McGraw-Hill.

76.) ONT. (1992). *Ontario Bridge Design Code*, Ottawa.

77.) Peronto, J.L. (2003). "High-Cycle Constant Amplitude Fatigue Life Variability of Welded Round HSS Y-Joints," MS Thesis, Marquette University, Milwaukee, WI.

78.) Rahimian, A., and Sifre, P. (1993) "Vortex Shedding Induced Fatigue Fracture of Mast Tower." *Structural Engineering in Natural Hazards Mitigation*, Ang, A.H.-S. and Villaverde, R.,Ed., Irvine, CA, April 19-21, American Society of Civil Engineers, 585-597.

79.) Repetto, M.P., and Solari, G. (2001). "Dynamic Alongwind Fatigue of Slender Vertical Structures." *Engineering Structures*, 23, 1622-1633.

80.) SAS. (2003a). “ANSYS 7.0 Element Library & Theory Reference.”, SAS IP, Inc.

81.) SAS. (2003b). ANSYS 7.0 Structural Analysis Guide, SAS IP, Inc., Houston, PA.

82.) Shinozuka, M., and Jan, C. (1972). “Digital Simulation of Random Processes and Its Applications.” *Journal of Sound and Vibration*, 25 (1), 111-128.

83.) Simiu, E., and Scanlon, R.H. (1996). *Wind Effects on Structures: Fundamentals and Applications to Design - 3rd Edition*, John Wiley & Sons, Inc., New York, NY.

84.) South, J. (1994). “Fatigue Analysis of Overhead Sign and Signal Structures.” *FHWA/IL/PR-115*, Illinois Department of Transportation, Springfield, IL.

85.) Thomson, W.T., and Dahleh, M.D. (1998). *Theory of Vibration with Applications, 5th Edition*, Prentice Hall, Inc., Upper Saddle River, NJ.

86.) Van Dien, J.P., Kaczinski, M.R., and Dexter, R.J. (1996) “Fatigue Testing of Anchor Bolts.” *Structures Congress XIV*Chicago, IL, American Society of Civil Engineers.

87.) Zettlemoyer, N., and Fisher, J.W. (1977). “Stress Gradient Correction Factor for Stress Intensity at Welded Stiffeners and Cover Plates.” *Welding Journal*, 56 (12), James F. Lincoln Arc Welding Foundation, 3938-3985.

Appendix A

Analytical Model Summaries

This appendix contains all information regarding the finite element models used in the present study. All models were generated using dimensional information contained WisDOT design drawings (and shop drawings if available) for the structure numbers indicated.

All FE models were created in the ANSYS Finite Element Analysis System and element types, material data, etc..., are consistent with the nomenclature found in this commercially available software.

A.1 Analytical Model Summary: S-40-404

GENERAL STRUCTURE INFORMATION:	
Sign Bridge Designation:	**S-40-404**
Span (between upright CL's):	**106'-3"**
Number of Truss Sections:	**3**
Section 1 Panel Point Spacing:	**9 panels @ 3'-9 2/3"**
Section 2 Panel Point Spacing:	**10 panels @ 3'-4 7/10"**
Section 3 Panel Point Spacing:	**9 panels @ 3'-9 2/3"**
Truss Depth:	**3'-9"**
Truss Width:	**3'-6"**
Material Type:	**Steel**
North (East) Upright Height:	**25'-0 3/4"**
Panel Point Spacing:	**5 panels @ 4'-7 7/8"**
South (West) Upright Height:	**22'-11 1/2"**
Panel Point Spacing:	**5 panels @ 4'-2 15/16"**
Sign Type:	**VMS**
Number of Sign & Catwalk Supports:	**9**

TRUSS & UPRIGHT MODEL INFORMATION:	
Truss Web Members:	
Element Type:	**PIPE16**
Real Constant:	**1**
Material Model:	**1**
Truss Chords:	
Element Type:	**PIPE16**
Real Constant:	**2**
Material Model:	**1**
South Uprights:	
Element Type:	**PIPE16**
Real Constant:	**3**
Material Model:	**1**
North Uprights:	
Element Type:	**PIPE16**
Real Constant:	**4**
Material Model:	**1**
Upright Web Members:	
Element Type:	**PIPE16**
Real Constant:	**5**
Material Model:	**1**
WT "Seat":	
Element Type:	**BEAM4**
Real Constant:	**6**
Material Model:	**1**

GENERAL MODEL INFORMATION:	
Number of Element Types:	**3**
Elements Used:	**PIPE16, BEAM4, SHELL63**
Number of Real Constants:	**10**
Number of Material Models:	**3**
Element Type 1:	**PIPE16**
Element Type 2:	**BEAM4**
Element Type 3:	**SHELL63**
Real Constant 1:	**1.625"o.d. x 0.140" wall (pipe)**
Real Constant 2:	**6.625"o.d. x 0.188" wall (pipe)**
Real Constant 3:	**8.625"o.d. x 0.219" wall (pipe)**
Real Constant 4:	**10.75"o.d. x 0.188" wall (pipe)**
Real Constant 5:	**2.375"o.d. x 0.154" wall (pipe)**
Real Constant 6:	**WT6x13**
Real Constant 7:	**thickness = 1/2" (VMS)**
Real Constant 8:	**W6x9**
Real Constant 9:	**thickness = 1" (grating)**
Real Constant 10:	**A=1/4in^2, Izz=Iyy=12in^4 (stiffeners)**
Material Model:	**1**
Young's Modulus:	**29e6 psi**
Poisson's Ratio:	**0.3**
Density:	**7.3e-4 lb-s^2/in^4**
Material Model:	**2**
Young's Modulus:	**29e6 psi**
Poisson's Ratio:	**0.3**
Density:	**1.8e-4 lb-s^2/in^4**
Material Model:	**3**
Young's Modulus:	**29e6 psi**
Poisson's Ratio:	**0.3**
Density:	**0**

SIGN MODEL INFORMATION:	
VMS Box:	
Element Type:	**SHELL63**
Real Constant:	**7**
Material Model:	**2**
Sign & Catwalk Supports:	
Element Type:	**BEAM4**
Real Constant:	**8**
Material Model:	**1**

CATWALK MODEL INFORMATION:	
Grating:	
Element Type:	**SHELL63**
Real Constant:	**9**
Material Model:	**2**
Catwalk Stiffeners:	
Element Type:	**BEAM4**
Real Constant:	**10**
Material Model:	**3**

A.2 Analytical Model Summary; S-67-402

GENERAL STRUCTURE INFORMATION:	
Sign Bridge Designation:	**S-67-402**
Span (between upright CL's):	**71'-3"**
Number of Truss Sections:	**2**
Section 1 Panel Point Spacing:	**9 panels @ 3'-9 15/16"**
Section 2 Panel Point Spacing:	**9 panels @ 3'-9 15/16"**
Truss Depth:	**3'-6"**
Truss Width:	**3'-6"**
Material Type:	**Steel**
North (East) Upright Height:	**19'-8 3/4"**
Panel Point Spacing:	**4 panels @ 4'-6 1/8"**
South (West) Upright Height:	**21'-7 1/2"**
Panel Point Spacing:	**5 panels @ 3'-11 7/8"**
Sign Type:	**VMS**
Number of Sign & Catwalk Supports:	**8**

TRUSS & UPRIGHT MODEL INFORMATION:	
Truss Diagonals:	
Element Type:	**PIPE16**
Real Constant:	**1**
Material Model:	**1**
Truss Struts:	
Element Type:	**PIPE16**
Real Constant:	**2**
Material Model:	**1**
Truss Chords:	
Element Type:	**PIPE16**
Real Constant:	**3**
Material Model:	**1**
Uprights:	
Element Type:	**PIPE16**
Real Constant:	**4**
Material Model:	**1**
Upright Web Members:	
Element Type:	**PIPE16**
Real Constant:	**5**
Material Model:	**1**
WT "Seat":	
Element Type:	**BEAM4**
Real Constant:	**6**
Material Model:	**1**

NORTH UPRIGHT BASE PLATE MODEL INFORMATION:	
Base Plate:	
Element Type:	**SHELL63**
Real Constant:	**9**
Material Model:	**1**
Anchor Bolts:	
Element Type:	**BEAM4**
Real Constant:	**10**
Material Model:	**1**

GENERAL MODEL INFORMATION:	
Number of Element Types:	**3**
Elements Used:	**PIPE16, BEAM4, SHELL63**
Number of Real Constants:	**12**
Number of Material Models:	**3**
Element Type 1:	**PIPE16**
Element Type 2:	**BEAM4**
Element Type 3:	**SHELL63**
Real Constant 1:	**1.625"o.d. x 0.140" wall (pipe)**
Real Constant 2:	**1.3125"o.d. x 0.133" wall (pipe)**
Real Constant 3:	**4.5"o.d. x 0.188" wall (pipe)**
Real Constant 4:	**8.625"o.d. x 0.188" wall (pipe)**
Real Constant 5:	**1.875"o.d. x 0.200" wall (pipe)**
Real Constant 6:	**WT6x13**
Real Constant 7:	**W6x9**
Real Constant 8:	**thickness = 1/2" (VMS)**
Real Constant 9:	**1" thick base plate**
Real Constant 10:	**1 1/2" dia. anchor bolts**
Real Constant 11:	**thickness = 1" (grating)**
Real Constant 12:	**A=1/4in^2, Izz=Iyy=12in^4 (stiffeners)**
Material Model:	**1**
Young's Modulus:	**29e6 psi**
Poisson's Ratio:	**0.3**
Density:	**7.3e-4 lb-s^2/in^4**
Material Model:	**2**
Young's Modulus:	**29e6 psi**
Poisson's Ratio:	**0.3**
Density:	**1.8e-4 lb-s^2/in^4**
Material Model:	**3**
Young's Modulus:	**29e6 psi**
Poisson's Ratio:	**0.3**
Density:	**0**

SIGN MODEL INFORMATION:	
VMS Box:	
Element Type:	**SHELL63**
Real Constant:	**8**
Material Model:	**2**
Sign & Catwalk Supports:	
Element Type:	**BEAM4**
Real Constant:	**7**
Material Model:	**1**

CATWALK MODEL INFORMATION:	
Grating:	
Element Type:	**SHELL63**
Real Constant:	**11**
Material Model:	**2**
Catwalk Stiffeners:	
Element Type:	**BEAM4**
Real Constant:	**12**
Material Model:	**3**

A.3 Analytical Model Summary; S-40-156

GENERAL STRUCTURE INFORMATION:	
Sign Bridge Designation:	**S-40-156**
Span (between upright CL's):	**67'-2"**
Number of Truss Sections:	**2**
Section 1 Panel Point Spacing:	**9 panels @ 3'-7 1/8"**
Section 2 Panel Point Spacing:	**9 panels @ 3'-7 1/8"**
Truss Depth:	**3'-6"**
Truss Width:	**3'-0 3/8"**
Material Type:	**Steel**
North (East) Upright Height:	**19'-0 3/4"**
Panel Point Spacing:	**4 panels @ 4'-6 1/4"**
South (West) Upright Height:	**21'-8 3/4"**
Panel Point Spacing:	**5 panels @ 4'-1 13/16"**
Sign Type:	**Type I**
Number of Sign & Catwalk Supports:	**7**

TRUSS & UPRIGHT MODEL INFORMATION:	
Truss Vertical Diagonals:	
Element Type:	**PIPE16**
Real Constant:	**1**
Material Model:	**1**
Truss Slanted Diagonals:	
Element Type:	**PIPE16**
Real Constant:	**2**
Material Model:	**1**
Truss Struts:	
Element Type:	**PIPE16**
Real Constant:	**3**
Material Model:	**1**
Truss Chords:	
Element Type:	**PIPE16**
Real Constant:	**4**
Material Model:	**1**
Uprights:	
Element Type:	**PIPE16**
Real Constant:	**5**
Material Model:	**1**
Upright Webs:	
Element Type:	**PIPE16**
Real Constant:	**6**
Material Model:	**1**
WT "Seat":	
Element Type:	**BEAM4**
Real Constant:	**7**
Material Model:	**1**

CATWALK MODEL INFORMATION:	
Grating:	
Element Type:	**SHELL63**
Real Constant:	**10**
Material Model:	**2**

GENERAL MODEL INFORMATION:	
Number of Element Types:	**3**
Elements Used:	**PIPE16, BEAM4, SHELL63**
Number of Real Constants:	**11**
Number of Material Models:	**4**
Element Type 1:	**PIPE16**
Element Type 2:	**BEAM4**
Element Type 3:	**SHELL63**
Real Constant 1:	**1.660"o.d. x 0.140" wall (pipe)**
Real Constant 2:	**1.900"o.d. x 0.145" wall (pipe)**
Real Constant 3:	**1.315"o.d. x 0.133" wall (pipe)**
Real Constant 4:	**5.563"o.d. x 0.219" wall (pipe)**
Real Constant 5:	**10.750"o.d. x 0.188" wall (pipe)**
Real Constant 6:	**2.375"o.d. x 0.218" wall (pipe)**
Real Constant 7:	**WT6x13**
Real Constant 8:	**W6x9**
Real Constant 9:	**thickness = 1/4" (Type I sign)**
Real Constant 10:	**thickness = 1" (grating)**
Real Constant 11:	**A=1/4in^2, Izz=Iyy=12in^4 (stiffeners)**
Material Model:	**1**
Young's Modulus:	**29e6 psi**
Poisson's Ratio:	**0.30**
Density:	**7.3e-4 lb-s^2/in^4**
Material Model:	**2**
Young's Modulus:	**29e6 psi**
Poisson's Ratio:	**0.30**
Density:	**1.8e-4 lb-s^2/in^4**
Material Model:	**3**
Young's Modulus:	**10e6 psi**
Poisson's Ratio:	**0.35**
Density:	**2.536e-4 lb-s^2/in^4**
Material Model:	**4**
Young's Modulus:	**29e6 psi**
Poisson's Ratio:	**0.30**
Density:	**0**

SIGN MODEL INFORMATION:	
Type I Sign:	
Element Type:	**SHELL63**
Real Constant:	**9**
Material Model:	**3**
Type I Sign Stiffeners:	
Element Type:	**BEAM4**
Real Constant:	**11**
Material Model:	**4**
Sign & Catwalk Supports:	
Element Type:	**BEAM4**
Real Constant:	**8**
Material Model:	**1**

Appendix B

Literature Review

B.1 Introduction

This appendix contains a complete review of the body of literature related to overhead sign and luminaire support structures. The review contains a variety of literature sources (*e.g.* research reports, journal articles, conference proceedings) and it is intended to end with the 2001 calendar year. It is recognized that a "flurry" of research activity has taken place since 2001, but this literature review, unfortunately, had to have an ending point.

B.2 Sign Support Structure Research

This segment of the chapter contains a literature review of past research related to sign support structures. The review is organized chronologically so as to offer insight to how past research efforts have laid the groundwork for subsequent studies, including the present research effort. The review is fairly detailed so that the present research effort can be properly tailored to add to the present body of literature as well as to justify the scope and direction of the present research effort.

Creamer et al. (1979)

This research report outlines an experimental and analytical study aimed at quantifying the loading applied to cantilevered sign support structures resulting from truck-induced pressure gusts and this type of structures' fatigue response to this loading. The end result of the study was recommendation of a procedure for designing cantilevered highway sign support structures for truck-induced gust pressure.

A field study was conducted to determine both the vibrational characteristics of the sign support structures being evaluated as well as these structures' response to various truck-induced gust events. Three cantilevered sign supports were instrumented with strain gauges located on the web members and the chords of the cantilevered truss structure. Manual excitation of the truss structure in both the horizontal (out-of-plane) and vertical (in-plane) directions and the corresponding strain gauge readings were used to estimate the natural frequency and inherent damping ratio of the support structure in these modes of vibration. The estimated damping ratios included aerodynamic damping present due to the buffeting of the supported sign through the air.

The experimentally determined horizontal and vertical damping ratios for the three sign support structures were both found to be relatively low (*e.g.* 0.40 % to 1.11 % of critical).

The member forces obtained experimentally were used to calibrate an analytical model of the sign structure and to develop an analytical loading function. Computed member forces from the analytical model for a specified loading function were compared to the experimentally obtained member forces resulting from truck gust events. This function was adjusted until the computed member forces were acceptably close to the experimentally obtained values. A pressure pulse due to passing trucks was developed using both an assumed triangular pulse as well as standard equations expressing pressure as a function of velocity. The resulting truck gust pressure loading function is shown in Figure B.1. The peak pressure of 1.23 psf and the pulse duration of 0.375 sec are notable characteristics of this truck-induced pressure pulse.

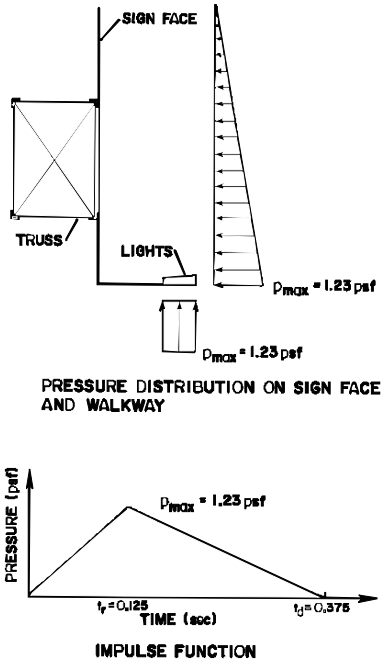

Figure B.1: Pressure Distribution and Impulse Forcing Function Resulting from Truck-Induced Gust Loading (Creamer *et al.* 1979).

A few important conclusions were drawn from the results of this study. One conclusion was that truck-induced gusts likely produce a significant cantilevered sign support response, which is in the form of a large number of stress ranges for each truck event. This is due in part to the relatively low inherent damping in these structures. However, the report also concluded that stress ranges measured in the superstructure of the sign support (*e.g.* web and chord truss

members) due to the truck-induced gusts are low and do not present a fatigue problem. Finally, fatigue design of the sign support structures for the truck-induced pressure loading can be accomplished by using either a static analysis and a pressure of 1.25 psf multiplied by an appropriate dynamic load factor (DLF), or it can be accomplished by conducting a dynamic analysis and using the computed triangular truck gust loading function directly.

Irwin and Peeters (1980)

This research effort evaluated the vibration and aerodynamic characteristics of monotube overhead sign support structures through the use of both field measurements and wind tunnel studies. A schematic drawing illustrating the type of sign support structure evaluated is shown in Figure B.2. Figure B.3 illustrates the wind tunnel model used to establish the aerodynamic characteristics of the sign and support.

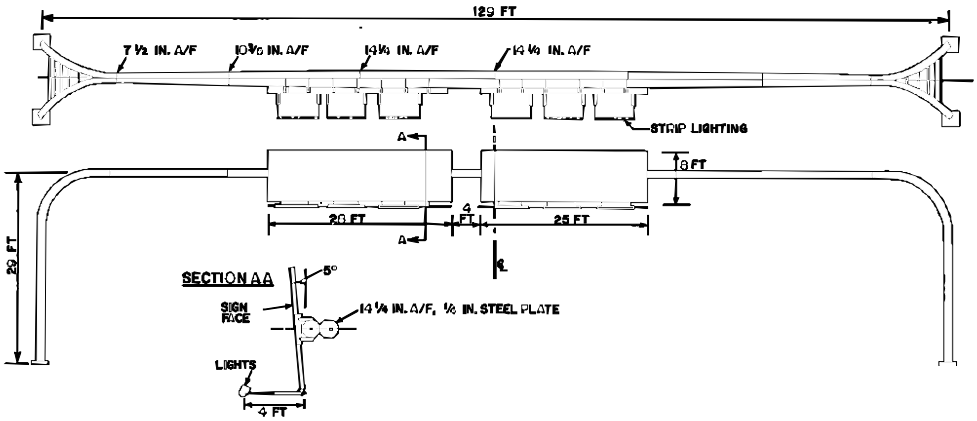

Figure B.2: Monotube Sign Support Structure Configuration (Irwin and Peeters 1980).

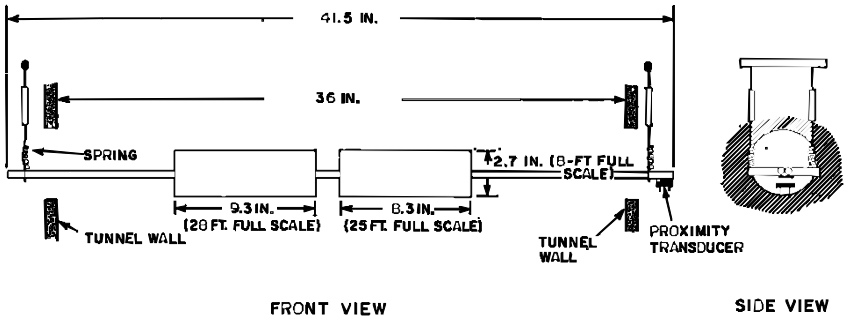

Figure B.3: Wind Tunnel Model of Monotube Sign Support Structure (Irwin and Peeters 1980).

A field investigation was conducted to determine natural frequencies and inherent damping. The field measurements indicated the following:

Bridge Spans Instrumented:	115 ft. to 145 ft. (non-uniform increments)
Natural (Inherent) Damping:	0.161 % to 0.276 % (with respect to critical)
Natural Frequency (Hz):	0.797 to 1.106

The horizontal (out-of-plane) aerodynamic damping was measured to be 0.595% of critical. The efforts behind the wind tunnel study were aimed at determining the aerodynamic stability of the sign bridge. The sign structure modeled was a dual octagonal tube with a 129-foot span and multiple signs mounted along the span (refer to Figures B.2 and B.3). The wind tunnel tests revealed a strong tendency for vortex-shedding induced oscillations. Therefore, further investigation focused on the following: (a) finding a level of damping that would suppress these oscillations; and (b) developing aerodynamic devices to counter vortex shedding induced vibrations.

Several observations and conclusions were drawn. Reducing the solidity of the sign was found to have a beneficial effect on the aerodynamic behavior of the structure. If 30-40% of the sign area was open, no significant oscillations occurred. However, in practical applications reducing the solidity of the sign is not permissible. Conversely, it was found that boxing in the back of the sign structure was found to have a negative effect on the aerodynamic behavior of the structure. It should be noted that Variable Message Signs (VMS) are already in the "boxed" configuration, and therefore, a support structure may be more susceptible to vortex shedding-induced vibrations. These two examples expose the importance of a structure's cross-section as it relates to the structure's susceptibility to vortex shedding. The wind tunnel testing concluded that a damping ratio of 1.8% of critical is sufficient to eliminate vortex shedding-induced vibrations for this particular sign bridge. Therefore, an airfoil configuration was recommended to provide additional aerodynamic damping to the support structure.

Edwards and Bingham (1984)

This study focused on wind loading and dynamic response of cantilevered truss sign support structures. The study included experimental work on existing structures, wind tunnel studies, and analytical efforts geared toward quantifying truss structure response. Wind tunnel models were used to evaluate the vortex shedding characteristics of the two-chord cantilever truss configuration. The wind tunnel experiments revealed a Strouhal number equal to 0.196, which is similar to a value of 0.20 for a circular cylinder.

Lock-in velocity ranges were found for both the circular cylinder and the two-chord configuration. A simulated cantilevered truss model was also studied in the wind tunnel. A

Strouhal number equal to 0.201 was determined for this configuration. An attempt was made to attach a flat plate to the truss model in order to simulate a sign. However, this plate attachment significantly altered the model behavior such that the wind tunnel could not develop the velocity necessary to excite vibration. This may suggest that the sign support structure is not susceptible to vortex shedding-induced vibrations when the sign is present. However, it is apparent in the report that the lack of vibration could have resulted from difficulties encountered in wind-tunnel modeling.

The study also attempted to measure the wind pressure that results from vehicular-induced wind gusts. The testing was done using hot film anemometer patches. A sign was instrumented with these "patches" located on both sides of the sign at the top corner near the vertical column support on both side of the sign. The location of the patches was less than ideal since they were not directly over the main vehicular traveling lanes, and the instrumented sign support was located over an exit ramp lane. The maximum pressure recorded on the sign due to vehicular-induced gusts was 1.41 psf. This is consistent with past research efforts (Creamer *et al.* 1979).

A theoretical investigation of wind loading on sign structures was also undertaken. The study was specifically set up to address the time-varying component of the wind pressure (*i.e.* wind turbulence). The following loading conditions were considered in the analytical studies:

1.) Vortex shedding from the cylindrical members of the structure, which included the vertical column.
2.) Wind buffeting against the flat surface of the sign where the time varying component was assumed to be a sine function with varying amplitude.
3.) Statistically varied turbulent wind velocities where the wind pressure was assumed to follow a sine function based on the Davenport wind velocity spectrum (Davenport 1961b);
4.) A randomly generated pressure spectrum.

Although not completely clear, it appears that the mean wind velocities used were taken from standard wind maps. The randomly generated pressure spectrum was developed using a random signal with a power spectral density that corresponded to measured values. The stochastic pressure loading used was based on a turbulent wind velocity component, which is shown in Figure B.4.

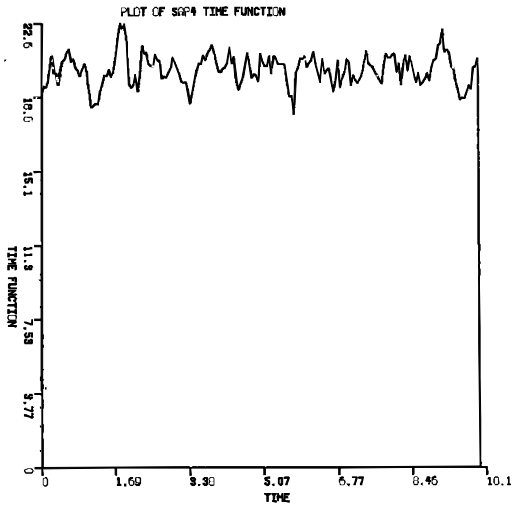

Figure B.4: Randomly Generated Turbulent Wind Velocity Function (Edwards and Bingham 1984).

The SAP IV finite element (FE) program was used to carry out the structural analysis. Three-dimensional analyses were carried out for the four-chord and two-chord configurations. The base conditions for the column in the analytical models were assumed to be rigid (*i.e.* fixed). The first four frequencies of vibration were computed for all of the analytical models. One interesting result of the analyses is that the first vibrational mode shapes of all the cantilevered truss models were in the horizontal plane (*i.e.* a torsion mode for the vertical column). This mode of vibration could be excited if the fluctuating frequency of the wind is similar in magnitude. The second fundamental modes of vibration were *hatchet-type*. It is possible that vortices shed off the truss members and/or sign(s) could excite this mode of vibration.

The analytical results obtained assuming vortex shedding-induced loading indicated that the stresses were very low (*i.e.* negligible). The vortex shedding in these cases was assumed to form off the cylindrical members of the structure, but the method used to load the structure with vortex shedding-induced pressure is not clear. It is assumed that a lock-in frequency was computed for the diameter of the cylinders considered. These lock-in frequencies were most likely compared to the modal frequencies of the structure. Matching lock-in frequencies with their vibrational shapes could then be used to develop vortex-shedding induced loading patterns (Johns and Dexter 1998b). However, these very important issues are not clearly outlined in the report. Therefore, it is felt that the vortex shedding induced loading analysis is suspect.

Analytical results from the buffeting wind response analysis seem reasonable, however, only a mean wind speed of 120 fps (82 mph) was evaluated. The fluctuating component of the wind in

this case was assumed to follow an amplitude-scaled sine function. The frequencies used in the sine function to simulate the turbulent component of wind were determined using a statistical procedure based on the Davenport Spectrum (Davenport 1961b). The range of frequencies considered was 0.35 to 9.1 Hz. This range covered the first few natural frequencies of vibration of the structures being considered. The report suggests that this loading causes large stresses, which is to be expected from such a severe mean wind speed.

The report also makes use of a wind power spectrum and a frequency domain analysis. A Fast Fourier Transform (FFT) was used to examine the frequency content of measured wind. A time-varying pressure function was generated and used in this analysis. The wind pressure used corresponds to a mean wind velocity of 82 mph (120 fps). Although the intention of this analysis is proper, the use of an 82 mph average wind with a turbulent component is quite severe. Using a typical probability density function (PDF) for peak mean wind speeds (*e.g.* Type I Extreme), this wind magnitude would be encountered very infrequently, if at all. If typical design wind maps were used in this analysis, the recurrence interval for this wind would be approximately 50 years, which corresponds to a 2% chance of exceedance in any given year. The stresses computed using these wind velocities were very large when considered in a fatigue analysis.

Field studies were carried out on one of the four-chord sign support structures. Strain gauges were mounted at various locations. The strain was monitored during passage of trucks beneath the sign as well as during natural wind events. Strain measured during the passage of vehicles beneath the sign did not cause stress magnitudes above 900 psi. If it is assumed that a rebound occurs, one might say that the maximum stress range would be 1,800 psi. These stress ranges are well below the CAFL for typical details in the cantilevered structures studied. The report does not mention the type of vehicle that caused each event. It does, however, mention a “box van” induced the maximum stress measured in the sign support. It is possible that a semi-tractor-trailer truck may cause more severe stress levels.

An attempt was made to measure the natural frequencies of vibration and damping percentages for the structure. An individual standing near the vertical pole centroid created oscillations in the structure to excite the cantilever horizontally (pole twisting mode) and vertically (hatchet mode). The horizontal mode (pole twisting) frequency was measured as 1.45 cycles per second, while the hatchet mode of vibration frequency was measured as 1.48 cycles per second. Damping in the vertical mode (hatchet-type) of vibration was measured to be 0.58% of critical. Aerodynamic damping was present in the horizontal mode of vibration, and its

magnitude was measured as 1.17% of critical. Aerodynamic damping found in this research is two times that found in Irwin and Peeters (1980) for the monotube sign support structure. Confirmation of these two magnitudes is difficult without additional experimentation.

A shaker was also used to provide vertical and horizontal motions to the cantilevered structure. The natural frequencies of vibration for the vertical mode and horizontal mode were measured as 1.49 and 1.46 cycles per second, respectively. Damping was also measured through the use of the shaker. The vertical mode of vibration had an inherent damping ratio of 1.4% of critical and the horizontal mode had a damping ratio of 1.85% of critical. The damping ratio measured in the horizontal mode is believed to have included both inherent as well as aerodynamic damping. Aerodynamic damping provided by the sign for the horizontal mode of vibration is thought to be significant; however, it was not mentioned nor quantified in this report.

The report contains several conclusions. First, it was noted that vortex shedding-induced vibrations of the structures and vehicle-induced gust loading do not significantly add to the stress levels in the structural members. However, the conclusion regarding stresses from vehicle-induced gusts is suspect since it was not mentioned that semi-tractor-trailer trucks passed beneath the sign during the field measurement period. The report also mentions that wind buffeting on the sign panels can cause large stress magnitudes. However, this conclusion was made assuming a high mean wind speed with a small recurrence interval. A broader range of wind speeds would provide a better understanding of these structures' responses to daily wind conditions.

South (1994)

This report is a detailed investigation of overhead sign and signal support structures. The over-riding goal of this report was "to combine pertinent existing wind loading and vibration theory, fatigue damage theory, and experimental data into a usable fatigue analysis method for overhead sign and signal structures". Furthermore, the report sought to develop factor of safety equations in order to estimate fatigue damage susceptibility.

The research included instrumentation of a traffic signal structure in Springfield, Illinois for the purpose of collecting wind speed data. An anemometer was mounted to a pole approximately 4 feet above the traffic signal mast-arm (25 feet above the ground). Wind speed data was collected from August 7, 1991 to January 25, 1993. Structures surrounding the site used for the data acquisition ranged from one to three stories in height with the nearest building structure being

200 feet from the site and having approximately two stories. The entire calendar year of data is represented in a histogram in Figure B.5.

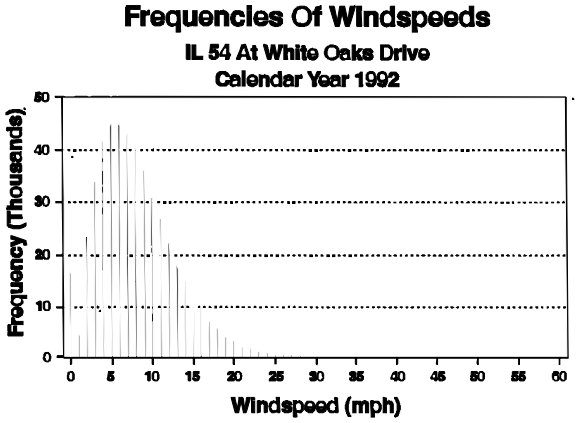

Figure B.5: Wind Speed Histogram for Springfield, Illinois (South 1994).

It appears that the wind loading for the year follows an "extreme" type distribution. Most wind velocity distributions are modeled using Type I, II or III Extreme probability density functions.

The report provides a fairly detailed discussion of the means and methods of quantifying fatigue damage. A procedure using a histogram of stress ranges and the Palmgren-Miner linear damage equation is suggested and used in the report. Proper use of stress-concentration factors is also emphasized and outlined. The report provides a detailed example of the fatigue damage analysis of a cantilevered mast arm traffic signal support structure. Both strain gauge readings and analytical methods are used in the example calculations. The example computations with strain-gauge data indicated approximately 30% of the fatigue damage is caused by a stress range of 4.5 ksi. The report emphasizes that fatigue life estimates should be determined with wind speed data measured over a number of years. The report also outlines a fatigue damage estimating procedure using wind speed histograms. The over-riding goal of the procedure is "to develop a stress range frequency histogram" (South 1994). This histogram can then be used to determine the number of available cycles at a given wind velocity and the fraction of total damage due to that wind speed. The analytical procedure used in the report indicated that all of the significant damage was due to wind speeds in a range from 16 to 27 miles per hour. Comparison with the AASHTO (1994) static procedure found that "... static methods overestimate the expected fatigue life of a given detail by a significant margin".

Cook et al. (1996)

This study contributed to the research effort of quantifying the truck-induced gust loading on overhead sign support elements. The main difference with this study when compared to Creamer *et al.* (1979) is that the former study did not include VMS. These signs have a substantial soffit as well as a large surface area perpendicular to traffic. This soffit is thought to receive significant upward/downward pressure from passing trucks. The Florida Department of Transportation (FLDOT) initiated this study in order to quantify these loading conditions.

Truck-induced pressures were quantified by means of experimental field measurements. An existing highway bridge structure was used to support a sturdy apparatus containing pitot-tube pressure sensors mounted in 15 degree increments between parallel and perpendicular to the flow of traffic (Figure B.6).

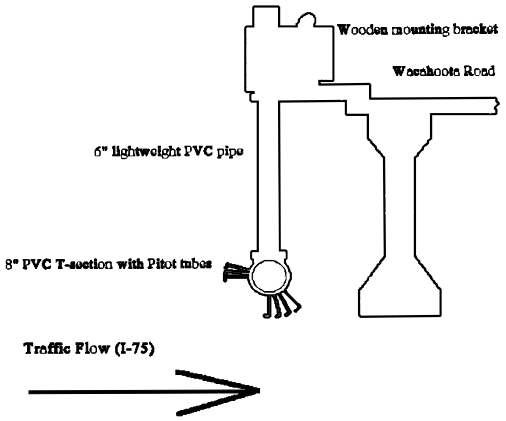

Figure B.6: Wind Velocity Measurement Devise (Cook *et al.* 1996).

The experimental apparatus had the capability of being raised and lowered so that a *gradient* of truck-induced pressures could be measured. In the initial stage of the work, pressures induced by 23 random trucks passing under the bridge were measured at a height of 17 feet above the roadway surface. The speed of each truck was determined using a radar gun, and a picture was taken of each truck. Truck-induced pressures versus time plots were recorded for each random truck event (Figure B.7). A power spectrum was also generated for each random truck-induced gust. The dominant frequencies in the power spectra were between approximately 0.6 Hz and 1.8 Hz.

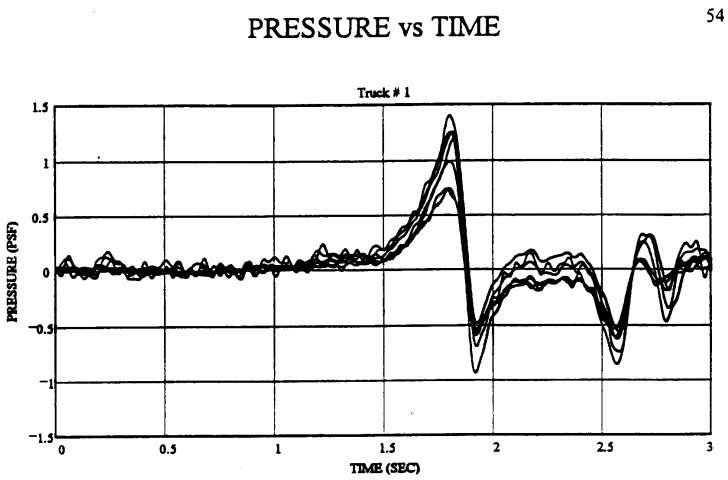

Figure B.7: Typical Truck-Induced Pressure Versus Time Plot (Cook *et al.* 1996).

Controlled truck passes were also used in the study. Tractor-trailer trucks were driven beneath the experimental apparatus at 65 mph. The pressure sensing device was set at four elevations: 17, 18, 19, and 20 feet above the roadway surface. These tests attempted to evaluate a *gradient* of truck-induced pressures while holding the speed and type of truck constant.

A few significant conclusions were drawn from this experimental research. First, the results indicate that passing trucks will induce a positive *and* negative pressure pulse on the VMS elements (refer to Fig. B.10). Second, the pressure magnitudes from the study were low with the *average* being approximately equal to 1 psf. It also was determined that for each foot of elevation over 17 feet above the roadway surface the truck-induced pressure on the sign elements reduces by approximately 10 percent. Lastly, it was found that the dominant frequencies of the truck-induced pressure pulses were in the range of 0.5 Hz to 2.0 Hz. As a result of this finding, the FLDOT currently makes attempts at ensuring that the natural frequency of the supporting structure does not approach these frequencies.

DeSantis and Haig (1996)

This paper outlines an investigation of the factors leading to the failure of a truss-type overhead cantilevered highway sign support structure in Virginia. The structure was less than one year old and supported a variable message sign with a 24-inch soffit. The horizontal mast-arm was composed of two parallel trusses, and the vertical upright was a single tapered pole. The failure mode described in the paper was said to be fatigue related and consisted of a circumferential crack around the steel pole at the toe of the base plate weld in the heat-affected zone (HAZ). The

opinion of this paper was that the soffit area of the VMS was being subjected to severe vertical pressures due to passing trucks.

An analytical investigation into the cause of the VMS collapse as a result of truck-induced gust pressure was undertaken. The investigation of the failure indicated, "…only loads that would explain the fatigue failure were vertical oscillations of the arm" (DeSantis and Haig 1996). This corresponds to a "hatchet" mode of vibration discussed in previous research efforts. This mode of vibration could be a result of vortex shedding, galloping, or truck-induced gusts on the VMS soffit. The investigators felt that this vibration condition was a result of only truck-induced pressures, and this decision guided the investigation. Highway workers validated this hypothesis, and mentioned that they observed the sign structure oscillating in the "hatchet" mode as trucks passed beneath the VMS.

The VMS support structure was designed according to the then current U.S. design specifications for highway sign and luminaire supports (AASHTO 1985). The fundamental vibration frequency for the VMS support was determined using a finite element analysis (SAS 2000). Using the computed natural frequency for the fundamental mode of vibration, the critical wind velocity for "lock-in" was computed as 1.34 mph. A bluff body dimension normal to the wind was assumed to be 7.38 inches, which is the average diameter of the truss chords. A Strouhal number of 0.18 was assumed, which is consistent with circular bluff bodies. Using the velocity of 1.34 mph it was found that the bending moments that result at the base using conventional pressures (AASHTO 1985) were negligible. The report stated that this calculation confirmed vortex shedding-induced vibrations were not the cause of the failure. This is questionable since the bluff body dimension perpendicular to the wind is much greater for the VMS and thus the "lock-in" wind velocity would be much greater. It is interesting to note that vortex shedding on the VMS was not considered in the analysis. This appears to be in error.

The effect of truck-induced loading was studied anecdotally. It was first assumed that, on average, a passing truck would have a velocity of 65 mph. It was then assumed that the truck would create an upward pulse of air (*i.e.* a gust) with a velocity equal to the passing truck's velocity (*i.e.* 65 mph). Using this wind velocity with appropriate drag and gust factors, the force applied to the underside of the VMS was computed using specification procedures (AASHTO 1985). Using this procedure, the pressure exerted on the underside of the sign was computed as 26.5 psf. If it is assumed that the upward lifting of the cantilever truss would be followed by a "rebound effect", it was shown that approximately 10.8 ksi of stress could exist at the base of the

vertical support each time a truck passed. One could also rationalize that the small damping of the VMS support could result in these upward pulses causing multiple damaging load cycles for each passing truck. Such severe stress ranges would promote a very short fatigue life. The truck-induced gust theory was further verified by using field crew observation which stated that the sign moved "about one foot" up and down each time a truck passed beneath. Using this third-hand information, the pressure beneath the sign required to cause this "observed" deformation corresponded to a truck speed of approximately 60 mph.

Gilani et al. (1997)

This report summarizes a research effort conducted for the California Department of Transportation (CALTRANS) after the collapse of a Changeable Message Sign (CMS or VMS) support structure. The research involved both a field investigation of a newly installed CMS cantilevered support structure as well as an analytical study of the same structure. The field studies were undertaken to quantify the natural frequencies of vibration and modal damping characteristics. FE analysis of the support structure was undertaken to evaluate stress distributions around access holes and within the base plate. Elastic analysis was utilized, and the mast-arm connection plates and base plate were modeled.

The experimental and analytical investigations revealed that the 4" x 6" conduit hole was a significant source of fatigue concern in the CMS support. Furthermore, it was felt that quality of workmanship was of major concern in the fabrication and erection of the CMS support structures. A mast-arm specimen that was tested developed micro-cracks as the flange-plate-to-mast-arm connection bolts were tightened. Further cracking was noticed in these locations during the experimental testing. The following recommendations were made upon completion of the experimental testing phase of the mast-arm. First, any conduit hole(s) in the mast-arm should be drilled and not flame cut. Second, a pre-qualified weld should be developed for the flange-plate-to-mast-arm connection. Inspection programs should be improved to ensure quality welding in these very sensitive structures. Also, an out-of-flatness limitation should be specified for flange plates. It was felt that this specification would minimize the formation of micro-cracks as the connection bolts are tightened. Lastly, the effort concluded that base plate flexibility should be included in the mathematical models.

This report also briefly evaluated the wind loading experienced by CMS support structures. It was mentioned that truck-induced gusts were expected to be severe. Vortex shedding was considered possible; however, it would likely occur at a low velocity (8.3 ft/sec or 5 mph) for

these structures, which is not expected to be a problem. Wind loading causing across wind oscillations of the support structure was attributed to galloping. It was the opinion of the authors that the low inherent damping of the structure makes the structure susceptible to negative damping which is the cause of galloping instability.

Chavez et al. (1997)

This research report outlines an effort undertaken to retrofit cantilevered CMS support structures with the goal being to eliminate the fatigue problems found in Gilani *et al.* (1997). It was felt that the cantilevered CMS structure from Gilani *et al.* could have been subjected to large dynamic stresses resulting from galloping-induced vibrations. The mast-arm-to-post flange connections and post-base plate connections were found to be critical. The retrofit schemes studied in the research effort focused on increasing the support structure stiffness, increasing the support structure damping, and moving the critical section away from the support post-base plate connection.

The research program evaluated two retrofit schemes experimentally and analytically. The first scheme involved gusset plates oriented radially around the post at the base plate. The second scheme utilized a concrete jacket at the base extending from the base plate to an elevation six feet above. The experimental testing concluded that the gusset plate scheme did not provide satisfactory performance. It was suggested that if the experimental conditions fully represent the in-field conditions, the concrete jacket retrofit scheme is the preferred approach for the cantilever CMS structure studied.

Johns and Dexter (1998b)

This research effort studied wind loads on cantilevered sign, signal, and luminaire support structures. Similar to the work of McDonald *et al.* (1995), it was found that excessive vibration of these types of structures may be caused by three different loading phenomena: (a) natural wind gust buffeting; (b) buffeting caused by truck-induced gusts; and (c) galloping. Field measurements of these three phenomena were gathered through instrumentation of a cantilevered VMS support structure. From these measurements, the study recommends static load ranges be used to simulate the dynamic nature of these loadings and to determine fatigue life.

The report offers a good discussion of possible wind loadings that might be recorded by the instrumented VMS support structure. It suggests “overhead sign support structures are not susceptible to galloping, but are potentially susceptible to vortex shedding” (Johns and Dexter

1998b). However, the report states that "vortex shedding has never been reported to be a problem for cantilevered support structures," and, as confirmed by the work of McDonald *et al.* (1995), vortex shedding was not considered in the study.

A review of the procedure used for modeling a structure's response to natural wind gusts using frequency-domain finite element analysis is given. The report also offers a brief discussion of the onset of galloping-induced oscillations by using the Den Hartog stability criterion. A summary of previous research efforts regarding truck-induced gusts is also described and used as a foundation for this study.

The remainder of the report is dedicated to a discussion of the experimental setup and measurements of a cantilevered VMS sign support structure. Short-term field tests were performed to obtain vibrational characteristics of the erected structure. The stiffness, natural frequency, and damping ratio of the cantilever support structure were determined. Two primary modes of vibration were studied: (a) hatchet or vertical mode; and (b) twisting mode. The natural damping of the structure was determined using the logarithmic decrement procedure. A Fast Fourier Transform (FFT) was used to determine the characteristic natural frequencies of the structure. The second phase of the short-term testing was to measure truck-induced gust pressures on the VMS support structure. The pressures, which were taken from test trucks driven under the sign at recorded velocities, were found to be "unpredictable". The transfer of pressure through pitot-tubes to the pressure transducers was thought to be unreliable due to the probable turbulent nature of the truck-induced gusts. However, the pitot-tube pressure transducer arrangement was thought to be useful for quantifying a pressure gradient along the height of the vertical surface of the VMS. The report suggests that the limited data taken from the tests indicates that two trucks running side-by-side under a VMS might have "twice" the effect on the structure as trucks running behind one another. The truck testing data also suggested suction was introduced to the soffit of the VMS prior to the upward gust of air. This result was consistent with other truck gust studies (Cook *et al.* 1996).

Additional steps were taken to more accurately quantify truck-induced pressure gusts. Figure B.8 illustrates the effect of truck-induced gusts resulting from 3 "controlled" truck runs. The very light damping magnitude exhibited by the "hatchet mode" vibration of the cantilever VMS support structure is apparent in the response.

The strain gauge measurements were used to back-calculate pressures acting upon the soffit of the VMS. Johns and Dexter (1998b) outline this "back-calculation process" and state that a pressure of 11 psf can be equated to a stress range of 14 MPa. The stress range for the "worst" truck event in Figure B.8 (Truck 3) can be conservatively taken to be 3.0 MPa. Therefore, the pressure acting upon the soffit of the VMS can be estimated as 2.4 psf. Trucks 1 and 2 have back-calculated soffit pressures that are of smaller magnitude: 1.2 psf and 1.96 psf, respectively. These pressures are definitely comparable to those measured by Cook *et al.* (1996) shown in Figure B.7. Although Johns and Dexter (1998b) indicate that pitot-tube pressure transducers can be unreliable, the truck-induced pressure gusts (with the exception of the "long-term measurements") calculated in Johns and Dexter (1998b) are consistent with the magnitudes reported by Creamer *et al.* (1979) and Cook *et al.* (1996).

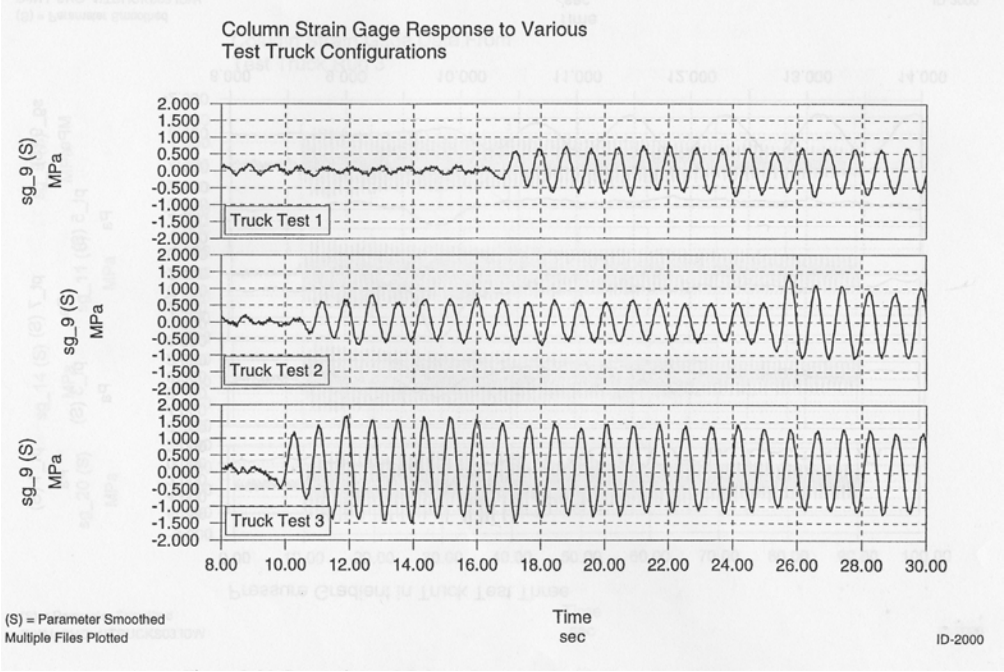

Figure B.8: Maximum Recorded Stress Ranges in Column Due to Truck-Induced Wind Gusts for Sign Vibrating in Hatchet-Mode (Johns and Dexter 1998b).

Long-term field-testing of the cantilevered support structure was carried out over a three-month period. Strain gages were mounted to the columns, the cantilevered truss upper chord, and the anchor bolts. Wind speed and direction were also monitored. It was reported that no "significant events" occurred over this monitoring period. "Galloping never did occur while the structure was monitored." However, the structure was found to be constantly vibrating at small

amplitudes due to some uncorrelated combination of natural wind gusts and truck-induced gusts. It was felt that the stress ranges due to these small vibrations were not sufficient to cause damage.

Johns and Dexter (1998c)

This journal paper is a condensed version of the Lehigh ATLSS research efforts (Johns and Dexter 1998a; Johns and Dexter 1998b; Kaczinski *et al.* 1998). However, there are several pieces of information found in this paper that are not easily found in the other research reports. Nonetheless, its condensed state allows for very direct interpretation of results, and, therefore, it will be reviewed in the present document.

One very convenient piece of information available in the paper is a table containing a "susceptibility matrix" for various sign and luminaire support structures. This matrix is reproduced in Table B.2.

Table B.2: Susceptibility Matrix for Sign, Signal, and Luminaire Supports (Johns and Dexter 1998c).

	Galloping	Vortex Shedding	Natural Wind Gusts	Truck-Induced Wind Gusts
Sign Support	X	(1)	X	X
Signal Support	X		X	X
Luminaire Support		X	X	

X - Indicates structure is susceptible to stated wind loading phenomena.
(1) - Vortex shedding was reported in an overhead sign support structure (Irwin and Peeters 1980).

A few conclusions, which may overlap with previous ATLSS research reports, were drawn from this paper in relation to sign support structure design. First, it was suggested that cantilevered sign and signal support structures should be designed for galloping-induced loads using a static (shear) pressure of 21 psf. This shear pressure should be made to act as a vertical loading on the vertical face of the supported sign. Second, truck-induced gust loadings can be considered in design using an equivalent static pressure of 37 psf multiplied by the appropriate drag coefficient. This pressure is to be applied to the horizontal surfaces of the support structure and/or the soffit of a VMS/CMS. The length of this pressure along the VMS or support structure should be 12 feet (*i.e.* the width of a passing truck). The source of this significant pressure magnitude is suspect.

Kaczinski et al. (1998)

This report contains results of experimental and analytical research performed to develop guidelines for the fatigue design of cantilevered sign, signal, and luminaire support structures. The study was motivated in part by a survey sent to state DOT's regarding the performance of cantilevered sign and signal support structures. In the responses to the survey, a total of 80 occurrences of fatigue damage in cantilevered support structures were reported. The majority of damage reported occurred in the mast-arm-to-column connection, the column-to-base-plate connection, and/or the anchor bolts. This report suggests that truck and natural wind-induced vibrations are responsible for the accumulation of fatigue damage in structures that have been in service for 15 to 20 years. The report attempts to address the above fatigue issues as well as the rather ambiguous nature of fatigue design outlined in the design specifications (AASHTO 1985; 1994).

As in previous reports, four wind loading types are identified in this report: (a) vortex shedding; (b) galloping; (c) natural wind gusts; and (d) truck-induced gusts. Vortex shedding is a potential wind load for those structures whose natural frequencies and Strouhal number yield a lock-in wind velocity in the range of 10 to 35 mph. Wind speeds below 10 mph are usually not sufficient to excite most structures, and wind speeds greater than 35 mph do not easily allow the formation of organized vortices. The report finds that, "cantilevered signal, sign, and luminaire support structures are generally not susceptible to significant vibrations due to the shedding of vortices" (Kaczinski *et al.* 1998). Galloping is believed to be the main cause of large amplitude oscillations in cantilevered structures. The report includes an extensive study of this, which will be discussed later. Natural wind gusts are characterized by a spectrum of fluctuating velocity components. These fluctuations in flow velocity induce fluctuating flow pressures on the various structural components, which in turn create vibrations in the structure. "The magnitudes of the variable stress ranges induced in the connection details of a structure may, in some cases, cause fatigue cracking due to the long-term cumulative effect of the natural wind gusts" (Kaczinski *et al.* 1998). Truck-induced gusts are also mentioned as an important component in the evaluation of the fatigue performance of cantilevered sign structures. It is noted that raising the lower surface of the sign structure relative to the road surface will reduce the magnitude of the vertical component of the truck-induced gust. This was evident in the research of Cook *et al.* (1996).

The report discusses aerodynamic and aero-elastic studies performed at MIT in the Wright Brothers Memorial Wind Tunnel. The aerodynamic research program was conducted to measure forces generated on model, cantilevered structures and to evaluate their susceptibility to

galloping-induced oscillations. Sign support structures are normally composed of circular cross-sectional elements. Circular cross-sections always exhibit positive aerodynamic damping, and, therefore, these structures are not susceptible to galloping-induced oscillations on their own. However, the aerodynamic study showed that cantilevered structures with signal attachments are susceptible to galloping. These structures become even more susceptible when back-plates are added to the signal attachments. These results were similar to conclusions drawn by other researchers (McDonald *et al.* 1995).

The aero-elastic study was used to explore the findings made in the aerodynamic wind tunnel study. In this study both vortex shedding-induced vibrations (without attachments) and galloping-induced vibrations (with attachments) of the structure were studied. The report suggests that vortex shedding does not need to be considered when lock-in wind velocities are less than 5 mph. It also noted that sign and signal attachments disrupt the formation of organized vortex streets due to three-dimensional effects. Therefore, as long as an overhead sign support structure has adequate attachments, vortex shedding does not need to be considered. The study also found that galloping-induced vibrations were possible for most types of sign and signal structures. However, it was concluded that the galloping phenomenon is very sensitive to a variety of conditions. Specific conditions related to the dynamic properties of the structure, the aerodynamic properties of the attachments, and the wind flow characteristics must all be "aligned" properly in order for galloping to take place. Because of these factors, galloping-induced oscillations were observed once in the wind tunnel tests but could not be reproduced.

Static and dynamic FE analyses were used to estimate wind pressures applied to cantilevered support structures during galloping, vortex shedding, and natural wind and truck-induced vibrations. The FE analyses omitted foundation flexibility and soil-structure interaction. An eigenvalue analysis was used to determine the natural frequencies and mode shapes corresponding to the first six modes of vibration. Load models for galloping and vortex shedding were developed based on the results of the aerodynamic and aero-elastic wind tunnel studies. The dynamic analyses consisted of linear modal analyses to determine the steady-state dynamic response of the sign support structure subjected to vortex shedding and/or galloping. Using a static FE analysis and assuming the applied load to be sinusoidal, an equivalent static pressure range was determined. An equivalent static lift-pressure range equal to 21 psf was recommended for the design of cantilevered sign support structures. This equivalent static wind pressure is to be applied vertically as a shear stress on the surface area of all sign and signal attachments as seen in the normal elevation, which are mounted to the horizontal mast-arm. Furthermore, it was

suggested that only those cantilevered support structures not having attachments and having lock-in velocities greater than 10 mph be considered susceptible to vortex shedding-induced vibrations. In most cases provisions contained in the design specification (AASHTO 1985; 1994) were thought to be adequate in this regard.

The report also discusses different methods of fatigue design. The report highlights and is more or less an advocate for an infinite-life fatigue design approach (Fisher *et al.* 1993). Infinite-life is achieved in any detail where the percentage of time the stress range exceeds the CAFL is acceptably low. Experimental results indicate that fatigue failure can occur if 0.05 percent or more of the stress ranges applied to a detail exceed the CAFL and infinite life resulted when fewer than 0.01 percent of the stress ranges exceeded the CAFL (Fisher *et al.* 1993). The infinite-life variable-amplitude fatigue design approach (Fisher *et al.* 1993) is also provided in the report. Using this approach, structure response and stress ranges, including any dynamic amplification, that have a probability of exceedance of 0.01 percent must be estimated. The 0.01 percent probability of exceedance stress ranges is termed the "fatigue limit-state" ranges. These stress ranges must be less than the CAFL of any detail considered. The infinite-life approach is considerably easier than trying to account for cumulative damage caused by a future distribution of wind loads as was done by South (1994). All that is required is to compute the strength limit-state as provided in the design specifications (AASHTO 1985; 1994) and to compute the fatigue limit-state governed by the 0.01 probability of exceedance.

Anchor bolt fatigue testing was also part of this study. The goal(s) of the testing was to develop a CAFL for snug-tight and fully tightened anchor bolts. The anchor bolt testing was motivated by the uncertainties involved in using welded component fatigue results for anchor bolt assessment. The report briefly summarized previous research by Frank (1980) that concluded that nominal diameter, galvanizing, thread-forming process (*e.g.* cut vs. rolled), thread series, and steel type bolts have a negligible effect on fatigue life. Dusel (1984) conducted similar testing and reached similar conclusions. These research efforts suggest that snug-tight anchor bolts adhere to AASHTO category E details while fully-tightened anchors adhere to category D details. Unfortunately, these past efforts did not arrive at a CAFL for snug-tight and fully-tightened anchor bolts. This was the motivation for the presently discussed effort.

The anchor bolt experimental investigation allowed the following conclusions to be drawn. First, axially loaded, snug-tight anchor rods should be designed for fatigue using Category E' in regions of *finite* fatigue life. Fully tightened bolts can be designed using Category E in the *finite*

fatigue life region. The CAFL for *all* anchor bolts was suggested as Category D provided beveled washers were utilized for a misaligned (1:40 max.) condition. Bending stresses resulting from misalignments less than 1:40 need not be explicitly considered if firm contact between the nut(s) and ply(s) exists (*e.g.* beveled washers). Furthermore it was suggested that prying should be minimized.

The report's final recommendation is that overhead sign and signal bridges be studied further. Specifically, it recommends that the literature and other design codes be reviewed. Furthermore, dynamic and static analyses should be conducted to determine and estimate equivalent static load ranges for vortex shedding, natural wind gusts, and truck-induced wind gusts.

Fouad et al. (1998)

The objective of the research outlined in this report was to "develop up-to-date, comprehensive specifications, and accompanying commentary, for structural supports for highway signs, luminaires, and traffic signals" (Fouad *et al.* 1998). The intent of this research was to provide revisions to many aspects of the then current sign and luminaire support specifications (AASHTO 1994). As a result, it recommends many changes and updates to parts of the design specifications. Some of these changes warrant a review as part of the present research effort.

This research report recommends moving from fastest-mile wind speed maps to 3-second gust maps for 50-year mean recurrence interval winds. This change directly affects the determination of drag coefficients, C_d, which are needed to compute effective velocity pressures. It would be required to make drag coefficients consistent with 3-second wind gust speeds. The report also recommends that a 3-second gust effect factor be defined. A second important proposed change to the wind design criteria is redefinition of the importance factor. The report recommends that the importance factor be redefined so that other mean recurrence interval winds may be computed using the traditional equation format of the design specifications. This proposed change to AASHTO would align the document with current wind loading provisions for buildings (ASCE 1998).

A major item also considered in this effort was the lack of recommendations regarding oscillations, fatigue, and resonance found in the previous specifications (AASHTO 1994). The major revision recommended was to include a section devoted to fatigue resistance and loading of signs, signals and luminaire support structures based on the work of Kaczinski *et al.* (1998). A brief study of the impact of the fatigue design criteria proposed resulted in the apparent over-

design of support structures. As a result, the report stopped short of recommending all fatigue design criteria as proposed in Kaczinski *et al.* (1998) in favor of recommending that: (1) only critical cantilevered structures be required to meet the proposed design criteria; and (2) fatigue design category III (Kaczinski *et al.* 1998) was recommended for support structures, but the more stringent categories (I and II) could not be recommended.

Fatigue design categories I, II, and III correspond to the AASHTO E' fatigue detail category. On average these three design categories were more conservative than the AASHTO E' detail category. Fatigue performance of anchor bolts also was considered in the proposed revisions to the design specifications. These revisions include allowable tensile stresses in anchor bolts consistent with group IV fatigue load combinations, which were also proposed by Kaczinski *et al.* (1998).

The new section proposed by this effort is related to fatigue design considerations, and it includes detail categories for connections similar to the categories found in the *LRFD Design Specifications for Highway Bridges* (AASHTO 1998). The proposed fatigue loading is based on an equivalent static loading intended to account for the dynamic loading effects. Galloping, vortex shedding, natural wind gusts, and truck-induced wind gusts are all considered in the proposed revisions. The proposed revisions to the structural supports specifications (AASHTO 1994) also include recommendations regarding anchor bolt fatigue considerations, which include guidance for installation and misalignment. All of the proposed fatigue related changes are limited to "critical" cantilevered overhead support structures. Fatigue related changes to the procedures used for full-span overhead support structures could not be recommended. As a result, these proposed changes and their impact on full-span overhead sign support structures require further evaluation.

Johns and Dexter (1999)

This paper outlines the ATLSS research undertaken to evaluate the effect of passing trucks on cantilevered sign support structures (Johns and Dexter 1998c). There are no additional pieces of information contained in this paper that are not contained in the other reports discussed previously in this chapter.

Kashar et al. (1999)

This paper outlines an investigation into the cause of a failed CMS (or VMS) structure for CALTRANS. It is believed that this investigation was conducted in parallel with that of Chavez

et al. (1997); Gilani and Whittaker (2000a,b); and Gilani *et al.* (1997) for the same CMS support structure. The paper explored both fabrication as well as wind loading contributions to the sudden failure of the structure.

The metallurgical investigation results provided in the paper suggest that the material and the welds used in the CMS structure were satisfactory and not likely the cause of the shortened fatigue life. The investigation estimated that approximately 1,000,000 trucks passed beneath the sign support prior to failure. A similar CMS structure was instrumented with strain gauges and dead load stresses measured were compared with analytically obtained quantities. The results of this comparison indicated that the grout used beneath the base plate provided sufficient restraint such that the fixed base condition assumed in the analytical studies was adequate.

The paper noted that the CMS support structure might have been subjected to both vortex shedding and galloping-induced vibrations prior to failure. A Strouhal number of 0.52 was assumed for the CMS. This led to a lock-in velocity for vortex shedding of 30 mph. It was mentioned in the paper that the wind averaged 31 mph during the 24 hours prior to failure and had gusts up to 60 mph. This would suggest that vortex shedding-induced vibrations contributed to the fatigue failure of the structure. The paper also reports that "galloping" was observed, with vertical oscillations of approximately 12 inches. One should be very careful interpreting this statement as vortex-shedding vibrations cause vertical oscillations. Therefore, one must assume the authors meant vortex-shedding. The measured results from the field instrumentation and the observations indicate that mild to strong winds and truck-induced pressures generated significant stresses within the support structure (6 ksi at height 3 feet from the base; 12-14 ksi just above the weld). Such severe stresses could easily have shortened the fatigue life of the structure.

Gilani and Whittaker (2000a;b)

These research papers summarize the research conducted at the University of California at Berkeley related to cantilevered CMS support structures (Chavez *et al.* 1997; Gilani *et al.* 1997). There are several conclusions related to the Berkeley research that are more pointedly stated in these research papers. First, it is mentioned that evaluation of the field recorded response data and the work of Kaczinski *et al.* (1998) suggest that galloping instability was a potential cause of the CMS support failure. As outlined previously, this is questionable. Furthermore, the paper mentions that the design procedure suggested in Kaczinski *et al.* (1998) should be reevaluated in light of the stress-ranges measured during the field experimentation. The second paper provided a concise summary of the laboratory experimentation conducted.

Dexter and Ricker (2002)

The research report can be considered the most current effort in relation to wind-induced failure of cantilevered sign support structures, cantilevered signal support structures, and luminaire support masts. The report outlines a problem of national scope in which in-service sign support and luminaire support structures are suffering collapse, or at the very least are being found with cracks. As a result, it specifically examines six issues (Dexter and Ricker 2002):

1. Variable Message Sign (VMS) issues;
2. vibration mitigation strategies;
3. characterization of at-risk structures;
4. quantification of importance factors
5. anchor rod tightening research
6. design examples, training materials, and guidance on installation, inspection, and maintenance.

The report provides a detailed summary of a survey administered to state DOT's outlining the severity and scope of the problem. It also presents and discusses the results of extensive analytical, field, and experimental work related to cantilevered sign and signal support structures as well as luminaire masts. The report also documents changes to the recommendations of Kaczinski *et al.* (1998), which evolved into the current standard for design of these structures (AASHTO 2001). Therefore, it is expected that Dexter and Ricker (2002) will become an added basis for the new revisions to the luminaire and sign support design standard.

B.3 High-Mast-Luminaire Support Structures

Unfortunately, the body of research literature related to luminaire support structures is less extensive than that devoted to cantilevered sign support structures. However, there is a small and significant set of research efforts that contributed to the present effort and warrant review as part of this synthesis. As with the sign-support work, the luminaire support research efforts are presented in chronological order.

Fisher et al. (1983)

This research effort focused on the fatigue performance of signal mast arms and their base plate connections. The base plate condition and the fatigue performance results obtained both analytically and experimentally are directly applicable to the present research effort.

Pipe base plate connections were fatigue tested to determine a representative AASHTO *Fatigue Detail Category* for the welded connection. It was determined that the welded pipe base detail can be categorized as a category E or E' detail depending upon the fillet weld profile at the base. It appeared that a "steeper" contact angle (*i.e.* greater than a 45 degree angle with respect to the horizontal) had a beneficial effect and increased the fatigue resistance.

An interesting finding of this research effort was with regard to galvanized coating and its effect on detecting cracks. When the specimens were hot-dip galvanized, the galvanized coating did not break and it concealed any evidence of a crack forming (Fisher *et al.* 1983). It was found that other NDT evaluation techniques (magnetic probe and eddy current probe) were adversely affected by the galvanized coating. Furthermore, the experimental evidence suggested that the cracks must extend almost completely through the pipe thickness prior to breaking the galvanized coating (Fisher *et al.* 1983).

A pre-existing (circa 1983) stress intensity factor formula for cover plate end welds (Zettlemoyer and Fisher 1977) was used to approximate the stress intensity factor at the pipe-to-base connection. The simplified procedure used tended to both over-estimate and under-estimate the fatigue resistance of the detail tested. It was suggested that axis-symmetry and fixity of the base plate could elevate the stress level in the pipe wall. The paper concludes with the recommendation that more accurate stress concentration factors and stress gradient correction factors be used for light pole details.

Kwok (1985)

Although this research effort focused on a free-standing light tower (similar to those used at athletic facilities), the effort demonstrated that finite element analysis could accurately predict vibrational mode shapes for tall HML-type structures. The light-tower studied in this effort was 214 feet tall and had a single, tapered mast.

Milford (1989)

The focus of this research effort was to develop gust factors for tall lighting support masts similar to those studied in Kwok (1985). The goal of the effort was to develop these gust factors for incorporation into code provisions.

Rahimian and Sifre (1993)

Although not devoted to a luminaire support, this contribution outlines a study of a dual-mast structure at the top of a forty-story building that developed fatigue cracks four months after its

installation. The masts investigated were 60-m (197 feet) in height. Although, providing conclusive recommendation that vortex-shedding was the likely cause for the failure, the analytical basis for this recommendation was slight. Nonetheless, the effort at least supports the notion that vortex-shedding induced vibrations may lead to failure of tapered mast structures.

Repetto and Solari (2001)

Along-wind response of slender support masts and a technique to estimate the fatigue life of such a structure is the focus of this effort. The research conducted and validated in this paper supports the use of simulated load histories and histograms of stress cycles to evaluate fatigue lives of mast structures. Although, focused on what amounts to single degree of freedom (SDOF) structures, the work suggests that finite element analysis and simulated loading histories can be candidates for generation of fatigue-life estimates.